Technical Report: USGS Award Number 08HQGR0017

Establishing Maximum Spectral Demand for Performance-Based Earthquake Engineering: Collaborative Research with the University at Buffalo and the USGS

Yin-Nan Huang
State University of New York, Buffalo
Buffalo, NY 14260
(716)645-4364
yh28@buffalo.edu

Andrew S. Whittaker
State University of New York, Buffalo
Buffalo, NY 14260
(716)645-4364
awhittak@buffalo.edu

Nicolas Luco
United States Geological Survey
Golden, CO 80401
(303)273-8683
nluco@usgs.gov

Award Term: December 2007 through December 2009

Abstract

Maximum spectral demand is used for design ground-motion parameters in ASCE/SEI 7-10, and FEMA P-750. The procedures presented in these documents to transform geometric mean horizontal spectral demand to maximum spectral demand were based initially on analysis of near-fault ground motions in the Western United States. The goals of this study are 1) to enable calculation of maximum spectral demand for all regions of seismic hazard in the United States, 2) to develop an understanding of the orientation of maximum spectral demand across different ranges of period for all regions of seismic hazard, and 3) to quantify the correlation of maximum spectral demand at different periods.

Three earthquake ground-motion databases are compiled for far-field Western United States (WUS), near-fault WUS and the Central and Eastern United States (CEUS). The database for the far-field WUS ground motions includes 165 pairs of ground motions with moment magnitude of 6.5 and greater and closest site-to-fault distance between 30 and 50 km. The database for the near-fault WUS ground motions includes 147 pairs of ground motions with moment magnitude of 6.5 and greater and closest site-to-fault distance of 15 km and less. The database for the CEUS ground motions includes 63 pairs of ground motions recorded from 19 earthquakes that occurred mostly in Eastern North America between 1976 and 2010.

The analysis results indicate that 1) the median ratios of maximum spectral demand to geometric-mean demand (GMRotI50) range between 1.1 and 1.4, increasing slightly with period, and the 84th percentile ratios range between 1.3 and 1.6; 2) the use of maximum spectral demand for force-based design is not overly conservative since there is typically an axis where the spectral demands are close or equal to the maximum demands; and 3) the model of Baker and Jayaram (2008), with some minor modification, can capture reasonably well the correlation of maximum spectral demand at different periods.

Contents

Section 1 Introduction 1-1

1.1 Motivation and objectives 1-1

1.2 Geometric-mean and maximum spectral demands 1-2

1.2.1 Geometric-mean spectral demand 1-2

1.2.2 Maximum spectral demand 1-4

1.2.3 Orientation of maximum spectral demand 1-5

1.2.4 Correlation of ground motions 1-6

1.3 Organization of the report 1-7

Section 2 WUS far-field ground motions 2-1

2.1 Datasets 2-1

2.2 NGA relationships 2-1

2.3 Geomean spectral demand representation 2-2

2.4 Maximum and geomean spectral demands 2-3

2.4.1 Relationships between maximum spectral demand and GMRotI50 2-3

2.4.2 Relationships between GMRotI50 and NGA-predicted GMRotI50 2-4

2.4.2.1 GMRotI50_BA 2-4

2.4.2.2 GMRotI50_CB 2-5

2.4.2.3 GMRotI50_CY 2-6

2.4.2.4 GMRotI50_ave 2-6

2.4.3 Relationships between maximum spectral demand and NGA-predicted GMRotI50 ..2-7

2.5 Orientation of maximum spectral demand 2-8

2.5.1 Methodology 2-8

2.5.2 Sample computations 2-9
2.5.3 Overall analysis results 2-10
2.6 Correlation of ground motions 2-11
2.6.1 Time series 2-11
2.6.1.1 Definition 2-11
2.6.1.2 The study of Hadjian (1981) 2-11
2.6.1.3 Correlation of the two time series for each pair of ground motions of Table 2-1 . 2-12
2.6.2 Spectral demand 2-13
2.6.2.1 The studies of Baker, Cornell and Jayaram 2-13
2.6.2.2 Correlation coefficient of maximum spectral demands at different periods 2-15

Section 3 WUS near-fault ground motions 3-1
3.1 Introduction 3-1
3.2 Geomean spectral demand representation 3-2
3.3 Maximum and geomean spectral demands 3-2
3.3.1 Relationships between maximum spectral demand and GMRotI50 3-2
3.3.2 Relationships between GMRotI50 and NGA-predicted GMRotI50 3-3
3.3.2.1 GMRotI50_BA 3-3
3.3.2.2 GMRotI50_CB 3-4
3.3.2.3 GMRotI50_CY 3-5
3.3.2.4 GMRotI50_ave 3-6
3.3.3 Relationships between maximum spectral demand and NGA-predicted GMRotI50 .. 3-7
3.4 Orientation of maximum spectral demand 3-8
3.4.1 Objectives 3-8
3.4.2 Sample computations 3-8

3.4.3 Overall analysis results 3-10

3.5 Correlation of ground motions 3-11

3.5.1 Time series.....3-11

3.5.2 Spectral demand 3-12

Section 4 CEUS ground motions 4-1

4.1 Datasets 4-1

4.2 Geomean spectral demand representation 4-3

4.3 Maximum and geomean spectral demands 4-3

4.4 Orientation of maximum spectral demand.....4-4

4.4.1 Sample computations.....4-4

4.4.2 Overall analysis results 4-5

4.5 Correlation of ground motions 4-5

4.5.1 Time series.....4-5

4.5.2 Spectral demand 4-6

4.5.2.1 Attenuation relationship.....4-6

4.5.2.2 Correlation coefficient of maximum spectral demands at different periods 4-7

Section 5 Summary and conclusions 5-1

5.1 Summary.....5-1

5.2 Conclusions.....5-2

5.2.1 WUS far-field ground motions 5-2

5.2.2 WUS near-fault ground motions 5-3

5.2.3 CEUS ground motions 5-5

Section 6 Acknowledgement and references 6-1

Figures

Figure 1-1. Definition of maximum spectral demand 1-8

Figure 2-1. Magnitude and distance distribution of the ground motions of Table 2-1 2-27

Figure 2-2. a) Eighty-fourth, 50th and 16th percentiles and b) cumulative distribution functions of normalized time difference between the peak accelerations parallel and perpendicular to the GMRotI50 direction for the records of Table 2-1.....2-28

Figure 2-3. Ratios of maximum spectral demand to GMRotI50 for the records of Table 2-1.2-29

Figure 2-4. Maximum, minimum, median and 84th and 16th percentiles of the ratios of maximum spectral demand to GMRotI50 for the records of Table 2-1.....2-29

Figure 2-5. Ratios of maximum spectral demand to GMRotI50 at periods of 0, 0.2, 0.5, 1, 2 and 3 seconds as a function of magnitude for the records of Table 2-1.....2-30

Figure 2-6. Ratios of maximum spectral demand to GMRotI50 at periods of 0, 0.2, 0.5, 1, 2 and 3 seconds as a function of distance for the records of Table 2-1 2-31

Figure 2-7. Ratios of GMRotI50 to GMRotI50_BA for the records of Table 2-1 2-32

Figure 2-8. Median and 84th and 16th percentiles of the ratios of GMRotI50 to GMRotI50_BA for the records of Table 2-1.....2-32

Figure 2-9. Ratios of GMRotI50 to GMRotI50_BA at periods of 0, 0.2, 0.5, 1, 2 and 3 seconds as a function of magnitude for the records of Table 2-1 2-33

Figure 2-10. Ratios of GMRotI50 to GMRotI50_BA at periods of 0, 0.2, 0.5, 1, 2 and 3 seconds as a function of distance for the records of Table 2-1 2-34

Figure 2-11. Stage-2 (Inter-event) residuals as a function of magnitude and fault types at periods of 0.2 and 3 seconds for the NGA B-A model (after Boore and Atkinson 2008).....2-35

Figure 2-12. Median and 84th and 16th percentiles of the ratios of GMRotI50 to GMRotI50_BA for all of the records of Table 2-1 except those of the 1999 Chi-Chi earthquake 2-35

Figure 2-13. Ratios of GMRotI50 to GMRotI50_CB for the records of Table 2-1 2-36

Figure 2-14. Median and 84th and 16th percentiles of the ratios of GMRotI50 to GMRotI50_CB for the records of Table 2-1 2-36

Figure 2-15. Ratios of GMRotI50 to GMRotI50_CB at periods of 0, 0.2, 0.5, 1, 2 and 3 seconds as a function of magnitude for the records of Table 2-1 2-37

Figure 2-16. Ratios of GMRotI50 to GMRotI50_CB at periods of 0, 0.2, 0.5, 1, 2 and 3 seconds as a function of distance for the records of Table 2-1 2-38

Figure 2-17. Inter-event residuals as a function of magnitude at periods of 0.2 and 3 seconds for the NGA C-B model (after Campbell and Bozorgnia 2008) 2-39

Figure 2-18. Median and 84th and 16th percentiles of the ratios of GMRotI50 to GMRotI50_CB for all of the records of Table 2-1 except those of the 1999 Chi-Chi earthquake 2-39

Figure 2-19. Ratios of GMRotI50 to GMRotI50_CY for the records of Table 2-1 2-40

Figure 2-20. Median and 84th and 16th percentiles of the ratios of GMRotI50 to GMRotI50_CY for the records of Table 2-1 2-40

Figure 2-21. Ratios of GMRotI50 to GMRotI50_CY at periods of 0, 0.2, 0.5, 1, 2 and 3 seconds as a function of magnitude for the records of Table 2-1 2-41

Figure 2-22. Ratios of GMRotI50 to GMRotI50_CY at periods of 0, 0.2, 0.5, 1, 2 and 3 seconds as a function of distance for the records of Table 2-1 2-42

Figure 2-23. Inter-event residuals as a function of magnitude at periods of 0.01, 0.2, 1 and 3 seconds for the NGA C-Y model (after Chiou and Youngs 2008) 2-43

Figure 2-24. Median and 84th and 16th percentiles of the ratios of GMRotI50 to GMRotI50_CY for all of the records of Table 2-1 except those of the 1999 Chi-Chi earthquake 2-43

Figure 2-25. Ratios of GMRotI50 to GMRotI50_ave for the records of Table 2-1 2-44

Figure 2-26. Median and 84th and 16th percentiles of the ratios of GMRotI50 to GMRotI50_ave for the records of Table 2-1 2-44

Figure 2-27. Ratios of GMRotI50 to GMRotI50_ave at periods of 0, 0.2, 0.5, 1, 2 and 3 seconds as a function of magnitude for the records of Table 2-1 2-45

Figure 2-28. Ratios of GMRotI50 to GMRotI50_ave at periods of 0, 0.2, 0.5, 1, 2 and 3 seconds as a function of distance for the records of Table 2-1 2-46

Figure 2-29. Median and 84th and 16th percentiles of the ratios of GMRotI50 to GMRotI50_ave for all of the records of Table 2-1 except those of the 1999 Chi-Chi earthquake 2-47

Figure 2-30. Ratios of GMRotI50 to GMRotI50_ave at periods of 0, 0.2, 0.5, 1, 2 and 3 seconds as a function of magnitude for all of the records of Table 2-1 except those of the 1999 Chi-Chi earthquake 2-48

Figure 2-31. Ratios of GMRotI50 to GMRotI50_ave at periods of 0, 0.2, 0.5, 1, 2 and 3 seconds as a function of distance for all of the records of Table 2-1 except those of the 1999 Chi-Chi earthquake 2-49

Figure 2-32. Ratios of maximum spectral demand to GMRotI50_BA for the records of Table 2-1 2-50

Figure 2-33. Median and 84th and 16th percentiles of the ratios of maximum spectral demand to GMRotI50_BA for the records of Table 2-1 2-50

Figure 2-34. Ratios of maximum spectral demand to GMRotI50_BA at periods of 0, 0.2, 0.5, 1, 2 and 3 seconds as a function of magnitude for the records of Table 2-1.....2-51

Figure 2-35. Ratios of maximum spectral demand to GMRotI50_BA at periods of 0, 0.2, 0.5, 1, 2 and 3 seconds as a function of distance for the records of Table 2-1 2-52

Figure 2-36. Median and 84th and 16th percentiles of the ratios of maximum spectral demand to GMRotI50_BA for all of the records of Table 2-1 except those of the 1999 Chi-Chi earthquake 2-53

Figure 2-37. Ratios of maximum spectral demand to GMRotI50_CB for the records of Table 2-1 2-54

Figure 2-38. Median and 84th and 16th percentiles of the ratios of maximum spectral demand to GMRotI50_CB for the records of Table 2-1.....2-54

Figure 2-39. Ratios of maximum spectral demand to GMRotI50_CB at periods of 0, 0.2, 0.5, 1, 2 and 3 seconds as a function of magnitude for the records of Table 2-1.....2-55

Figure 2-40. Ratios of maximum spectral demand to GMRotI50_CB at periods of 0, 0.2, 0.5, 1, 2 and 3 seconds as a function of distance for the records of Table 2-1 2-56

Figure 2-41. Median and 84th and 16th percentiles of the ratios of maximum spectral demand to GMRotI50_CB for all of the records of Table 2-1 except those of the 1999 Chi-Chi earthquake 2-57

Figure 2-42. Ratios of maximum spectral demand to GMRotI50_CY for the records of Table 2-1 2-58

Figure 2-43. Median and 84th and 16th percentiles of the ratios of maximum spectral demand to GMRotI50_CY for the records of Table 2-1.....2-58

Figure 2-44. Ratios of maximum spectral demand to GMRotI50_CY at periods of 0, 0.2, 0.5, 1, 2 and 3 seconds as a function of magnitude for the records of Table 2-1.....2-59

Figure 2-45. Ratios of maximum spectral demand to GMRotI50_CY at periods of 0, 0.2, 0.5, 1, 2 and 3 seconds as a function of distance for the records of Table 2-1 2-60

Figure 2-46. Median and 84th and 16th percentiles of the ratios of maximum spectral demand to GMRotI50_CY for all of the records of Table 2-1 except those of the 1999 Chi-Chi earthquake 2-61

Figure 2-47. Ratios of maximum spectral demand to GMRotI50_ave for the records of Table 2-1 2-62

Figure 2-48. Median and 84th and 16th percentiles of the ratios of maximum spectral demand to GMRotI50_ave for the records of Table 2-1.....2-62

Figure 2-49. Ratios of maximum spectral demand to GMRotI50_ave at periods of 0, 0.2, 0.5, 1, 2 and 3 seconds as a function of magnitude for the records of Table 2-1 2-63

Figure 2-50. Ratios of maximum spectral demand to GMRotI50_ave at periods of 0, 0.2, 0.5, 1, 2 and 3 seconds as a function of distance for the records of Table 2-1 2-64

Figure 2-51. Median and 84th and 16th percentiles of the ratios of maximum spectral demand to GMRotI50_ave for all of the records of Table 2-1 except those of the 1999 Chi-Chi earthquake 2-65

Figure 2-52. Ratios of maximum spectral demand to GMRotI50_ave at sample periods as a function of magnitude for all of the records of Table 2-1 except those of the Chi-Chi earthquake 2-66

Figure 2-53. Ratios of maximum spectral demand to GMRotI50_ave at sample periods as a function of distance for all of the records of Table 2-1 except those of the Chi-Chi earthquake 2-67

Figure 2-54. Acceleration orbit of a 2-degree-of-freedom oscillator used to compute the maximum shaking orientation 2-68

Figure 2-55. Sample results for EQ15 of Table 2-1 2-69

Figure 2-56. Cumulative distribution function for $\bar{R}_{S_a,\max}$ for period ranges R1 through R4 of Table 2-7 2-70

Figure 2-57. Correlation coefficient for a sample pair of ground motions as a function of orientation 2-71

Figure 2-58. Cumulative distribution functions for ρ_{Max}, ρ_{FN_FP} and $\rho_{Max_S_a}$ for the records of Table 2-1 2-71

Figure 2-59. Contours of correlation coefficients between the maximum spectral demands at T_1 and T_2 computed using the B-A, C-B, C-Y and averaged NGA models for all of the records of Table 2-1 and the model of Baker and Jayaram (2008) 2-72

Figure 2-60. Correlation coefficients between the maximum spectral demands at T_1 and T_2 computed using the averaged NGA results for all of the records of Table 2-1 and the model of Baker and Jayaram (2008) 2-73

Figure 2-61. Correlation coefficients between the maximum spectral demands at T_1 and a given T_2 computed using the averaged NGA results for all of the records of Table 2-1 and the model of Baker and Jayaram (2008) 2-74

Figure 3-1. Magnitude and distance distribution of the ground motions of Table 3-1 3-26

Figure 3-2. a) Eighty-fourth, 50th and 16th percentiles and b) cumulative distribution functions of normalized time difference between the peak accelerations parallel and perpendicular to the GMRotI50 direction for the records of Table 3-1.....3-27

Figure 3-3. Ratios of maximum spectral demand to GMRotI50 for the records of Table 3-1..... 3-28

Figure 3-4. Maximum, minimum, median and 84th and 16th percentiles of the ratios of maximum spectral demand to GMRotI50 for the records of Table 3-1.....3-28

Figure 3-5. Ratios of maximum spectral demand to GMRotI50 at periods of 0, 0.2, 0.5, 1, 2 and 3 seconds as a function of magnitude for the records of Table 3-1.....3-29

Figure 3-6. Ratios of maximum spectral demand to GMRotI50 at periods of 0, 0.2, 0.5, 1, 2 and 3 seconds as a function of distance for the records of Table 3-1 3-30

Figure 3-7. Ratios of GMRotI50 to GMRotI50_BA for the records of Table 3-1 3-31

Figure 3-8. Median and 84th and 16th percentiles of the ratios of GMRotI50 to GMRotI50_BA for the records of Table 3-1.....3-31

Figure 3-9. Ratios of GMRotI50 to GMRotI50_BA at periods of 0, 0.2, 0.5, 1, 2 and 3 seconds as a function of magnitude for the records of Table 3-1.....3-32

Figure 3-10. Ratios of GMRotI50 to GMRotI50_BA at periods of 0, 0.2, 0.5, 1, 2 and 3 seconds as a function of distance for the records of Table 3-1 3-33

Figure 3-11. Median and 84th and 16th percentiles of the ratios of GMRotI50 to GMRotI50_BA for all of the records of Table 3-1 except those of the 1999 Chi-Chi earthquake 3-34

Figure 3-12. Median ratios of GMRotI50 to GMRotI50_BA computed using (3.1) for all of the records of Table 3-1 and for all of the records except those of the 1999 Chi-Chi earthquake 3-34

Figure 3-13. Ratios of GMRotI50 to GMRotI50_CB for the records of Table 3-1 3-35

Figure 3-14. Median and 84th and 16th percentiles of the ratios of GMRotI50 to GMRotI50_CB for the records of Table 3-1 3-35

Figure 3-15. Ratios of GMRotI50 to GMRotI50_CB at periods of 0, 0.2, 0.5, 1, 2 and 3 seconds as a function of magnitude for the records of Table 3-1 3-36

Figure 3-16. Ratios of GMRotI50 to GMRotI50_CB at periods of 0, 0.2, 0.5, 1, 2 and 3 seconds as a function of distance for the records of Table 3-1 3-37

Figure 3-17. Median and 84th and 16th percentiles of the ratios of GMRotI50 to GMRotI50_CB for all the records of Table 3-1 except those of the 1999 Chi-Chi earthquake 3-38

Figure 3-18. Median ratios of GMRotI50 to GMRotI50_CB computed using (3.1) for all of the records of Table 3-1 and for all of the records except those of the 1999 Chi-Chi earthquake 3-38

Figure 3-19. Ratios of GMRotI50 to GMRotI50_CY for the records of Table 3-1 3-39

Figure 3-20. Median and 84th and 16th percentiles of the ratios of GMRotI50 to GMRotI50_CY for the records of Table 3-1 3-39

Figure 3-21. Ratios of GMRotI50 to GMRotI50_CY at periods of 0, 0.2, 0.5, 1, 2 and 3 seconds as a function of magnitude for the records of Table 3-1 3-40

Figure 3-22. Ratios of GMRotI50 to GMRotI50_CY at periods of 0, 0.2, 0.5, 1, 2 and 3 seconds as a function of distance for the records of Table 3-1 3-41

Figure 3-23. Median and 84th and 16th percentiles of the ratios of GMRotI50 to GMRotI50_CY for all of the records of Table 3-1 except those of the 1999 Chi-Chi earthquake 3-42

Figure 3-24. Median ratios of GMRotI50 to GMRotI50_CY computed using (3.1) for all of the records of Table 3-1 and for all of the records except those of the 1999 Chi-Chi earthquake 3-42

Figure 3-25. Ratios of GMRotI50 to GMRotI50_ave for the records of Table 3-1 3-43

Figure 3-26. Median and 84th and 16th percentiles of the ratios of GMRotI50 to GMRotI50_ave for the records of Table 3-1 3-43

Figure 3-27. Ratios of GMRotI50 to GMRotI50_ave at periods of 0, 0.2, 0.5, 1, 2 and 3 seconds as a function of magnitude for the records of Table 3-1 3-44

Figure 3-28. Ratios of GMRotI50 to GMRotI50_ave at periods of 0, 0.2, 0.5, 1, 2 and 3 seconds as a function of distance for the records of Table 3-1 3-45

Figure 3-29. Median and 84th and 16th percentiles of the ratios of GMRotI50 to GMRotI50_ave for all of the records of Table 3-1 except those of the 1999 Chi-Chi earthquake 3-46

Figure 3-30. Median ratios of GMRotI50 to GMRotI50_ave computed using (3.1) for all of the records of Table 3-1 and for all of the records except those of the 1999 Chi-Chi earthquake 3-46

Figure 3-31. Ratios of GMRotI50 to GMRotI50_ave at periods of 0, 0.2, 0.5, 1, 2 and 3 seconds as a function of magnitude for all of the records of Table 3-1 except those of the 1999 Chi-Chi earthquake 3-47

Figure 3-32. Ratios of GMRotI50 to GMRotI50_ave at periods of 0, 0.2, 0.5, 1, 2 and 3 seconds as a function of distance for all of the records of Table 3-1 except those of the 1999 Chi-Chi earthquake 3-48

Figure 3-33. Ratios of maximum spectral demand to GMRotI50_BA for the records of Table 3-1 3-49

Figure 3-34. Median and 84th and 16th percentiles of the ratios of maximum spectral demand to GMRotI50_BA for the records of Table 3-1 3-49

Figure 3-35. Ratios of maximum spectral demand to GMRotI50_BA at periods of 0, 0.2, 0.5, 1, 2 and 3 seconds as a function of magnitude for the records of Table 3-1 3-50

Figure 3-36. Ratios of maximum spectral demand to GMRotI50_BA at periods of 0, 0.2, 0.5, 1, 2 and 3 seconds as a function of distance for the records of Table 3-1 3-51

Figure 3-37. Median and 84th and 16th percentiles of the ratios of maximum spectral demand to GMRotI50_BA for all of the records of Table 3-1 except those of the 1999 Chi-Chi earthquake 3-52

Figure 3-38. Median ratios of maximum spectral demand to GMRotI50_BA computed using (3.1) for all of the records of Table 3-1 and for all of the records except those of the 1999 Chi-Chi earthquake 3-52

Figure 3-39. Ratios of maximum spectral demand to GMRotI50_CB for the records of Table 3-1 3-53

Figure 3-40. Median and 84th and 16th percentiles of the ratios of maximum spectral demand to GMRotI50_CB for the records of Table 3-1.....3-53

Figure 3-41. Ratios of maximum spectral demand to GMRotI50_CB at periods of 0, 0.2, 0.5, 1, 2 and 3 seconds as a function of magnitude for the records of Table 3-1.....3-54

Figure 3-42. Ratios of maximum spectral demand to GMRotI50_CB at periods of 0, 0.2, 0.5, 1, 2 and 3 seconds as a function of distance for the records of Table 3-1 3-55

Figure 3-43. Median and 84th and 16th percentiles of the ratios of maximum spectral demand to GMRotI50_CB for all of the records of Table 3-1 except those of the 1999 Chi-Chi earthquake 3-56

Figure 3-44. Median ratios of maximum spectral demand to GMRotI50_CB computed using (3.1) for all the records of Table 3-1 and for all of the records except those of the 1999 Chi-Chi earthquake 3-56

Figure 3-45. Ratios of maximum spectral demand to GMRotI50_CY for the records of Table 3-1 3-57

Figure 3-46. Median and 84th and 16th percentiles of the ratios of maximum spectral demand to GMRotI50_CY for the records of Table 3-1 3-57

Figure 3-47. Ratios of maximum spectral demand to GMRotI50_CY at periods of 0, 0.2, 0.5, 1, 2 and 3 seconds as a function of magnitude for the records of Table 3-1 3-58

Figure 3-48. Ratios of maximum spectral demand to GMRotI50_CY at periods of 0, 0.2, 0.5, 1, 2 and 3 seconds as a function of distance for the records of Table 3-1 3-59

Figure 3-49. Median and 84th and 16th percentiles of the ratios of maximum spectral demand to GMRotI50_CY for all of the records of Table 3-1 except those of the 1999 Chi-Chi earthquake 3-60

Figure 3-50. Median ratios of maximum spectral demand to GMRotI50_CY computed using (3.1) for all the records of Table 3-1 and for all of the records except those of the 1999 Chi-Chi earthquake 3-60

Figure 3-51. Ratios of maximum spectral demand to GMRotI50_ave for the records of Table 3-1 3-61

Figure 3-52. Median and 84th and 16th percentiles of the ratios of maximum spectral demand to GMRotI50_ave for the records of Table 3-1 3-61

Figure 3-53. Ratios of maximum spectral demand to GMRotI50_ave at periods of 0, 0.2, 0.5, 1, 2 and 3 seconds as a function of magnitude for the records of Table 3-1 3-62

Figure 3-54. Ratios of maximum spectral demand to GMRotI50_ave at periods of 0, 0.2, 0.5, 1, 2 and 3 seconds as a function of distance for the records of Table 3-1 3-63

Figure 3-55. Median and 84th and 16th percentiles of the ratios of maximum spectral demand to GMRotI50_ave for all of the records of Table 3-1 except those of the 1999 Chi-Chi earthquake 3-64

Figure 3-56. Median ratios of maximum spectral demand to GMRotI50_ave computed using (3.1) for all of the records of Table 3-1 and for all of the records except those of the 1999 Chi-Chi earthquake 3-64

Figure 3-57. Ratios of maximum spectral demand to GMRotI50_ave at sample periods as a function of magnitude for all of the records of Table 3-1 except those of the Chi-Chi earthquake 3-65

Figure 3-58. Ratios of maximum spectral demand to GMRotI50_ave at sample periods as a function of distance for all of the records of Table 3-1 except those of the Chi-Chi earthquake 3-66

Figure 3-59. Sample results for EQ77 of Table 3-1 3-67

Figure 3-60. Sample results for EQ162 of Table 3-1 3-68

Figure 3-61. Cumulative distribution function for $\bar{R}_{S_a,\max}$ for period ranges R1 through R4 of Table 3-11 3-69

Figure 3-62. Distributions of $\theta_{\max}$ as a function of r for period ranges R1 through R4 of Table 3-11 3-70

Figure 3-63. Cumulative distribution functions for ρ_{Max}, ρ_{FN_FP} and $\rho_{Max_S_a}$ for the records of Table 3-1 3-71

Figure 3-64. Contours of correlation coefficients between the maximum spectral demands at T_1 and T_2 computed using the B-A, C-B, C-Y and averaged NGA models for the records of Table 3-1 and the model of Baker and Jayaram (2008) 3-72

Figure 3-65. Correlation coefficients between the maximum spectral demands at T_1 and T_2 computed using the averaged NGA results for the records of Table 3-1 and the model of Baker and Jayaram (2008) 3-73

Figure 3-66. Correlation coefficients between the maximum spectral demands at T_1 and a given T_2 computed using the averaged NGA results for the records of Table 3-1 and the model of Baker and Jayaram (2008) 3-74

Figure 4-1. Magnitude and distance distribution of the ground motions of Table 4-2 4-17

Figure 4-2. Distributions of peak ground acceleration as a function of a) moment magnitude and b) epicentral distance for the ground motions of Table 4-2 4-18

Figure 4-3. a) Eighty-fourth, 50th and 16th percentiles and b) cumulative distribution functions of normalized time difference between the peak accelerations parallel and perpendicular to the GMRotI50 direction for the records of Table 4-2.....4-19

Figure 4-4. Eighty-fourth, 50th and 16th percentiles of spectral acceleration for the records of Table 4-2.....4-20

Figure 4-5. Ratios of maximum spectral demand to GMRotI50 for the records of Table 4-2.....4-21

Figure 4-6. Maximum, minimum, median and 84th and 16th percentiles of the ratios of maximum spectral demand to GMRotI50 for the records of Table 4-2.....4-21

Figure 4-7. Ratios of maximum spectral demand to GMRotI50 at periods of 0, 0.2, 0.5, 1, 2 and 3 seconds as a function of magnitude for the records of Table 4-2.....4-22

Figure 4-8. Ratios of maximum spectral demand to GMRotI50 at periods of 0, 0.2, 0.5, 1, 2 and 3 seconds as a function of distance for the records of Table 4-2.....4-23

Figure 4-9. Sample results for EQ8 of Table 4-2.....4-24

Figure 4-10. Cumulative distribution function for $\bar{R}_{S_a,\max}$ for period ranges R1 through R4 of Table 4-4.....4-25

Figure 4-11. Cumulative distribution functions for ρ_{Max}, ρ_{FN_FP} and $\rho_{Max_S_a}$ for the records of Table 4-2.....4-25

Figure 4-12. Ratios of maximum spectral demand to θ_{CEUS} at sample periods as a function of magnitude for all of the records of Table 4-2.....4-26

Figure 4-13. Ratios of maximum spectral demand to θ_{CEUS} at sample periods as a function of distance for all of the records of Table 4-2.....4-27

Figure 4-14. Contours of correlation coefficients between the maximum spectral demands at T_1 and T_2 for the records of Table 4-2 and the model of (4.3) through (4.7).....4-28

Figure 4-15. Correlation coefficients between the maximum spectral demands at T_1 and T_2 for the records of Table 4-2 and the model of (4.3) through (4.7).....4-29

Figure 4-16. Correlation coefficients between the maximum spectral demands at T_1 and a given T_2 for the records of Table 4-2 and the model of (4.3) through (4.7).....4-30

Tables

Table 2-1. Far-field earthquake ground motion records for the WUS study 2-17

Table 2-2. Median and 84th percentile of the ratio of maximum spectral demand to GMRotI50 for all of the records of Table 2-1 2-23

Table 2-3. Median and 84th percentile of the ratio of GMRotI50 to GMRotI50_BA, GMRotI50_CB, GMRotI50_BA and GMRotI50_ave for all of the records of Table 2-1 2-24

Table 2-4. Median and 84th percentile of the ratio of GMRotI50 to GMRotI50_BA, GMRotI50_CB, GMRotI50_BA and GMRotI50_ave for all of the records of Table 2-1 except those of the 1999 Chi-Chi earthquake 2-24

Table 2-5. Median and 84th percentile of the ratio of maximum spectral demand to GMRotI50_BA, GMRotI50_CB, GMRotI50_BA and GMRotI50_ave for all of the records of Table 2-1 2-25

Table 2-6. Median and 84th percentile of the ratio of maximum spectral demand to GMRotI50_BA, GMRotI50_CB, GMRotI50_BA and GMRotI50_ave for all of the records of Table 2-1 except those of the 1999 Chi-Chi earthquake 2-25

Table 2-7. Medians, means and standard deviations of $\overline{R}_{S_a,\max}$ and T_L and T_U for R1 through R4 2-26

Table 2-8. Statistics of the correlation coefficients of Figure 2-58 2-26

Table 3-1. Near-fault earthquake ground motion records for the WUS study.....3-14

Table 3-2. Median and 84th percentile of the ratio of maximum spectral demand to GMRotI50 for all the records of Table 3-1 3-19

Table 3-3. Median and 84th percentile of the ratio of GMRotI50 to GMRotI50_BA, GMRotI50_CB, GMRotI50_BA and GMRotI50_ave for all of the records of Table 3-1 3-20

Table 3-4. Median and 84th percentile of the ratio of GMRotI50 to GMRotI50_BA, GMRotI50_CB, GMRotI50_BA and GMRotI50_ave for all of the records of Table 3-1 except those of the 1999 Chi-Chi earthquake 3-20

Table 3-5. Median and 84th percentile of the ratio of GMRotI50 to GMRotI50_BA, GMRotI50_CB, GMRotI50_BA and GMRotI50_ave computed using (3.1) through (3.3) for all of the records of Table 3-1 3-21

Table 3-6. Median and 84th percentile of the ratio of GMRotI50 to GMRotI50_BA, GMRotI50_CB, GMRotI50_BA and GMRotI50_ave computed using (3.1) through (3.3) for all of the records of Table 3-1 except those of the 1999 Chi-Chi earthquake 3-21

Table 3-7. Median and 84th percentile of the ratio of maximum spectral demand to GMRotI50_BA, GMRotI50_CB, GMRotI50_BA and GMRotI50_ave for all of the records of Table 3-1 3-22

Table 3-8. Median and 84th percentile of the ratio of maximum spectral demand to GMRotI50_BA, GMRotI50_CB, GMRotI50_BA and GMRotI50_ave for all of the records of Table 3-1 except those of the 1999 Chi-Chi earthquake 3-22

Table 3-9. Median and 84th percentile of the ratio of maximum spectral demand to GMRotI50_BA, GMRotI50_CB, GMRotI50_BA and GMRotI50_ave computed using (3.1) through (3.3) for all of the records of Table 3-1.....3-23

Table 3-10. Median and 84th percentile of the ratio of maximum spectral demand to GMRotI50_BA, GMRotI50_CB, GMRotI50_BA and GMRotI50_ave computed using (3.1) through (3.3) for all of the records of Table 3-1 except those of the 1999 Chi-Chi earthquake.....3-23

Table 3-11. Medians, means and standard deviations of $\bar{R}_{S_a,\max}$ and T_L and T_U for R1 through R4 3-24

Table 3-12. Numbers of ground-motion pairs as a function of period, distance and $\theta_{\max}$ 3-24

Table 3-13. Statistics of the correlation coefficients of Figure 3-63 3-25

Table 4-1. List of earthquakes for the CEUS study 4-10

Table 4-2. Earthquake ground motion records for the CEUS study 4-11

Table 4-3. Median and 84th percentile of the ratio of maximum spectral demand to GMRotI50 for the ground motions of Table 4-2 4-14

Table 4-4. Medians, means and standard deviations of $\bar{R}_{S_a,\max}$ and T_L and T_U for R1 through R4 for the ground motions of Table 4-2.....4-15

Table 4-5. Statistics of the correlation coefficients of Figure 4-11 4-15

Table 4-6. Coefficients for the attenuation relationship of (4.1) 4-16

SECTION 1
INTRODUCTION

1.1 Motivation and objectives

The values of the seismic design parameters reported in the 2010 *Minimum Design Loads for Buildings and Other Structures*, ASCE/SEI 7-10 (ASCE 2010, termed the "2010 ASCE-7 Standard" hereafter), the 2009 *NEHRP Recommended Seismic Provisions for New Buildings and Other Structures*, FEMA P-750 (FEMA 2009, termed the "2009 NEHRP Provisions" hereafter), and the not yet published 2012 *International Building Code* will be identical. Both the probabilistic and deterministic values of the design parameters are defined in terms of maximum spectral demand rather than geometric-mean[1] (termed geomean hereafter) demand.

Structural engineers in the United States have not necessarily understood the important difference between maximum and geomean spectral demands. Work by the authors of this report (Huang et al. 2008), in part for the Building Seismic Safety Council Project 07, has led to an improved understanding of the relationship between maximum and geomean spectral demands in the near-fault region. The knowledge gained from these studies provides the technical basis for the calculation of maximum spectral demand in the aforementioned three design-oriented documents.

In this report, the work of Huang et al. (2008) is extended to the far-field region in the Western United States (WUS) and to the Central and Eastern United States (CEUS). Additional studies are performed for WUS near-fault motions. The major goal of the study is to enable calculation of maximum spectral demand for all regions of the United States. For this purpose, we focus on three tasks: 1) establishing the relationships between maximum and geometric-mean spectral demands, 2) identifying the orientation of maximum spectral demand, and 3) computing the correlation of maximum spectral demands at different periods. The product of the first task when used with reliable estimates of geomean spectral demand can be used to determine the magnitude

[1] The geometric-mean (geomean) demand is computed as the square root of the product of two spectral demands at a given period in two orthogonal horizontal directions.

of maximum spectral demand. The second task addresses the concern that it might be overly conservative to use maximum spectral demand for force-based (*R*-factor) design wherein design lateral forces are computed independently along each axis of a building. The product of the third task enables the correlation of spectral demand at different periods to be included in the shape of a maximum spectrum.

Section 1.2 below provides background information on geomean and maximum spectral demand. The organization of the report is presented in Section 1.3.

1.2 Geometric-mean and maximum spectral demands

1.2.1 Geometric-mean spectral demand

Ground-motion attenuation relationships typically predict the median and logarithmic standard deviation of spectral acceleration of a single degree-of-freedom (SDOF) oscillator given an earthquake magnitude, a site-to-source distance and the local site conditions. For horizontal shaking, the relationships generally output a median estimate of the geomean spectral demand for two orthogonal horizontal components of ground motion. Geomean horizontal spectral demand is then used either directly or indirectly (through probabilistic seismic hazard analysis) as input to numerical models to calculate forces and deformations in buildings, bridges and infrastructure.

Geomean spectral demand, which is predicted by most attenuation relationships, has two advantages: 1) it is easy to compute; and 2) the aleatory uncertainty in attenuation relationships using this measure is smaller than that calculated with other representations of demand, for example, spectral demand of the strike-normal component, the strike-parallel component, or either of the as-recorded horizontal components (Beyer and Bommer 2006). Although widely used, the geomean spectral demand has no physical significance since the peak structural response in the two horizontal directions seldom occurs at the same time (see the discussion in Sections 2.3, 3.2 and 4.2). Also, the value of the geomean demand depends on the orientation of the sensors recording the pair of motions. To address this issue, Boore et al. (2006) defined a *rotated* geomean, GMRotI50, where “GM” stands for geometric mean; “Rot” indicates that the geomean spectral demands at all non-redundant rotation angles are considered; “I” identifies that the rotation angle is independent of period; and “50” represents the percentile value used for the

measure. The procedures for the computation of GMRotI50 of a pair of perpendicular horizontal ground motions are summarized below from Boore et al. (2006):

1. Rotate the pair of as-recorded ground motions θ_j degree and compute the geomean spectral demand of the rotated pair. The spectral demand at a given period T_i is termed $\mathrm{GM}(\theta_j, T_i)$. The rotation angle θ_j is increased from 0 to 89 degrees in increments of 1 degree. The median of the 90 geomean spectral demands for T_i is termed $\mathrm{GMRotD50}(T_i)$, where "D" indicates that the rotation angle of the demand is period-dependent.

2. Compute the penalty function defined below:

$$\mathrm{penalty}(\theta_j) = \frac{1}{N_{per}} \sum_{i=l}^{h} [\mathrm{GM}(\theta_j, T_i) / \mathrm{GMRotD50}(T_i) - 1]^2 \tag{1.1}$$

   where the lower and upper bounds of period, termed T_l and T_h, respectively, depend on the procedure used to remove noise from the records; and N_{per} is the number of periods included in the computation. The value of $\mathrm{penalty}(\theta_j)$ is an index for the difference between the geomean spectral demand for θ_j and GMRotD50 over the period range of T_l and T_h.

3. The rotation angle corresponding to the minimum of the penalty function is termed $\theta_{\min}$ and the geomean spectral demand for $\theta_{\min}$ is defined as GMRotI50; that is,

$$\mathrm{GMRotI50}(T_i) = \mathrm{GM}(\theta_{\min}, T_i) \tag{1.2}$$

GMRotI50 is the geomean spectral demand of a pair of ground motions rotated by an angle of $\theta_{\min}$ from their recorded orientation to minimize the difference between the geomean spectral demand of the pair and its GMRotD50 over the period range of T_l and T_h. Boore et al. (2006) showed that the average effect on geomean spectral demand of rotating the pair of ground motions from the recorded orientation was less than 3%. The measure "GMRotI50" has been adopted in the "Next Generation Attenuation (NGA) Relationships" project coordinated by the Lifelines Program of the Pacific Earthquake Engineering Research (PEER) Center. All five sets

of attenuation relationships developed in the NGA project estimate the distribution of GMRotI50 for shallow crustal earthquakes in the WUS.

1.2.2 Maximum spectral demand

Figure 1-1 illustrates the computation of maximum spectral demand of a sample pair of ground motions. A 5%-damped linear oscillator with a period of 1-second in both horizontal directions is subjected to the *X* and *Y* components of the sample pair; the acceleration orbit of the oscillator with respect to the *X* and *Y* directions is shown in the figure. The maximum acceleration and its orientation (α) with respect to the *Y* direction are identified by the point on the orbit farthest from the origin (solid circle in the upper-left quadrant in the figure). The process was repeated at all periods considered in the studies of this report to construct the maximum spectrum for the ground-motion pair. For a given ground-motion pair, α varies as a function of period.

Maximum spectral demand and several similar measures of spectral demand have been studied previously. Howard et al. (2005) characterized directivity effects using a spectral intensity index that integrates spectral acceleration over a period range from 0.5 to 3 seconds. A polarity azimuth range is identified for a pair of ground motions using the velocity orbit of the pair. The time-series is then rotated within this azimuth range until one component produces the greatest spectral intensity. The orientation and spectral demand for this component, termed the SA_{MAX} component, were compared with those for the strike-normal (SN) component using 29 pairs of near-fault ground motions. They concluded that 1) the SN spectral demand estimated by Somerville et al. (1997) and modified by Abrahamson (2000) adequately predicted the average spectral demand for the SA_{MAX} component for sites within 5 km of a strike-skip fault, and 2) the average spectral demand for the SA_{MAX} component exceeded the predictions of Somerville et al. (1997) and Abrahamson (2000) for the SN component by a factor between 1.7 and 2 for reverse faults.

Beyer and Bommer (2006) investigated the ratio of the maximum to recorded geomean spectral demands using 949 earthquake records with moment magnitude ranging between 4.2 and 7.9 and hypocentral distance ranging between 5 and 200 km. They reported that the median of the ratio varied between 1.2 and 1.3, depending on the period. Campbell and Bozorgnia (2007) computed the ratio of the greater spectral demand for a pair of recorded ground motions to GMRotI50 for

the pair using 1561 records with magnitudes and distances similar to those of Beyer and Bommer (2006). The median of the ratio varied between 1.11 and 1.2.

Huang et al. (2008) studied the differences between strike-normal, strike-parallel, geomean and maximum spectral demands in the near-fault region using 147 pairs of records with moment magnitude greater than 6.5 and closest site-to-fault distance less than 15 km selected from the NGA strong motion database. In their study, the geomean spectral demand, termed MMgm, was computed using the horizontal components of ground motions parallel and perpendicular to the orientation of maximum spectral demand. They reported that the median of the ratio of maximum spectral demand to MMgm ranges from 1.2 to 1.45. The ratio of maximum spectral demand to the median GMRotI50 generated using three of the NGA relationships was also computed for the 147 pairs of ground motions. Scale factors were developed to transform NGA-predicted GMRotI50 to maximum demand in the near-fault region for average directivity, the forward directivity and worst-case directivity.

In this study, the work of Huang et al. (2008) is extended to far-field WUS and all CEUS ground motions and relationships between maximum spectral demand and GMRotI50 are developed.

1.2.3 Orientation of maximum spectral demand

For a pair of horizontal ground motions, the orientation of maximum spectral demand (α of Figure 1-1) is a function of period. The use of a maximum demand spectrum for force-based design against building collapse might be overly conservative for a structure with significant higher-mode effects and/or large ductility if the orientation of the maximum spectral demand either varies widely as a function of period or is random.

The orientation of maximum spectral demand has been studied. Howard et al. (2005) investigated 15 pairs of strike-slip and 14 pairs of reverse faulting records with a closest distance from the site to the fault rupture plane of less than 10 km. They defined a spectral intensity index that integrates spectral acceleration over a range of period from 0.5 to 3 seconds and observed that the orientation associated with the greatest value of the index agrees reasonably well with the SN direction for ground motions recorded within 5 km of strike-slip faults and can depart

significantly from the SN direction for reverse faults. Watson-Lamprey and Boore (2007) studied the relationship between the geomean spectral demand and spectral demands for maximum, SN and randomly chosen components of a pair of ground motions at discrete periods. They reported that for distance greater than about 3 km, the SN component seldom corresponds to the maximum spectral demand, and for distances smaller than 3 km, the orientation of maximum spectral demand is essentially SN at long periods but somewhat random at short periods. The variation in the orientation of maximum spectral demand over a wide range of period for a pair of ground motions was not investigated in either study. Hong and Goda (2007) proposed a model to predict the ratio of the spectral acceleration for a pair of ground motions at a given orientation and period to the maximum spectral demand at the period. The orientation of the maximum spectral demand with respect to the strike of the fault was not discussed.

1.2.4 Correlation of ground motions

Two types of correlation of ground motions are discussed in this report. One is the correlation between two orthogonal horizontal acceleration *time series* for a pair of ground motions and the other is the correlation of *maximum spectral demand* at different periods.

Current seismic design codes for buildings do not include a requirement on the correlation of the two orthogonal horizontal ground-motion time series used for response-history analysis. However, design standards for safety-related nuclear facilities such as ASCE Standard 4-98 (ASCE 2000) and ASCE Standard 43-05 (ASCE 2005) require the correlation coefficient for two orthogonal components of ground motion for response-history analysis to be less than 0.3. The technical basis of this requirement was developed by Hadjian (1981) using 50 pairs of recorded ground motions that were available at that time (see Section 2.6.1.2 for more information). Since then a significant number of ground-motion records have been acquired. The limiting value of 0.3 presented in ASCE Standards 4-98 and 43-05 is re-evaluated in this study using records from large ground-motion databases compiled recently for the WUS and the CEUS.

In the past five years, research has addressed the correlation of spectral demand at different periods as well as its impact on the performance of structures. Baker and Cornell (2006b) and Baker et al. (2009) performed a series of nonlinear response-history analyses to study the impact

of ground motion selection and modification methods on the story drift response of buildings. Similar conclusions were drawn in both studies: analyses using ground motions matched to a uniform hazard spectrum (UHS) where the correlation of spectral demand is not considered consistently overestimate peak story drift response; those analyses using carefully chosen ground motions scaled to a target spectrum that preserves the correlation of spectral demand lead to unbiased estimates of response.

The correlation of geomean spectral demand in the WUS was studied and reported by Cornell, Baker and their students (e.g., Baker and Cornell 2006a, Baker and Jayaram 2008). In this report, we compute the correlation coefficients of maximum spectral demands at different periods and compare our results with those of Baker and Jayaram (2008) for geomean spectral demand. The utility of using the model of Baker and Jayaram (2008) for maximum spectral demand is discussed.

1.3 Organization of the report

This report includes five sections and a list of references (Section 6). Sections 2, 3 and 4 present results of analysis for far-field WUS, near-fault WUS and CEUS ground motions, respectively. Each of Sections 2, 3 and 4 includes results for 1) the distribution of the ratio of maximum spectral demand to GMRotI50, 2) the orientation of maximum spectral demand, 3) the correlation between two orthogonal horizontal acceleration time series, and 4) the correlation of maximum spectral demands at different periods. Sections 2 and 3 also present the relationships 1) between measured and NGA-predicted GMRotI50, and 2) between maximum spectral demand and NGA-predicted GMRotI50. Section 5 summarizes the results of Sections 2, 3 and 4.

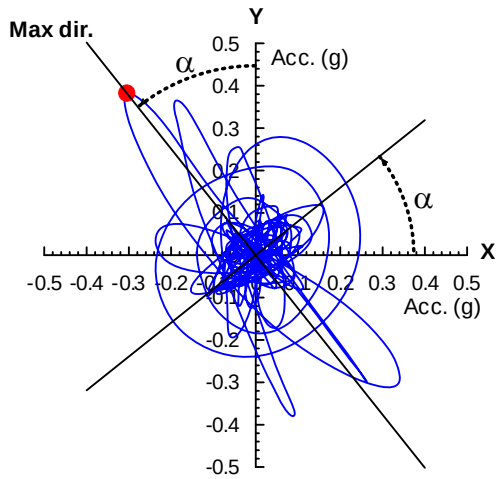

Figure 1-1. Definition of maximum spectral demand

SECTION 2
WUS FAR-FIELD GROUND MOTIONS

2.1 Datasets

The Lifelines Program of the Pacific Earthquake Engineering Research Center (PEER) coordinated a research program, known as the "Next Generation Attenuation (NGA) Relationships" project, to develop new ground-motion prediction models for shallow crustal earthquakes. The NGA project developed a global strong-motion database (http://peer.berkeley.edu/nga/), which includes more than 3500 sets of recordings from 173 earthquakes.

The dataset used in this section is a subset of the PEER NGA ground motion database. Since the focus of this section is far-field shaking with significant potential to cause building damage, all pairs of ground motions from earthquakes with moment magnitude (M_W) of 6.5 and greater, and closest site-to-fault-rupture distance (r) between 30 and 50 km, were extracted from the PEER database for the analysis of this section. Table 2-1 lists the 165 ground-motion pairs in the dataset for this section. Each pair of time series was rotated to the strike-normal (SN) and strike-parallel (SP) directions by the PEER researchers. Of the 165 pairs of motions, the numbers of records associated with strike-slip, normal, reverse and reverse-oblique faulting are 20, 2, 60 and 83, respectively. The dataset is governed by the 1989 Loma Prieta earthquake (21 pairs, reverse-oblique faulting), 1994 Northridge earthquake (51 pairs, reverse faulting) and 1999 Chi-Chi earthquake in Taiwan (62 pairs, reverse-oblique faulting).

Figure 2-1 characterizes the ground motions in the dataset of Table 2-1 with respect to moment magnitude and site-to-source distance. The data at magnitudes of 6.69, 6.93 and 7.62 are those for the Northridge, Loma Prieta and Chi-Chi earthquakes, respectively.

2.2 NGA relationships

The focus of the NGA project was the development of new ground-motion prediction models for shallow crustal earthquakes with moment magnitude between 5 and 8.5 and site-to-source distance between 0 and 200 km (Power et al. 2008). Five attenuation relationships were prepared:

1) Abrahamson and Silva (2008), 2) Boore and Atkinson (2008), 3) Campbell and Bozorgnia (2008), 4) Chiou and Youngs (2008), and 5) Idriss (2008). The United States Geological Survey (USGS) used three of the NGA relationships, namely, Boore and Atkinson (B-A), Campbell and Bozorgnia (C-B), and Chiou and Youngs (C-Y), to generate the 2008 seismic hazard maps for crustal faults in the Western United States (WUS). The 2008 USGS seismic hazard maps provide the basis for the seismic design parameters of the 2009 NEHRP Provisions (FEMA 2009), 2010 ASCE-7 Standard (ASCE 2010) and 2012 International Building Code.

The output of all NGA relationships is the distribution of spectral demand in the direction of GMRotI50: a rotated geomean spectral demand independent of sensor orientation (see Section 1.2.1). In this report, the rotated geomean demand predicted by the NGA relationships is termed NGA-predicted GMRotI50 and the rotated geomean computed per Boore et al. (2006) using a pair of earthquake records is termed GMRotI50. The relationships between 1) maximum spectral demand and GMRotI50, 2) GMRotI50 and NGA-predicted GMRotI50, and 3) maximum spectral demand and NGA-predicted GMRotI50 are studied and presented in Sections 2.4.1, 2.4.2 and 2.4.3, respectively. For NGA-predicted GMRotI50, we focus on the three NGA relationships used to generate the 2008 USGS seismic hazard maps. The terms “GMRotI50_BA”, “GMRotI50_CB” and “GMRotI50_CY” represent the median spectral demand computed using the B-A, C-B and C-Y NGA relationships, respectively, given an earthquake scenario. The notation “GMRotI50_ave” is the average of “GMRotI50_BA”, “GMRotI50_CB” and “GMRotI50_CY” given an earthquake scenario.

2.3 Geomean spectral demand representation

This section presents a study that investigates the time difference between the peak spectral acceleration response at a given period in two perpendicular directions for each pair of ground motions of Table 2-1. The study was performed using a series of 5%-damped elastic single degree-of-freedom oscillators with periods between 0 and 4 seconds. Each pair of records of Table 2-1 was rotated to be parallel and perpendicular to the orientation of GMRotI50 and used for the response-history analysis. For a given pair of ground motions, the time difference between the two spectral accelerations at a given period was computed and normalized by the period.

Panel a of Figure 2-2 presents the 84th, 50th and 16th percentiles of the normalized time differences for the 165 pairs of records of Table 2-1. The percentiles presented in this report were computed by counting unless noted otherwise. The median normalized time differences are greater than 1 at all periods considered in the study and exceed 5 in the short period range. Panel b of Figure 2-2 presents the cumulative distribution functions of the normalized time differences at periods of 0.2, 0.5, 1 and 2 seconds. Each distribution of Figure 2-2b was developed by sorting the 165 realizations from smallest to largest and assigning a probability from 1/165 to 1.00 in increments of 1/165 for each of the results. Over 70% (50%) of the records have the normalized time differences at periods of 0.2 and 0.5 second (1 and 2 seconds) greater than 2; the percentages increase to 80% (70%) for the normalized time differences greater than 1.

2.4 Maximum and geomean spectral demands

2.4.1 Relationships between maximum spectral demand and GMRotI50

Figure 2-3 presents the residual between maximum spectral demand and GMRotI50, defined as the natural logarithm of the ratio of maximum spectral demand to GMRotI50, as a function of period, for the records of Table 2-1. Figure 2-4 presents the maximum, minimum, median and 84th and 16th percentiles of the ratios of maximum spectral demand to GMRotI50 for the records of Table 2-1 through counting exercise. The median and 84th percentile of the ratios of Figure 2-4 at periods of 0, 0.2, 0.5, 1, 2, 3 and 4 seconds are presented in Table 2-2. The median ratios range between 1.2 and 1.3 and the 84th percentile ratios range between 1.3 and 1.5 across most of the period range of Figure 2-4. The median and 84th percentile results increase slightly with period.

To study the dependence of the residual between maximum spectral demand and GMRotI50 on M_W and r, the residuals of Figure 2-3 at periods of 0, 0.2, 0.5, 1, 2 and 3 seconds were re-plotted in the six panels of Figure 2-5 (Figure 2-6), respectively, as a function of M_W (r). The blue line in each panel presents a linear regression fit to the data. The residuals at a period of 0 second show clear dependence on M_W. The dependence on M_W at the other periods, and on r at all periods of Figure 2-6, is moderate.

2.4.2 Relationships between GMRotI50 and NGA-predicted GMRotI50

2.4.2.1 GMRotI50_BA

The results for the ratios of GMRotI50 to each of GMRotI50_BA, GMRotI50_CB, GMRotI50_CY and GMRotI50_ave are presented in Sections 2.4.2.1 through 2.4.2.4, respectively.

Figure 2-7 presents the residuals between GMRotI50 and GMRotI50_BA as a function of period for the records of Table 2-1. Figure 2-8 presents the median and 84th and 16th percentiles of the ratios of GMRotI50 to GMRotI50_BA for the records of Table 2-1. The median ratios of Figure 2-8 range between 0.7 and 0.9. The median ratio is much smaller than 1 at periods close to 0 second. The residuals of Figure 2-7 at periods of 0, 0.2, 0.5, 1, 2 and 3 seconds are re-plotted in the six panels of Figure 2-9 (Figure 2-10), respectively, as a function of M_W (r). The dependence of the residuals on M_W at periods 0 and 0.2 second is evident and decreases as the period increases. The dependence on r is insignificant at all periods of Figure 2-10.

The regression results of Figure 2-9 are governed by the data at magnitudes of 6.69, 6.93 and 7.62. The B-A attenuation relationship overestimates the spectral demand of the magnitude 7.62 event (the 1999 Chi-Chi earthquake) at periods of 0 and 0.2 second (see panels a and b of Figure 2-9) resulting in the small median ratio of GMRotI50 to GMRotI50_BA of Figure 2-8 at those periods.

Figure 2-11 is a figure extracted from Boore and Atkinson (2008) to support the results of Figure 2-8 and Figure 2-9. Figure 2-11 presents the Stage-2 (inter-event) residuals as a function of magnitude and fault types for the B-A attenuation relationship. The Stage-2 residual is the residual between the inter-event term for a given earthquake event and the prediction of the model for magnitude dependence in the B-A attenuation relationship[1].

---

[1] The development of a ground-motion attenuation relationship often involves two stages. In Stage 1, the event term for a specific earthquake event at a given period is subtracted (normalized) from the spectral ordinates of the records for the event at the given period and the normalized data from all events

The left panel of Figure 2-11 presents the data for a period of 0.2 second. The solid red square at a magnitude of 7.6 is for the 1999 Chi-Chi earthquake; the residual is about 0.55 and much smaller than 1. As a point of reference, the median of the ratios of GMRotI50 to GMRotI50_BA at a magnitude of 7.62 in Figure 2-9b is 0.6. We conclude that the bias in the median ratio of GMRotI50 to GMRotI50_BA in the short period range, as presented in Figure 2-8, is due mainly to the residual between the event term for the Chi-Chi earthquake and the prediction of the model for magnitude dependence in the B-A attenuation relationship.

In the right panel of Figure 2-11, the residual at a magnitude of 7.6 for the Chi-Chi earthquake is about 1 for a period of 3 seconds, which implies that the bias in the long period range in Figure 2-8 is not due to the records of the Chi-Chi earthquake. If the records of the Chi-Chi earthquake are removed from the data of Figure 2-8, the median curve will be closer to 1 in the short period range and will not be significantly changes in the long period range. To confirm this hypothesis, we repeated the analysis of Figure 2-8 using all of the records of Table 2-1 except those of the Chi-Chi earthquake. Results are presented in Figure 2-12. The median and 84th percentile results of Figure 2-8 (Figure 2-12) at periods of 0, 0.2, 0.5, 1, 2, 3 and 4 seconds are presented in the 2nd and 3rd columns of Table 2-3 (Table 2-4). In Table 2-4, the median ratios are very close to 1 at periods between 0.2 and 2 seconds and the differences between Table 2-3 and Table 2-4 for the B-A model are greater at 0.2 second than at 3 seconds. The bias in the ratio of GMRotI50 to GMRotI50_BA still exists in Figure 2-12 in the long period range, likely due to the inter-event residuals for other earthquakes.

2.4.2.2 GMRotI50_CB

The analyses of Figure 2-7 through Figure 2-12 were repeated for GMRotI50_CB. Results are presented in Figure 2-13 through Figure 2-18, respectively. The median and 84th percentile results of Figure 2-14 (Figure 2-18) at periods of 0, 0.2, 0.5, 1, 2, 3 and 4 seconds are presented in the 4th and 5th columns of Table 2-3 (Table 2-4).

---

considered are put together for Stage-1 regression to establish the model for distance dependence. The event terms from Stage 1 are used in a Stage-2 regression to establish the model for magnitude dependence.

The trends in the data for the C-B model are similar to those for the B-A model. The C-B model also overestimates the median GMRotI50 of the records of Table 2-1 and the bias in the short period range of Figure 2-14 is due to the inter-event residual for the Chi-Chi earthquake (see the solid red squares in Figure 2-17). The bias is eliminated at periods between 0.2 and 2 seconds when the analysis is performed without the records of the Chi-Chi earthquake.

2.4.2.3 GMRotI50_CY

The analyses of Figure 2-7 through Figure 2-12 were repeated for GMRotI50_CY. Results are presented in Figure 2-19 through Figure 2-24, respectively. The median and 84th percentile results of Figure 2-20 (Figure 2-24) at periods of 0, 0.2, 0.5, 1, 2, 3 and 4 seconds are presented in the 6th and 7th columns of Table 2-3 (Table 2-4).

In Figure 2-20, the C-Y model overestimates the median GMRotI50 of the records of Table 2-1 for more than 20% for periods less than 0.2 second but predicts the median GMRotI50 within 10% for periods greater than 0.3 second. This observation can be explained using Figure 2-23 (Chiou and Youngs 2008) that presents the inter-event residuals for the C-Y model at periods of 0.01, 0.2, 1 and 3 seconds. The solid circle in each panel of Figure 2-20 at a magnitude of 7.6 is the residual for the Chi-Chi earthquake. Significant residuals are observed for the event at periods of 0.01 and 0.2 seconds but those at periods of 1 and 3 seconds are small.

In Figure 2-21 and Figure 2-22, the magnitude dependence of the residual between GMRotI50 and GMRotI50_CY is evident at periods of 0, 0.2 and 0.5 second. The distance dependence is insignificant at all periods presented in the study.

2.4.2.4 GMRotI50_ave

The analyses of Figure 2-7 through Figure 2-10 were repeated for GMRotI50_ave. Results are presented in Figure 2-25 through Figure 2-28, respectively. The trend in the data for GMRotI50_ave is similar to those for GMRotI50_BA and GMRotI50_CB.

The analyses of Figure 2-26 through Figure 2-28 were repeated using all of the records of Table 2-1 except those of the Chi-Chi earthquake. Results are presented in Figure 2-29 through Figure 2-31, respectively. The median and 84th percentile results of Figure 2-26 (Figure 2-29) at periods

of 0, 0.2, 0.5, 1, 2, 3 and 4 seconds are presented in the 8th and 9th columns of Table 2-3 (Table 2-4).

The median ratio of GMRotI50 to GMRotI50_ave ranges between 0.9 and 1.1 at almost all the periods of Figure 2-29. The ratio does not depend on distance (see Figure 2-31). The magnitude dependence presented in Figure 2-30 should be interpreted with care since the regression is governed by the data at magnitudes 6.69 and 6.93: a very narrow range of magnitude.

2.4.3 Relationships between maximum spectral demand and NGA-predicted GMRotI50

The analyses of Figure 2-7 through Figure 2-10 and Figure 2-12 were repeated using the ratio of maximum spectral demand to GMRotI50_BA (GMRotI50_CB, GMRotI50_CY). Results are presented in Figure 2-32 (Figure 2-37, Figure 2-42) through Figure 2-36 (Figure 2-41, Figure 2-46), respectively. The analyses of Figure 2-25 through Figure 2-31 for the ratio of GMRotI50 to GMRotI50_ave were repeated using the ratio of maximum spectral demand to GMRotI50_ave and the results are presented in Figure 2-47 through Figure 2-53, respectively.

The median and 84th percentile of the ratios of maximum spectral demand to each of GMRotI50_BA, GMRotI50_CB, GMRotI50_CY and GMRotI50_ave for all of the records of Table 2-1 are presented in Table 2-5 and those for all records except those of the Chi-Chi earthquake are presented in Table 2-6 at periods of 0, 0.2, 0.5, 1, 2, 3 and 4 seconds.

The four sets of median values of Table 2-5 are much smaller than the corresponding median values of Table 2-2, except for the results of the C-Y model at periods greater than 1 second, because the B-A and C-B models overestimate the median GMRotI50 of the records of Table 2-1 for the whole period range studied herein, as does the C-Y model in the short period range. The median GMRotI50 of the records of the Chi-Chi earthquake, which include 38% of the records of Table 2-1, is significantly overestimated in the short period range. The median ratios of maximum spectral demand to NGA-predicted GMRotI50 become closer to the median values of Table 2-2 in the short period range when the analysis is performed without the records of the Chi-Chi earthquake (see Table 2-6).

Based on the results of Figure 2-35, Figure 2-40 and Figure 2-45, the distance dependence of the ratio of maximum spectral demand to NGA-predicted GMRotI50 is insignificant. Based on the results of Figure 2-34, Figure 2-39 and Figure 2-44, the magnitude dependence of the ratio is evident in the short period range. We note that this observation should be interpreted with care since each data point was weighted equally in the regression analysis and 38% of the data are at a magnitude of 7.62; that is, the weighting factor for each magnitude is not equal and the regression analysis is highly influenced by the records of the Chi-Chi earthquake.

2.5 Orientation of maximum spectral demand

2.5.1 Methodology

The procedure used to investigate the relationship between the maximum spectral demand and the corresponding orientation for a given period and pair of earthquake records is illustrated in Figure 2-54. A 5%-damped linear oscillator with a period of 1 second in each horizontal direction was subjected to the SN and SP components of a ground motion. The acceleration orbit of the oscillator with respect to the SN and SP axes is shown in the figure. The maximum spectral acceleration (termed $S_{a,\max}(T_i)$, where T_i is the period of the oscillator) and its orientation with respect to the SN direction are identified by the solid circle shown in the figure: the point on the orbit farthest from the origin. The axis of Figure 2-54 was rotated counter-clockwise from the SN axis in increments of 1° from the SN axis through 180° as shown. For each angle of rotation (θ_j), the history of acceleration response along the rotated axis, $A(t,T_i,\theta_j)$, was computed as:

$$A(t,T_i,\theta_j) = A(t,T_i,SN)\times\cos(\theta_j) + A(t,T_i,SP)\times\sin(\theta_j) \tag{2.1}$$

where $A(t,T_i,SN)$ and $A(t,T_i,SP)$ are the acceleration response of the oscillator subjected to the SN and SP components of the ground motion, respectively, at time t. The maximum value of $A(t,T_i,\theta_j)$ was identified and denoted $S_a(T_i,\theta_j)$. The 180 values of $S_a(T_i,\theta_j)$ were binned into 18 groups, where Bin 1 is for θ_j from 1° through 10°, Bin 2 is for θ_j from 11° through 20°, and so forth. The ratio of the maximum value of the 10 $S_a(T_i,\theta_j)$ in each bin to $S_{a,\max}(T_i)$ was computed and denoted $R_{S_a}(T_i,\theta_{\mathrm{Bin}\,k})$, where k ranges from 1 to 18. The analysis was then repeated for the same pair of ground motions and another value of T_i. Forty-one values of T_i from 0

through 4 seconds in increments of 0.1 second were analyzed for each of the 165 pairs of records in the dataset.

2.5.2 Sample computations

Sample results are presented in Figure 2-55 using EQ15, the first pair of ground motions of Table 2-1. EQ15 was recorded during the 1952 Kern County earthquake. The values of M_W and r for EQ15 are 7.4 and 39 km, respectively. Panel a of Figure 2-55 presents the response spectra for the SN and SP components of EQ15. Panels c and e present the acceleration orbits of 0.2- and 2-second oscillators, respectively, subjected to EQ15. For T_i = 0.2 second, the peak acceleration demands at the SN and SP directions are close and the maximum acceleration demand occurs at θ_j = 89° (see the solid circle in panel c). For T_i = 2 second, the demand along the SP direction is much greater than that along the SN direction.

Panel b of Figure 2-55 presents R_{S_a} for Bins 1 (θ_j = 1° through 10°), 4 (31° through 40°) and 7 (61° through 70°) at periods of 0 through 4 seconds. Panel d presents identical information for Bins 10 (91° through 100°), 13 (121° through 130°) and 16 (151° through 160°). In this case, the values of R_{S_a} for orientations close to the SP direction (Bins 7 and 10) are greater than those close to the SN direction (Bins 1 and 16) at most periods between 0 and 4 seconds.

We note that the data of Figure 2-55 are sample results. The direction of maximum acceleration demand does not have significant correlation with either the SN or SP direction for far-field ground motions. The data presented in Section 3 for near-fault ground motions show that the strong correlation between the SN and maximum-demand directions does not exist for r greater than 3 to 5 km.

A parameter is defined in (2.2) to study the relationship between the rotation angle and the spectral demand averaged over four ranges of period:

$$\overline{R}_{S_a}(\theta_{\text{Bin } k}) = \frac{1}{N_T} \sum_{T_i=T_L}^{T_U} R_{S_a}(T_i, \theta_{\text{Bin } k}) \tag{2.2}$$

where T_L and T_U are lower- and upper-bound periods, respectively, for each of the four period ranges; and N_T is the number of periods in each range. The period ranges are 0 to 4.0 seconds

(R1), 0 to 1.0 second (R2), 1.0 to 2.0 seconds (R3) and 2.0 to 4.0 seconds (R4); the values of T_L and T_U for each range are listed in Table 2-7. A value of 1 for $\overline{R}_{S_a}(\theta_{\text{Bin}\,k})$ indicates that the maximum shaking demand at all periods between T_L and T_U is achieved between the rotation angles associated with Bin *k*.

Panel f of Figure 2-55 presents the value of $\overline{R}_{S_a}$ for all four ranges of period at the midpoint rotation angle for each bin. For all four curves of Panel f, the value of $\overline{R}_{S_a}$ increases as the angle approaches 90° (the SP direction) and decreases as it approaches 0° and 180° (the SN direction). For range R1, the maximum value of $\overline{R}_{S_a}$ over the 18 bins of angles (termed $\overline{R}_{S_a,\max}$) is 0.97 and the corresponding midpoint rotation angle (termed $\theta_{\max}$) is 85°. The minimum value of $\overline{R}_{S_a}$ is 0.7 and the corresponding midpoint rotation angle is 5°. For ranges R2, R3 and R4, the values of $\overline{R}_{S_a,\max}$ are 0.96, 0.97 and 0.98, respectively, and the values of $\theta_{\max}$ are 85°, 95° and 85°. For EQ77, $\theta_{\max}$ is similar to the SP direction, regardless of the range of period.

2.5.3 Overall analysis results

The parameter $\overline{R}_{S_a,\max}$ can be used to address the following question: Is the orientation of maximum spectral demand for a pair of recorded ground motions somewhat constant across oscillator periods? For example, if the value of $\overline{R}_{S_a,\max}$ for R1 is greater than 0.9, it is very likely that the spectral demands in that range of orientation angle are equal or nearly equal to the maximum spectral demands for a wide range of the periods between 0 and 4 seconds, or, put differently, there is an axis of strongest shaking, where the use of a maximum spectrum for design is not overly conservative even for structures with response in two or more modes.

Figure 2-56 presents the distributions of $\overline{R}_{S_a,\max}$ for R1, R2, R3 and R4 for all 165 pairs of records. Each distribution of Figure 2-56 was developed by sorting the 165 realizations from smallest to largest and assigning a probability from 1/165 to 1.00 in increments of 1/165 for each of the results to develop the cumulative distribution function (CDF). Seventy-three percent of the records have $\overline{R}_{S_a,\max}$ greater than 0.95 for the long period range (R4); the percentage drops to 42% for the short period range (R2). The medians (by counting), means and standard deviations of the 165 realizations for R1 through R4 are presented in Table 2-7. The median and mean values of $\overline{R}_{S_a,\max}$ for all cases range between 0.93 and 0.97 and the standard deviation is 0.03 for

all cases. The results of Figure 2-56 and Table 2-7 indicate that there is typically an axis of strongest shaking.

2.6 Correlation of ground motions

2.6.1 Time series

2.6.1.1 Definition

Two types of correlation of ground motions are studied and presented in Section 2.6. Section 2.6.1 presents the correlation between two orthogonal horizontal acceleration *time series* for each pair of the ground-motion records of Table 2-1. Section 2.6.2 presents the correlation of *spectral demands* (maximum demand at different periods) for each pair of the records of Table 2-1.

In Section 2.6.1, the correlation between a pair of ground-motion time series is measured using a correlation coefficient (ρ) defined as:

$$\rho = \frac{E\{(X_1 - m_1)(X_2 - m_2)\}}{s_1 s_2} \tag{2.3}$$

where X_1 (X_2) is the ground acceleration for component 1 (2) of a pair of orthogonal horizontal ground-motion time series; m_1 and s_1 (m_2 and s_2) are the mean and standard deviation of X_1 (X_2), respectively; and $E\{\ \}$ is the expectation operator (Soong 2004). For a given acceleration time series with n data points, m_1 and s_1 (m_2 and s_2) are computed using the following equations:

$$m = \frac{1}{n}\sum_{i=1}^{n} x(t_i) \tag{2.4}$$

$$s = \sqrt{\frac{1}{n-1}\sum_{i=1}^{n}\left(x(t_i) - m\right)^2} \tag{2.5}$$

where $x(t_i)$ is the acceleration at a time instant t_i .

2.6.1.2 The study of Hadjian (1981)

For a pair of orthogonal horizontal ground motions recorded at a site, the value of correlation coefficient depends on the orientation of observation for the records (Hadjian 1978, 1981). Figure 2-57 presents the correlation coefficient of a sample pair of ground motions as a function of the

angle of the observation. For the computation of Figure 2-57, the sample pair of ground motions was rotated from 1° to 180° in increments of 1°. For each rotation angle, the correlation coefficient of the rotated time series was computed using (2.3) through (2.5) and presented in Figure 2-57. The plot of the correlation coefficient as a function of rotation angle is sinusoidal since the rotation matrix used to rotate the ground motion is composed of sine and cosine functions and $E\{\ \}$ of (2.3) is a linear operator. For example, the curve of correlation coefficient of Figure 2-57 is identical to the function of $0.22\sin(2\phi - 38.55^{\circ})$, where ϕ is the rotation angle and 0.22 is the maximum correlation coefficient of the sample pair of ground motions over all rotation angles, termed ρ_{Max} hereafter.

Hadjian (1981) developed 1) the probability density function (PDF) of ρ conditioned on ρ_{Max} and 2) the PDF of ρ_{Max}, and combined the two PDFs to establish the PDF of ρ. The first PDF, developed based on the observation that the function of ρ in terms of ϕ is sinusoidal, was used to address the variability in ρ due to the randomness in the orientation of ground motions. The second PDF, developed using 50 pairs of recorded ground motions available at that time, was used to address the variability in ρ_{Max}. Based on the distribution of ρ, Hadjian recommended that the correlation coefficient of the horizontal components of ground motion used in response-history analysis should be less than 0.32. The results of Hadjian (1981) provide the technical basis for design codes ASCE Standard 4-98 (ASCE 2000) and ASCE Standard 43-05 (ASCE 2005), where an upper bound of 0.3 is required on the correlation coefficient of two orthogonal horizontal ground-motion time series used for analysis.

2.6.1.3 Correlation of the two time series for each pair of ground motions of Table 2-1

For the records of Table 2-1, the distributions of three correlation coefficients of orthogonal horizontal ground-motion time series were investigated, namely, ρ_{Max}, ρ_{FN_FP} and $\rho_{Max_S_a}$, where ρ_{Max}, as defined in the Section 2.6.1.2, is the maximum correlation coefficient of a pair of ground motions over all rotation angles; ρ_{FN_FP} is the correlation coefficient of the ground-motion components in the FN and FP orientations; and $\rho_{Max_S_a}$ is the correlation coefficient in the orientations parallel and perpendicular to the direction associated with $\overline{R}_{S_a,\max}$.

For each of the 165 pairs of ground motions of Table 2-1, the values of ρ_{Max}, ρ_{FN_FP} and $\rho_{Max_S_a}$ were computed. The CDFs of ρ_{Max}, ρ_{FN_FP} and $\rho_{Max_S_a}$ are presented in Figure 2-58.

For the three CDFs of Figure 2-58, the values of correlation coefficient at cumulative probabilities of 0.5 and 0.9 and the cumulative probability at a correlation coefficient of 0.3 are presented in Table 2-8 together with the mean and standard deviation of the 165 realizations for ρ_{Max}, ρ_{FN_FP} and $\rho_{Max_S_a}$ for the records of Table 2-8.

The mean and standard deviation for ρ_{Max} are 0.21 and 0.13, respectively, in Table 2-8. As a point of reference, the mean and standard deviation for ρ_{Max} reported in Hadjian (1981) are 0.234 and 0.109, respectively. In Table 2-8, the probability for ρ_{Max} less than 0.3 is 79%[2] and almost all realizations for $\rho_{Max_S_a}$ are less than 0.3. The mean and median values for $\rho_{Max_S_a}$ are about one half those for ρ_{Max}. The data of Figure 2-58 and Table 2-8 support the upper bound on the correlation coefficient (0.3) specified in the ASCE Standard 4-98 (ASCE 2000) and ASCE Standard 43-05 (ASCE 2005).

2.6.2 Spectral demand

2.6.2.1 The studies of Baker, Cornell and Jayaram

Much recent discussion on selection and scaling ground motions for long return-period earthquake shaking has centered on the ground-motion randomness index known as epsilon (ε). Epsilon is defined as the number of logarithmic standard deviations by which the underlying logarithmic spectral acceleration [$\ln(x_{S_a})$] deviates from the median value, where the median and the logarithmic standard deviation of spectral acceleration (denoted as θ_{S_a} and β_{S_a}, respectively) are predicted by an attenuation relationship (McGuire 1995; Baker and Cornell 2005):

$$\varepsilon = \frac{\ln(x_{S_a}) - \ln(\theta_{S_a})}{\beta_{S_a}} \tag{2.6}$$

Baker and Cornell (2005) proposed that the effect of ε on structural response given $S_a(T_1)$ is greater than that of either magnitude or distance because ε is an indicator of spectral shape. A

---

[2] Note that the probability for ρ less than 0.3 will be greater than the probability for $\rho_{\max}$ less than 0.3 since the value of ρ for a pair of ground motions depends on both the orientation of the components and the value of $\rho_{\max}$.

positive value of ε at a given period tends to indicate a relative peak in the acceleration response spectrum at that period. To address this observation, Baker and Cornell (2005, 2006b) introduced a Conditional Mean Spectrum (CMS), which considers the correlation of spectral demands (in the form of ε) at different periods. A CMS is computed using the following equation:

$$\mu_{\ln Sa(T_2)|\ln Sa(T_1)=\ln Sa(T_1)^*} = \mu_{\ln Sa}(\bar{M},\bar{R},T_2) + \sigma_{\ln Sa}(\bar{M},T_2)\rho_{\ln Sa(T_1),\ln Sa(T_2)} \cdot \bar{\varepsilon}(T_1) \tag{2.7}$$

where $Sa(T_1)$ and $Sa(T_2)$ are spectral accelerations at periods T_1 and T_2; T_1 is the fundamental period of a structure; $Sa(T_1)*$ is the value of $Sa(T_1)$ corresponding to a given annual frequency of exceedance; $\bar{M}$, $\bar{R}$ and $\bar{\varepsilon}$ are the mean magnitude (M), distance (r) and ε values, respectively, that produce $Sa(T_1)*$; $\mu_{\ln Sa(T_2)|\ln Sa(T_1)=\ln Sa(T_1)^*}$ is the mean of $\ln Sa(T_2)$ given that $\ln Sa(T_1) = \ln Sa(T_1)*$; $\mu_{\ln Sa}$ and $\sigma_{\ln Sa}$ are the mean and standard deviation of $\ln Sa$, respectively, obtained from a ground motion attenuation relationship; and $\rho_{\ln Sa(T_1),\ln Sa(T_2)}$ is the correlation coefficient of $\ln Sa(T_1)$ and $\ln Sa(T_2)$.

The development of a CMS requires the correlation coefficient of $\ln Sa(T_1)$ and $\ln Sa(T_2)$. For a combination of ground motion parameters (M , r , shear wave velocity, fault type, etc.), the correlation of $\ln Sa(T_1)$ and $\ln Sa(T_2)$ can be completely described by the correlation of ε at periods T_1 and T_2, termed $\rho_{\varepsilon(T_1),\varepsilon(T_2)}$ (Baker and Jayaram 2008). Baker and Jayaram (2008) developed a model for $\rho_{\varepsilon(T_1),\varepsilon(T_2)}$ using the ground-motion records in the NGA database (http://peer.berkeley.edu/nga/) and four NGA attenuation relationships, namely, Abrahamson and Silva (2008), B-A, C-B and C-Y. The model is presented below:

$$\begin{aligned}
&\text{if } T_{\max} < 0.109 \quad \rho_{\varepsilon(T_1),\varepsilon(T_2)} = C_2 \\
&\text{else if } T_{\min} > 0.109 \quad \rho_{\varepsilon(T_1),\varepsilon(T_2)} = C_1 \\
&\text{else if } T_{\max} < 0.2 \quad \rho_{\varepsilon(T_1),\varepsilon(T_2)} = \min(C_2,\ C_4) \\
&\text{else} \quad \rho_{\varepsilon(T_1),\varepsilon(T_2)} = C_4
\end{aligned} \tag{2.8}$$

where $T_{\min} = \min(T_1,T_2)$, $T_{\max} = \max(T_1,T_2)$ and

$$C_1 = 1 - \cos\left(\frac{\pi}{2} - 0.366\ln\left(\frac{T_{\max}}{\max(T_{\min},0.109)}\right)\right) \tag{2.9}$$

$$C_2 = \begin{cases} 1 - 0.105\left(1 - \dfrac{1}{1+e^{100T_{\max}-5}}\right)\left(\dfrac{T_{\max} - T_{\min}}{T_{\max} - 0.0099}\right) & \text{if } T_{\max} < 0.2 \\ 0 & \text{otherwise} \end{cases} \tag{2.10}$$

$$C_3 = \begin{cases} C_2 & \text{if } T_{\max} < 0.109 \\ C_1 & \text{otherwise} \end{cases} \tag{2.11}$$

$$C_4 = C_1 + 0.5\left(\sqrt{C_3} - C_3\right)\left(1 + \cos\left(\frac{\pi T_{\min}}{0.109}\right)\right) \tag{2.12}$$

2.6.2.2 Correlation coefficient of maximum spectral demands at different periods

This subsection presents the correlation of maximum spectral demands at periods of T_1 and T_2. A parameter, $\varepsilon_{\max}(T_i)$, is defined as

$$\varepsilon_{\max}(T_i) = \frac{\ln(x_{\max}(T_i)) - \ln(SF(T_i)\cdot\theta_{NGA})}{\beta_{NGA}} \tag{2.13}$$

where $x_{\max}(T_i)$ is the maximum spectral demand at the period T_i for a set of ground motions of Table 2-1; θ_{NGA} is GMRotI50_BA, GMRotI50_CB, GMRotI50_CY or GMRotI50_ave at the period T_i for the set of ground motions; β_{NGA} is the dispersion corresponding to θ_{NGA} predicted by the NGA models and $SF(T_i)$ is a factor to scale the median NGA-predicted GMRotI50 to median maximum spectral demand at the period T_i. The parameter $SF(T_i)$ is based on the median ratio of maximum spectral demand to NGA-predicted GMRotI50 presented in Figure 2-33, Figure 2-38, Figure 2-43, and Figure 2-48 for GMRotI50_BA, GMRotI50_CB, GMRotI50_CY and GMRotI50_ave, respectively. It is likely more appropriate to use $\sqrt{\beta_{NGA}^2 + \beta_{\max/GMRotI50}^2}$ rather than β_{NGA} for the denominator in (2.13), where $\beta_{\max/GMRotI50}$ is the dispersion for the ratio of maximum spectral demand to (observed) GMRotI50, which can be computed using the data of Figure 2-4. The typical value of β_{NGA} ranges between 0.55 and 0.8 and that of $\beta_{\max/GMRotI50}$ ranges between 0.1 and 0.15. The difference between $\sqrt{\beta_{NGA}^2 + \beta_{\max/GMRotI50}^2}$ and β_{NGA} is less than 5%.

The values of $\varepsilon_{\max}(T_i)$ for all records of Table 2-1 were computed at periods between 0 and 4 seconds for each of GMRotI50_BA, GMRotI50_CB, GMRotI50_CY and GMRotI50_ave, and the correlation coefficients between $\varepsilon_{\max}(T_1)$ and $\varepsilon_{\max}(T_2)$, termed $\rho_{\varepsilon_{\max}(T_1),\varepsilon_{\max}(T_2)}$, were obtained. The contours of $\rho_{\varepsilon_{\max}(T_1),\varepsilon_{\max}(T_2)}$ are presented in panels a through d of Figure 2-59 for

GMRotI50_BA, GMRotI50_CB, GMRotI50_CY and GMRotI50_ave, respectively. Panel e of Figure 2-59 presents the contours of correlation coefficients per (2.8), that is, the model of Baker and Jayaram (2008). The distributions presented in the five panels of Figure 2-59 are similar.

Panels a and b of Figure 2-60 presents $\rho_{\varepsilon_{\max}(T_1),\varepsilon_{\max}(T_2)}$ for GMRotI50_ave and Baker and Jayaram (2008), respectively, in a 3-dimensional format. Similar distributions are observed in both panels.

Panels a through d of Figure 2-61 present the values of $\rho_{\varepsilon_{\max}(T_1),\varepsilon_{\max}(T_2)}$ as a function of T_1 given that T_2 is equal to 0.2, 0.5, 1 and 3 seconds, respectively. The solid and dashed lines in each panel present the data for Baker and Jayaram (2008) and GMRotI50_ave, respectively. The differences between the data for Baker and Jayaram (2008) and GMRotI50_ave are insignificant. At periods smaller than 0.1 second, the value of $\rho_{\varepsilon_{\max}(T_1),\varepsilon_{\max}(T_2)}$ for Baker and Jayaram (2008) is always 0.1 (or more) smaller than that for GMRotI50_ave.

The results of Figure 2-59 through Figure 2-61 suggest that the model of Baker and Jayaram (2008), with minor modification in the short period range, can be used to capture the correlation between the maximum spectral demands at different periods for the far-field motions of Table 2-1.

Table 2-1. Far-field earthquake ground motion records for the WUS study

Record Sequence Number	Earthquake Name	Station Name	Year	M_W	r (km)	V_{S30} (m/s)
15	Kern County	Taft Lincoln School	1952	7.36	38.89	385.4
36	Borrego Mtn	El Centro Array #9	1968	6.63	45.66	213.4
63	San Fernando	Fairmont Dam	1971	6.61	30.19	684.9
65	San Fernando	Gormon - Oso Pump Plant	1971	6.61	46.78	308.4
81	San Fernando	Pearblossom Pump	1971	6.61	38.97	529.1
87	San Fernando	Santa Anita Dam	1971	6.61	30.70	684.9
93	San Fernando	Whittier Narrows Dam	1971	6.61	39.45	298.7
121	Friuli, Italy-01	Barcis	1976	6.50	49.38	424.8
122	Friuli, Italy-01	Codroipo	1976	6.50	33.40	274.5
186	Imperial Valley-06	Niland Fire Station	1979	6.53	36.92	207.5
188	Imperial Valley-06	Plaster City	1979	6.53	30.33	345.4
191	Imperial Valley-06	Victoria	1979	6.53	31.92	274.5
287	Irpinia, Italy-01	Bovino	1980	6.90	46.25	274.5
291	Irpinia, Italy-01	Rionero In Vulture	1980	6.90	30.07	530.0
731	Loma Prieta	APEEL 10 - Skyline	1989	6.93	41.88	391.9
732	Loma Prieta	APEEL 2 - Redwood City	1989	6.93	43.23	133.1
735	Loma Prieta	APEEL 7 - Pulgas	1989	6.93	41.86	415.3
736	Loma Prieta	APEEL 9 - Crystal Springs Res	1989	6.93	41.03	449.6
748	Loma Prieta	Belmont - Envirotech	1989	6.93	44.11	627.6
751	Loma Prieta	Calaveras Reservoir	1989	6.93	35.49	513.7
757	Loma Prieta	Dumbarton Bridge West End FF	1989	6.93	35.52	274.5
759	Loma Prieta	Foster City - APEEL 1	1989	6.93	43.94	116.4
760	Loma Prieta	Foster City - Menhaden Court	1989	6.93	45.58	126.4
761	Loma Prieta	Fremont - Emerson Court	1989	6.93	39.85	284.8
762	Loma Prieta	Fremont - Mission San Jose	1989	6.93	39.51	367.6
772	Loma Prieta	Halls Valley	1989	6.93	30.49	281.6
775	Loma Prieta	Hollister - SAGO Vault	1989	6.93	30.24	684.9
781	Loma Prieta	Lower Crystal Springs Dam dwnst	1989	6.93	48.39	712.8
782	Loma Prieta	Monterey City Hall	1989	6.93	44.35	684.9
786	Loma Prieta	Palo Alto - 1900 Embarc.	1989	6.93	30.81	209.9

Record Sequence Number	Earthquake Name	Station Name	Year	M_W	r (km)	V_{S30} (m/s)
787	Loma Prieta	Palo Alto - SLAC Lab	1989	6.93	30.86	425.3
791	Loma Prieta	SAGO South - Surface	1989	6.93	34.32	684.9
800	Loma Prieta	Salinas - John & Work	1989	6.93	32.78	271.4
807	Loma Prieta	Sunol - Forest Fire Station	1989	6.93	47.57	400.6
812	Loma Prieta	Woodside	1989	6.93	34.09	454.0
826	Cape Mendocino	Eureka - Myrtle & West	1992	7.01	41.97	338.5
838	Landers	Barstow	1992	7.28	34.86	370.8
884	Landers	Palm Springs Airport	1992	7.28	36.15	207.5
897	Landers	Twentynine Palms	1992	7.28	41.43	684.9
942	Northridge-01	Alhambra - Fremont School	1994	6.69	36.77	550.0
945	Northridge-01	Anaverde Valley - City R	1994	6.69	38.00	446.0
946	Northridge-01	Antelope Buttes	1994	6.69	46.91	821.7
947	Northridge-01	Arcadia - Arcadia Av	1994	6.69	39.73	308.6
948	Northridge-01	Arcadia - Campus Dr	1994	6.69	41.41	367.5
950	Northridge-01	Baldwin Park - N Holly	1994	6.69	47.98	308.6
951	Northridge-01	Bell Gardens - Jaboneria	1994	6.69	44.11	308.6
958	Northridge-01	Camarillo	1994	6.69	40.34	234.9
962	Northridge-01	Carson - Water St	1994	6.69	49.81	160.6
964	Northridge-01	Compton - Castlegate St	1994	6.69	47.04	308.6
967	Northridge-01	Downey - Birchdale	1994	6.69	48.87	245.1
968	Northridge-01	Downey - Co Maint Bldg	1994	6.69	46.74	271.9
969	Northridge-01	Duarte - Mel Canyon Rd.	1994	6.69	48.63	446.0
970	Northridge-01	El Monte - Fairview Av	1994	6.69	44.79	308.6
971	Northridge-01	Elizabeth Lake	1994	6.69	36.55	234.9
981	Northridge-01	Inglewood - Union Oil	1994	6.69	42.20	316.0
984	Northridge-01	LA - 116th St School	1994	6.69	41.17	301.0
990	Northridge-01	LA - City Terrace	1994	6.69	36.62	365.2
991	Northridge-01	LA - Cypress Ave	1994	6.69	30.70	446.0
992	Northridge-01	LA - E Vernon Ave	1994	6.69	36.75	308.6
997	Northridge-01	LA - N Figueroa St	1994	6.69	31.16	405.2
999	Northridge-01	LA - Obregon Park	1994	6.69	37.36	349.4
1000	Northridge-01	LA - Pico & Sentous	1994	6.69	31.33	270.2

Record Sequence Number	Earthquake Name	Station Name	Year	M_W	r (km)	V_{S30} (m/s)
1001	Northridge-01	LA - S Grand Ave	1994	6.69	33.99	308.6
1002	Northridge-01	LA - S. Vermont Ave	1994	6.69	32.27	270.2
1005	Northridge-01	LA - Temple & Hope	1994	6.69	31.48	376.1
1007	Northridge-01	LA - Univ. Hospital	1994	6.69	34.20	376.1
1019	Northridge-01	Lake Hughes #1	1994	6.69	35.81	425.3
1021	Northridge-01	Lake Hughes #4 - Camp Mend	1994	6.69	31.66	821.7
1022	Northridge-01	Lake Hughes #4B - Camp Mend	1994	6.69	31.69	554.0
1026	Northridge-01	Lawndale - Osage Ave	1994	6.69	39.91	361.2
1027	Northridge-01	Leona Valley #1	1994	6.69	37.19	684.9
1028	Northridge-01	Leona Valley #2	1994	6.69	37.24	446.0
1029	Northridge-01	Leona Valley #3	1994	6.69	37.33	684.9
1030	Northridge-01	Leona Valley #4	1994	6.69	37.57	446.0
1031	Northridge-01	Leona Valley #5 - Ritter	1994	6.69	37.80	446.0
1032	Northridge-01	Leona Valley #6	1994	6.69	38.03	327.4
1033	Northridge-01	Littlerock - Brainard Can	1994	6.69	46.58	821.7
1034	Northridge-01	Malibu - Point Dume Sch	1994	6.69	33.67	349.5
1035	Northridge-01	Manhattan Beach - Manhattan	1994	6.69	39.29	405.2
1038	Northridge-01	Montebello - Bluff Rd.	1994	6.69	45.03	405.2
1041	Northridge-01	Mt Wilson - CIT Seis Sta	1994	6.69	35.88	821.7
1053	Northridge-01	Palmdale - Hwy 14 & Palmdale	1994	6.69	41.67	551.6
1055	Northridge-01	Pasadena - N Sierra Madre	1994	6.69	36.12	455.4
1057	Northridge-01	Playa Del Rey - Saran	1994	6.69	31.74	405.2
1058	Northridge-01	Point Mugu - Laguna Peak	1994	6.69	41.93	376.1
1065	Northridge-01	Rolling Hills Est-Rancho Vista	1994	6.69	49.32	376.1
1070	Northridge-01	San Gabriel - E Grand Ave	1994	6.69	39.31	401.4
1072	Northridge-01	San Marino - SW Academy	1994	6.69	35.02	379.4
1074	Northridge-01	Sandberg - Bald Mtn	1994	6.69	41.56	821.7
1095	Northridge-01	Whittier - S. Alta Dr	1994	6.69	49.10	376.1
1102	Kobe, Japan	Chihaya	1995	6.90	49.91	609.0
1118	Kobe, Japan	Tadoka	1995	6.90	31.69	312.0
1144	Gulf of Aqaba	Eilat	1995	7.20	44.10	354.9
1162	Kocaeli, Turkey	Goynuk	1999	7.51	31.74	424.8

Record Sequence Number	Earthquake Name	Station Name	Year	M_W	r (km)	V_{S30} (m/s)
1166	Kocaeli, Turkey	Iznik	1999	7.51	30.74	274.5
1181	Chi-Chi, Taiwan	CHY004	1999	7.62	47.34	271.3
1183	Chi-Chi, Taiwan	CHY008	1999	7.62	40.44	210.7
1186	Chi-Chi, Taiwan	CHY014	1999	7.62	34.18	473.9
1187	Chi-Chi, Taiwan	CHY015	1999	7.62	38.14	228.7
1196	Chi-Chi, Taiwan	CHY027	1999	7.62	42.00	210.0
1199	Chi-Chi, Taiwan	CHY032	1999	7.62	35.44	192.7
1200	Chi-Chi, Taiwan	CHY033	1999	7.62	43.83	197.6
1204	Chi-Chi, Taiwan	CHY039	1999	7.62	31.88	201.2
1210	Chi-Chi, Taiwan	CHY050	1999	7.62	44.76	473.9
1211	Chi-Chi, Taiwan	CHY052	1999	7.62	39.02	473.9
1212	Chi-Chi, Taiwan	CHY054	1999	7.62	48.49	172.1
1228	Chi-Chi, Taiwan	CHY076	1999	7.62	42.16	169.8
1230	Chi-Chi, Taiwan	CHY079	1999	7.62	47.53	473.9
1232	Chi-Chi, Taiwan	CHY081	1999	7.62	41.67	473.9
1233	Chi-Chi, Taiwan	CHY082	1999	7.62	36.11	193.7
1236	Chi-Chi, Taiwan	CHY088	1999	7.62	37.48	272.6
1239	Chi-Chi, Taiwan	CHY093	1999	7.62	49.83	190.5
1240	Chi-Chi, Taiwan	CHY094	1999	7.62	37.12	221.9
1245	Chi-Chi, Taiwan	CHY102	1999	7.62	37.72	553.4
1248	Chi-Chi, Taiwan	CHY109	1999	7.62	41.03	473.9
1249	Chi-Chi, Taiwan	CHY110	1999	7.62	41.03	473.9
1252	Chi-Chi, Taiwan	ESL	1999	7.62	44.54	553.4
1258	Chi-Chi, Taiwan	HWA005	1999	7.62	47.58	272.6
1259	Chi-Chi, Taiwan	HWA006	1999	7.62	47.86	272.6
1270	Chi-Chi, Taiwan	HWA020	1999	7.62	44.54	375.3
1273	Chi-Chi, Taiwan	HWA024	1999	7.62	43.15	553.4
1279	Chi-Chi, Taiwan	HWA030	1999	7.62	46.95	272.6
1281	Chi-Chi, Taiwan	HWA032	1999	7.62	47.16	473.9
1283	Chi-Chi, Taiwan	HWA034	1999	7.62	44.32	379.2
1284	Chi-Chi, Taiwan	HWA035	1999	7.62	48.35	473.9
1285	Chi-Chi, Taiwan	HWA036	1999	7.62	43.80	272.6

Record Sequence Number	Earthquake Name	Station Name	Year	M_W	r (km)	V_{S30} (m/s)
1286	Chi-Chi, Taiwan	HWA037	1999	7.62	46.20	272.6
1287	Chi-Chi, Taiwan	HWA038	1999	7.62	42.54	642.7
1288	Chi-Chi, Taiwan	HWA039	1999	7.62	45.89	375.3
1289	Chi-Chi, Taiwan	HWA041	1999	7.62	47.76	272.6
1299	Chi-Chi, Taiwan	HWA054	1999	7.62	43.01	272.6
1300	Chi-Chi, Taiwan	HWA055	1999	7.62	47.46	272.6
1301	Chi-Chi, Taiwan	HWA056	1999	7.62	41.10	511.3
1303	Chi-Chi, Taiwan	HWA058	1999	7.62	45.77	553.4
1304	Chi-Chi, Taiwan	HWA059	1999	7.62	49.15	473.9
1350	Chi-Chi, Taiwan	ILA067	1999	7.62	38.82	553.4
1351	Chi-Chi, Taiwan	KAU001	1999	7.62	44.93	473.9
1377	Chi-Chi, Taiwan	KAU050	1999	7.62	40.49	553.4
1380	Chi-Chi, Taiwan	KAU054	1999	7.62	30.85	473.9
1402	Chi-Chi, Taiwan	NST	1999	7.62	38.43	375.3
1407	Chi-Chi, Taiwan	STY	1999	7.62	40.49	553.4
1471	Chi-Chi, Taiwan	TCU015	1999	7.62	49.81	426.0
1477	Chi-Chi, Taiwan	TCU031	1999	7.62	30.18	489.2
1478	Chi-Chi, Taiwan	TCU033	1999	7.62	40.89	423.4
1479	Chi-Chi, Taiwan	TCU034	1999	7.62	35.69	393.8
1487	Chi-Chi, Taiwan	TCU047	1999	7.62	35.00	520.4
1524	Chi-Chi, Taiwan	TCU095	1999	7.62	45.18	446.6
1526	Chi-Chi, Taiwan	TCU098	1999	7.62	47.67	375.3
1539	Chi-Chi, Taiwan	TCU113	1999	7.62	31.07	230.3
1544	Chi-Chi, Taiwan	TCU119	1999	7.62	37.95	215.0
1552	Chi-Chi, Taiwan	TCU140	1999	7.62	32.97	215.0
1554	Chi-Chi, Taiwan	TCU145	1999	7.62	35.34	215.0
1585	Chi-Chi, Taiwan	TTN040	1999	7.62	48.33	728.0
1586	Chi-Chi, Taiwan	TTN041	1999	7.62	45.35	418.2
1594	Chi-Chi, Taiwan	TTN051	1999	7.62	36.70	553.4
1597	Chi-Chi, Taiwan	WSF	1999	7.62	42.16	169.8
1598	Chi-Chi, Taiwan	WTC	1999	7.62	42.25	215.0
1619	Duzce, Turkey	Mudurnu	1999	7.14	34.30	659.6

Record Sequence Number	Earthquake Name	Station Name	Year	M_W	r (km)	V_{S30} (m/s)
1620	Duzce, Turkey	Sakarya	1999	7.14	45.16	471.0
1626	Sitka, Alaska	Sitka Observatory	1972	7.68	34.61	659.6
1636	Manjil, Iran	Qazvin	1990	7.37	49.97	274.5
1762	Hector Mine	Amboy	1999	7.13	43.05	271.4
1794	Hector Mine	Joshua Tree	1999	7.13	31.06	379.3
1836	Hector Mine	Twentynine Palms	1999	7.13	42.06	684.9
2111	Denali, Alaska	R109 (temp)	2002	7.90	43.00	963.9

Table 2-2. Median and 84th percentile of the ratio of maximum spectral demand to GMRotI50 for all of the records of Table 2-1

Period (sec)	$\frac{\text{Maximum demand}}{\text{GMRotI50}}$	
	Median	84th percentile
0	1.18	1.31
0.2	1.20	1.36
0.5	1.23	1.39
1	1.27	1.44
2	1.27	1.44
3	1.27	1.41
4	1.31	1.50

Table 2-3. Median and 84th percentile of the ratio of GMRotI50 to GMRotI50_BA, GMRotI50_CB, GMRotI50_BA and GMRotI50_ave for all of the records of Table 2-1

Period (sec)	GMRotI50 / GMRotI50_BA		GMRotI50 / GMRotI50_CB		GMRotI50 / GMRotI50_CY		GMRotI50 / GMRotI50_ave	
	Median	84th percentile	Median	84th percentile	Median	84th percentile	Median	84th percentile
0	0.73	1.24	0.86	1.51	0.80	1.32	0.79	1.32
0.2	0.73	1.24	0.86	1.52	0.83	1.53	0.81	1.49
0.5	0.74	1.24	0.92	1.69	0.92	1.68	0.89	1.61
1	0.72	1.26	0.87	1.53	0.99	1.65	0.90	1.53
2	0.74	1.27	0.79	1.57	0.95	1.86	0.83	1.57
3	0.76	1.40	0.80	1.60	1.05	1.88	0.87	1.68
4	0.77	1.35	0.75	1.51	1.11	2.28	0.86	1.74

Table 2-4. Median and 84th percentile of the ratio of GMRotI50 to GMRotI50_BA, GMRotI50_CB, GMRotI50_BA and GMRotI50_ave for all of the records of Table 2-1 except those of the 1999 Chi-Chi earthquake

Period (sec)	GMRotI50 / GMRotI50_BA		GMRotI50 / GMRotI50_CB		GMRotI50 / GMRotI50_CY		GMRotI50 / GMRotI50_ave	
	Median	84th percentile	Median	84th percentile	Median	84th percentile	Median	84th percentile
0	0.87	1.34	0.99	1.59	0.92	1.53	0.91	1.53
0.2	0.96	1.61	0.99	1.77	1.04	1.77	0.97	1.67
0.5	0.98	1.55	0.95	1.69	1.15	1.87	1.03	1.63
1	0.97	1.64	0.97	1.78	1.08	2.06	0.99	1.85
2	0.95	1.52	0.95	1.71	1.03	1.92	0.95	1.70
3	0.86	1.67	0.90	1.80	1.08	2.12	0.93	1.81
4	0.83	1.61	0.81	1.54	1.09	2.31	0.89	1.77

Table 2-5. Median and 84th percentile of the ratio of maximum spectral demand to GMRotI50_BA, GMRotI50_CB, GMRotI50_BA and GMRotI50_ave for all of the records of Table 2-1

Period (sec)	Max. Demand / GMRotI50_BA		Max. Demand / GMRotI50_CB		Max. Demand / GMRotI50_CY		Max. Demand / GMRotI50_ave	
	Median	84th percentile	Median	84th percentile	Median	84th percentile	Median	84th percentile
0	0.92	1.47	1.07	1.75	0.98	1.61	0.96	1.65
0.2	0.96	1.74	1.06	1.89	1.00	1.87	0.99	1.79
0.5	1.07	1.93	1.11	2.07	1.17	2.12	1.09	2.04
1	1.13	1.89	1.12	1.93	1.24	2.22	1.16	2.04
2	1.12	2.00	1.04	2.06	1.25	2.45	1.11	2.13
3	1.06	2.03	1.03	2.13	1.28	2.42	1.10	2.07
4	1.04	2.26	1.00	2.13	1.44	3.00	1.10	2.42

Table 2-6. Median and 84th percentile of the ratio of maximum spectral demand to GMRotI50_BA, GMRotI50_CB, GMRotI50_BA and GMRotI50_ave for all of the records of Table 2-1 except those of the 1999 Chi-Chi earthquake

Period (sec)	Max. Demand / GMRotI50_BA		Max. Demand / GMRotI50_CB		Max. Demand / GMRotI50_CY		Max. Demand / GMRotI50_ave	
	Median	84th percentile	Median	84th percentile	Median	84th percentile	Median	84th percentile
0	1.06	1.60	1.18	1.91	1.20	1.85	1.16	1.77
0.2	1.18	2.02	1.19	2.24	1.27	2.17	1.17	2.10
0.5	1.22	1.93	1.21	2.04	1.42	2.36	1.28	2.04
1	1.27	2.13	1.26	2.27	1.42	2.69	1.27	2.27
2	1.20	2.07	1.20	2.29	1.32	2.66	1.23	2.36
3	1.09	2.11	1.13	2.27	1.40	2.83	1.15	2.35
4	1.04	2.27	1.02	2.36	1.40	3.17	1.10	2.60

Table 2-7. Medians, means and standard deviations of $\overline{R}_{S_a,\max}$ and T_L and T_U for R1 through R4

Bin	T_L (sec)	T_U (sec)	Median	Mean	Standard deviation
R1	0	4	0.93	0.93	0.03
R2	0	1	0.95	0.94	0.03
R3	1	2	0.96	0.96	0.03
R4	2	4	0.97	0.96	0.03

Table 2-8. Statistics of the correlation coefficients of Figure 2-58

Type of correlation coefficient	**Mean**	**Standard deviation**	**Median**	**Ninetieth percentile**	**Cumulative probability for $\rho = 0.3$**
ρ_{Max}	0.21	0.13	0.18	0.38	0.79
ρ_{FN_FP}	0.14	0.11	0.11	0.29	0.91
$\rho_{Max_S_a}$	0.11	0.10	0.09	0.26	0.96

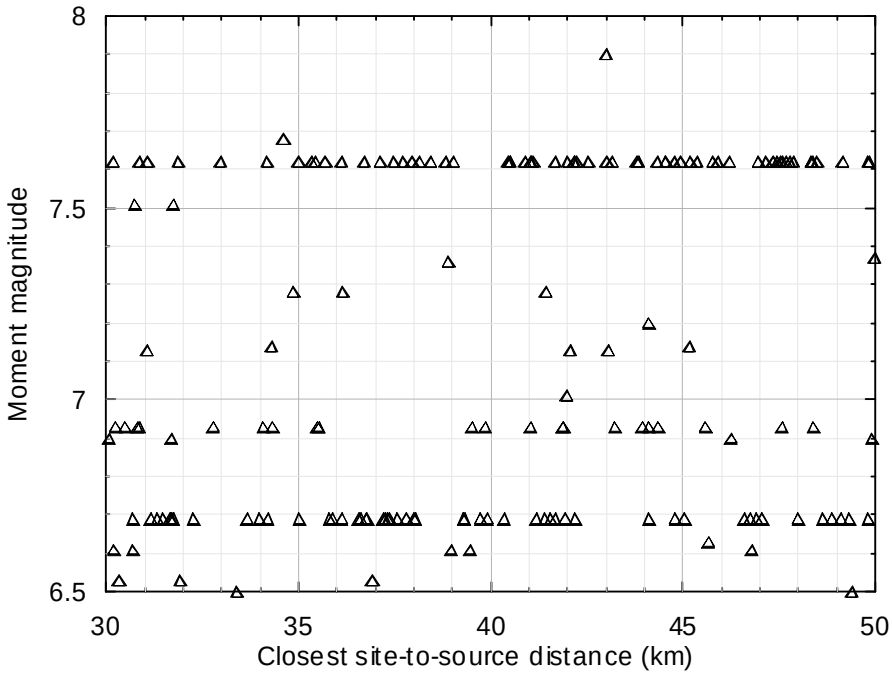

Figure 2-1. Magnitude and distance distribution of the ground motions of Table 2-1

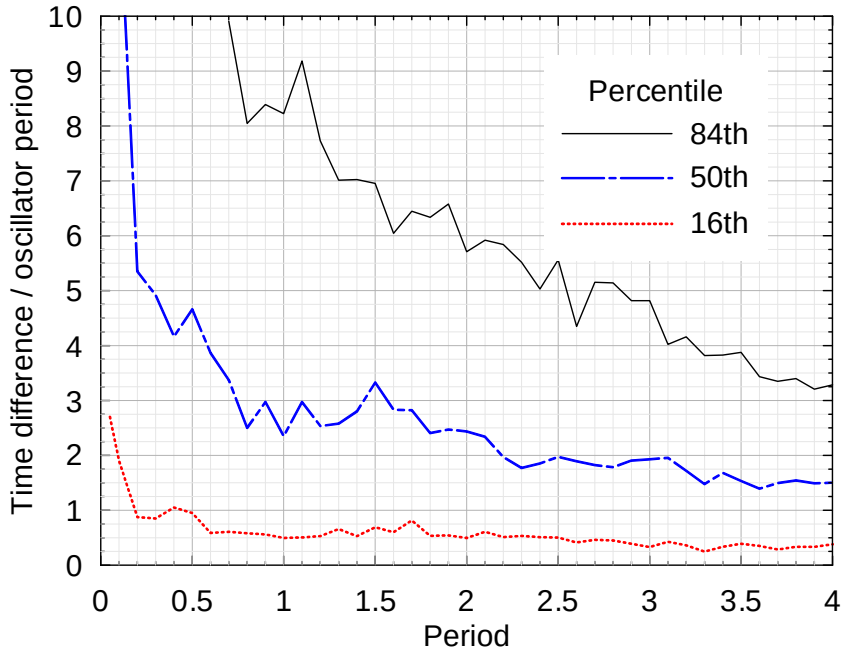

a. 84th, 50th and 16th percentiles

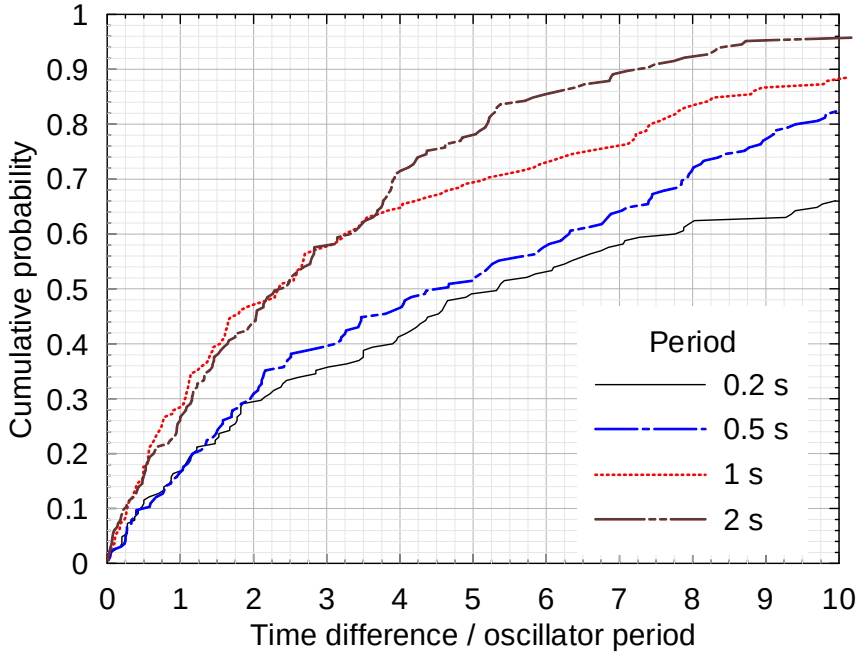

b. CDFs

Figure 2-2. a) Eighty-fourth, 50th and 16th percentiles and b) cumulative distribution functions of normalized time difference between the peak accelerations parallel and perpendicular to the GMRotI50 direction for the records of Table 2-1

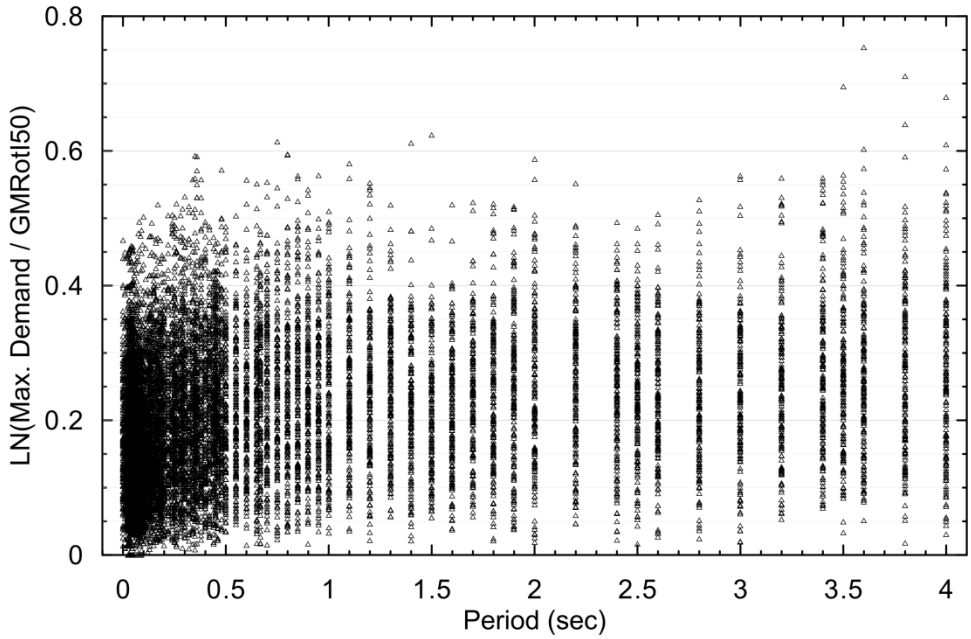

Figure 2-3. Ratios of maximum spectral demand to GMRotI50 for the records of Table 2-1

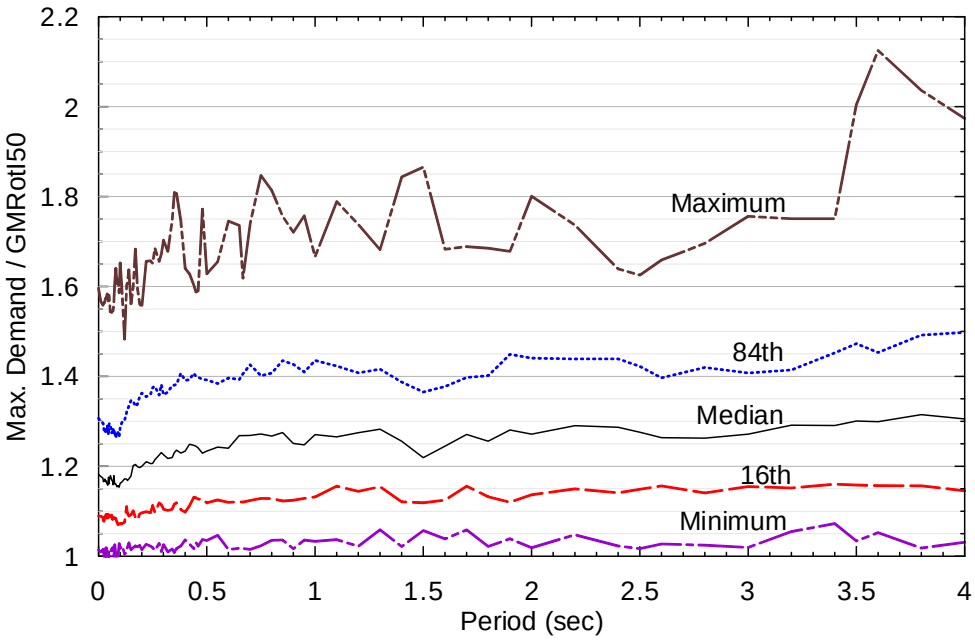

Figure 2-4. Maximum, minimum, median and 84th and 16th percentiles of the ratios of maximum spectral demand to GMRotI50 for the records of Table 2-1

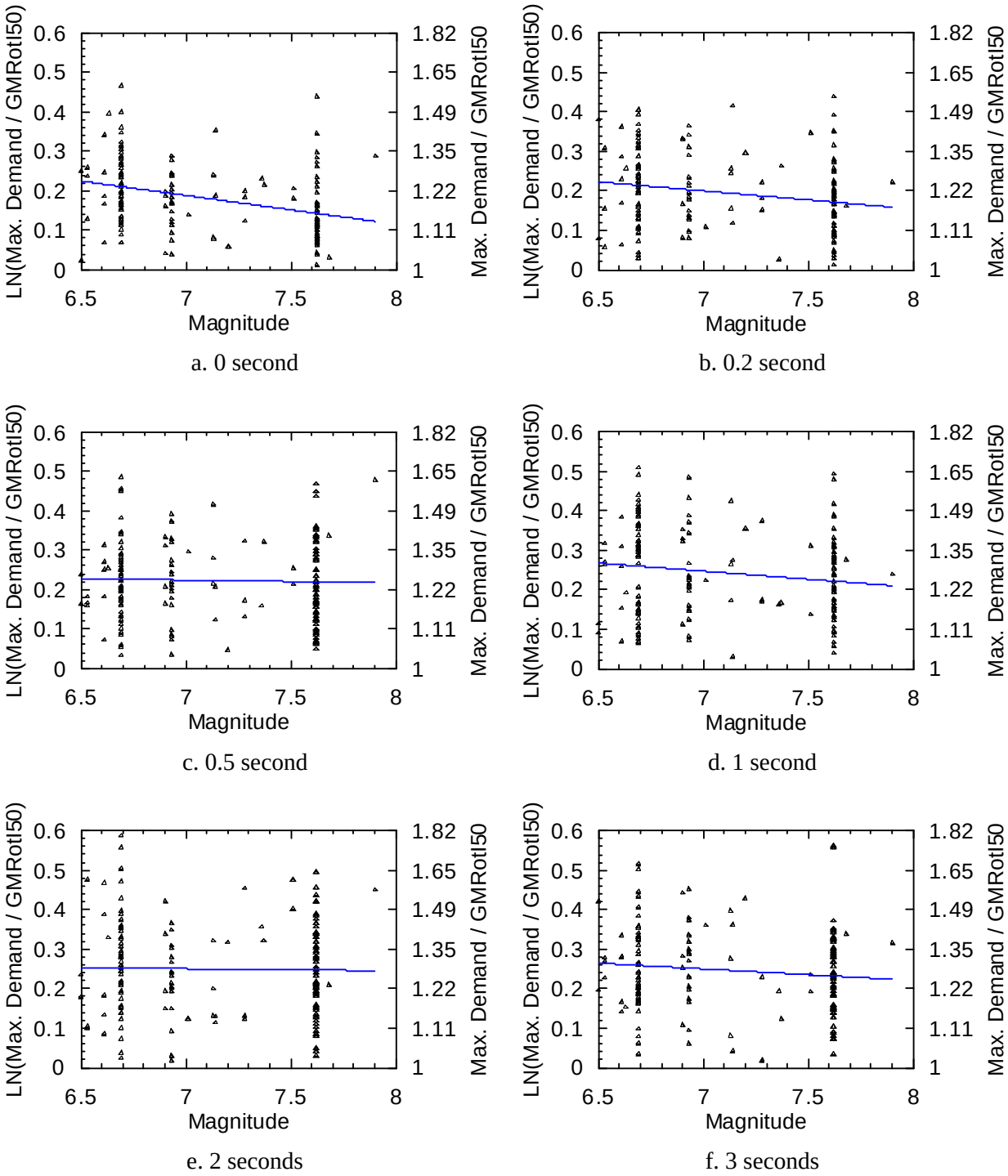

Figure 2-5. Ratios of maximum spectral demand to GMRotI50 at periods of 0, 0.2, 0.5, 1, 2 and 3 seconds as a function of magnitude for the records of Table 2-1

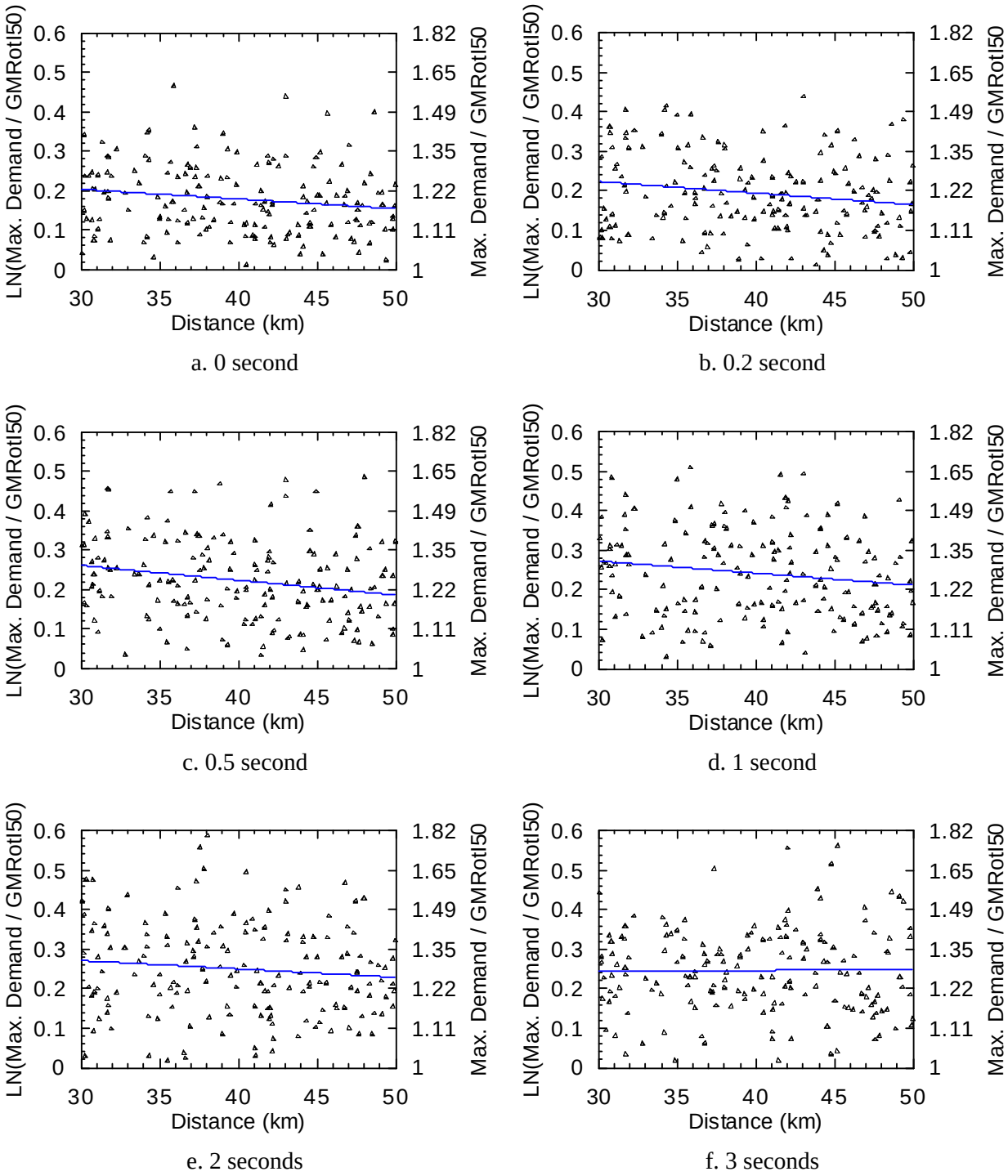

Figure 2-6. Ratios of maximum spectral demand to GMRotI50 at periods of 0, 0.2, 0.5, 1, 2 and 3 seconds as a function of distance for the records of Table 2-1

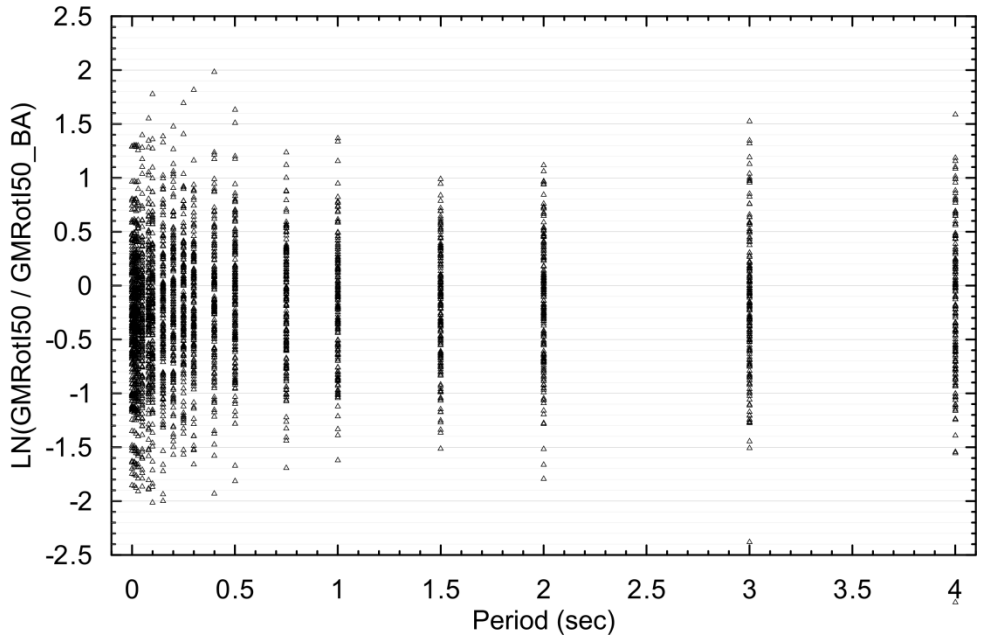

Figure 2-7. Ratios of GMRotI50 to GMRotI50_BA for the records of Table 2-1

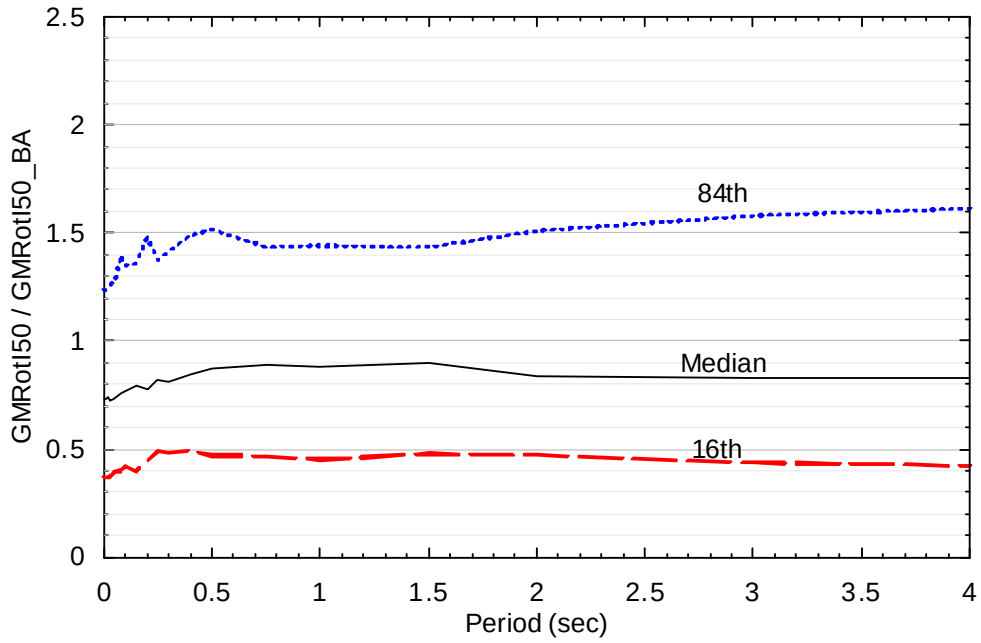

Figure 2-8. Median and 84th and 16th percentiles of the ratios of GMRotI50 to GMRotI50_BA for the records of Table 2-1

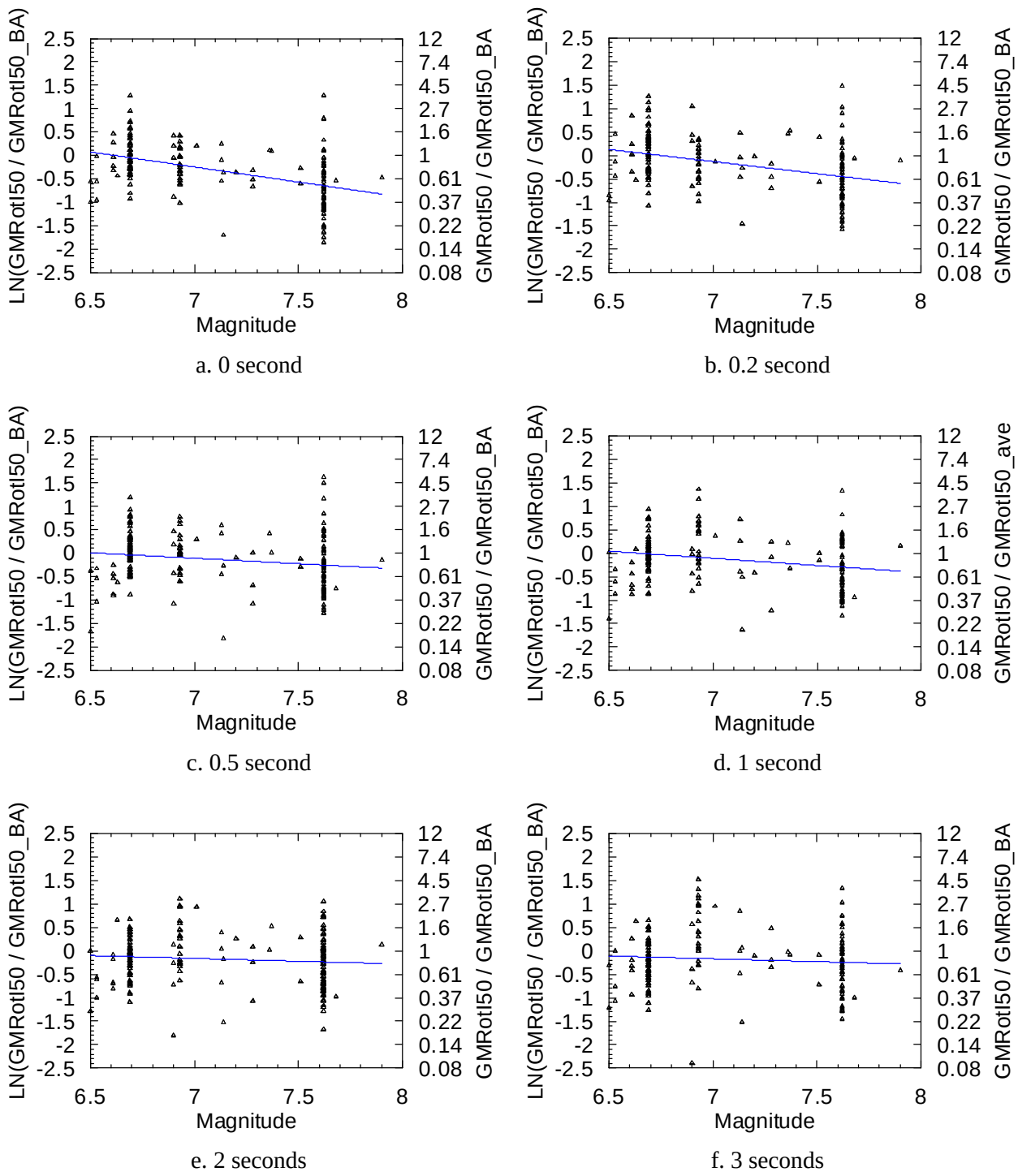

Figure 2-9. Ratios of GMRotI50 to GMRotI50_BA at periods of 0, 0.2, 0.5, 1, 2 and 3 seconds as a function of magnitude for the records of Table 2-1

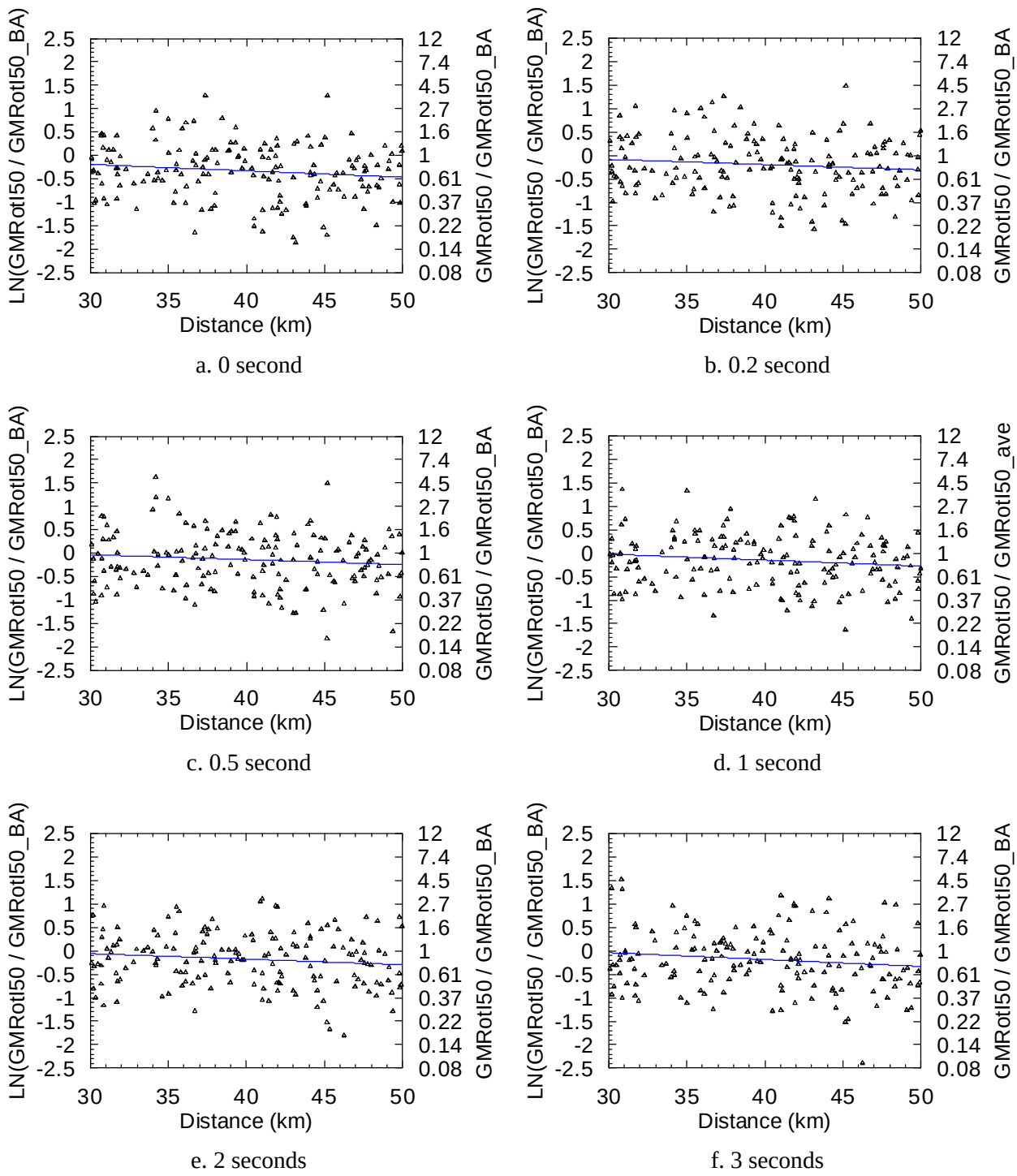

Figure 2-10. Ratios of GMRotI50 to GMRotI50_BA at periods of 0, 0.2, 0.5, 1, 2 and 3 seconds as a function of distance for the records of Table 2-1

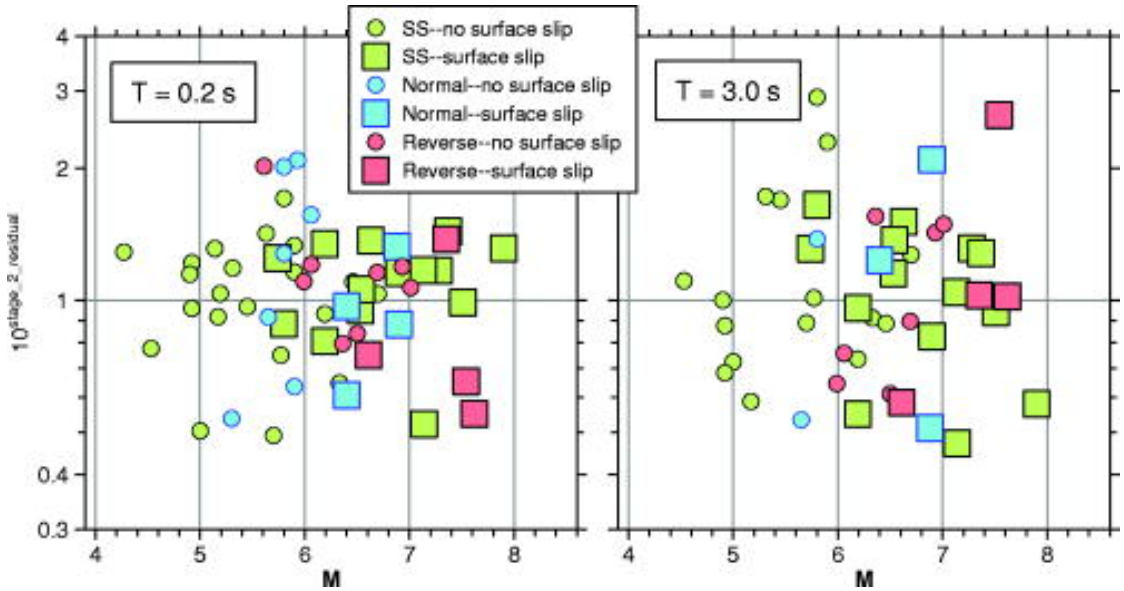

Figure 2-11. Stage-2 (Inter-event) residuals as a function of magnitude and fault types at periods of 0.2 and 3 seconds for the NGA B-A model (after Boore and Atkinson 2008)

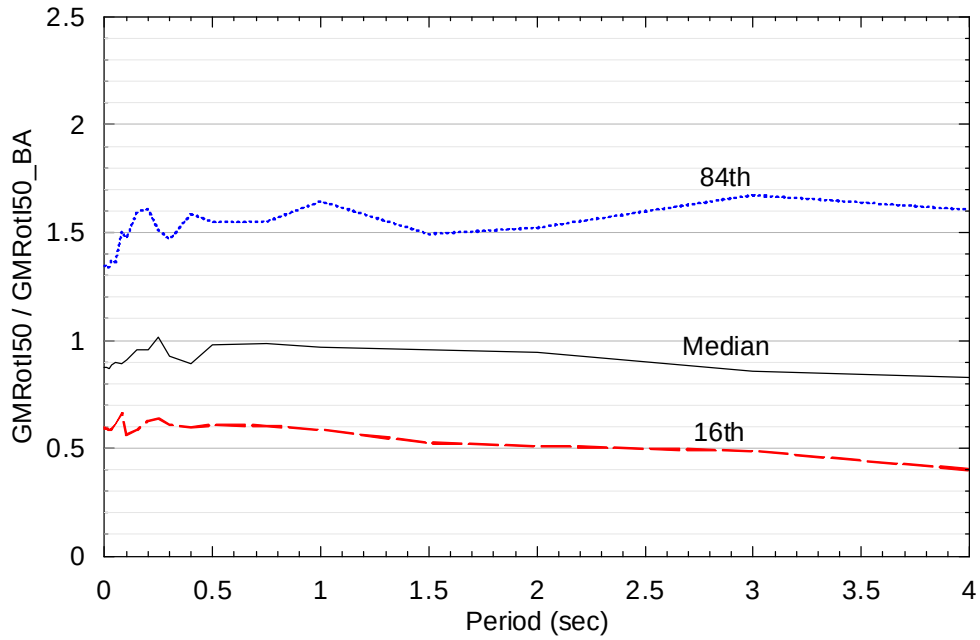

Figure 2-12. Median and 84th and 16th percentiles of the ratios of GMRotI50 to GMRotI50_BA for all of the records of Table 2-1 except those of the 1999 Chi-Chi earthquake

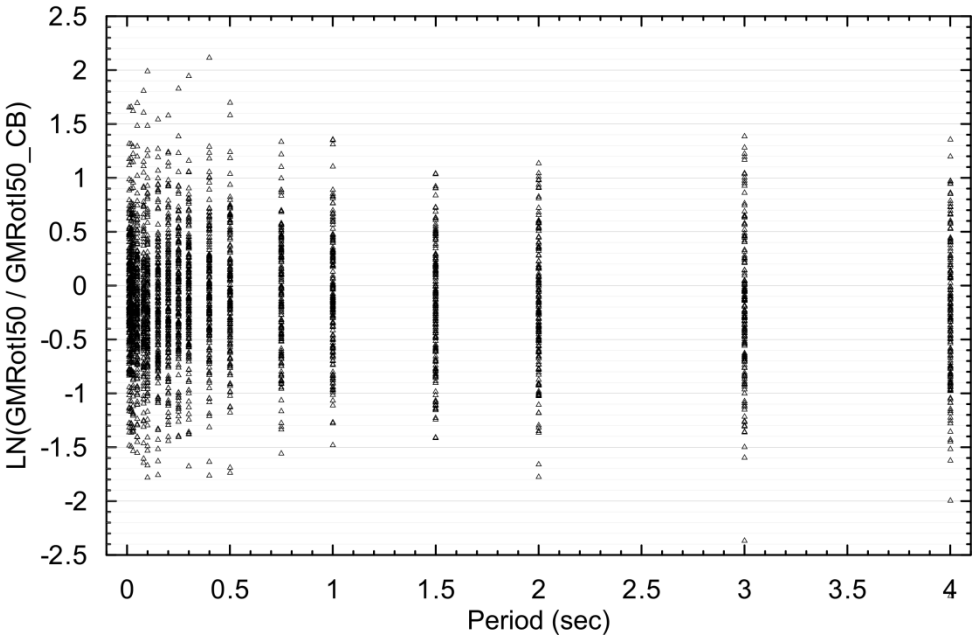

Figure 2-13. Ratios of GMRotI50 to GMRotI50_CB for the records of Table 2-1

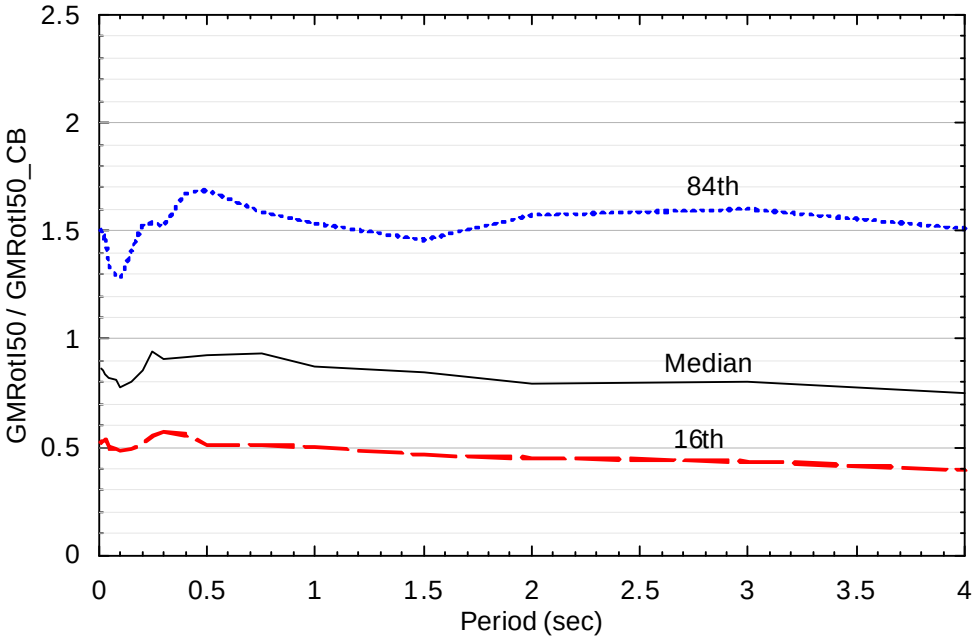

Figure 2-14. Median and 84th and 16th percentiles of the ratios of GMRotI50 to GMRotI50_CB for the records of Table 2-1

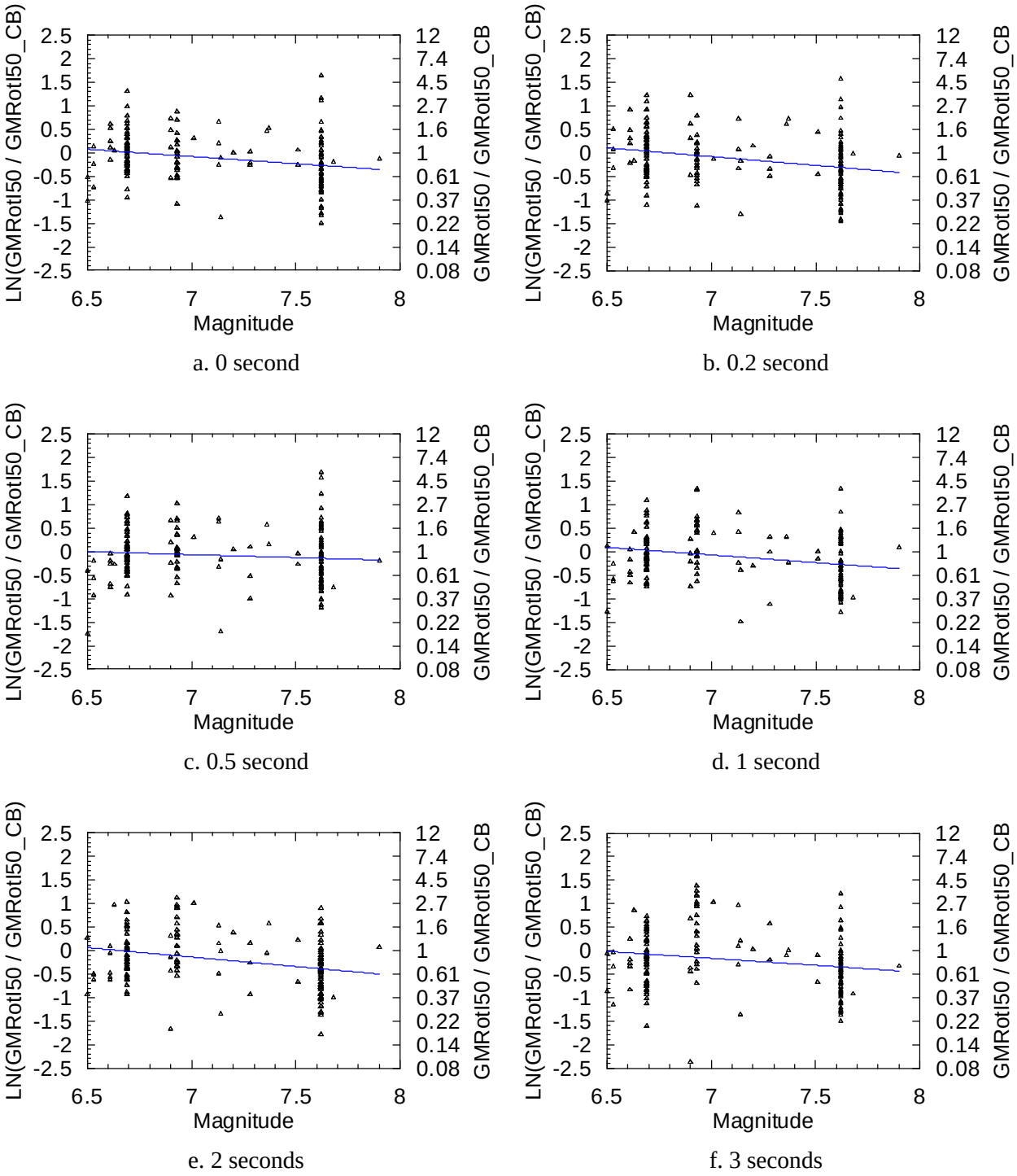

Figure 2-15. Ratios of GMRotI50 to GMRotI50_CB at periods of 0, 0.2, 0.5, 1, 2 and 3 seconds as a function of magnitude for the records of Table 2-1

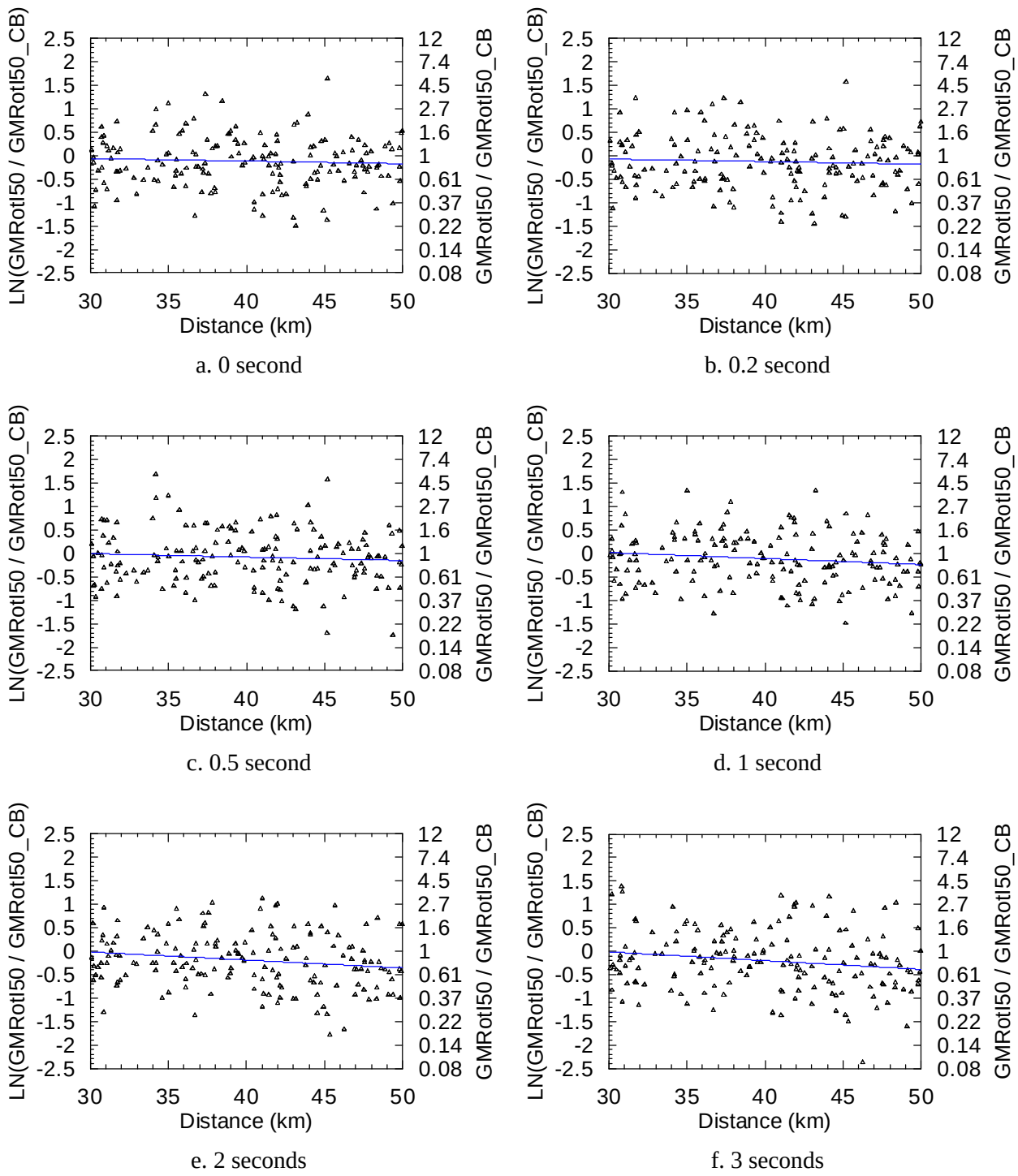

Figure 2-16. Ratios of GMRotI50 to GMRotI50_CB at periods of 0, 0.2, 0.5, 1, 2 and 3 seconds as a function of distance for the records of Table 2-1

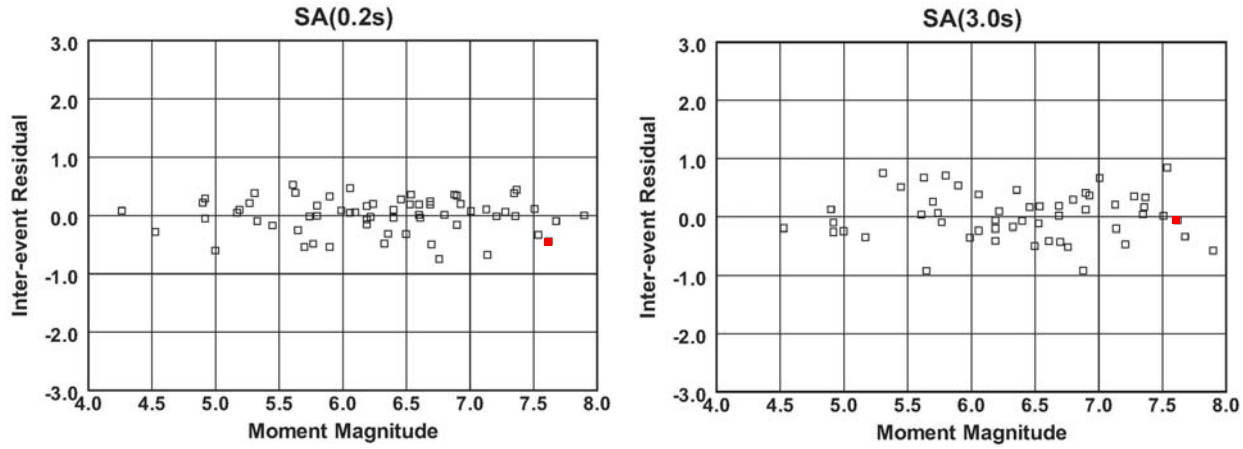

Figure 2-17. Inter-event residuals as a function of magnitude at periods of 0.2 and 3 seconds for the NGA C-B model (after Campbell and Bozorgnia 2008)

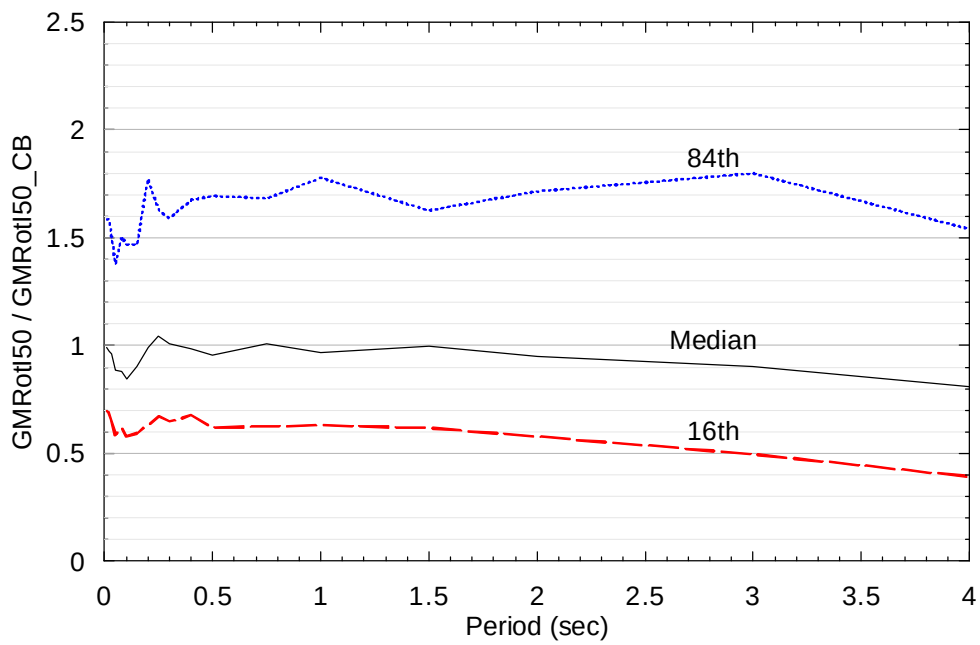

Figure 2-18. Median and 84th and 16th percentiles of the ratios of GMRotI50 to GMRotI50_CB for all of the records of Table 2-1 except those of the 1999 Chi-Chi earthquake

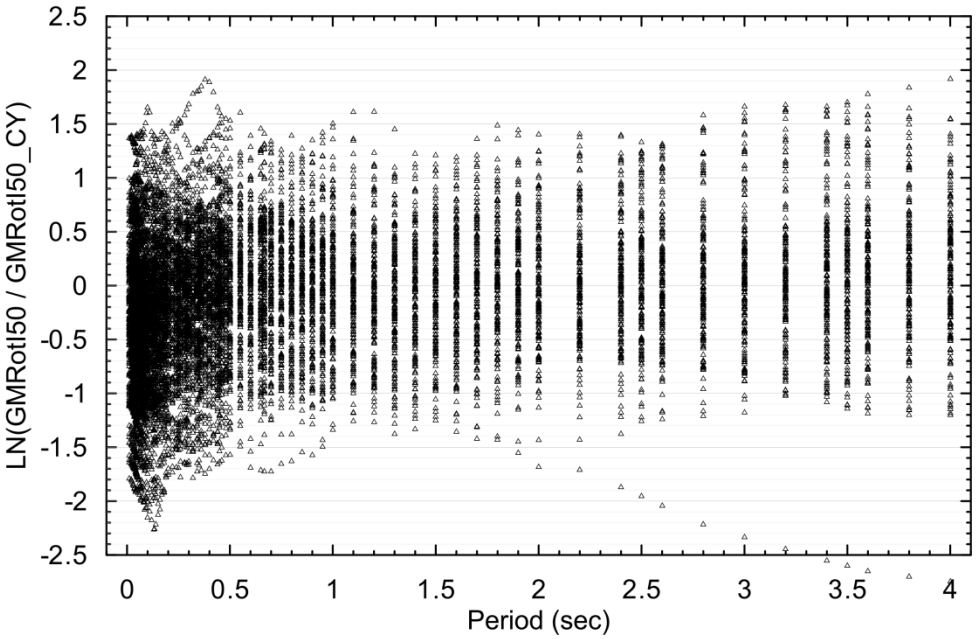

Figure 2-19. Ratios of GMRotI50 to GMRotI50_CY for the records of Table 2-1

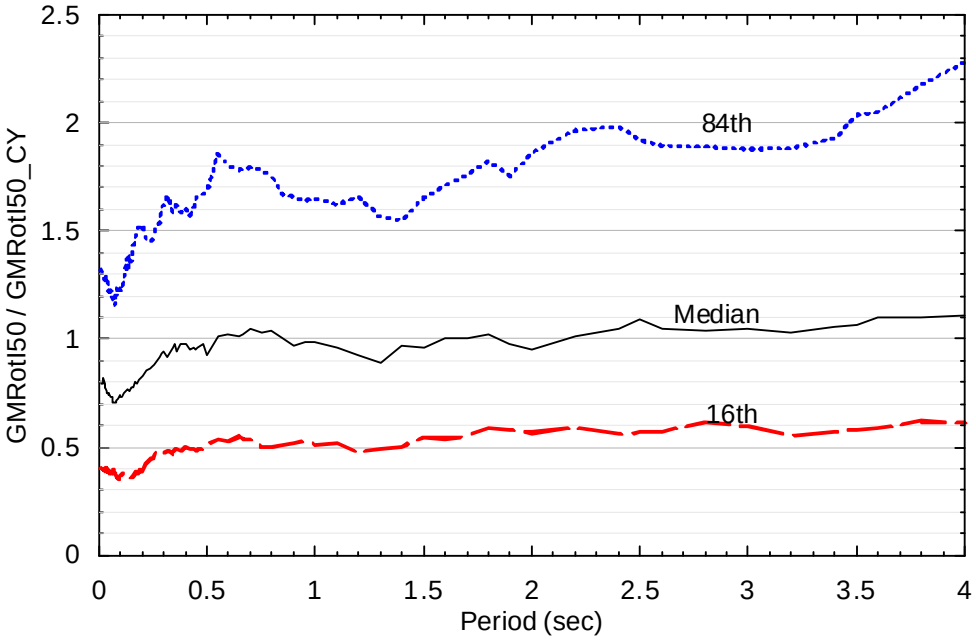

Figure 2-20. Median and 84th and 16th percentiles of the ratios of GMRotI50 to GMRotI50_CY for the records of Table 2-1

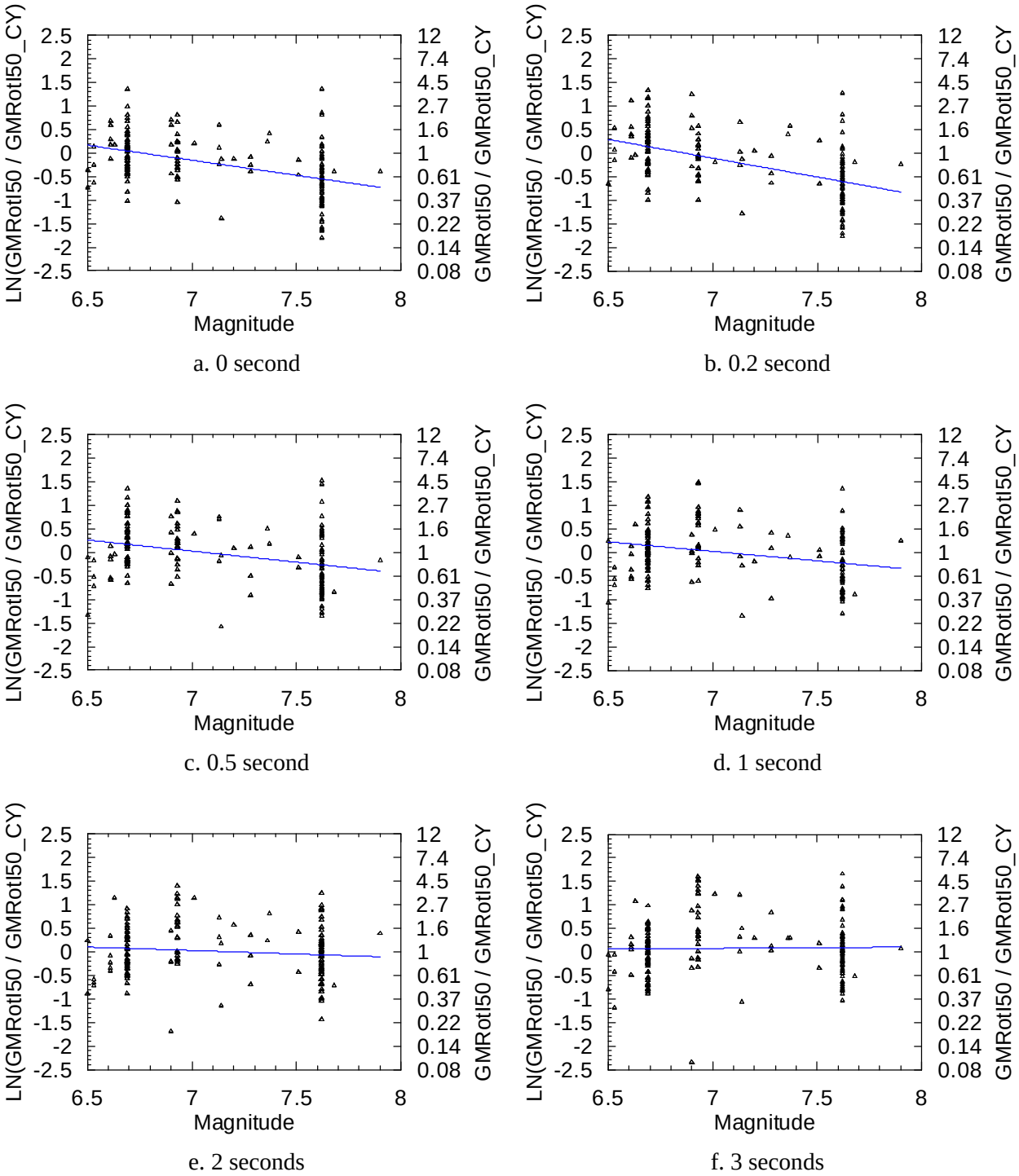

Figure 2-21. Ratios of GMRotI50 to GMRotI50_CY at periods of 0, 0.2, 0.5, 1, 2 and 3 seconds as a function of magnitude for the records of Table 2-1

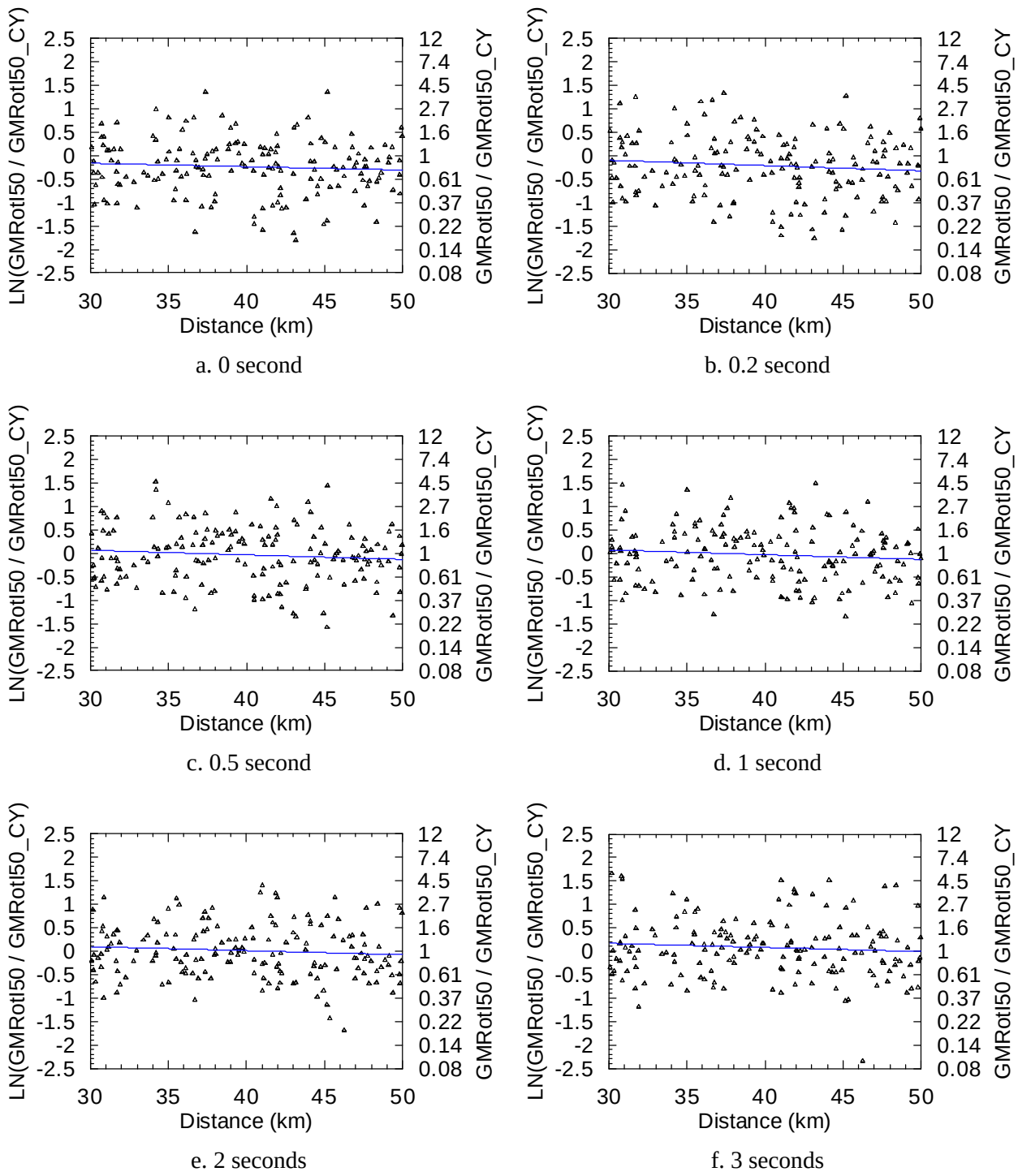

Figure 2-22. Ratios of GMRotI50 to GMRotI50_CY at periods of 0, 0.2, 0.5, 1, 2 and 3 seconds as a function of distance for the records of Table 2-1

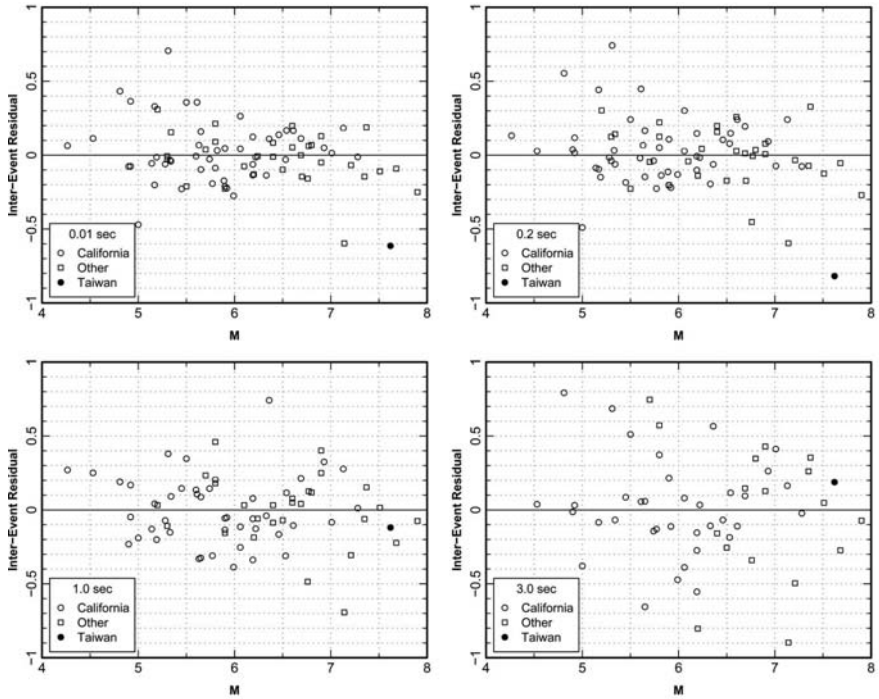

Figure 2-23. Inter-event residuals as a function of magnitude at periods of 0.01, 0.2, 1 and 3 seconds for the NGA C-Y model (after Chiou and Youngs 2008)

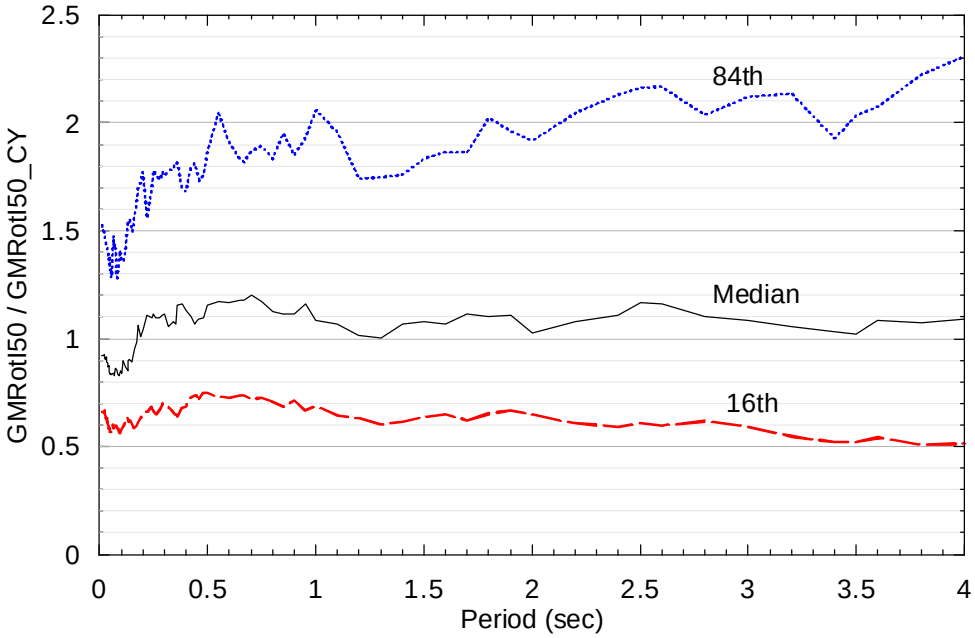

Figure 2-24. Median and 84th and 16th percentiles of the ratios of GMRotI50 to GMRotI50_CY for all of the records of Table 2-1 except those of the 1999 Chi-Chi earthquake

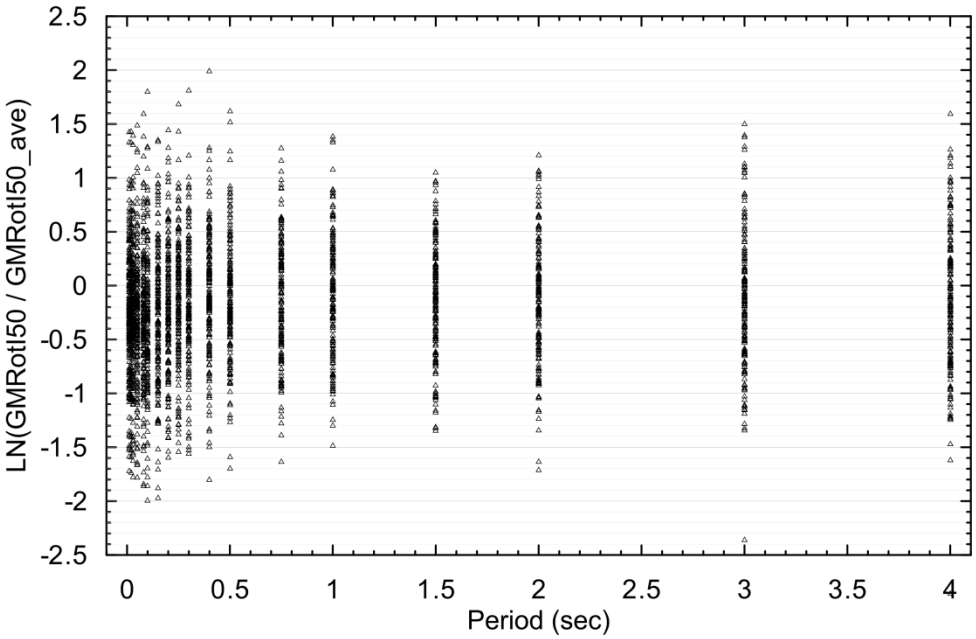

Figure 2-25. Ratios of GMRotI50 to GMRotI50_ave for the records of Table 2-1

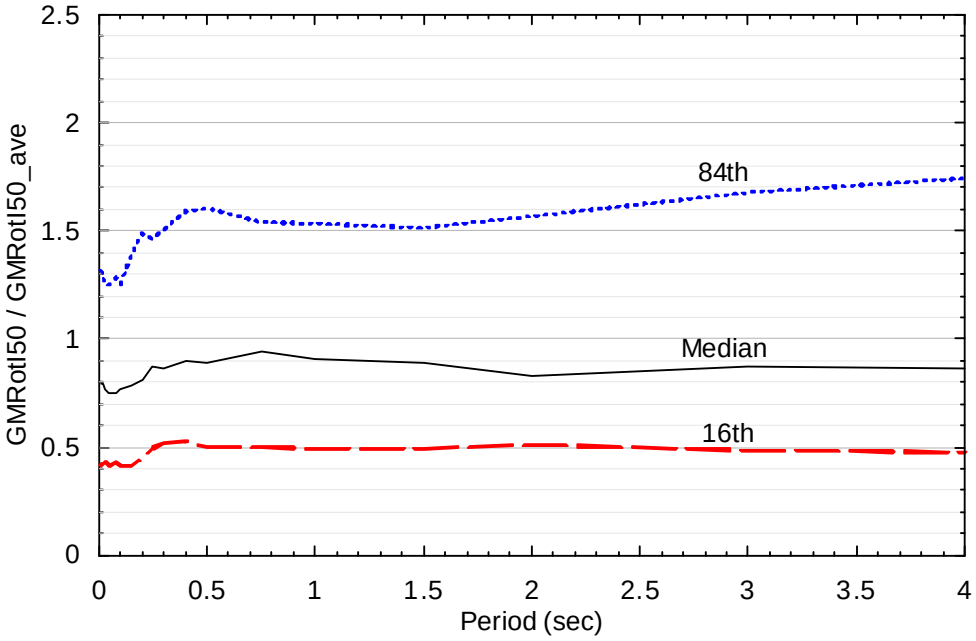

Figure 2-26. Median and 84th and 16th percentiles of the ratios of GMRotI50 to GMRotI50_ave for the records of Table 2-1

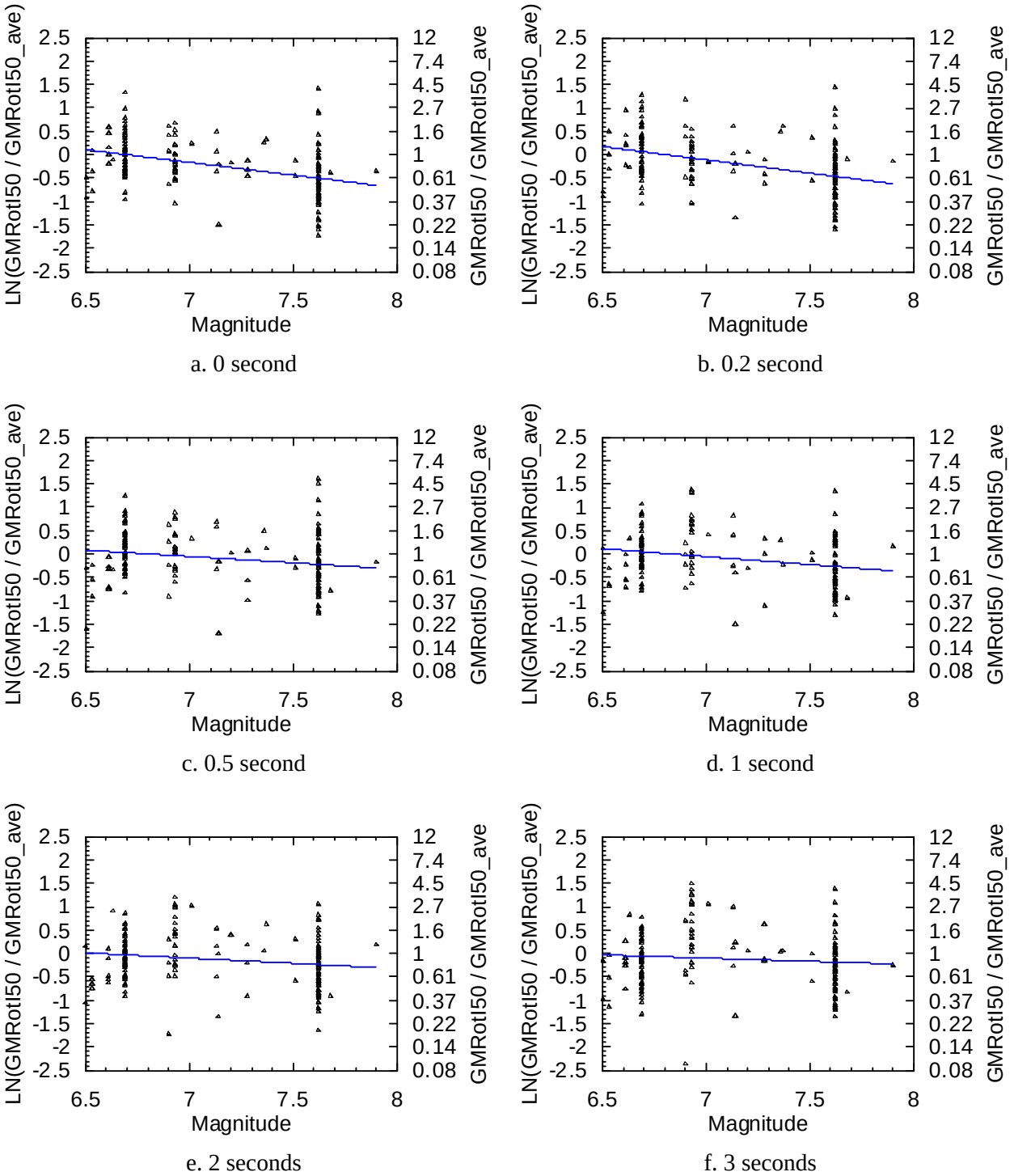

a. 0 second

b. 0.2 second

c. 0.5 second

d. 1 second

e. 2 seconds

f. 3 seconds

Figure 2-27. Ratios of GMRotI50 to GMRotI50_ave at periods of 0, 0.2, 0.5, 1, 2 and 3 seconds as a function of magnitude for the records of Table 2-1

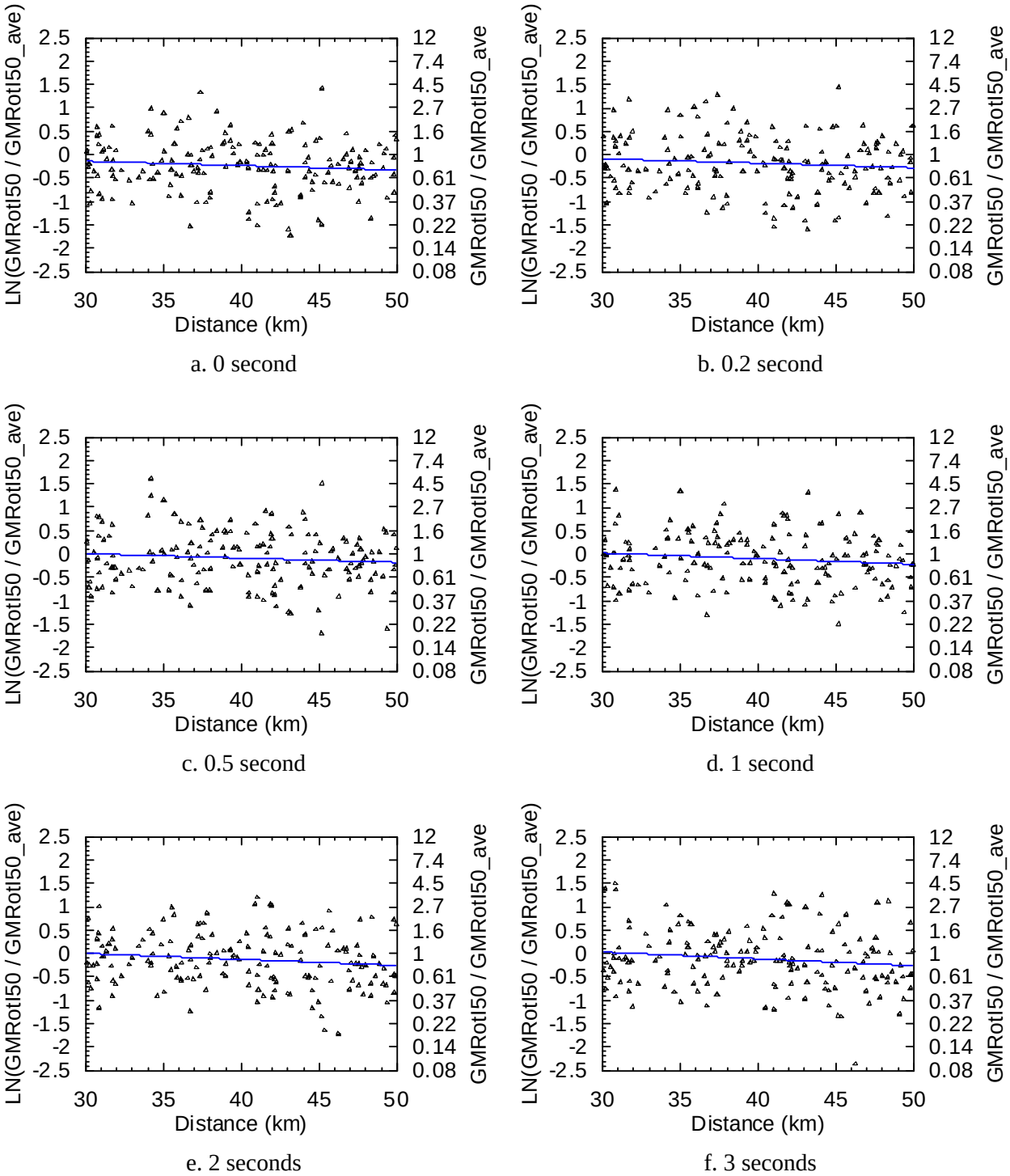

Figure 2-28. Ratios of GMRotI50 to GMRotI50_ave at periods of 0, 0.2, 0.5, 1, 2 and 3 seconds as a function of distance for the records of Table 2-1

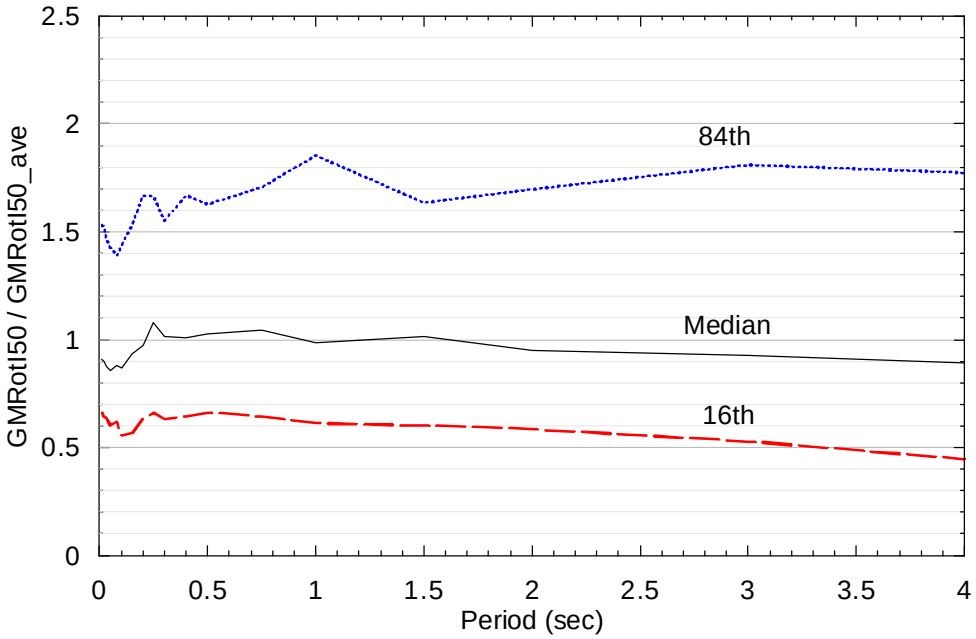

Figure 2-29. Median and 84th and 16th percentiles of the ratios of GMRotI50 to GMRotI50_ave for all of the records of Table 2-1 except those of the 1999 Chi-Chi earthquake

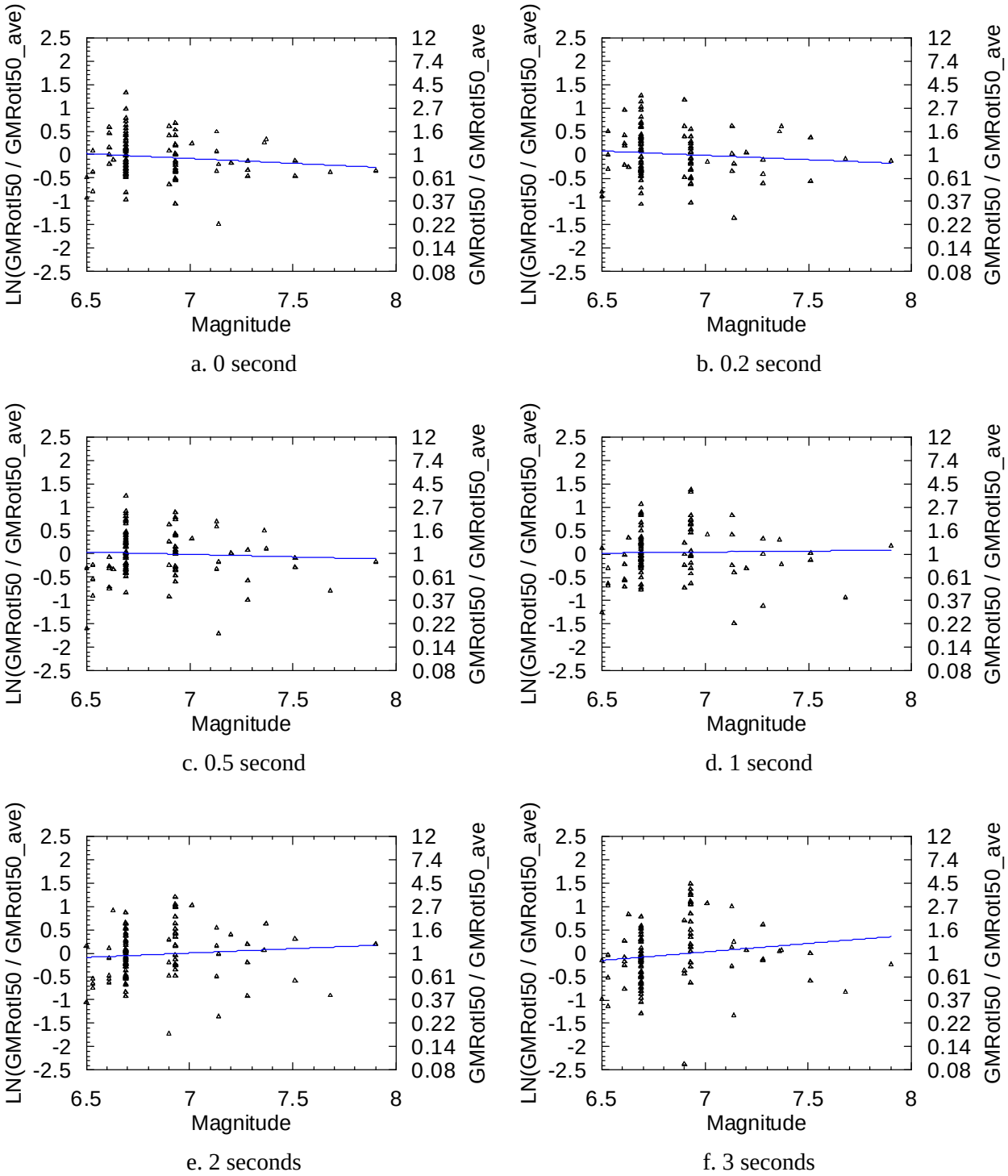

Figure 2-30. Ratios of GMRotI50 to GMRotI50_ave at periods of 0, 0.2, 0.5, 1, 2 and 3 seconds as a function of magnitude for all of the records of Table 2-1 except those of the 1999 Chi-Chi earthquake

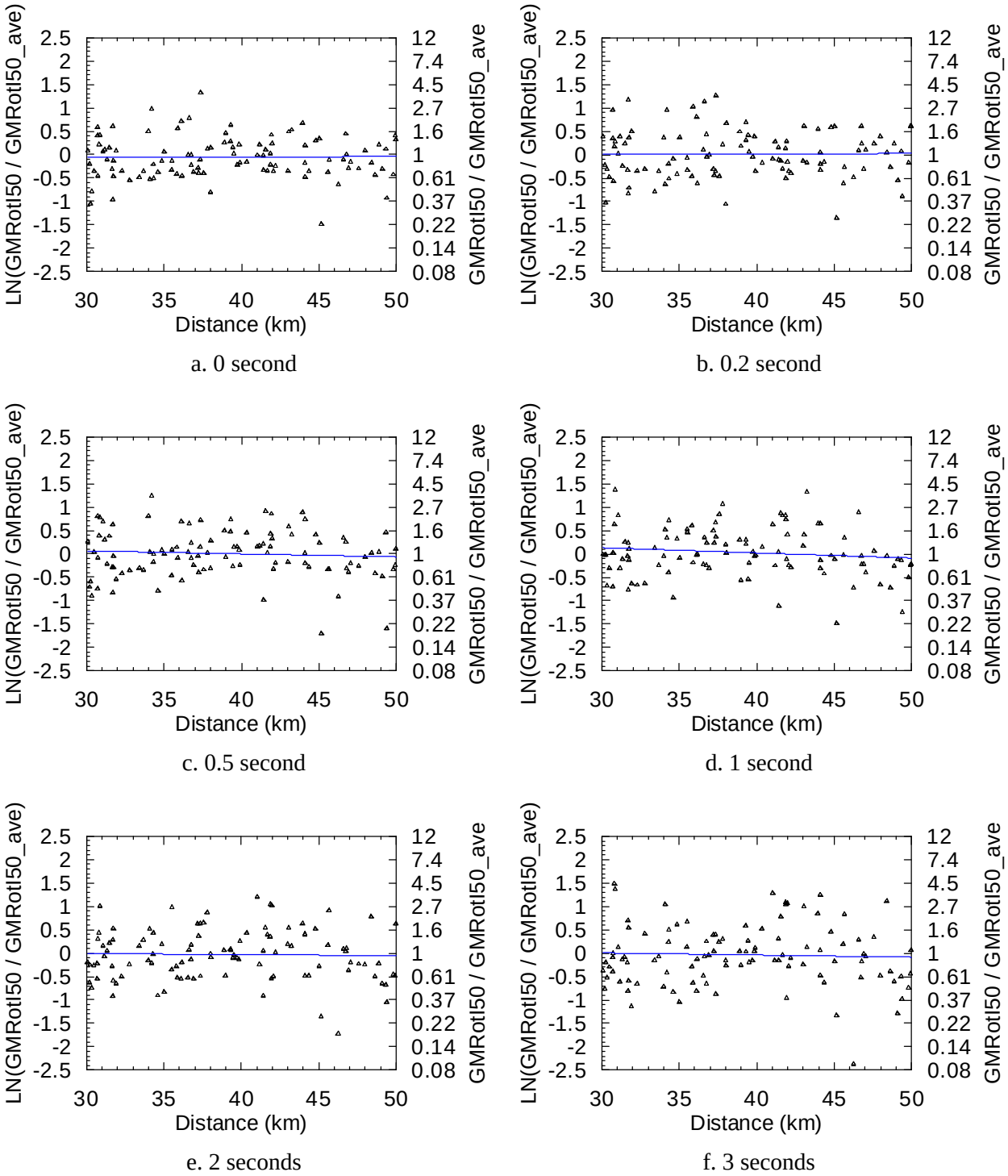

Figure 2-31. Ratios of GMRotI50 to GMRotI50_ave at periods of 0, 0.2, 0.5, 1, 2 and 3 seconds as a function of distance for all of the records of Table 2-1 except those of the 1999 Chi-Chi earthquake

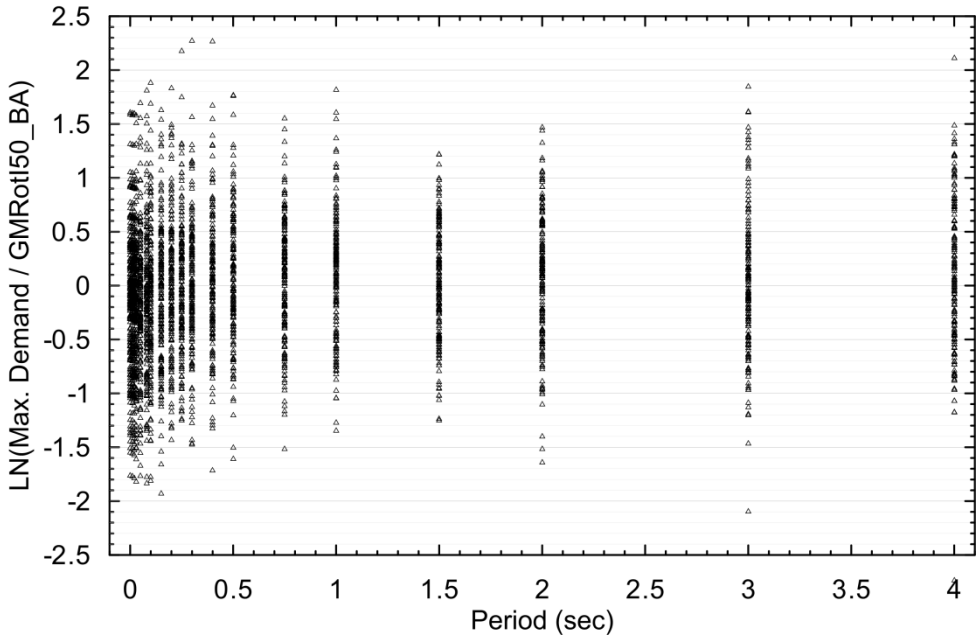

Figure 2-32. Ratios of maximum spectral demand to GMRotI50_BA for the records of Table 2-1

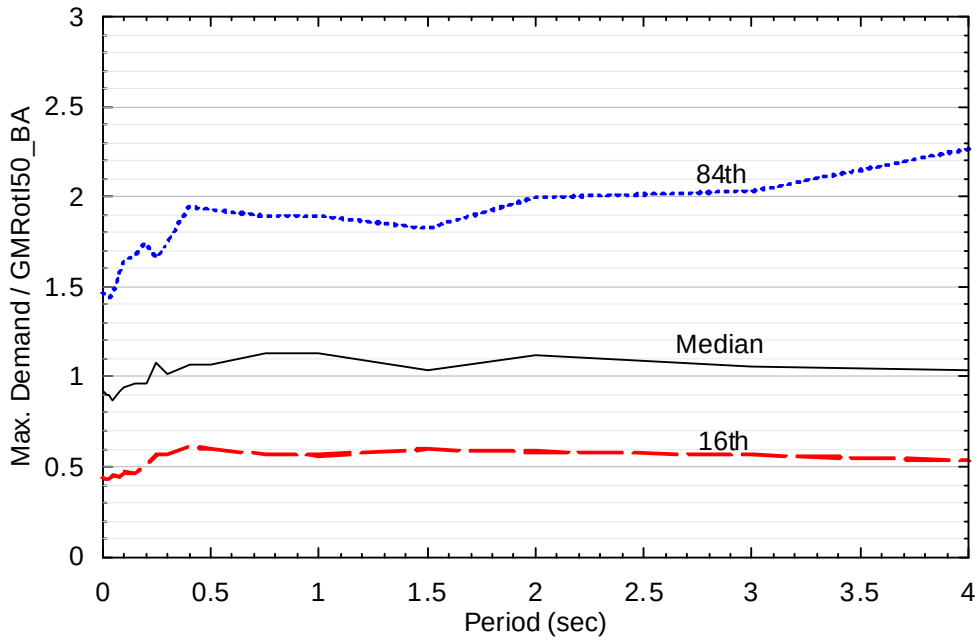

Figure 2-33. Median and 84th and 16th percentiles of the ratios of maximum spectral demand to GMRotI50_BA for the records of Table 2-1

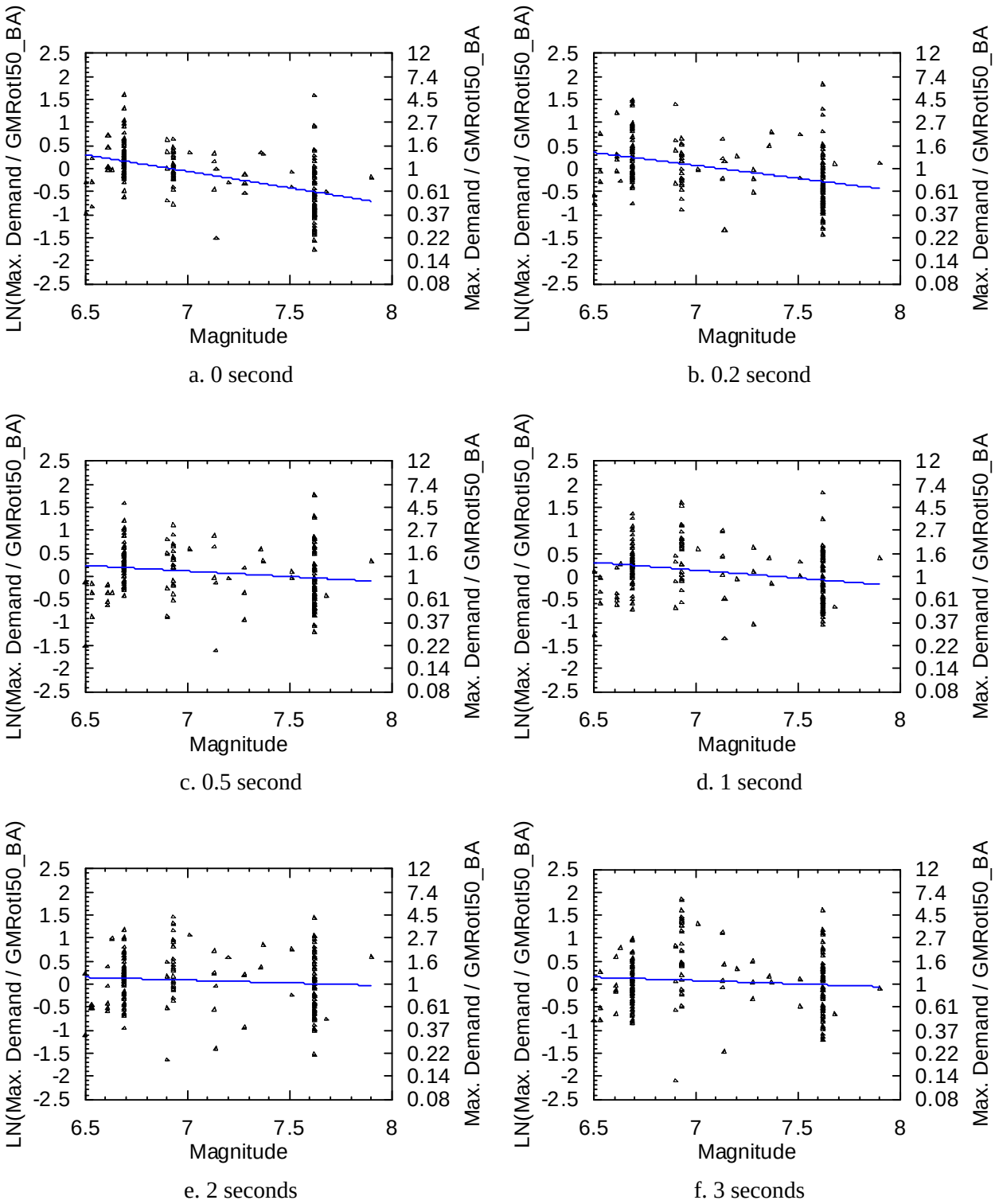

Figure 2-34. Ratios of maximum spectral demand to GMRotI50_BA at periods of 0, 0.2, 0.5, 1, 2 and 3 seconds as a function of magnitude for the records of Table 2-1

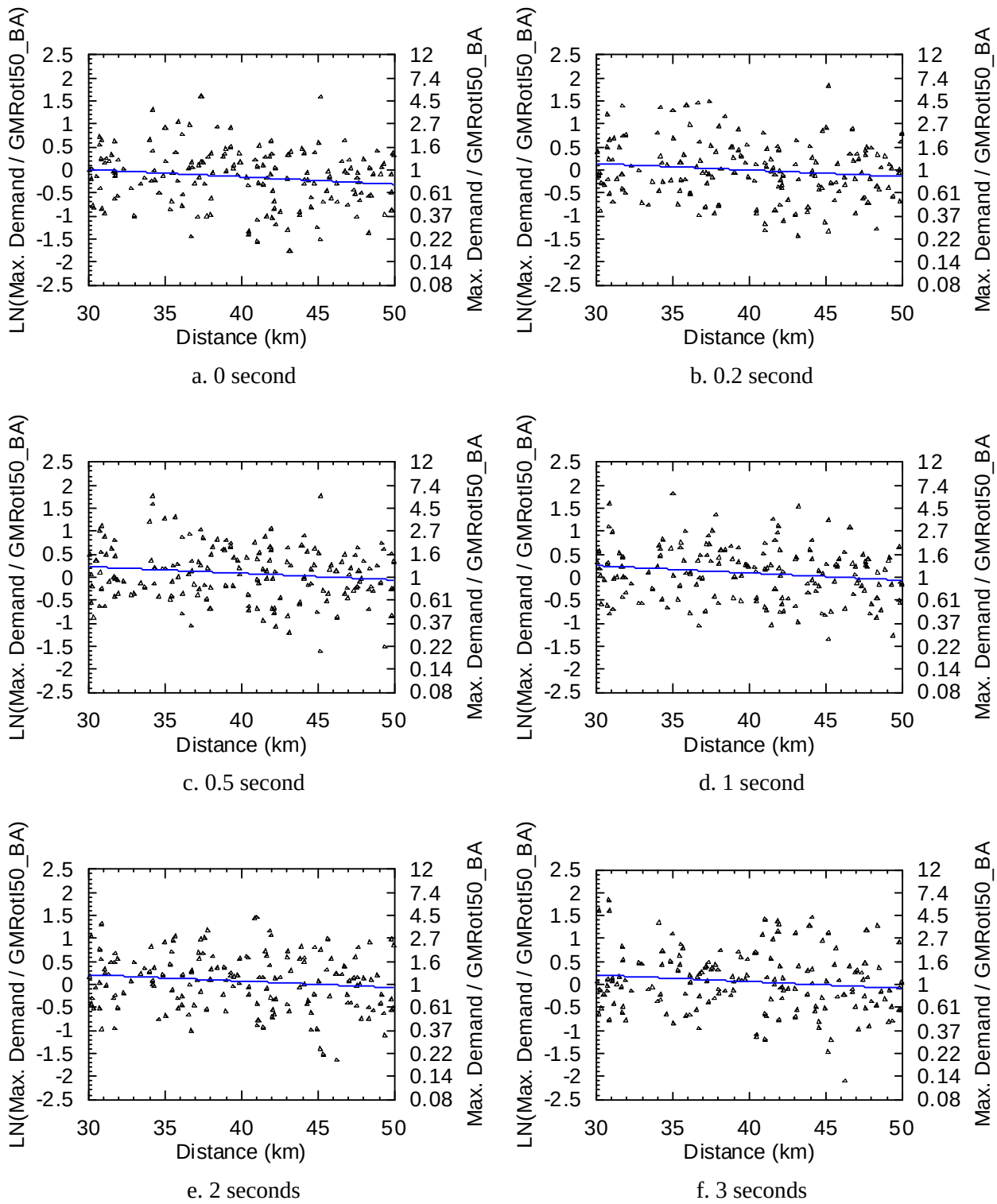

Figure 2-35. Ratios of maximum spectral demand to GMRotI50_BA at periods of 0, 0.2, 0.5, 1, 2 and 3 seconds as a function of distance for the records of Table 2-1

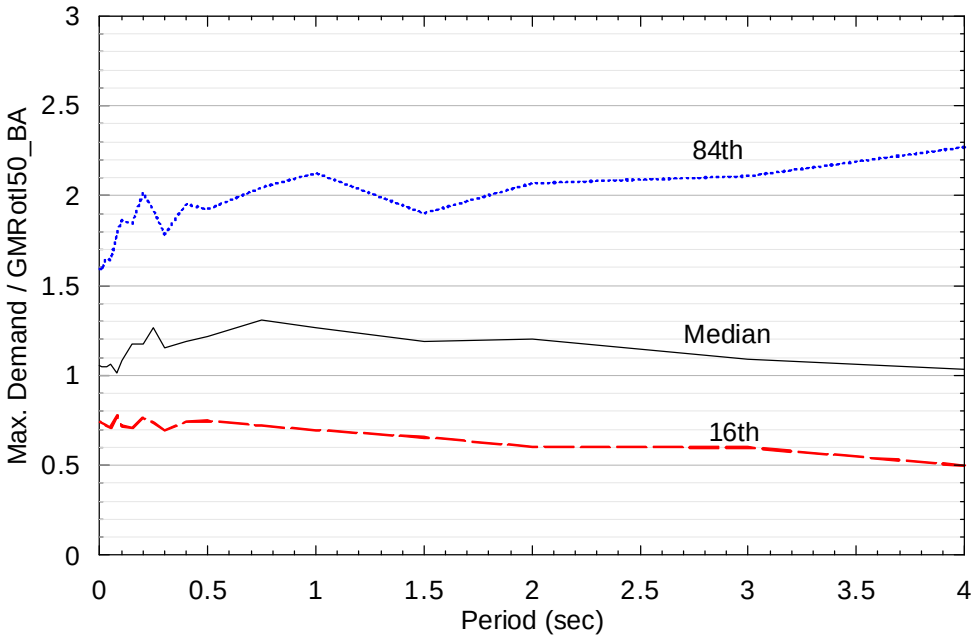

Figure 2-36. Median and 84th and 16th percentiles of the ratios of maximum spectral demand to GMRotI50_BA for all of the records of Table 2-1 except those of the 1999 Chi-Chi earthquake

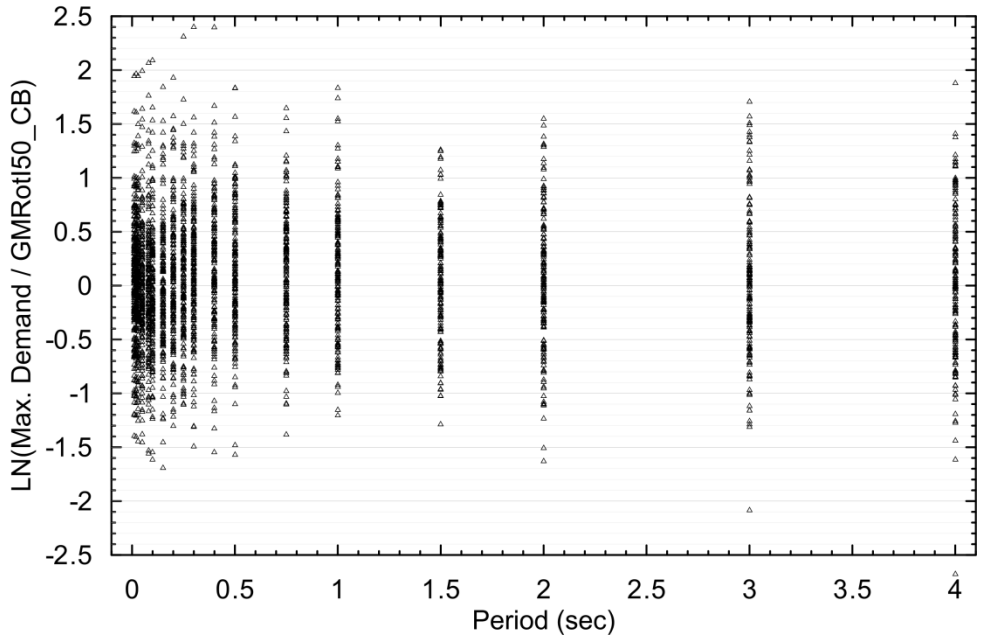

Figure 2-37. Ratios of maximum spectral demand to GMRotI50_CB for the records of Table 2-1

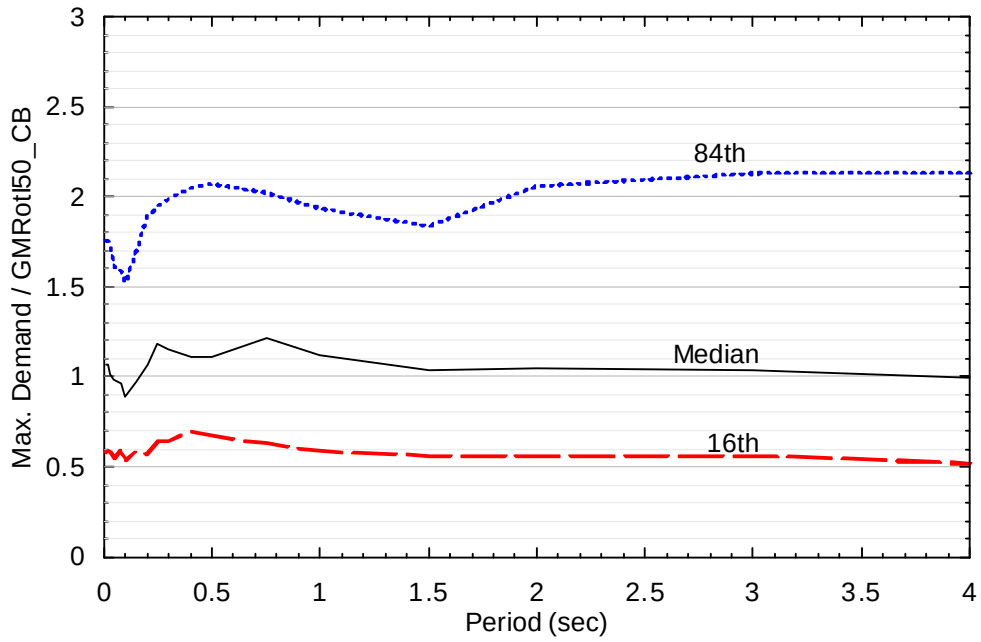

Figure 2-38. Median and 84th and 16th percentiles of the ratios of maximum spectral demand to GMRotI50_CB for the records of Table 2-1

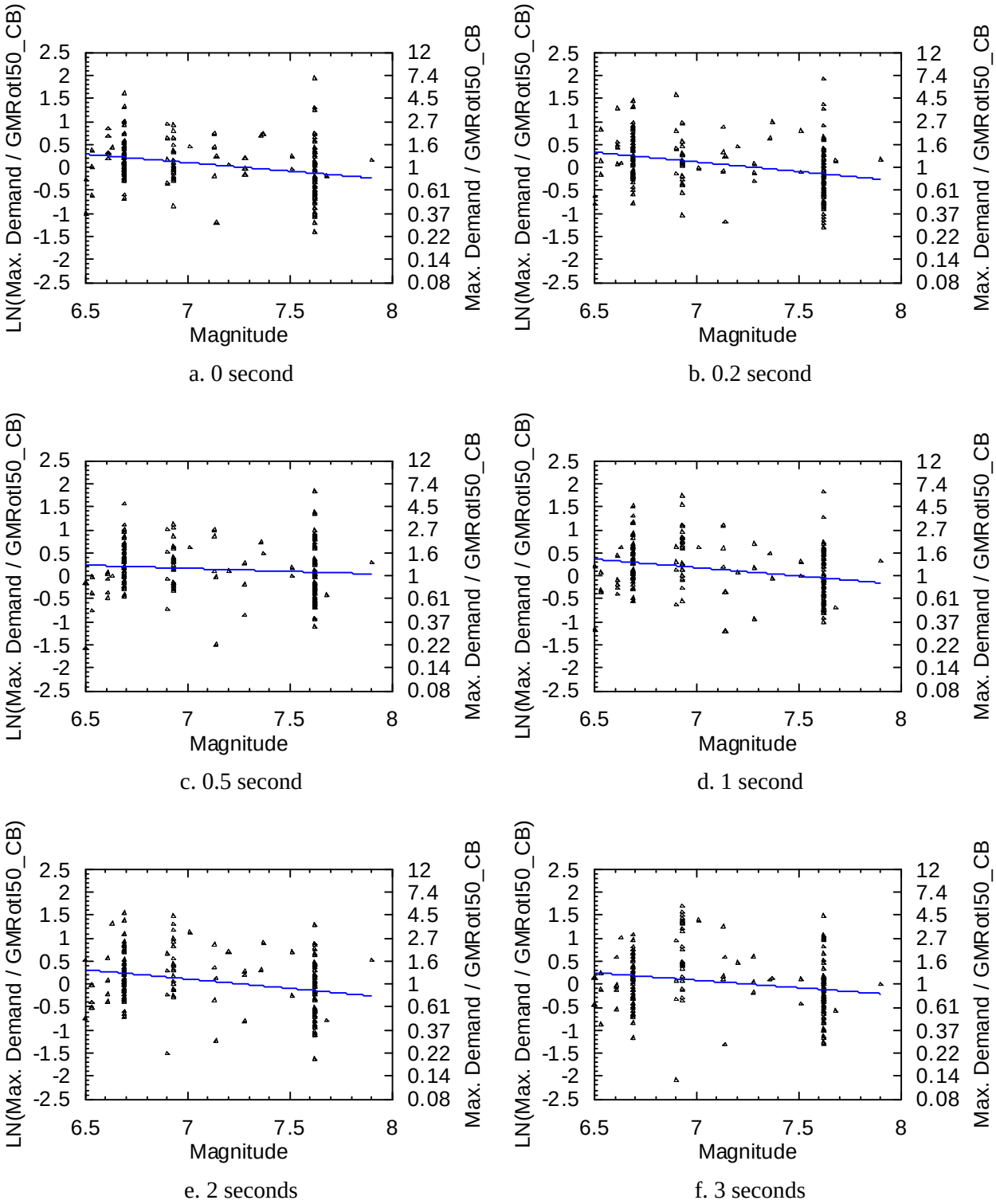

Figure 2-39. Ratios of maximum spectral demand to GMRotI50_CB at periods of 0, 0.2, 0.5, 1, 2 and 3 seconds as a function of magnitude for the records of Table 2-1

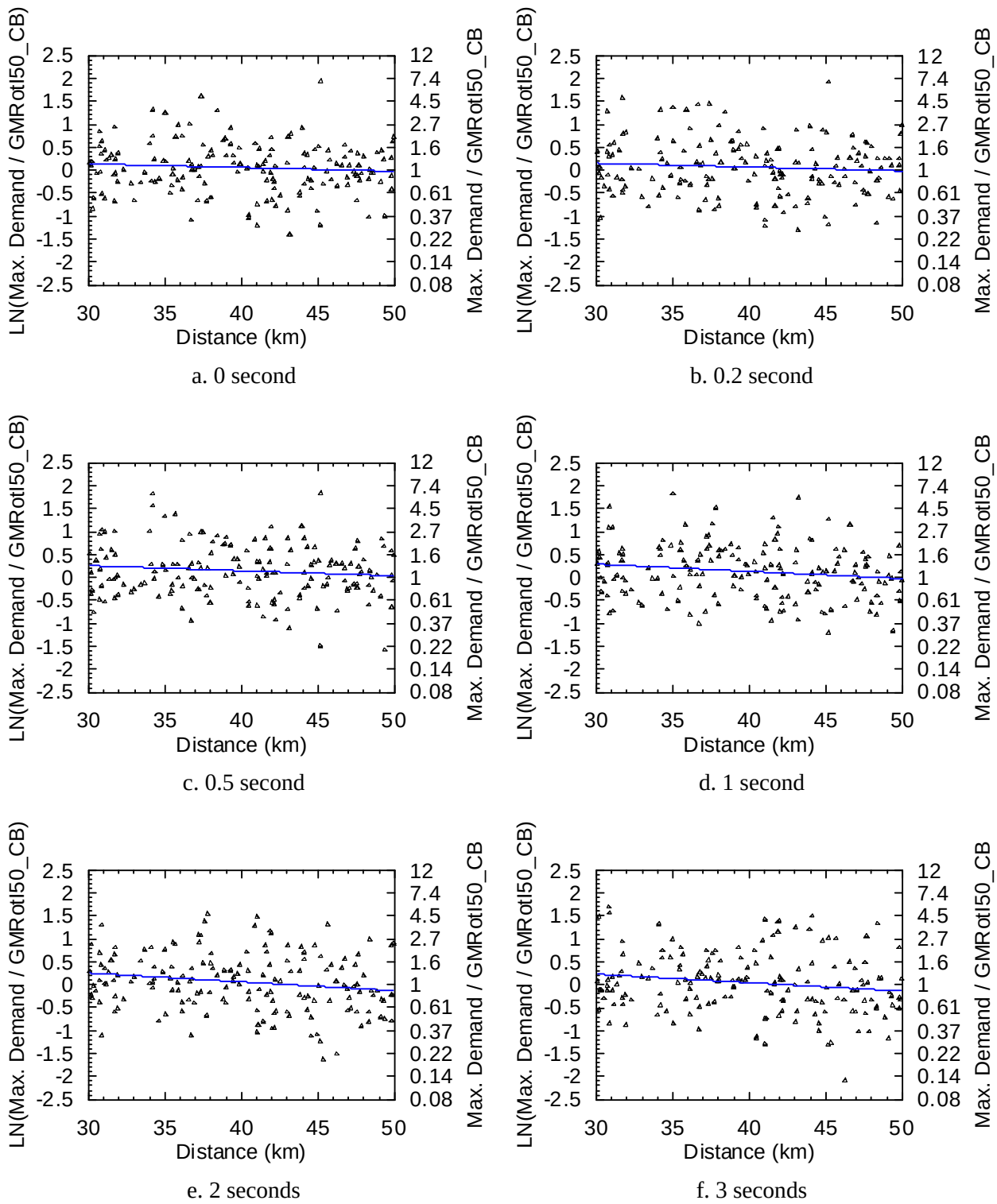

Figure 2-40. Ratios of maximum spectral demand to GMRotI50_CB at periods of 0, 0.2, 0.5, 1, 2 and 3 seconds as a function of distance for the records of Table 2-1

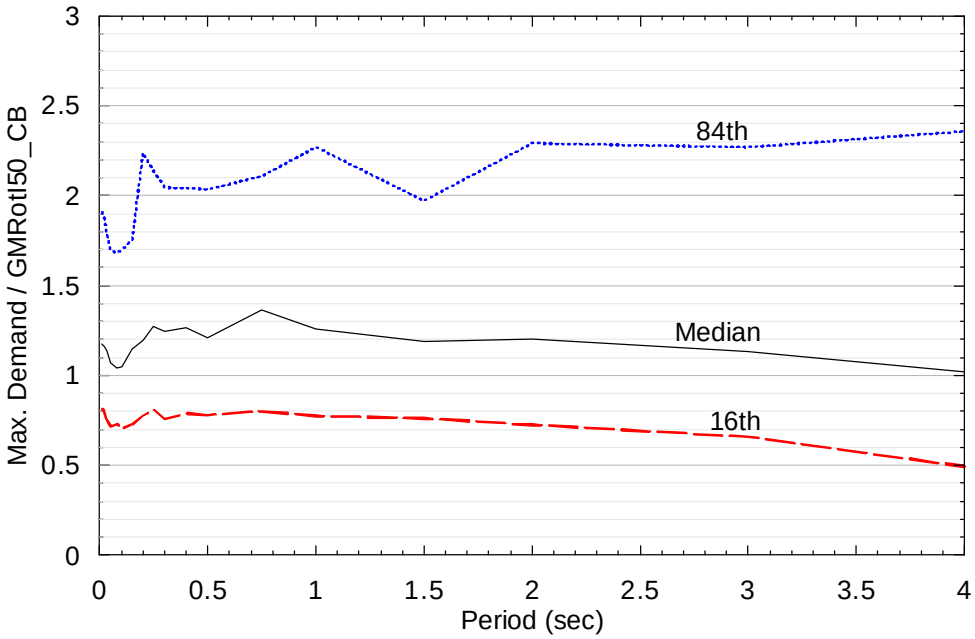

Figure 2-41. Median and 84th and 16th percentiles of the ratios of maximum spectral demand to GMRotI50_CB for all of the records of Table 2-1 except those of the 1999 Chi-Chi earthquake

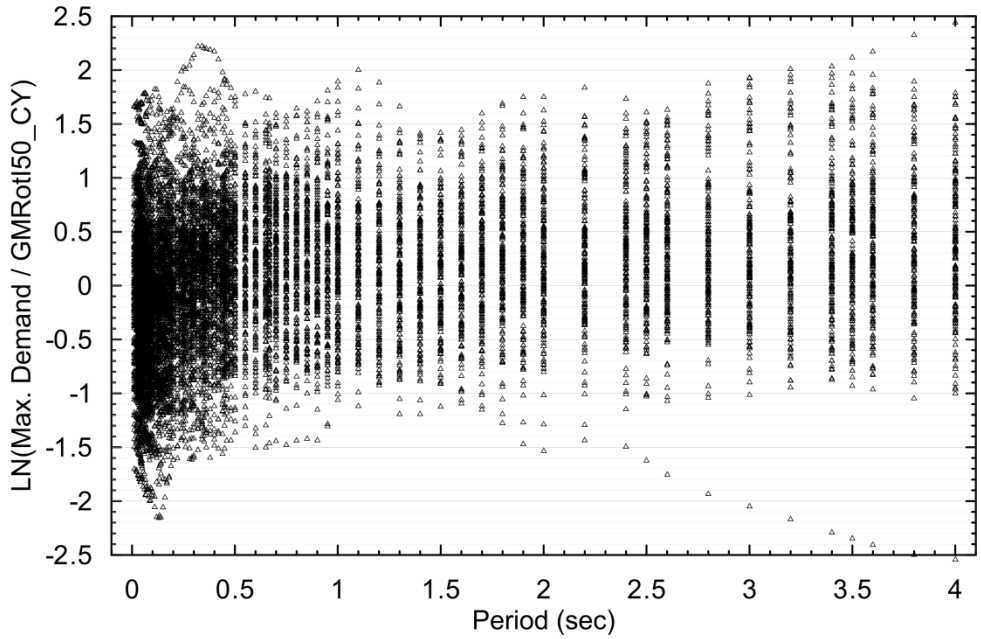

Figure 2-42. Ratios of maximum spectral demand to GMRotI50_CY for the records of Table 2-1

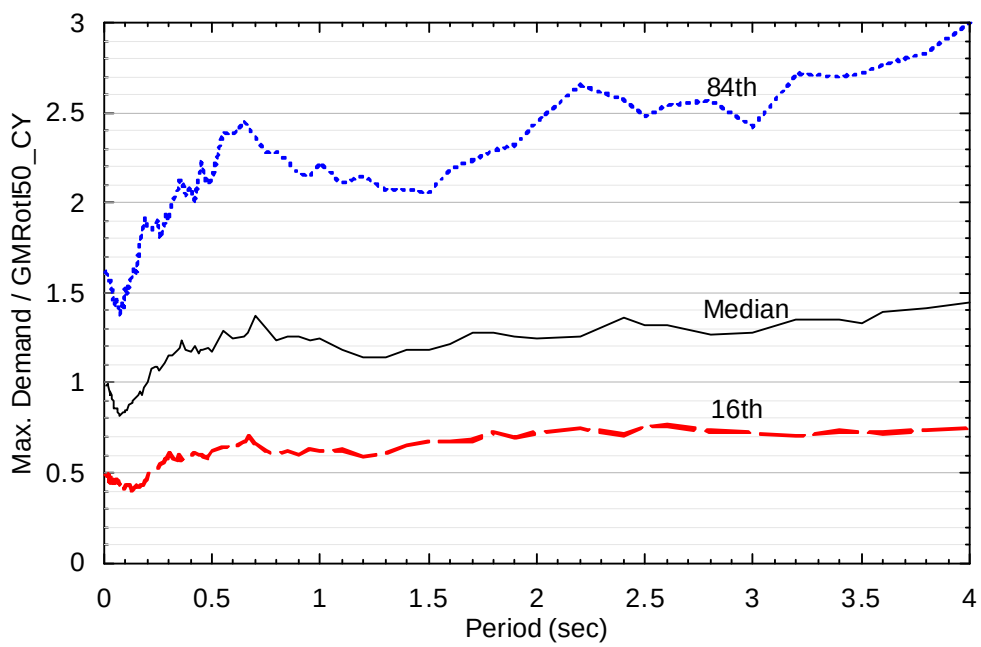

Figure 2-43. Median and 84th and 16th percentiles of the ratios of maximum spectral demand to GMRotI50_CY for the records of Table 2-1

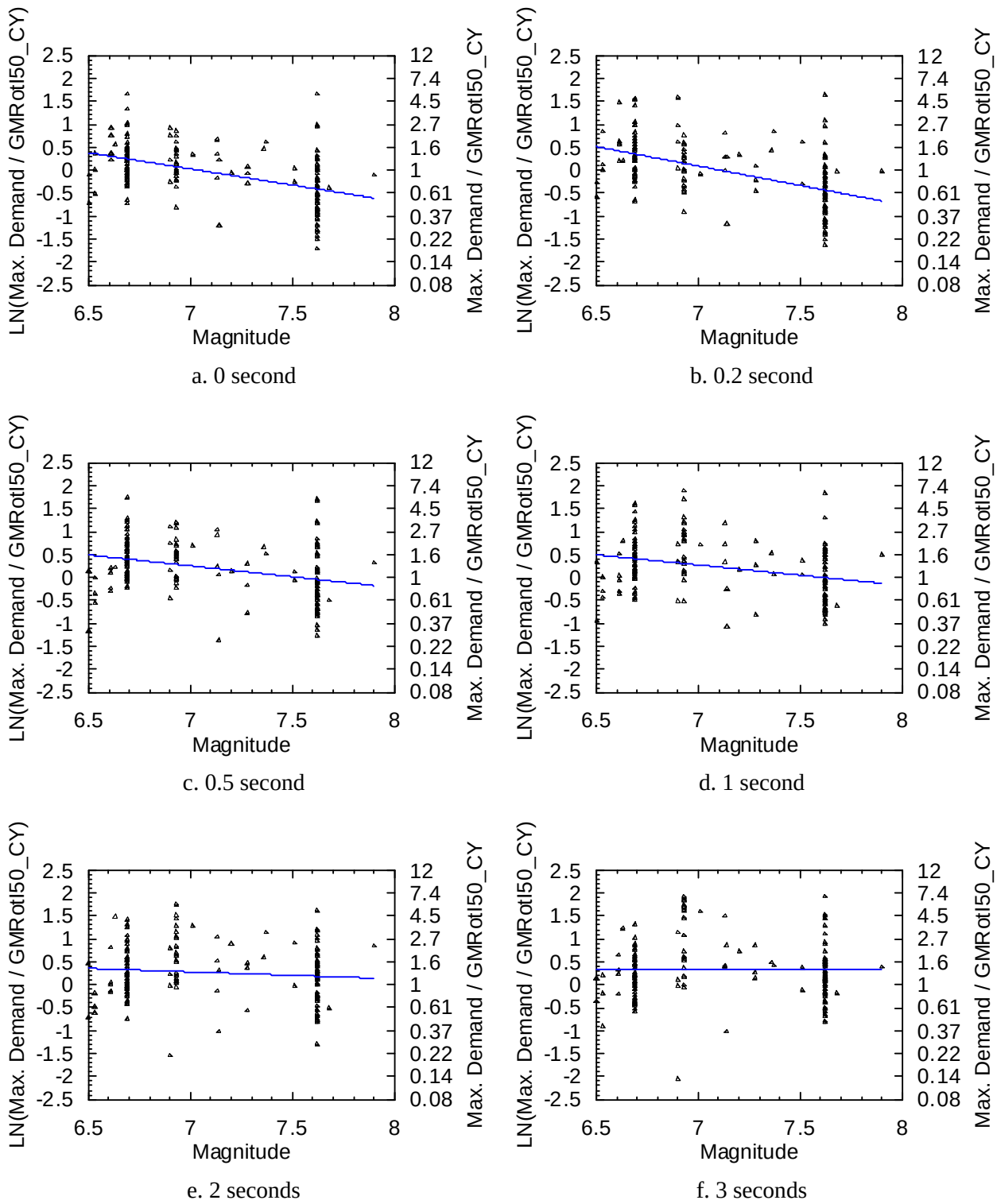

Figure 2-44. Ratios of maximum spectral demand to GMRotI50_CY at periods of 0, 0.2, 0.5, 1, 2 and 3 seconds as a function of magnitude for the records of Table 2-1

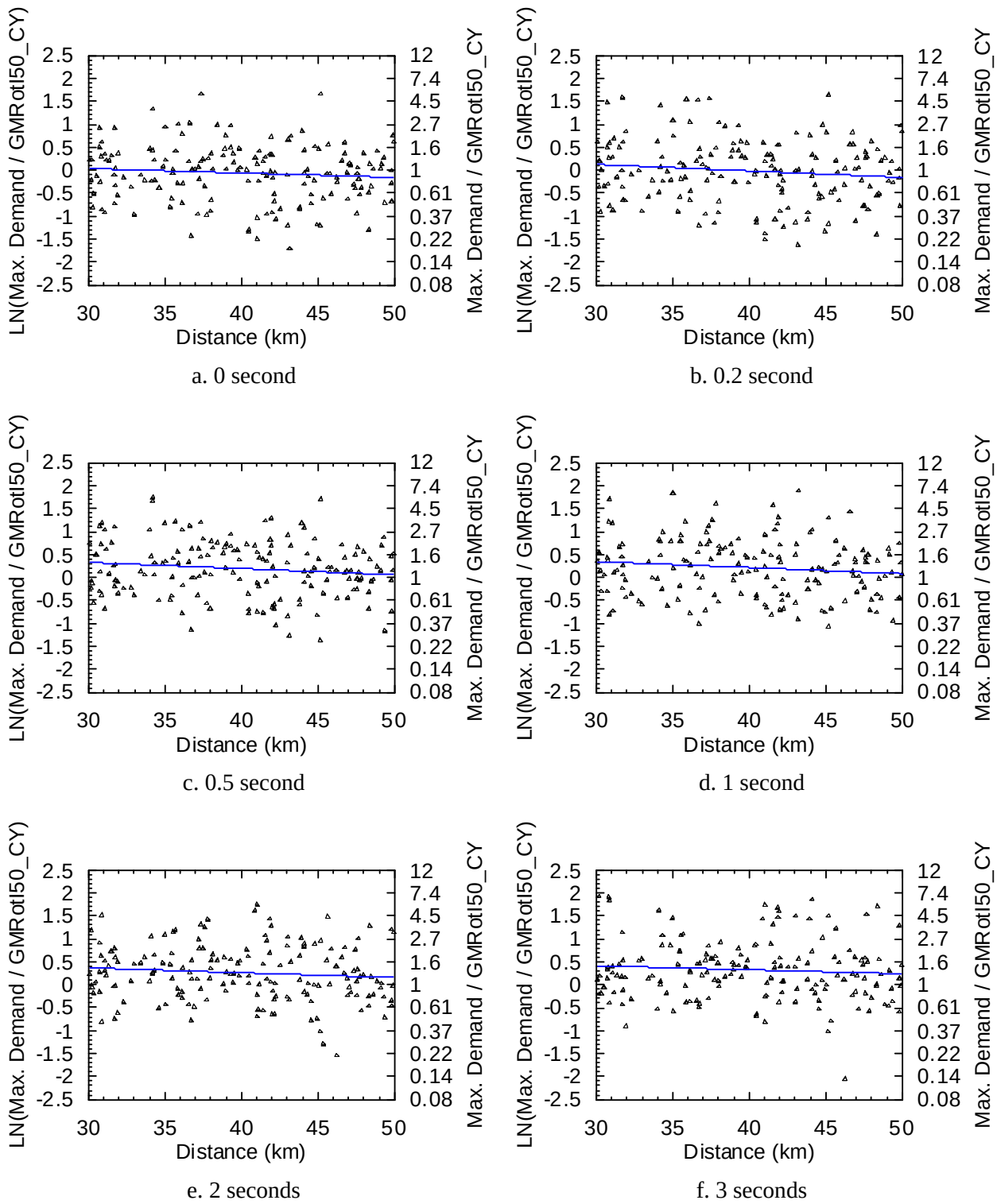

Figure 2-45. Ratios of maximum spectral demand to GMRotI50_CY at periods of 0, 0.2, 0.5, 1, 2 and 3 seconds as a function of distance for the records of Table 2-1

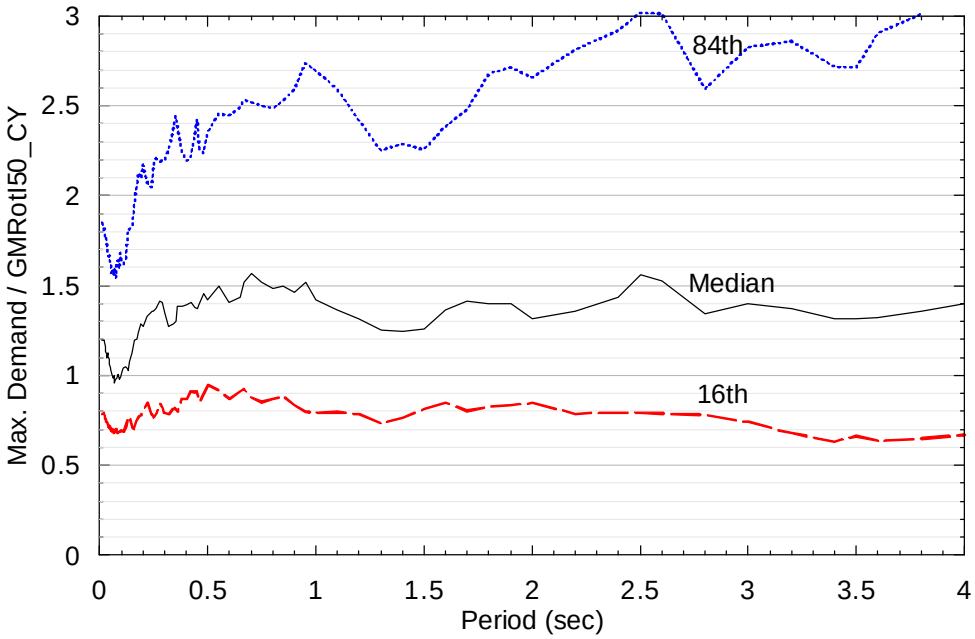

Figure 2-46. Median and 84th and 16th percentiles of the ratios of maximum spectral demand to GMRotI50_CY for all of the records of Table 2-1 except those of the 1999 Chi-Chi earthquake

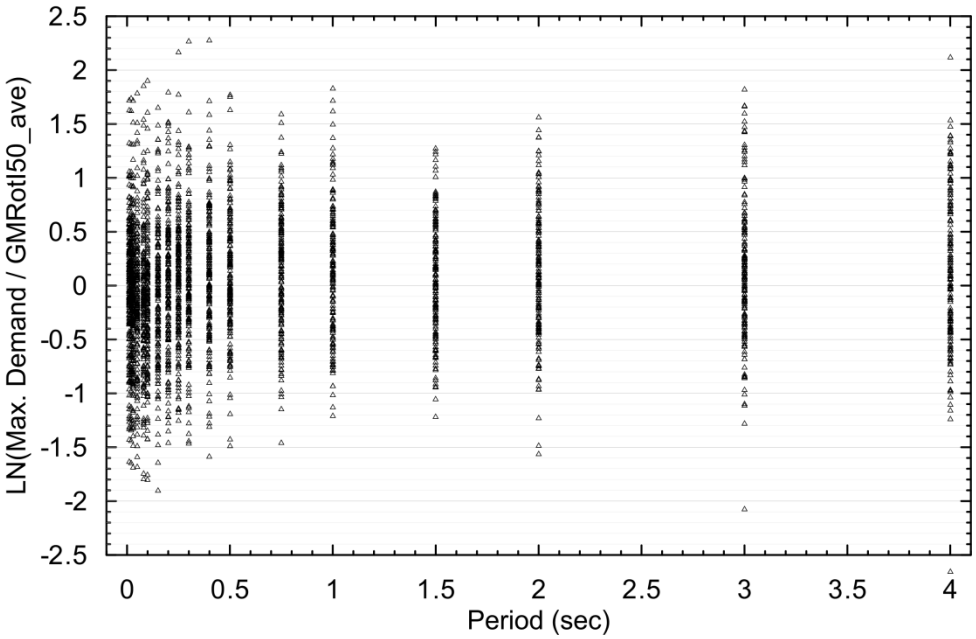

Figure 2-47. Ratios of maximum spectral demand to GMRotI50_ave for the records of Table 2-1

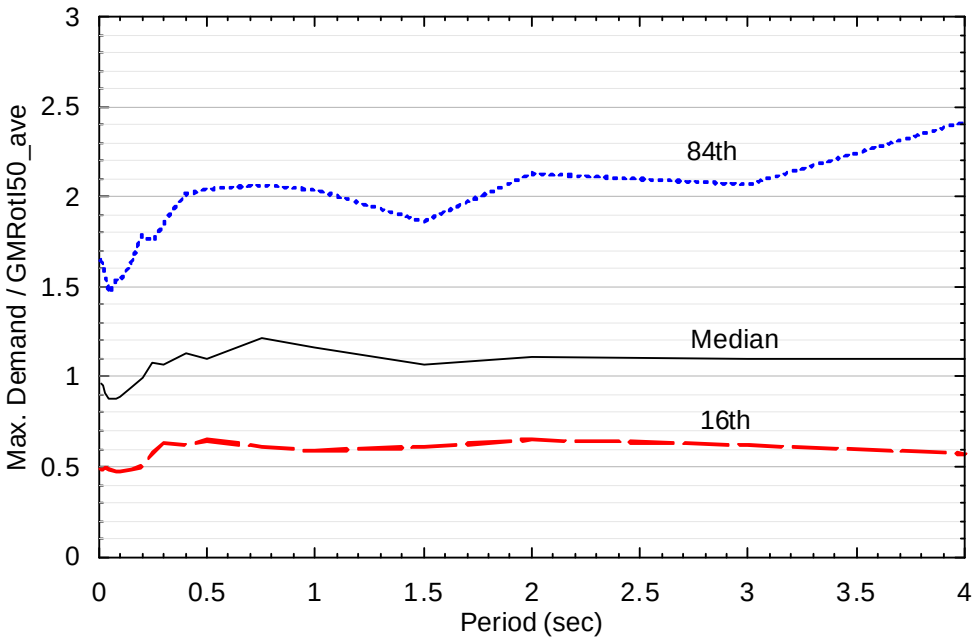

Figure 2-48. Median and 84th and 16th percentiles of the ratios of maximum spectral demand to GMRotI50_ave for the records of Table 2-1

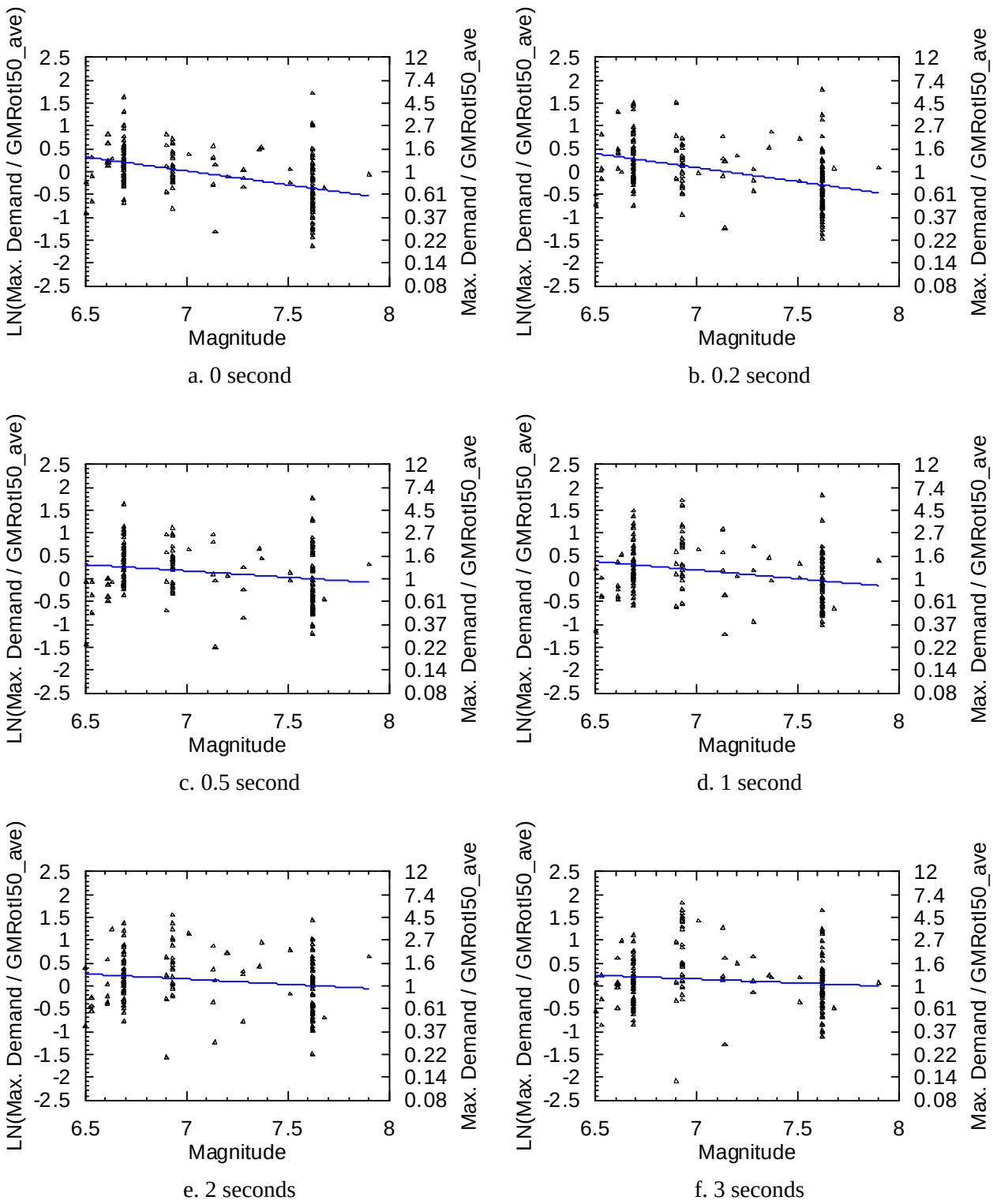

a. 0 second

b. 0.2 second

c. 0.5 second

d. 1 second

e. 2 seconds

f. 3 seconds

Figure 2-49. Ratios of maximum spectral demand to GMRotI50_ave at periods of 0, 0.2, 0.5, 1, 2 and 3 seconds as a function of magnitude for the records of Table 2-1

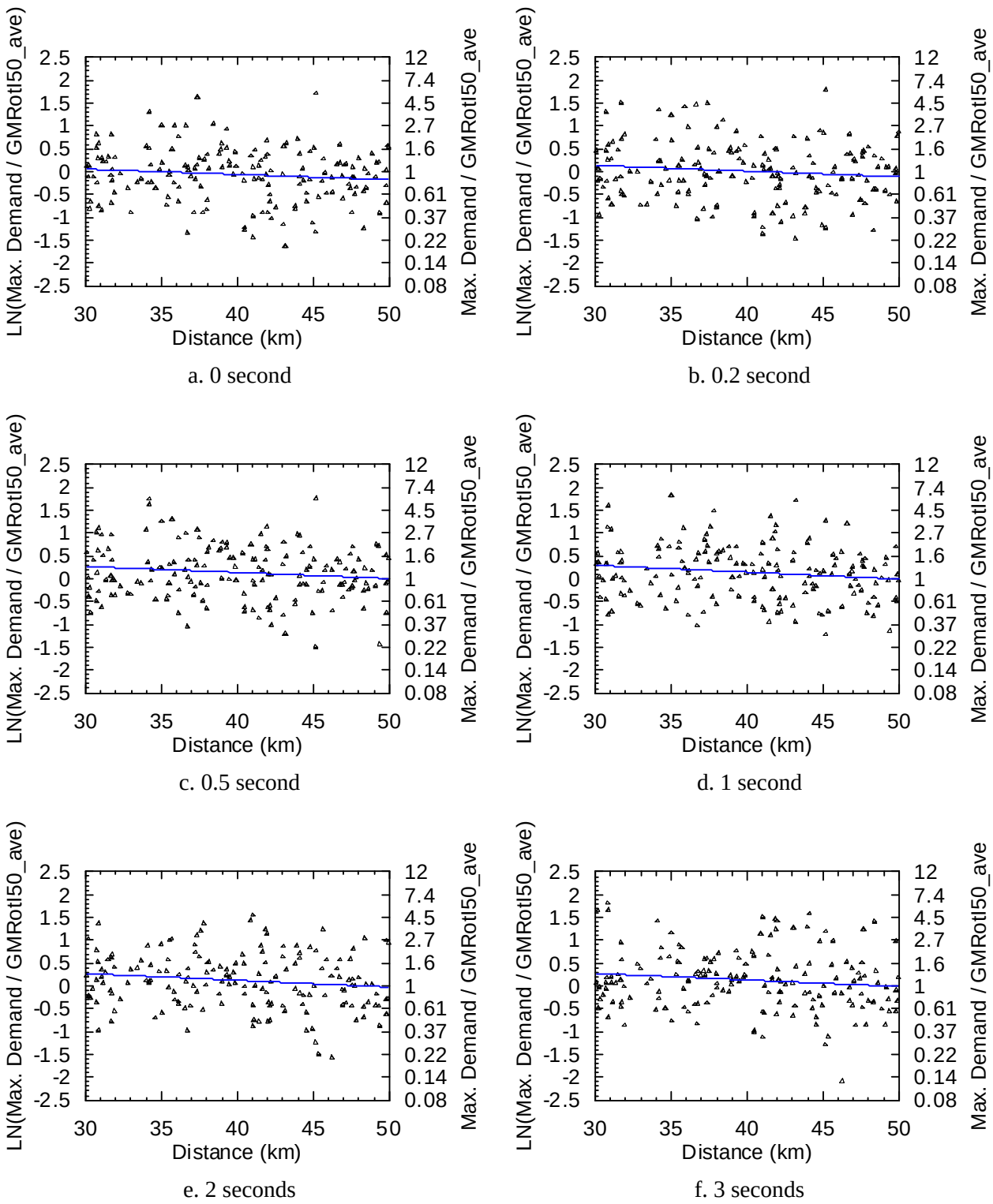

Figure 2-50. Ratios of maximum spectral demand to GMRotI50_ave at periods of 0, 0.2, 0.5, 1, 2 and 3 seconds as a function of distance for the records of Table 2-1

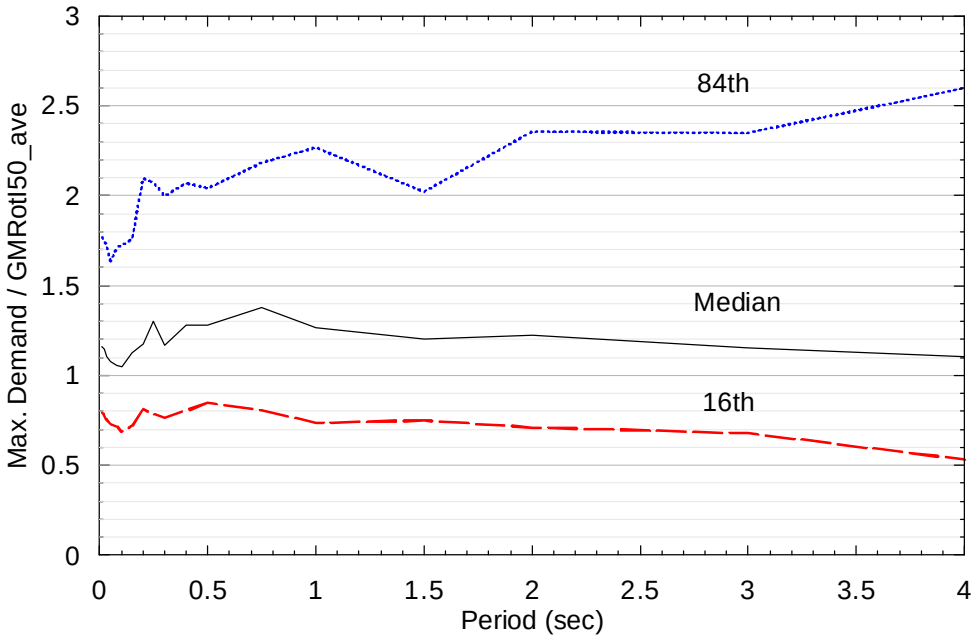

Figure 2-51. Median and 84th and 16th percentiles of the ratios of maximum spectral demand to GMRotI50_ave for all of the records of Table 2-1 except those of the 1999 Chi-Chi earthquake

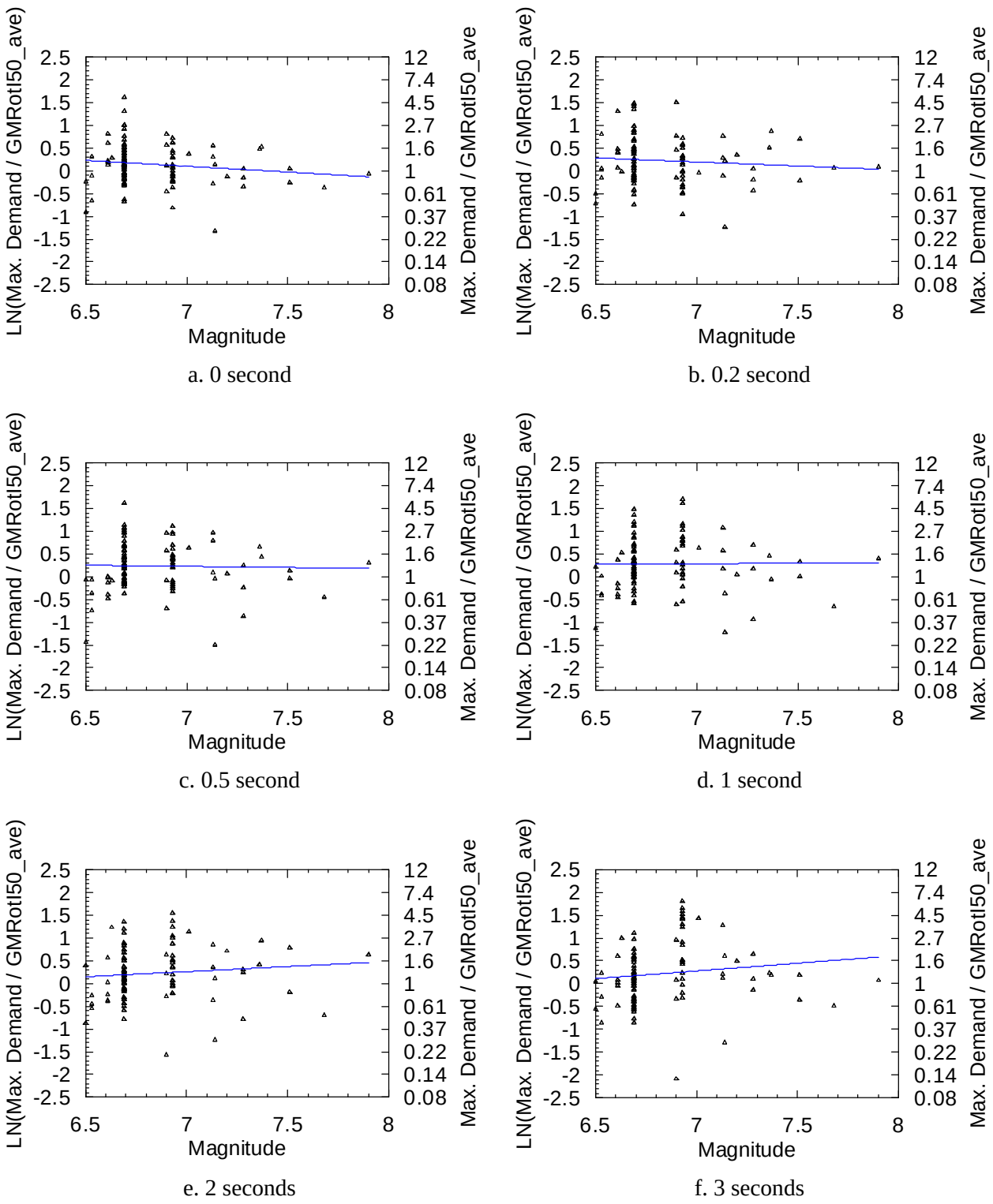

Figure 2-52. Ratios of maximum spectral demand to GMRotI50_ave at sample periods as a function of magnitude for all of the records of Table 2-1 except those of the Chi-Chi earthquake

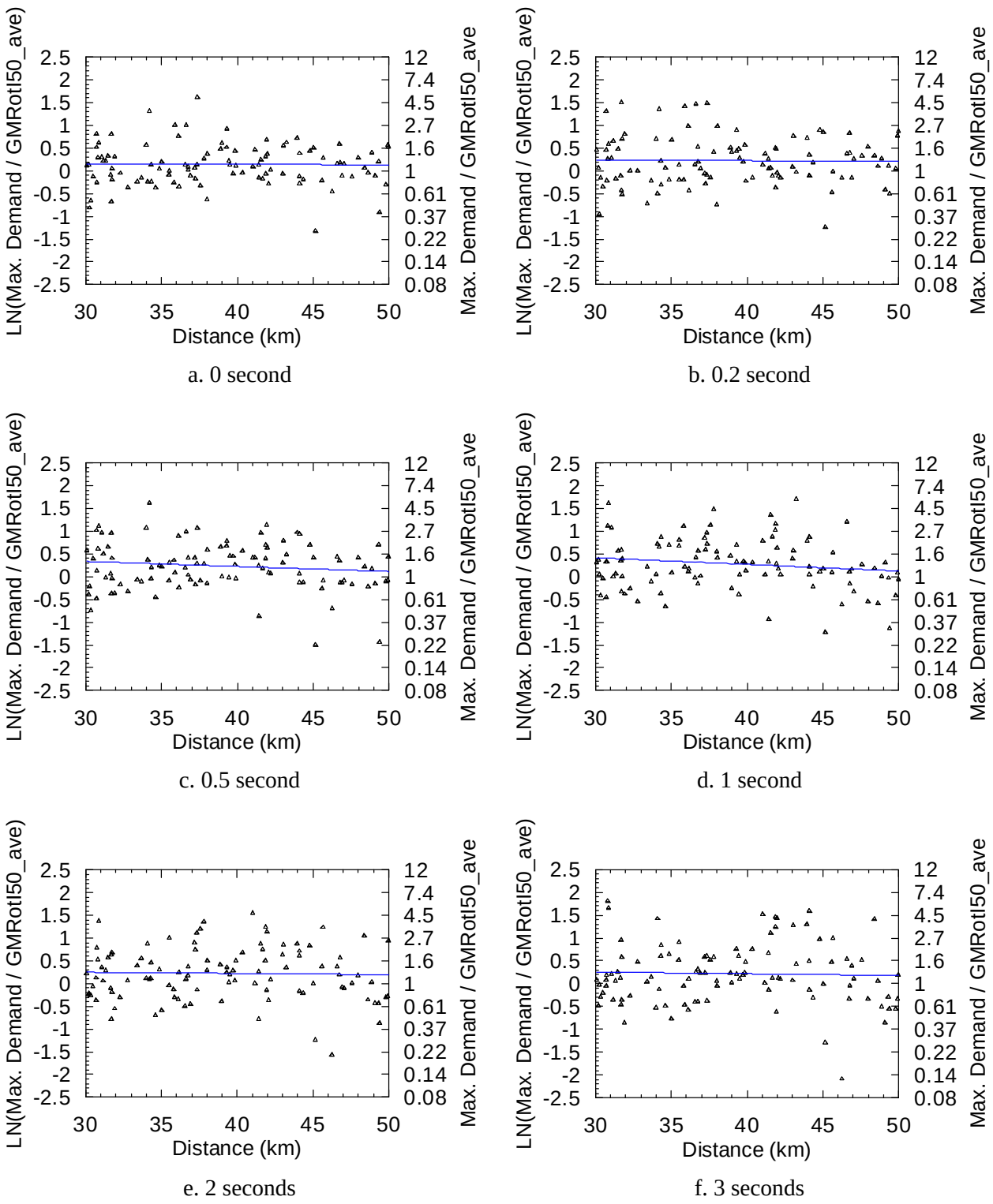

Figure 2-53. Ratios of maximum spectral demand to GMRotI50_ave at sample periods as a function of distance for all of the records of Table 2-1 except those of the Chi-Chi earthquake

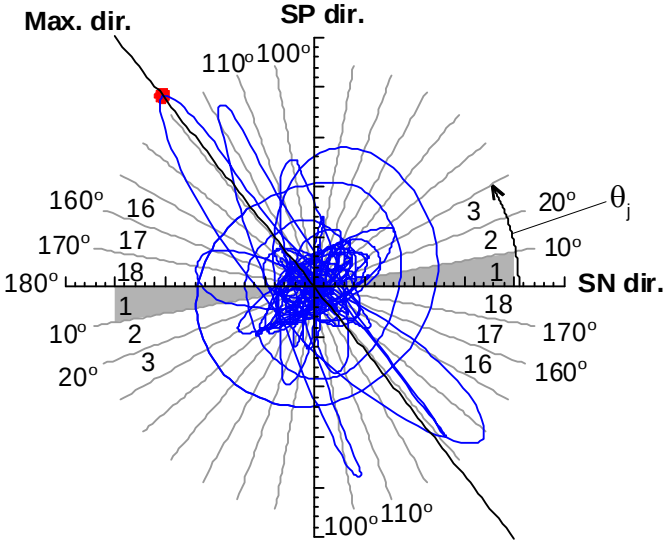

Figure 2-54. Acceleration orbit of a 2-degree-of-freedom oscillator used to compute the maximum shaking orientation

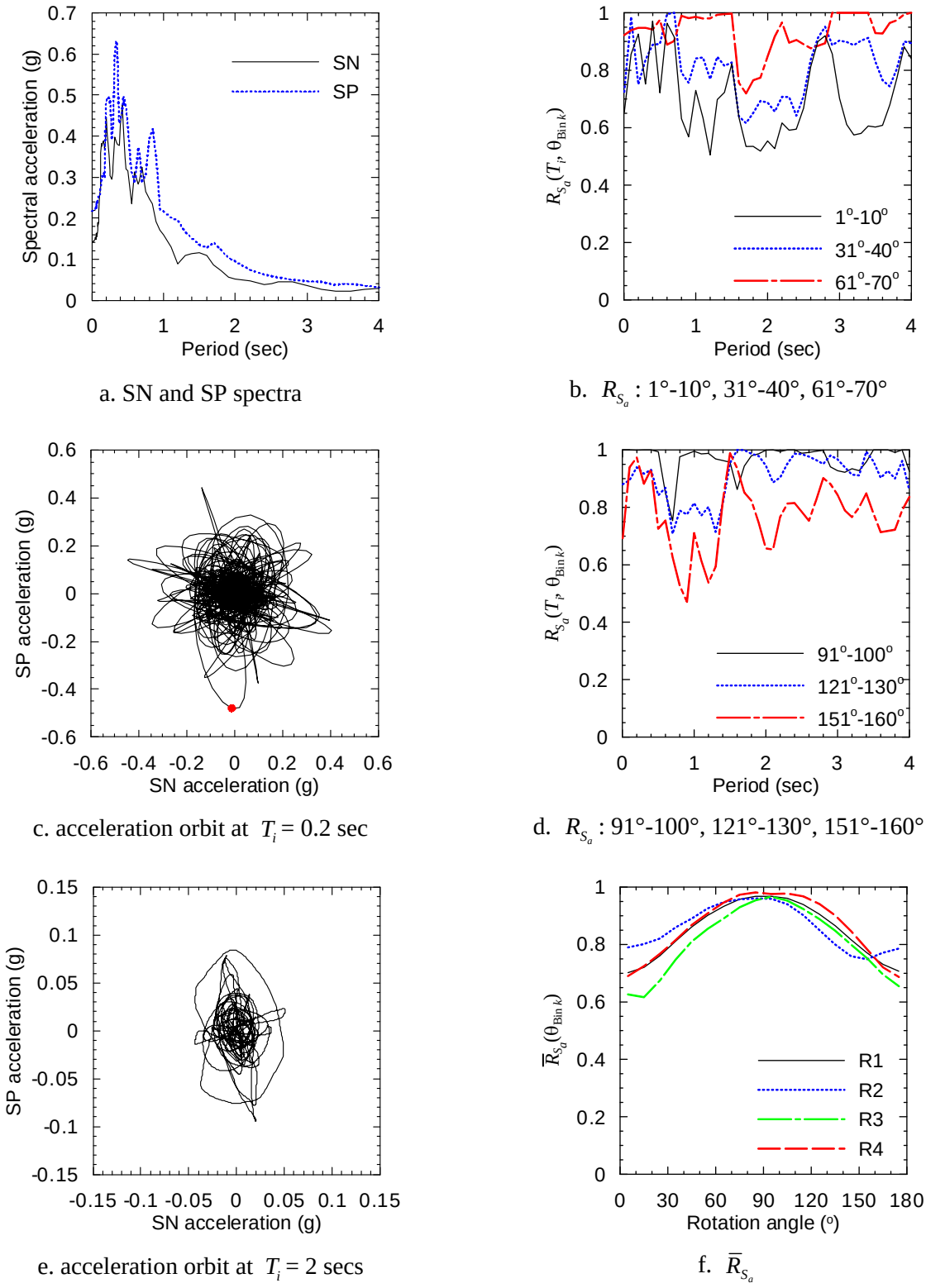

a. SN and SP spectra

b. R_{S_a} : 1°-10°, 31°-40°, 61°-70°

c. acceleration orbit at $T_i = 0.2$ sec

d. R_{S_a} : 91°-100°, 121°-130°, 151°-160°

e. acceleration orbit at $T_i = 2$ secs

f. $\overline{R}_{S_a}$

Figure 2-55. Sample results for EQ15 of Table 2-1

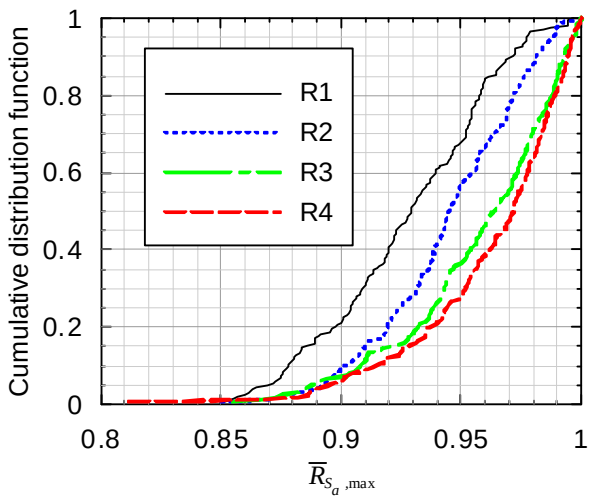

Figure 2-56. Cumulative distribution function for $\overline{R}_{S_a,\max}$ for period ranges R1 through R4 of Table 2-7

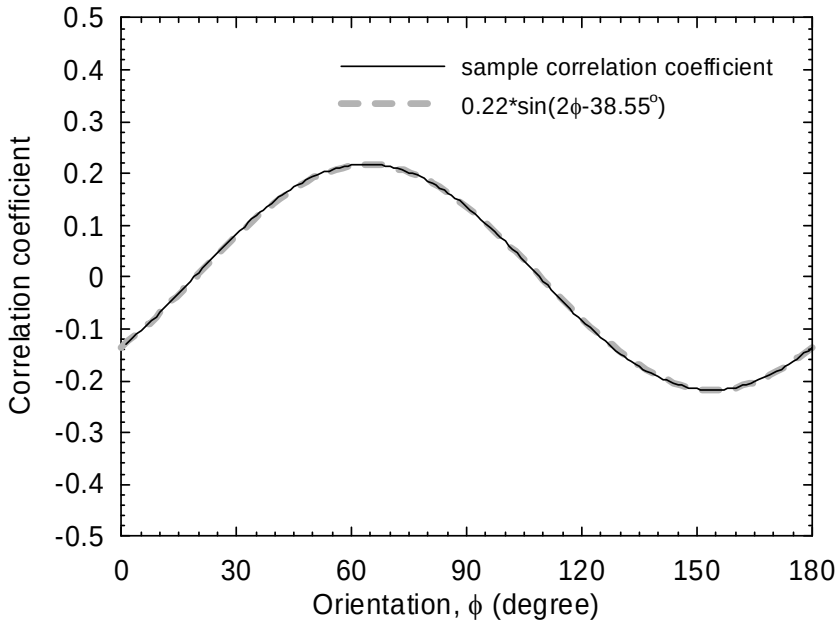

Figure 2-57. Correlation coefficient for a sample pair of ground motions as a function of orientation

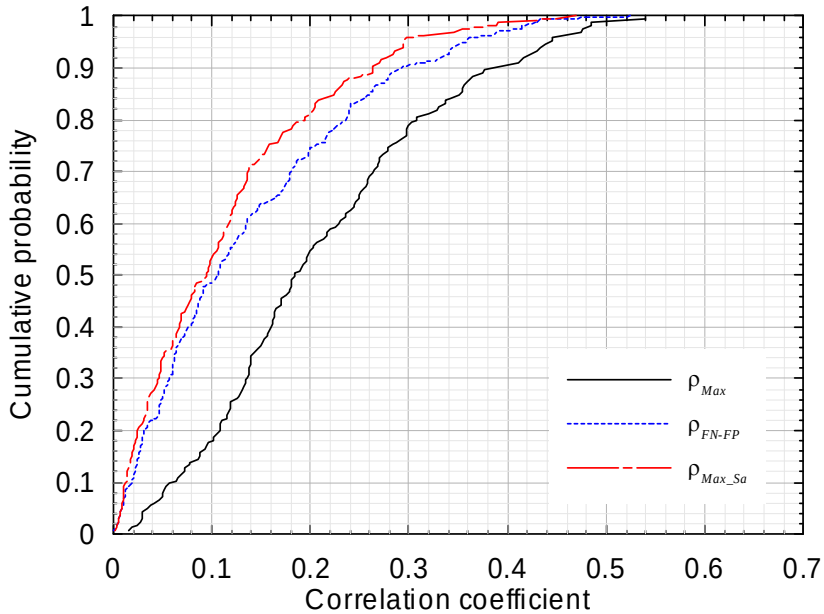

Figure 2-58. Cumulative distribution functions for ρ_{Max}, ρ_{FN_FP} and $\rho_{Max_S_a}$ for the records of Table 2-1

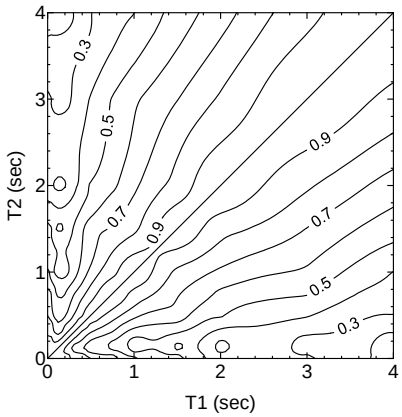

a. B-A model

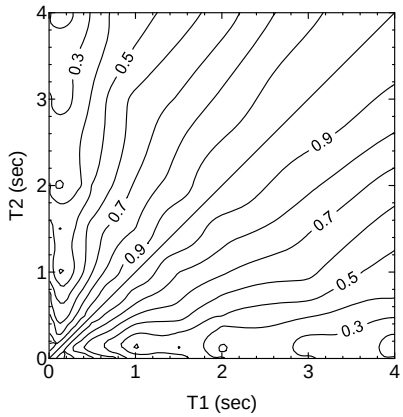

b. C-B model

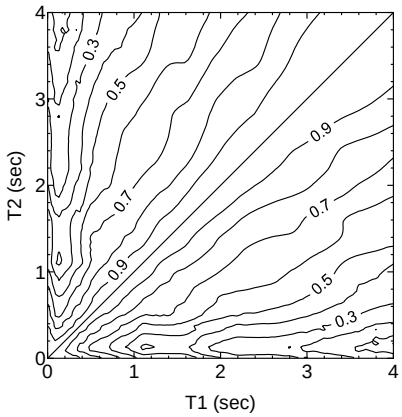

c. C-Y model

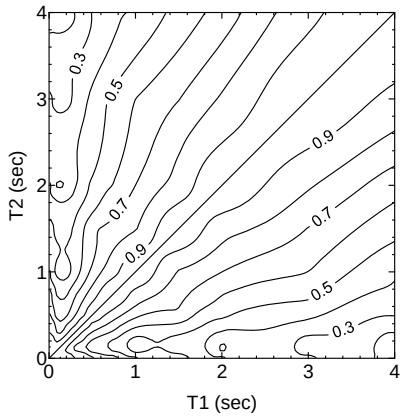

d. averaged NGA results

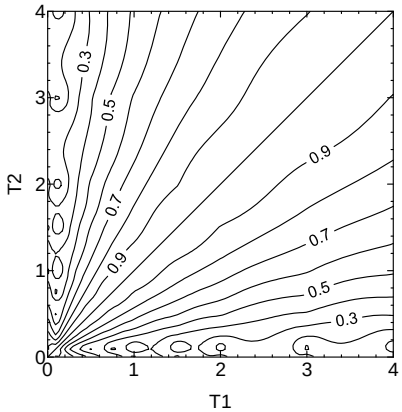

e. Baker and Jayaram (2008)

Figure 2-59. Contours of correlation coefficients between the maximum spectral demands at T_1 and T_2 computed using the B-A, C-B, C-Y and averaged NGA models for all of the records of Table 2-1 and the model of Baker and Jayaram (2008)

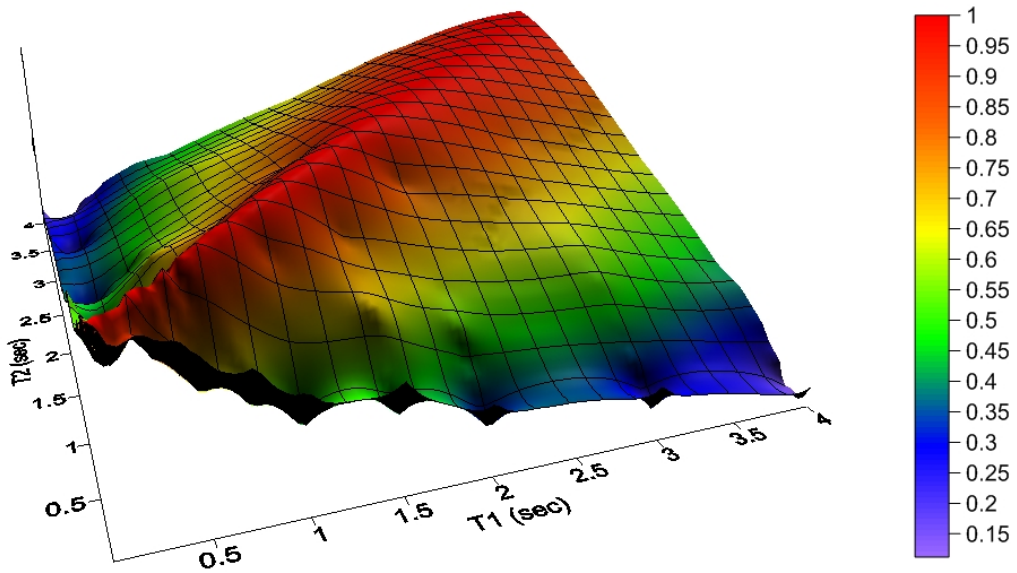

a. averaged NGA results

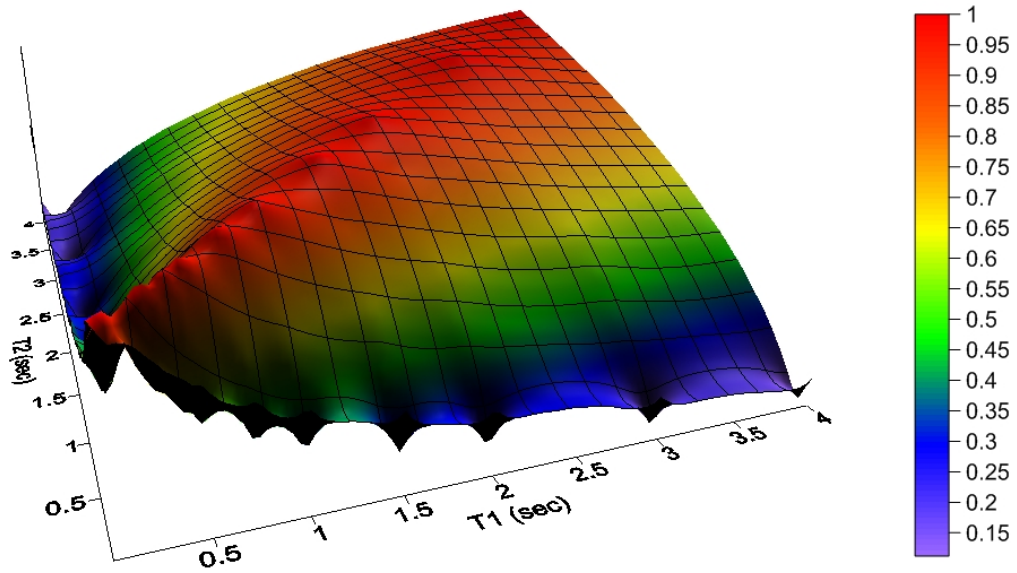

b. Baker and Jayaram (2008)

Figure 2-60. Correlation coefficients between the maximum spectral demands at T_1 and T_2 computed using the averaged NGA results for all of the records of Table 2-1 and the model of Baker and Jayaram (2008)

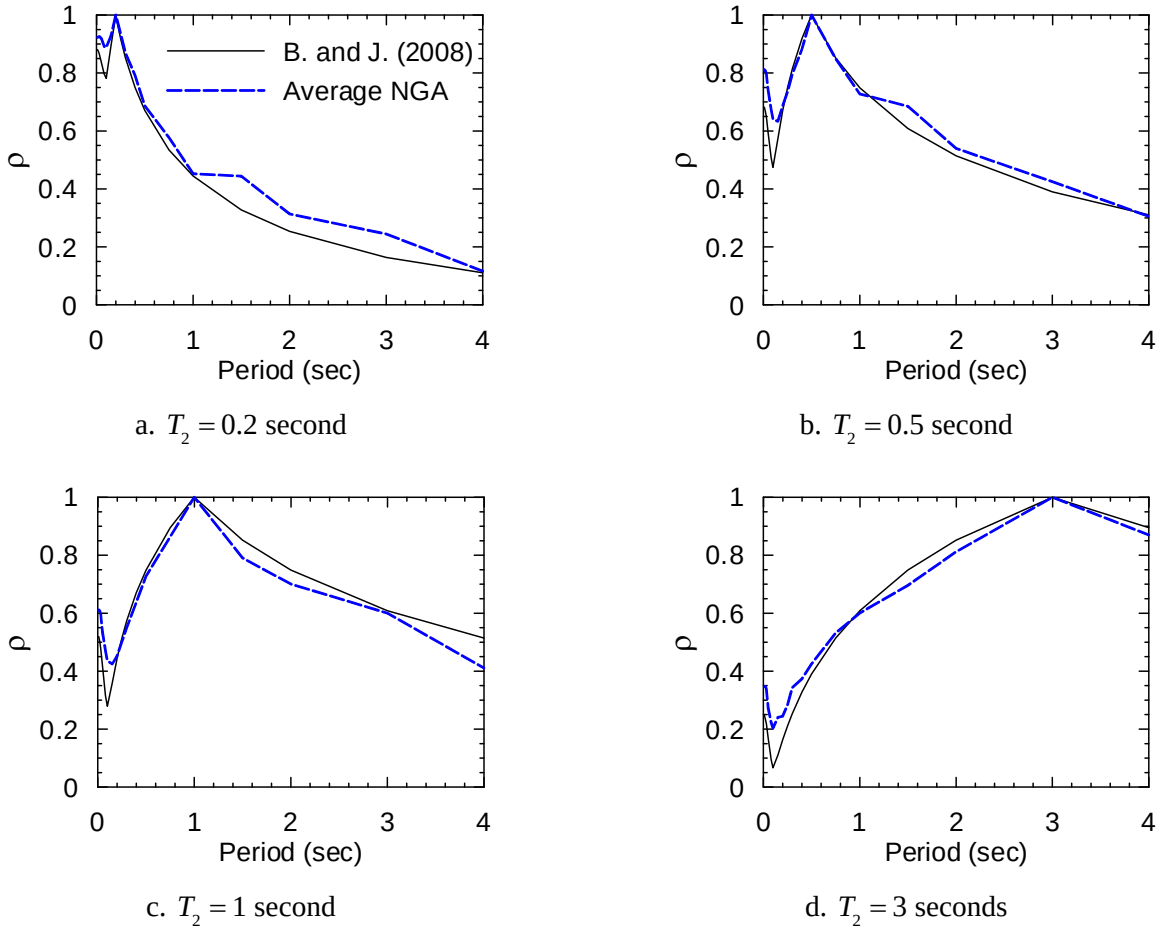

a. $T_2 = 0.2$ second

b. $T_2 = 0.5$ second

c. $T_2 = 1$ second

d. $T_2 = 3$ seconds

Figure 2-61. Correlation coefficients between the maximum spectral demands at T_1 and a given T_2 computed using the averaged NGA results for all of the records of Table 2-1 and the model of Baker and Jayaram (2008)

SECTION 3
WUS NEAR-FAULT GROUND MOTIONS

3.1 Introduction

The focus of this section is strong near-fault shaking in the Western United States (WUS). Similar to the records of Table 2-1 for far-field ground motions, the dataset used in this section is a subset of the PEER NGA ground motion database. All pairs of ground motions in the PEER NGA database for earthquakes with moment magnitude (M_W) of 6.5 and greater, and with closest distance from the recording site to the ruptured area (r) of 15 km and less are studied in this section. The 147 ground-motion pairs used in this section are listed in Table 3-1. Each pair of time series was rotated to the strike-normal (SN) and strike-parallel (SP) directions by the PEER researchers.

Figure 3-1 presents the distribution of the 147 ground-motion pairs as a function of M_W and r. Of the 147 pairs of motions, 46 are associated with strike-slip faulting and 101 with dip-slip faulting; 3, 7, 78, 58 and 1 pairs of motions are associated with Site Classes A through E, respectively, per the site classification of the 2009 NEHRP *Recommended Seismic Provisions* (FEMA 2009). Fifty-six pairs of motions are from the 1999 Chi-Chi earthquake in Taiwan. The data of Figure 3-1 at a magnitude of 7.62 are those for the Chi-Chi earthquake.

The analyses of Section 2 were repeated using the records of Table 3-1. Results are presented in this section. Section 3.2 presents the time difference between the peak accelerations in the two orthogonal horizontal directions. Sections 3.3.1, 3.3.2 and 3.3.3 present the relationships between 1) maximum spectral demand and GMRotI50, 2) GMRotI50 and NGA-predicted GMRotI50, and 3) maximum spectral demand and NGA-predicted GMRotI50, respectively. Identical to the notation used in Section 2, “GMRotI50_BA”, “GMRotI50_CB” and “GMRotI50_CY” are the median spectral demand computed using the B-A, C-B and C-Y NGA relationships. The parameter “GMRotI50_ave” is the average of “GMRotI50_BA”, “GMRotI50_CB” and “GMRotI50_CY” for a given earthquake scenario. Section 3.4 presents information on the orientation of maximum spectral demand. Section 3.5 presents information on the correlation of components of ground motion.

3.2 Geomean spectral demand representation

The subsection presents the time difference between the peak spectral acceleration response at a given period in two perpendicular directions for each pair of ground motions of Table 3-1. The study was performed using a series of 5%-damped elastic single degree-of-freedom oscillators with periods between 0 and 4 seconds. Each pair of records of Table 3-1 was rotated to be parallel and perpendicular to the orientation of GMRotI50 and used for response-history analysis. For a given pair of ground motions, the time difference between the two spectral accelerations at a given period was computed and then normalized by the period.

Panel a of Figure 3-2 presents the 84th, 50th and 16th percentiles of the normalized time difference for the 147 pairs of records of Table 3-1. The median normalized time differences are a) greater than 5 at the periods smaller than 0.2 second, b) greater than 1 at all periods smaller than 3 seconds, and c) between 1 and 0.5 at the periods between 3 and 4 seconds. Panel b of Figure 3-2 presents the cumulative distribution functions of the normalized time differences at periods of 0.2, 0.5, 1 and 2 seconds. Over 75%, 70%, 55% and 55% of the records have the normalized time differences greater than 1 at periods of 0.2, 0.5, 1 and 2 seconds, respectively.

3.3 Maximum and geomean spectral demands

3.3.1 Relationships between maximum spectral demand and GMRotI50

Figure 3-3 presents the residual between maximum spectral demand and GMRotI50, defined as the natural logarithm of the ratio of maximum spectral demand to GMRotI50, as a function of period, for the records of Table 3-1. Figure 3-4 presents the maximum, minimum, median and 84th and 16th percentiles of the ratios of maximum spectral demand to GMRotI50 for the records of Table 3-1. The median and 84th percentile of the ratios of Figure 3-4 at periods of 0, 0.2, 0.5, 1, 2, 3 and 4 seconds are presented in Table 3-2. The median ratios range between 1.2 and 1.4 and the 84th percentile ratios range between 1.3 and 1.5 across most of the period range of Figure 3-4. The median and 84th percentile results increase slightly with period, which is similar to that of Figure 2-4 for far-field WUS records.

To study the dependence of the residual between maximum spectral demand and GMRotI50 on M_W and r, the residuals of Figure 3-3 at periods of 0, 0.2, 0.5, 1, 2 and 3 seconds were re-plotted in the six panels of Figure 3-5 (Figure 3-6), respectively, as a function of M_W (r). The blue line in each panel presents a linear regression fit to the data. The residuals at a period of 3 second show clear dependence on M_W. The dependence on M_W at the other periods, and on r at all periods of Figure 3-6, is either insignificant or moderate.

3.3.2 Relationships between GMRotI50 and NGA-predicted GMRotI50

3.3.2.1 GMRotI50_BA

Figure 3-7 presents the residuals between GMRotI50 and GMRotI50_BA as a function of period for the records of Table 3-1. Figure 3-8 presents the median and 84th and 16th percentiles of the ratios of GMRotI50 to GMRotI50_BA for the records of Table 3-1. The median ratios of Figure 3-8 range between 0.8 and 1.3. The median ratio is smaller than 1 at periods less than 0.5 second and about 1.2 at periods greater than 1 second. The median and 84th percentile results of Figure 3-8 at periods of 0, 0.2, 0.5, 1, 2, 3 and 4 seconds are presented in the 2nd and 3rd columns of Table 3-3. The residuals of Figure 3-7 at periods of 0, 0.2, 0.5, 1, 2 and 3 seconds are re-plotted in the six panels of Figure 3-9 (Figure 3-10), respectively, as a function of M_W (r). The dependence of the residuals on M_W at periods 0 and 0.2 second is evident and decreases as the period increases. The dependence on r is insignificant at all periods of Figure 3-10.

The bias in the median curve of Figure 3-8 in the short period range is expected since 38% of the records of Table 3-1 are from the 1999 Chi-Chi earthquake and the inter-event residual of the B-A attenuation relationship for the Chi-Chi earthquake is much smaller than 1 in the short period range (see Figure 2-11 and the discussion presented in Section 2.4.2.1).

To investigate the impact of the 1999 Chi-Chi earthquake data on our results, we repeated the analysis of Figure 3-8 using all of the records of Table 3-1 bar those of the Chi-Chi earthquake. Results are presented in Figure 3-11. The median and 84th percentile results of Figure 3-11 at periods of 0, 0.2, 0.5, 1, 2, 3 and 4 seconds are presented in the 2nd and 3rd columns of Table 3-4. The median values in the 2nd column of Table 3-4 are higher than those of Table 3-3 at

periods of 0, 0.2 and 0.5 second and similar at periods of 1, 2 and 4 seconds. A peak occurs in the median curve of Figure 3-11 at a period of 3 seconds.

The results of Figure 3-8 and Figure 3-11 were computed by counting, which may be sensitive to the number of realizations. If we assume the distribution of the ratio of GMRotI50 to GMRotI50_BA to be lognormal, the median and 84th percentile values of the ratio can be estimated using the following equations:

$$\theta_Y = \exp\left(\frac{1}{n}\sum_{i=1}^{n}\ln y_i\right) \tag{3.1}$$

$$\beta_Y = \sqrt{\frac{1}{n-1}\sum_{i=1}^{n}(\ln y_i - \ln\theta_Y)^2} \tag{3.2}$$

$$y_{84th} = \theta_Y \cdot e^{\beta_Y} \tag{3.3}$$

where y_i is the the ratio of GMRotI50 to GMRotI50_BA for the *i*th ground-motion pair of Table 3-1, and θ_Y, β_Y and y_{84th} are the median, logarithmic standard deviation and 84th percentile of the ratio, respectively. The median estimations for the ratio of GMRotI50 to GMRotI50_BA computed using (3.1) are presented in Figure 3-12 for all of the records of Table 3-1 and for all of the records except those of the Chi-Chi earthquake. The median and 84th percentile results for the ratio of GMRotI50 to GMRotI50_BA computed using (3.1) through (3.3) at periods of 0, 0.2, 0.5, 1, 2, 3 and 4 seconds are presented in the 2nd and 3rd columns of Table 3-5 and Table 3-6 for all the records of Table 3-1 and for all the records except those of the Chi-Chi earthquake, respectively. The peak in the median curve of Figure 3-11 at a period of 3 seconds does not appear in Figure 3-12. In Figure 3-12, the impact of the records from the Chi-Chi earthquake is limited to the short period range. This observation is expected since the inter-event residual of the B-A attenuation relationship for the Chi-Chi earthquake is close to 1 in the long period range (see Figure 2-11).

3.3.2.2 GMRotI50_CB

The analyses of Figure 3-7 through Figure 3-12 were repeated for GMRotI50_CB. Results are presented in Figure 3-13 through Figure 3-18, respectively. The median and 84th percentile results of Figure 3-14 (Figure 3-17) at periods of 0, 0.2, 0.5, 1, 2, 3 and 4 seconds are presented in the 4th and 5th columns of Table 3-3 (Table 3-4).

The C-B model also overestimates the median GMRotI50 of the records of Table 3-1 in the short period range of Figure 3-14 and the bias is due to the inter-event residual for the Chi-Chi earthquake (see Figure 2-17). The bias in the short period range is reduced when the analysis is performed without the records of the Chi-Chi earthquake.

The dependence of the residuals on M_W and r is either insignificant or moderate in Figure 3-15 and Figure 3-16. The dependence on M_W is greatest at periods of 0 and 0.2 second and decreases as the period increases since the regression results of Figure 3-15 are heavily weighted at a magnitude of 7.62 (the Chi-Chi earthquake), where the attenuation relationship overestimates the median GMRotI50 of the recorded ground motions in the short period range.

The median estimations for the ratio of GMRotI50 to GMRotI50_CB computed using (3.1) are presented in Figure 3-18 for all the records of Table 3-1 and for all the records except those of the Chi-Chi earthquake. The median and 84th percentile results for the ratio of GMRotI50 to GMRotI50_CB computed using (3.1) through (3.3) at periods of 0, 0.2, 0.5, 1, 2, 3 and 4 seconds are presented in the 4th and 5th columns of Table 3-5 and Table 3-6 for all of the records of Table 3-1 and for all of the records except those of the Chi-Chi earthquake, respectively. The bias in the short period range is again reduced when the analysis is performed without the records of the Chi-Chi earthquake. The median values of the ratio for the analysis without the records of the Chi-Chi earthquake are very close to 1 for most of the periods presented in Figure 3-18.

3.3.2.3 GMRotI50_CY

The analyses of Figure 3-7 through Figure 3-12 were repeated for GMRotI50_CY. Results are presented in Figure 3-19 through Figure 3-24, respectively. The median and 84th percentile results of Figure 3-20 (Figure 3-23) at periods of 0, 0.2, 0.5, 1, 2, 3 and 4 seconds are presented in the 6th and 7th columns of Table 3-3 (Table 3-4). The median and 84th percentile results for the ratio of GMRotI50 to GMRotI50_CY computed using (3.1) through (3.3) at periods of 0, 0.2, 0.5, 1, 2, 3 and 4 seconds are presented in the 6th and 7th columns of Table 3-5 and Table 3-6 for all the records of Table 3-1 and for all the records except those of the Chi-Chi earthquake, respectively.

In Figure 3-20, the C-Y model overestimates the median GMRotI50 of the records of Table 3-1 in the short period range but underestimates the median GMRotI50 for periods greater than 2.5 seconds. This observation can be explained using Figure 2-23 that presents the inter-event residuals for the C-Y model at periods of 0.01, 0.2, 1 and 3 seconds. The residuals are smaller than -0.5 at periods of 0.01 and 0.2 second and increase to 0.1 at a period of 3 seconds. As presented in Figure 3-23, the bias in the median curve of Figure 3-20 is greatly reduced both in the short and long period ranges when the analysis is performed without the records of the Chi-Chi earthquake. Similar trends are observed in Figure 3-24 for the median results computed using (3.1).

In Figure 3-21 and Figure 3-22, the magnitude dependence of the residual between GMRotI50 and GMRotI50_CY is evident at periods of 0, 0.2 and 0.5 second. The distance dependence is either insignificant or moderate at all periods presented in Figure 3-22.

3.3.2.4 GMRotI50_ave

Figure 3-25 presents the residuals between GMRotI50 and GMRotI50_ave as a function of period for the records of Table 3-1. Figure 3-26 presents the median and 84th and 16th percentiles of the ratios of Figure 3-25. The residuals of Figure 3-25 at periods of 0, 0.2, 0.5, 1, 2 and 3 seconds are re-plotted in the six panels of Figure 3-27 (Figure 3-28), respectively, as a function of M_w (r). The trends in these figures are similar to those for other NGA-predicted GMRotI50. The parameter GMRotI50_ave overestimates the median GMRotI50 of the records of Table 3-1 in the short period range (see Figure 3-26) and the magnitude dependence of the residual is evident in that range (see panels a and b of Figure 3-27). The reason for this bias has been discussed in Sections 3.3.2.1 through 3.3.2.3.

The analyses of Figure 3-26 through Figure 3-28 were repeated using all the records of Table 3-1 except those of the 1999 Chi-Chi earthquake. Results are presented in Figure 3-29, Figure 3-31 and Figure 3-32, respectively. The median and 84th percentile results of Figure 3-26 (Figure 3-29) at periods of 0, 0.2, 0.5, 1, 2, 3 and 4 seconds are presented in the 8th and 9th columns of Table 3-3 (Table 3-4). The bias in the short period range is greatly reduced.

The median estimations for the ratio of GMRotI50 to GMRotI50_ave computed using (3.1) are presented in Figure 3-30 for all of the records of Table 3-1 and for all of the records except those of the Chi-Chi earthquake. The median and 84th percentile results for the ratio of GMRotI50 to GMRotI50_ave computed using (3.1) through (3.3) at periods of 0, 0.2, 0.5, 1, 2, 3 and 4 seconds are presented in the 8th and 9th columns of Table 3-5 and Table 3-6 for all of the records of Table 3-1 and for all of the records except those of the Chi-Chi earthquake, respectively. Figure 3-30 clearly presents the impact of the records of the Chi-Chi earthquake on the ratio of GMRotI50 to GMRotI50_ave. The median ratios for the analysis without the records of the Chi-Chi earthquake are very close to 1 for most of the periods presented in Figure 3-30.

3.3.3 Relationships between maximum spectral demand and NGA-predicted GMRotI50

The analyses of Figure 3-7 through Figure 3-12 were repeated using the ratio of maximum spectral demand to GMRotI50_BA (GMRotI50_CB, GMRotI50_CY). Results are presented in Figure 3-33 (Figure 3-39, Figure 3-45) through Figure 3-38 (Figure 3-44, Figure 3-50), respectively. The analyses of Figure 3-25 through Figure 3-32 for the ratio of GMRotI50 to GMRotI50_ave were repeated for the ratio of maximum spectral demand to GMRotI50_ave and the results are presented in Figure 3-51 through Figure 3-58, respectively.

The median and 84th percentile of the ratios of maximum spectral demand to each of GMRotI50_BA, GMRotI50_CB, GMRotI50_CY and GMRotI50_ave for all of the records of Table 3-1 by counting (using (3.1) through (3.3)) are presented in Table 3-7 (Table 3-9) and those for all of the records except those of the Chi-Chi earthquake are presented in Table 3-8 (Table 3-10) at periods of 0, 0.2, 0.5, 1, 2, 3 and 4 seconds.

The four sets of median values of Table 3-7 are much smaller than the corresponding median values of Table 3-2 in the short period range, because the median GMRotI50 of the records of the Chi-Chi earthquake, which include 38% of the records of Table 3-1, is significantly overestimated by the B-A, C-B and C-Y models in the short period range. The median ratios of maximum spectral demand to NGA-predicted GMRotI50 are more similar to the median values of Table 3-2 in the short period range when the analysis is performed without the records of the Chi-Chi earthquake (see Table 3-8). The median ratios are similar to the median values of Table

3-2 throughout the entire period range when the median ratios are computed using (3.1) and without the records of the Chi-Chi earthquake (see Table 3-10).

Based on the results of Figure 3-36, Figure 3-42 and Figure 3-48, the distance dependence of the ratio of maximum spectral demand to NGA-predicted GMRotI50 is insignificant. Based on the results of Figure 3-35, Figure 3-41 and Figure 3-47, the ratio is dependent on magnitude in the short period range only, which is an expected result because the regression is governed by the realizations for the Chi-Chi earthquake and the three NGA models studied herein overestimate the median GMRotI50 of the records of the Chi-Chi earthquake in Table 3-1.

3.4 Orientation of maximum spectral demand

3.4.1 Objectives

The analyses of Section 2.5 were repeated using the records of Table 3-1 and the results are presented in this subsection. The definitions of all terms used in this subsection are presented in Section 2.5 and not repeated herein. Section 3.4.2 presents results for sample pairs of ground motions. Section 3.4.3 presents results for the analyses using all the records of Table 3-1 to answer the questions:

1. Is the orientation of maximum spectral demand for a pair of recorded ground motions somewhat constant over a wide range of period or is the orientation of maximum demand random?
2. Can the SN direction be used as a surrogate for the direction of maximum shaking in the near-fault region?

3.4.2 Sample computations

Sample results are presented using two pairs of ground motions. The first pair, termed EQ77, was numbered 77 in the NGA flatfile and obtained from the Pacoima Dam site during the 1971 San Fernando earthquake. The values of M_W and r for EQ77 are 6.61 and 1.8 km, respectively. The second pair, EQ162, was recorded at the Calexico Fire Station during the 1979 Imperial Valley earthquake, with M_W = 6.53 and r = 10.5 km. The analysis of Figure 2-55 was repeated using EQ77 and EQ162.

Figure 3-59 presents the results for EQ77. Panel a of Figure 3-59 presents the response spectra for the SN and SP components of EQ77. The SN component produces greater spectral demands than the SP component for periods greater than 0.4 second. Panels c and e present the acceleration orbits of 0.2- and 2-second oscillators, respectively, subjected to EQ77. For T_i = 0.2 second, the maximum acceleration demand occurs at θ_j = 136° (see the solid circle in panel c) although the response along the SN direction is also significant. For T_i = 2 second, the SN component of EQ77 clearly dominates the response of the oscillator.

Panel b of Figure 3-59 presents R_{S_a}, which is a function of period and bin of rotation angles θ_j, for Bins 1 (θ_j = 1° through 10°), 2 (11° through 20°) and 8 (71° through 80°) at periods of 0 through 4 seconds. Panel d presents R_{S_a} for Bins 10 (91° through 100°), 14 (131° through 140°) and 18 (171° through 180°). In both panels, the values of R_{S_a} for orientations close to the SN direction (Bins 1 and 18) are greater than 0.95 across most of the period range. The values of R_{S_a} for Bins 8 and 10 are much smaller than those for Bins 1 and 18 at periods greater than about 0.3 second, that is, the intensity of the shaking along axes oriented between 71° through 80° and 91° through 100° from the SN axis is much smaller than that in the SN direction.

Panel f of Figure 3-59 presents the value of $\overline{R}_{S_a}(\theta_{\text{Bin}\,k})$ for four ranges of period at the midpoint rotation angle for each bin. The four ranges of period are 0 to 4 seconds (R1), 0 to 1 second (R2), 1 to 2 seconds (R3) and 2 to 4 seconds (R4). For given rotation angles associated with Bin *k*, a value of 1 for $\overline{R}_{S_a}(\theta_{\text{Bin}\,k})$ indicates that the maximum shaking demand is achieved across the entire range of period included in the computation. The trends in the four curves in panel f are similar, namely, the value of $\overline{R}_{S_a}$ decreases as the angle approaches 90° (the SP direction) and increases as it approaches 0° and 180° (the SN direction). For range R1, the maximum value of $\overline{R}_{S_a}$ over the 18 bins of angles (termed $\overline{R}_{S_a,\max}$) is 0.98 and the corresponding midpoint rotation angle (termed $\theta_{\max}$) is 175°: close to the SN direction. The minimum value of $\overline{R}_{S_a}$ is 0.35 and the corresponding midpoint rotation angle is 75°: close to the SP direction. For ranges R2, R3 and R4, the values of $\overline{R}_{S_a,\max}$ are 0.98, 1 and 1, respectively, and the values of $\theta_{\max}$ are 15°, 175° and 165°. For EQ77, $\theta_{\max}$ is close to the SN direction regardless of the range of period.

Figure 3-60 presents results for EQ162. The shapes of $\overline{R}_{S_a}$ for EQ162 (see panel f) are very different from those for EQ77. For range R1, $\overline{R}_{S_a,\max}$ does not occur in Bins 1 or 18 but in Bin 4,

with a value of 0.94. The results of panel b show that the value of R_{S_a} for Bin 4 is smaller than that for Bin 1 at periods smaller than 0.4 second (see panel c for the acceleration orbit of an oscillator with T_i = 0.2 second), is comparable with that for Bin 1 at periods between 0.4 and 1.2 seconds, and greater than that for Bin 1 at periods greater than 1.2 seconds (see panel e for the acceleration orbit of an oscillator with T_i = 2 seconds). For ranges R2, R3 and R4, the values of $\overline{R}_{S_a,\max}$ are 0.98, 0.94 and 0.99, respectively, and the values of $\theta_{\max}$ are 5°, 65° and 45°. For EQ162, the orientation of maximum demand is dependent on the range of period considered. However, the value of $\overline{R}_{S_a,\max}$ for range R1 is close to 1 (=0.94), which suggests that there is a small range of orientation (between 30° and 40° in this example) where the spectral demands are very close or equal to the maximum demands for most of the periods in the range of 0 to 4 seconds.

3.4.3 Overall analysis results

Figure 3-61 presents the distributions of $\overline{R}_{S_a,\max}$ for R1, R2, R3 and R4 for all 147 pairs of records. Each distribution of Figure 3-61 was developed by sorting the 147 results from smallest to largest and assigning a probability from 1/147 to 1.00 in increments of 1/147 for each of the results. The medians, (arithmetic) means and standard deviations of the 147 results for R1 through R4 are presented in Table 3-11. The median values of $\overline{R}_{S_a,\max}$ for all cases are greater than 0.94, which indicates clearly that there is typically an axis of strongest shaking.

Figure 3-62 presents the distributions of $\theta_{\max}$ as a function of r and fault type for R1 through R4. Table 3-12 identifies three ground-motion bins by r ($r \leq 3$ km, $r \leq 5$ km and $5 < r \leq 15$ km) for each period range and presents values of a) n_{all}, b) $n_{\pm 30^\circ}$, and c) $n_{\pm 30^\circ} / n_{all}$ for each bin, where n_{all} is the number of ground-motion pairs in each bin and $n_{\pm 30^\circ}$ is the number of ground-motion pairs with $\theta_{\max}$ between $\pm 30^\circ$ of the SN direction in each bin.

For period ranges R1 through R4, the probability of $\theta_{\max}$ being within $\pm 30^\circ$ of the SN direction for $r \leq 3$ km is similar to that for $r \leq 5$ km. For r less than 5 km, the probabilities of $\theta_{\max}$ being within $\pm 30^\circ$ of the SN direction are 64%, 53%, 61% and 72% for R1 through R4, respectively. For r greater than 5 km, these probabilities decrease to 44%, 39%, 48% and 46%. Fault strike-normal cannot be assumed as the direction of maximum shaking for r greater than 5 km for any

of the period ranges considered here. Importantly, for closest site-to-source distance less than 5 km, the probability of $\theta_{\max}$ differing from the SN direction by more than 30° is significant for short periods (47% for R2), which is a similar observation to that drawn by Watson-Lamprey and Boore (2007).

3.5 Correlation of ground motions

3.5.1 Time series

The analyses of Sections 2.6.1 and 2.6.2 were repeated using the records of Table 3-1 and presented in Sections 3.5.1 and 3.5.2, respectively. The notation presented in Section 2.6 is used here. Section 3.5.1 presents the correlation between two orthogonal horizontal acceleration *time series* for each pair of the ground-motion records of Table 3-1. Section 3.5.2 presents the correlation of *spectral demands* (maximum demand at different periods) for each pair of the records of Table 3-1.

For the records of Table 3-1, the distributions of three correlation coefficients of orthogonal horizontal ground-motion time series were investigated, namely, ρ_{Max}, ρ_{FN_FP} and $\rho_{Max_S_a}$, where ρ_{Max} is the maximum correlation coefficient of a pair of ground motions over all rotation angles; ρ_{FN_FP} is the correlation coefficient of the ground-motion components in the FN and FP orientations; and $\rho_{Max_S_a}$ is the correlation coefficient in the orientations parallel and perpendicular to the direction associated with $\overline{R}_{S_a,\max}$.

The CDFs of ρ_{Max}, ρ_{FN_FP} and $\rho_{Max_S_a}$ are presented in Figure 3-63. For the three CDFs of Figure 3-63, the values of correlation coefficient at cumulative probabilities of 0.5 and 0.9 and the cumulative probability at a correlation coefficient of 0.3 are presented in Table 3-13 together with the mean and standard deviation of the 147 realizations for each of ρ_{Max}, ρ_{FN_FP} and $\rho_{Max_S_a}$.

In Table 3-13, the mean and standard deviation for ρ_{Max} are 0.24 and 0.15, respectively. As a point of reference, the mean and standard deviation for ρ_{Max} reported in Hadjian (1981) are 0.234 and 0.109, respectively. The probabilities for ρ_{Max}, ρ_{FN_FP} and $\rho_{Max_S_a}$ less than 0.3 are 74% , 89% and 92%, respectively. The data of Figure 3-63 and Table 3-13 for near-fault ground motions support the upper bound on the correlation coefficient (0.3) specified in the ASCE

Standard 4-98 (ASCE 2000) and ASCE Standard 43-05 (ASCE 2005): the same conclusion as that drawn in Section 2.6.1.3 for far-field ground motions.

3.5.2 Spectral demand

This subsection presents the correlation of maximum spectral demands at periods of T_1 and T_2. Identical to Section 2.6.2.2, the variable, $\varepsilon_{\max}(T_i)$, is used for computations:

$$\varepsilon_{\max}(T_i) = \frac{\ln(x_{\max}(T_i)) - \ln(SF(T_i) \cdot \theta_{NGA})}{\beta_{NGA}} \tag{3.4}$$

where $x_{\max}(T_i)$ is the maximum spectral demand at the period T_i for a set of ground motions of Table 3-1; θ_{NGA} is GMRotI50_BA, GMRotI50_CB, GMRotI50_CY or GMRotI50_ave at the period T_i for the set of ground motions; β_{NGA} is the dispersion corresponding to θ_{NGA} predicted by the NGA models and $SF(T_i)$ is a factor to scale the median NGA-predicted GMRotI50 to median maximum spectral demand at the period T_i. The parameter $SF(T_i)$ is based on the median ratio of maximum spectral demand to NGA-predicted GMRotI50 presented in Figure 3-34, Figure 3-40, Figure 3-46, and Figure 3-52 for GMRotI50_BA, GMRotI50_CB, GMRotI50_CY and GMRotI50_ave, respectively.

The correlation coefficients between $\varepsilon_{\max}(T_1)$ and $\varepsilon_{\max}(T_2)$, termed $\rho_{\varepsilon_{\max}(T_1),\varepsilon_{\max}(T_2)}$, were computed and the contours of $\rho_{\varepsilon_{\max}(T_1),\varepsilon_{\max}(T_2)}$ are presented in panels a through d of Figure 3-64 for GMRotI50_BA, GMRotI50_CB, GMRotI50_CY and GMRotI50_ave, respectively. Panel e of Figure 3-64 presents the contours of correlation coefficients per the model of Baker and Jayaram (2008), as described in (2.8) through (2.12). The distributions presented in the five panels of Figure 3-64 are similar.

Panels a and b of Figure 3-65 presents $\rho_{\varepsilon_{\max}(T_1),\varepsilon_{\max}(T_2)}$ for GMRotI50_ave and Baker and Jayaram (2008), respectively, in a 3-dimensional format. The two distributions are similar.

Panels a through d of Figure 3-66 present the values of $\rho_{\varepsilon_{\max}(T_1),\varepsilon_{\max}(T_2)}$ as a function of T_1 given that T_2 is equal to 0.2, 0.5, 1 and 3 seconds, respectively. The solid and dashed lines in each panel present the data for Baker and Jayaram (2008) and GMRotI50_ave, respectively. The differences between the data for Baker and Jayaram (2008) and GMRotI50_ave are insignificant for most of

periods presented in Figure 3-66. At $T_1 = 0.1$ second, the value of $\rho_{\varepsilon_{\max}(T_1),\varepsilon_{\max}(T_2)}$ for Baker and Jayaram (2008) is about 0.15 (0.1) smaller than that for GMRotI50_ave given that T_2 is equal to 0.5 second (1 and 3 seconds).

The results of Figure 3-64 through Figure 3-66 suggest that the model of Baker and Jayaram (2008), with minor modification in the short period range, can be used to capture the correlation between the maximum spectral demands at different periods for the near-fault ground motions of Table 3-1.

Table 3-1. Near-fault earthquake ground motion records for the WUS study

Record Sequence Number	Earthquake Name	Station Name	Year	M_W	r (km)	V_{S30} (m/s)
6	Imp. Valley-02	El Centro #9	1940	6.95	6.09	213.4
77	San Fernando	Pacoima Dam	1971	6.61	1.81	2016.1
126	Gazli, USSR	Karakyr	1976	6.80	5.46	659.6
158	Imp. Valley-06	Aeropuerto Mexicali	1979	6.53	0.34	274.5
159	Imp. Valley-06	Agrarias	1979	6.53	0.65	274.5
160	Imp. Valley-06	Bonds Corner	1979	6.53	2.68	223.0
161	Imp. Valley-06	Brawley Airport	1979	6.53	10.42	208.7
162	Imp. Valley-06	Calexico Fire St.	1979	6.53	10.45	231.2
165	Imp. Valley-06	Chihuahua	1979	6.53	7.29	274.5
170	Imp. Valley-06	EC County Center FF	1979	6.53	7.31	192.1
171	Imp. Valley-06	EC Meloland Overpass FF	1979	6.53	0.07	186.2
173	Imp. Valley-06	El Centro #10	1979	6.53	6.17	202.9
174	Imp. Valley-06	El Centro #11	1979	6.53	12.45	196.3
178	Imp. Valley-06	El Centro #3	1979	6.53	12.85	162.9
179	Imp. Valley-06	El Centro #4	1979	6.53	7.05	208.9
180	Imp. Valley-06	El Centro #5	1979	6.53	3.95	205.6
181	Imp. Valley-06	El Centro #6	1979	6.53	1.35	203.2
182	Imp. Valley-06	El Centro #7	1979	6.53	0.56	210.5
183	Imp. Valley-06	El Centro #8	1979	6.53	3.86	206.1
184	Imp. Valley-06	El Centro Differential Array	1979	6.53	5.09	202.3
185	Imp. Valley-06	Holtville Post Office	1979	6.53	7.65	202.9
187	Imp. Valley-06	Parachute Test Site	1979	6.53	12.69	348.7
189	Imp. Valley-06	SAHOP Casa Flores	1979	6.53	9.64	338.6
284	Irpinia, Italy-01	Auletta	1980	6.90	9.55	1000.0
285	Irpinia, Italy-01	Bagnoli Irpinio	1980	6.90	8.18	1000.0
292	Irpinia, Italy-01	Sturno	1980	6.90	10.84	1000.0
495	Nahanni, Canada	Site 1	1985	6.76	9.60	659.6
496	Nahanni, Canada	Site 2	1985	6.76	4.93	659.6
497	Nahanni, Canada	Site 3	1985	6.76	5.32	659.6
723	Superst. Hills-02	Parachute Test Site	1987	6.54	0.95	348.7
725	Superst. Hills-02	Poe Road	1987	6.54	11.16	207.5

Record Sequence Number	Earthquake Name	Station Name	Year	M_W	r (km)	V_{S30} (m/s)
727	Superst. Hills-02	Superstition Mtn. Camera	1987	6.54	5.61	362.4
728	Superst. Hills-02	Westmorland Fire Sta.	1987	6.54	13.03	193.7
741	Loma Prieta	BRAN	1989	6.93	10.72	376.1
753	Loma Prieta	Corralitos	1989	6.93	3.85	462.2
763	Loma Prieta	Gilroy - Gavilan Coll.	1989	6.93	9.96	729.7
764	Loma Prieta	Gilroy - Historic Bldg.	1989	6.93	10.97	338.5
765	Loma Prieta	Gilroy Array #1	1989	6.93	9.64	1428.0
766	Loma Prieta	Gilroy Array #2	1989	6.93	11.07	270.8
767	Loma Prieta	Gilroy Array #3	1989	6.93	12.82	349.9
768	Loma Prieta	Gilroy Array #4	1989	6.93	14.34	221.8
779	Loma Prieta	LGPC	1989	6.93	3.88	477.7
801	Loma Prieta	San Jose - Santa Teresa Hills	1989	6.93	14.69	671.8
802	Loma Prieta	Saratoga - Aloha Ave	1989	6.93	8.50	370.8
803	Loma Prieta	Saratoga - W Valley Coll.	1989	6.93	9.31	370.8
821	Erzican, Turkey	Erzincan	1992	6.69	4.38	274.5
825	Cape Mendocino	Cape Mendocino	1992	7.01	6.96	513.7
828	Cape Mendocino	Petrolia	1992	7.01	8.18	712.8
829	Cape Mendocino	Rio Dell Overpass - FF	1992	7.01	14.33	311.8
864	Landers	Joshua Tree	1992	7.28	11.03	379.3
879	Landers	Lucerne	1992	7.28	2.19	684.9
949	Northridge-01	Arleta - Nordhoff Fire Sta.	1994	6.69	8.66	297.7
959	Northridge-01	Canoga Park - Topanga Can	1994	6.69	14.70	267.5
960	Northridge-01	Canyon Country - W Lost Cany	1994	6.69	12.44	308.6
982	Northridge-01	Jensen Filter Plant	1994	6.69	5.43	373.1
983	Northridge-01	Jensen Filter Plant Generator	1994	6.69	5.43	525.8
1004	Northridge-01	LA - Sepulveda VA Hospital	1994	6.69	8.44	380.1
1013	Northridge-01	LA Dam	1994	6.69	5.92	629.0
1042	Northridge-01	N Hollywood - Coldwater Can	1994	6.69	12.51	446.0
1044	Northridge-01	Newhall - Fire Sta.	1994	6.69	5.92	269.1
1045	Northridge-01	Newhall - W Pico Canyon Rd.	1994	6.69	5.48	285.9
1048	Northridge-01	Northridge - 17645 Saticoy St	1994	6.69	12.09	280.9
1050	Northridge-01	Pacoima Dam (downstr)	1994	6.69	7.01	2016.1

Record Sequence Number	Earthquake Name	Station Name	Year	M_W	r (km)	V_{S30} (m/s)
1051	Northridge-01	Pacoima Dam (upper left)	1994	6.69	7.01	2016.1
1052	Northridge-01	Pacoima Kagel Canyon	1994	6.69	7.26	508.1
1063	Northridge-01	Rinaldi Receiving Sta.	1994	6.69	6.50	282.3
1080	Northridge-01	Simi Valley - Katherine Rd	1994	6.69	13.42	557.4
1082	Northridge-01	Sun Valley - Roscoe Blvd	1994	6.69	10.05	308.6
1083	Northridge-01	Sunland - Mt Gleason Ave	1994	6.69	13.35	446.0
1084	Northridge-01	Sylmar - Converter Sta.	1994	6.69	5.35	251.2
1085	Northridge-01	Sylmar - Converter Sta. East	1994	6.69	5.19	370.5
1086	Northridge-01	Sylmar - Olive View Med FF	1994	6.69	5.30	440.5
1106	Kobe, Japan	KJMA	1995	6.90	0.96	312.0
1111	Kobe, Japan	Nishi-Akashi	1995	6.90	7.08	609.0
1119	Kobe, Japan	Takarazuka	1995	6.90	0.27	312.0
1120	Kobe, Japan	Takatori	1995	6.90	1.47	256.0
1148	Kocaeli, Turkey	Arcelik	1999	7.51	13.49	523.0
1161	Kocaeli, Turkey	Gebze	1999	7.51	10.92	792.0
1165	Kocaeli, Turkey	Izmit	1999	7.51	7.21	811.0
1176	Kocaeli, Turkey	Yarimca	1999	7.51	4.83	297.0
1178	Chi-Chi, Taiwan	ALS	1999	7.62	10.80	553.4
1182	Chi-Chi, Taiwan	CHY006	1999	7.62	9.77	438.2
1193	Chi-Chi, Taiwan	CHY024	1999	7.62	9.64	427.7
1197	Chi-Chi, Taiwan	CHY028	1999	7.62	3.14	542.6
1198	Chi-Chi, Taiwan	CHY029	1999	7.62	10.97	544.7
1201	Chi-Chi, Taiwan	CHY034	1999	7.62	14.82	378.8
1202	Chi-Chi, Taiwan	CHY035	1999	7.62	12.65	473.9
1227	Chi-Chi, Taiwan	CHY074	1999	7.62	10.80	553.4
1231	Chi-Chi, Taiwan	CHY080	1999	7.62	2.69	553.4
1244	Chi-Chi, Taiwan	CHY101	1999	7.62	9.96	258.9
1403	Chi-Chi, Taiwan	NSY	1999	7.62	13.15	599.6
1462	Chi-Chi, Taiwan	TCU	1999	7.62	5.18	472.8
1488	Chi-Chi, Taiwan	TCU048	1999	7.62	13.55	473.9
1489	Chi-Chi, Taiwan	TCU049	1999	7.62	3.78	487.3
1490	Chi-Chi, Taiwan	TCU050	1999	7.62	9.51	272.6

Record Sequence Number	Earthquake Name	Station Name	Year	M_W	r (km)	V_{S30} (m/s)
1491	Chi-Chi, Taiwan	TCU051	1999	7.62	7.66	272.6
1492	Chi-Chi, Taiwan	TCU052	1999	7.62	0.66	393.2
1493	Chi-Chi, Taiwan	TCU053	1999	7.62	5.97	454.6
1494	Chi-Chi, Taiwan	TCU054	1999	7.62	5.30	460.7
1495	Chi-Chi, Taiwan	TCU055	1999	7.62	6.36	272.6
1496	Chi-Chi, Taiwan	TCU056	1999	7.62	10.50	272.6
1497	Chi-Chi, Taiwan	TCU057	1999	7.62	11.84	473.9
1499	Chi-Chi, Taiwan	TCU060	1999	7.62	8.53	272.6
1501	Chi-Chi, Taiwan	TCU063	1999	7.62	9.80	272.6
1503	Chi-Chi, Taiwan	TCU065	1999	7.62	0.59	305.9
1504	Chi-Chi, Taiwan	TCU067	1999	7.62	0.64	433.6
1505	Chi-Chi, Taiwan	TCU068	1999	7.62	0.32	487.3
1507	Chi-Chi, Taiwan	TCU071	1999	7.62	5.31	624.9
1508	Chi-Chi, Taiwan	TCU072	1999	7.62	7.03	468.1
1509	Chi-Chi, Taiwan	TCU074	1999	7.62	13.46	549.4
1510	Chi-Chi, Taiwan	TCU075	1999	7.62	0.91	573.0
1511	Chi-Chi, Taiwan	TCU076	1999	7.62	2.76	615.0
1512	Chi-Chi, Taiwan	TCU078	1999	7.62	8.20	443.0
1513	Chi-Chi, Taiwan	TCU079	1999	7.62	10.97	364.0
1515	Chi-Chi, Taiwan	TCU082	1999	7.62	5.18	472.8
1517	Chi-Chi, Taiwan	TCU084	1999	7.62	11.24	553.4
1519	Chi-Chi, Taiwan	TCU087	1999	7.62	7.00	473.9
1521	Chi-Chi, Taiwan	TCU089	1999	7.62	8.88	553.4
1527	Chi-Chi, Taiwan	TCU100	1999	7.62	11.39	473.9
1528	Chi-Chi, Taiwan	TCU101	1999	7.62	2.13	272.6
1529	Chi-Chi, Taiwan	TCU102	1999	7.62	1.51	714.3
1530	Chi-Chi, Taiwan	TCU103	1999	7.62	6.10	494.1
1531	Chi-Chi, Taiwan	TCU104	1999	7.62	12.89	473.9
1533	Chi-Chi, Taiwan	TCU106	1999	7.62	14.99	473.9
1535	Chi-Chi, Taiwan	TCU109	1999	7.62	13.08	473.9
1536	Chi-Chi, Taiwan	TCU110	1999	7.62	11.60	212.7
1541	Chi-Chi, Taiwan	TCU116	1999	7.62	12.40	493.1

Record Sequence Number	Earthquake Name	Station Name	Year	M_W	r (km)	V_{S30} (m/s)
1545	Chi-Chi, Taiwan	TCU120	1999	7.62	7.41	459.3
1546	Chi-Chi, Taiwan	TCU122	1999	7.62	9.35	475.5
1547	Chi-Chi, Taiwan	TCU123	1999	7.62	14.93	272.6
1548	Chi-Chi, Taiwan	TCU128	1999	7.62	13.15	599.6
1549	Chi-Chi, Taiwan	TCU129	1999	7.62	1.84	664.4
1550	Chi-Chi, Taiwan	TCU136	1999	7.62	8.29	473.9
1551	Chi-Chi, Taiwan	TCU138	1999	7.62	9.79	652.9
1595	Chi-Chi, Taiwan	WGK	1999	7.62	9.96	258.9
1596	Chi-Chi, Taiwan	WNT	1999	7.62	1.84	664.4
1602	Duzce, Turkey	Bolu	1999	7.14	12.04	326.0
1605	Duzce, Turkey	Duzce	1999	7.14	6.58	276.0
1611	Duzce, Turkey	Lamont 1058	1999	7.14	0.21	424.8
1612	Duzce, Turkey	Lamont 1059	1999	7.14	4.17	424.8
1614	Duzce, Turkey	Lamont 1061	1999	7.14	11.46	481.0
1615	Duzce, Turkey	Lamont 1062	1999	7.14	9.15	338.0
1617	Duzce, Turkey	Lamont 375	1999	7.14	3.93	424.8
1618	Duzce, Turkey	Lamont 531	1999	7.14	8.03	659.6
1787	Hector Mine	Hector	1999	7.13	11.66	684.9
2114	Denali, Alaska	TAPS Pump Station #10	2002	7.90	2.74	329.4
3548	Loma Prieta	Los Gatos-Lexington Dam	1989	6.93	5.02	1070.3

Table 3-2. Median and 84th percentile of the ratio of maximum spectral demand to GMRotI50 for all the records of Table 3-1

Period (sec)	$\frac{\text{Maximum demand}}{\text{GMRotI50}}$	
	Median	84th percentile
0	1.21	1.32
0.2	1.22	1.36
0.5	1.29	1.41
1	1.31	1.44
2	1.31	1.45
3	1.31	1.47
4	1.37	1.52

Table 3-3. Median and 84th percentile of the ratio of GMRotI50 to GMRotI50_BA, GMRotI50_CB, GMRotI50_BA and GMRotI50_ave for all of the records of Table 3-1

Period (sec)	GMRotI50 / GMRotI50_BA		GMRotI50 / GMRotI50_CB		GMRotI50 / GMRotI50_CY		GMRotI50 / GMRotI50_ave	
	Median	84th percentile	Median	84th percentile	Median	84th percentile	Median	84th percentile
0	0.92	1.54	0.87	1.47	0.70	1.22	0.84	1.36
0.2	0.81	1.43	0.84	1.48	0.64	1.21	0.74	1.35
0.5	0.99	1.59	0.91	1.57	0.81	1.51	0.89	1.55
1	1.18	1.74	0.97	1.50	0.93	1.55	1.02	1.58
2	1.16	1.85	0.97	1.57	1.04	1.75	1.04	1.67
3	1.25	2.13	1.09	1.61	1.24	1.95	1.16	1.77
4	1.24	2.16	1.01	1.65	1.21	2.07	1.12	1.80

Table 3-4. Median and 84th percentile of the ratio of GMRotI50 to GMRotI50_BA, GMRotI50_CB, GMRotI50_BA and GMRotI50_ave for all of the records of Table 3-1 except those of the 1999 Chi-Chi earthquake

Period (sec)	GMRotI50 / GMRotI50_BA		GMRotI50 / GMRotI50_CB		GMRotI50 / GMRotI50_CY		GMRotI50 / GMRotI50_ave	
	Median	84th percentile	Median	84th percentile	Median	84th percentile	Median	84th percentile
0	1.17	1.76	1.02	1.54	0.96	1.36	1.04	1.53
0.2	1.02	1.57	1.08	1.66	0.96	1.40	1.04	1.55
0.5	1.10	1.83	1.00	1.63	1.03	1.76	1.01	1.67
1	1.21	1.74	0.98	1.50	0.96	1.60	1.05	1.64
2	1.17	1.89	1.02	1.72	1.01	2.00	1.05	1.71
3	1.43	2.24	1.21	1.65	0.98	1.91	1.18	1.73
4	1.23	2.07	0.99	1.54	1.05	1.89	1.06	1.71

Table 3-5. Median and 84th percentile of the ratio of GMRotI50 to GMRotI50_BA, GMRotI50_CB, GMRotI50_BA and GMRotI50_ave computed using (3.1) through (3.3) for all of the records of Table 3-1

Period (sec)	GMRotI50 / GMRotI50_BA		GMRotI50 / GMRotI50_CB		GMRotI50 / GMRotI50_CY		GMRotI50 / GMRotI50_ave	
	Median	84th percentile	Median	84th percentile	Median	84th percentile	Median	84th percentile
0	0.92	1.59	0.89	1.45	0.71	1.22	0.82	1.38
0.2	0.82	1.45	0.83	1.47	0.66	1.23	0.75	1.35
0.5	0.99	1.74	0.92	1.59	0.82	1.51	0.90	1.57
1	1.09	1.95	0.94	1.68	0.87	1.61	0.95	1.70
2	1.13	2.13	0.92	1.70	0.97	1.88	0.99	1.83
3	1.15	2.20	0.97	1.79	1.09	2.11	1.05	1.93
4	1.17	2.25	0.94	1.73	1.14	2.25	1.05	1.95

Table 3-6. Median and 84th percentile of the ratio of GMRotI50 to GMRotI50_BA, GMRotI50_CB, GMRotI50_BA and GMRotI50_ave computed using (3.1) through (3.3) for all of the records of Table 3-1 except those of the 1999 Chi-Chi earthquake

Period (sec)	GMRotI50 / GMRotI50_BA		GMRotI50 / GMRotI50_CB		GMRotI50 / GMRotI50_CY		GMRotI50 / GMRotI50_ave	
	Median	84th percentile	Median	84th percentile	Median	84th percentile	Median	84th percentile
0	1.12	1.89	1.00	1.64	0.89	1.45	0.99	1.61
0.2	0.99	1.74	0.99	1.73	0.87	1.52	0.94	1.62
0.5	1.09	2.06	0.97	1.83	0.97	1.89	1.00	1.88
1	1.11	2.08	0.94	1.77	0.89	1.79	0.96	1.82
2	1.12	2.29	0.95	1.89	0.92	1.95	0.98	1.95
3	1.16	2.42	0.98	1.97	0.96	2.02	1.01	2.02
4	1.10	2.23	0.89	1.75	0.94	1.91	0.95	1.85

Table 3-7. Median and 84th percentile of the ratio of maximum spectral demand to GMRotI50_BA, GMRotI50_CB, GMRotI50_BA and GMRotI50_ave for all of the records of Table 3-1

Period (sec)	Max. Demand / GMRotI50_BA		Max. Demand / GMRotI50_CB		Max. Demand / GMRotI50_CY		Max. Demand / GMRotI50_ave	
	Median	84th percentile	Median	84th percentile	Median	84th percentile	Median	84th percentile
0	1.08	1.98	1.06	1.78	0.86	1.51	1.01	1.65
0.2	0.96	1.75	1.05	1.83	0.78	1.51	0.91	1.63
0.5	1.25	2.12	1.16	1.93	1.03	1.97	1.13	2.00
1	1.45	2.46	1.26	2.11	1.15	2.05	1.29	2.14
2	1.54	2.60	1.20	2.08	1.29	2.48	1.33	2.35
3	1.59	2.92	1.41	2.29	1.50	2.76	1.45	2.53
4	1.67	3.19	1.37	2.25	1.61	2.97	1.49	2.69

Table 3-8. Median and 84th percentile of the ratio of maximum spectral demand to GMRotI50_BA, GMRotI50_CB, GMRotI50_BA and GMRotI50_ave for all of the records of Table 3-1 except those of the 1999 Chi-Chi earthquake

Period (sec)	Max. Demand / GMRotI50_BA		Max. Demand / GMRotI50_CB		Max. Demand / GMRotI50_CY		Max. Demand / GMRotI50_ave	
	Median	84th percentile	Median	84th percentile	Median	84th percentile	Median	84th percentile
0	1.43	2.09	1.25	1.80	1.13	1.57	1.26	1.75
0.2	1.22	2.15	1.26	2.01	1.14	1.79	1.23	1.82
0.5	1.44	2.36	1.33	2.13	1.26	2.17	1.30	2.23
1	1.53	2.50	1.28	2.11	1.25	2.28	1.33	2.26
2	1.63	2.73	1.31	2.35	1.28	2.69	1.39	2.49
3	1.74	3.21	1.53	2.43	1.39	2.76	1.55	2.72
4	1.49	3.19	1.36	2.24	1.37	2.69	1.41	2.59

Table 3-9. Median and 84th percentile of the ratio of maximum spectral demand to GMRotI50_BA, GMRotI50_CB, GMRotI50_BA and GMRotI50_ave computed using (3.1) through (3.3) for all of the records of Table 3-1

Period (sec)	Max. Demand / GMRotI50_BA		Max. Demand / GMRotI50_CB		Max. Demand / GMRotI50_CY		Max. Demand / GMRotI50_ave	
	Median	84th percentile	Median	84th percentile	Median	84th percentile	Median	84th percentile
0	1.12	1.96	1.07	1.78	0.85	1.50	0.99	1.69
0.2	1.01	1.82	1.03	1.85	0.81	1.54	0.93	1.69
0.5	1.27	2.31	1.18	2.11	1.06	2.00	1.15	2.08
1	1.43	2.63	1.23	2.25	1.13	2.17	1.24	2.29
2	1.48	2.89	1.20	2.30	1.27	2.54	1.29	2.48
3	1.51	3.01	1.28	2.43	1.43	2.83	1.38	2.62
4	1.59	3.19	1.28	2.44	1.56	3.15	1.44	2.75

Table 3-10. Median and 84th percentile of the ratio of maximum spectral demand to GMRotI50_BA, GMRotI50_CB, GMRotI50_BA and GMRotI50_ave computed using (3.1) through (3.3) for all of the records of Table 3-1 except those of the 1999 Chi-Chi earthquake

Period (sec)	Max. Demand / GMRotI50_BA		Max. Demand / GMRotI50_CB		Max. Demand / GMRotI50_CY		Max. Demand / GMRotI50_ave	
	Median	84th percentile	Median	84th percentile	Median	84th percentile	Median	84th percentile
0	1.36	2.32	1.21	2.00	1.07	1.77	1.19	1.97
0.2	1.24	2.21	1.23	2.19	1.09	1.93	1.17	2.06
0.5	1.41	2.76	1.25	2.43	1.26	2.52	1.29	2.50
1	1.47	2.85	1.25	2.40	1.19	2.44	1.28	2.48
2	1.48	3.12	1.25	2.57	1.22	2.64	1.29	2.66
3	1.56	3.39	1.32	2.73	1.30	2.78	1.36	2.81
4	1.53	3.24	1.23	2.51	1.30	2.73	1.32	2.66

Table 3-11. Medians, means and standard deviations of $\overline{R}_{S_a,\max}$ and T_L and T_U for R1 through R4

Bin	T_L (sec)	T_U (sec)	Median	Mean	Standard deviation
R1	0	4	0.94	0.94	0.04
R2	0	1	0.96	0.95	0.04
R3	1	2	0.98	0.97	0.03
R4	2	4	0.98	0.97	0.03

Table 3-12. Numbers of ground-motion pairs as a function of period, distance and $\theta_{\max}$

Range	T_L (sec)	T_U (sec)	Parameter	$r \le 3$ km	$r \le 5$ km	$5 < r \le 15$ km
R1	0	4	n_{all}	25	36	111
			$n_{\pm 30^\circ}$	16	23	49
			$n_{\pm 30^\circ}/n_{\text{all}}$	0.64	0.64	0.44
R2	0	1	$n_{\pm 30^\circ}$	14	19	43
			$n_{\pm 30^\circ}/n_{\text{all}}$	0.56	0.53	0.39
R3	1	2	$n_{\pm 30^\circ}$	17	22	53
			$n_{\pm 30^\circ}/n_{\text{all}}$	0.68	0.61	0.48
R4	2	4	$n_{\pm 30^\circ}$	19	26	51
			$n_{\pm 30^\circ}/n_{\text{all}}$	0.76	0.72	0.46

Table 3-13. Statistics of the correlation coefficients of Figure 3-63

Type of correlation coefficient	Mean	Standard deviation	Median	Ninetieth percentile	Cumulative probability for $\rho = 0.3$
ρ_{Max}	0.24	0.15	0.21	0.44	0.74
ρ_{FN_FP}	0.14	0.12	0.12	0.31	0.89
$\rho_{Max_S_a}$	0.12	0.11	0.09	0.26	0.92

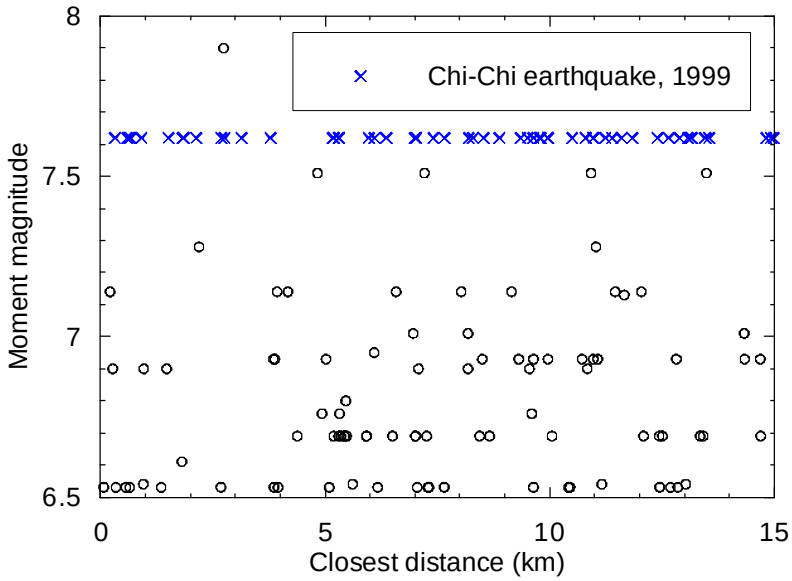

Figure 3-1. Magnitude and distance distribution of the ground motions of Table 3-1

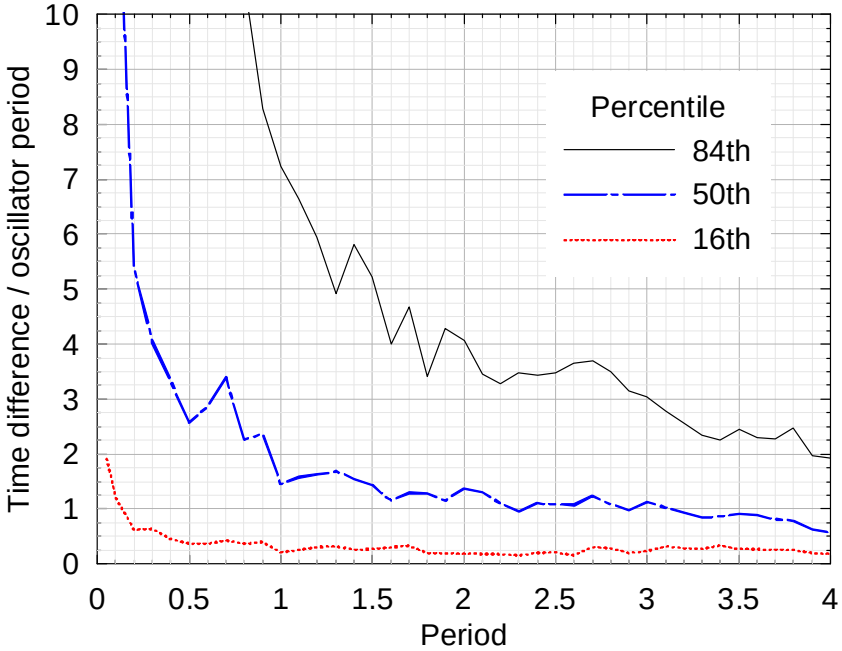

a. 84th, 50th and 16th percentiles

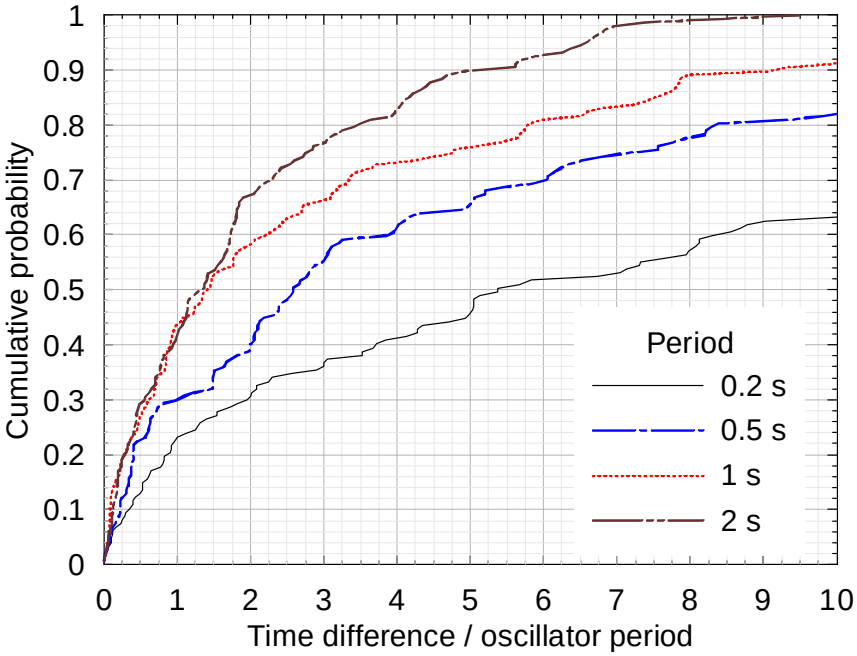

b. CDFs

Figure 3-2. a) Eighty-fourth, 50th and 16th percentiles and b) cumulative distribution functions of normalized time difference between the peak accelerations parallel and perpendicular to the GMRotI50 direction for the records of Table 3-1

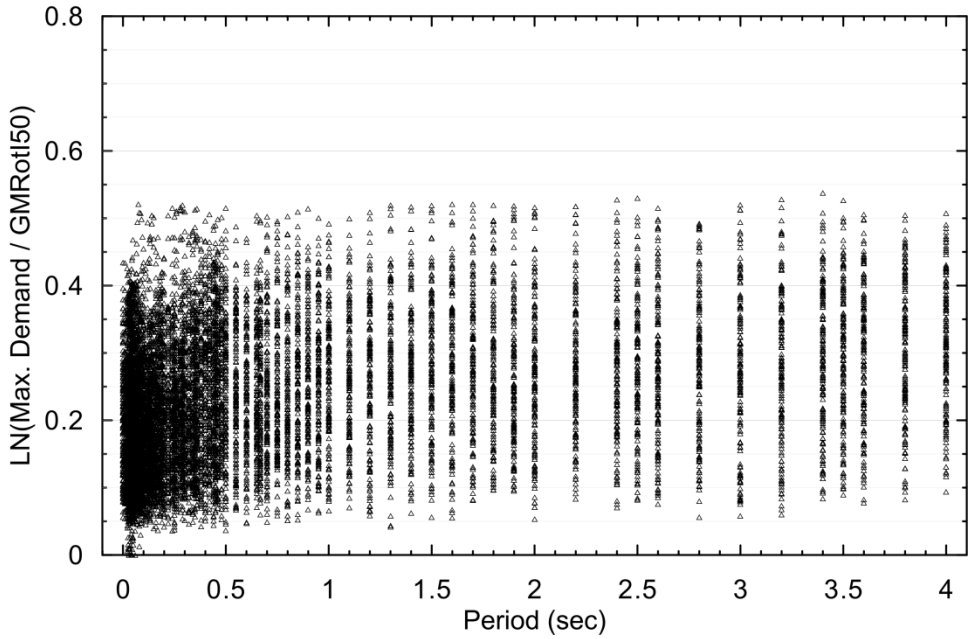

Figure 3-3. Ratios of maximum spectral demand to GMRotI50 for the records of Table 3-1

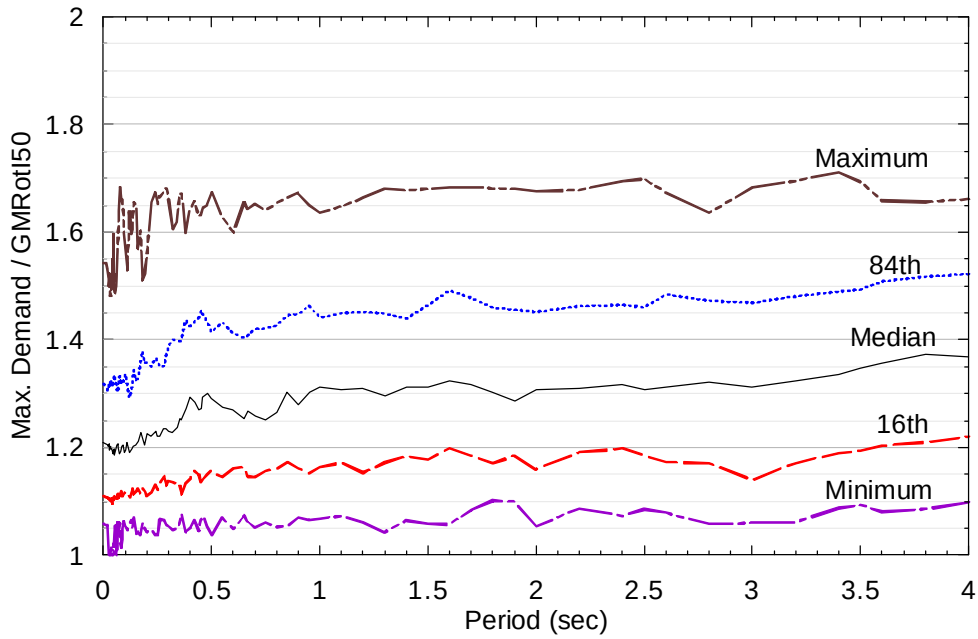

Figure 3-4. Maximum, minimum, median and 84th and 16th percentiles of the ratios of maximum spectral demand to GMRotI50 for the records of Table 3-1

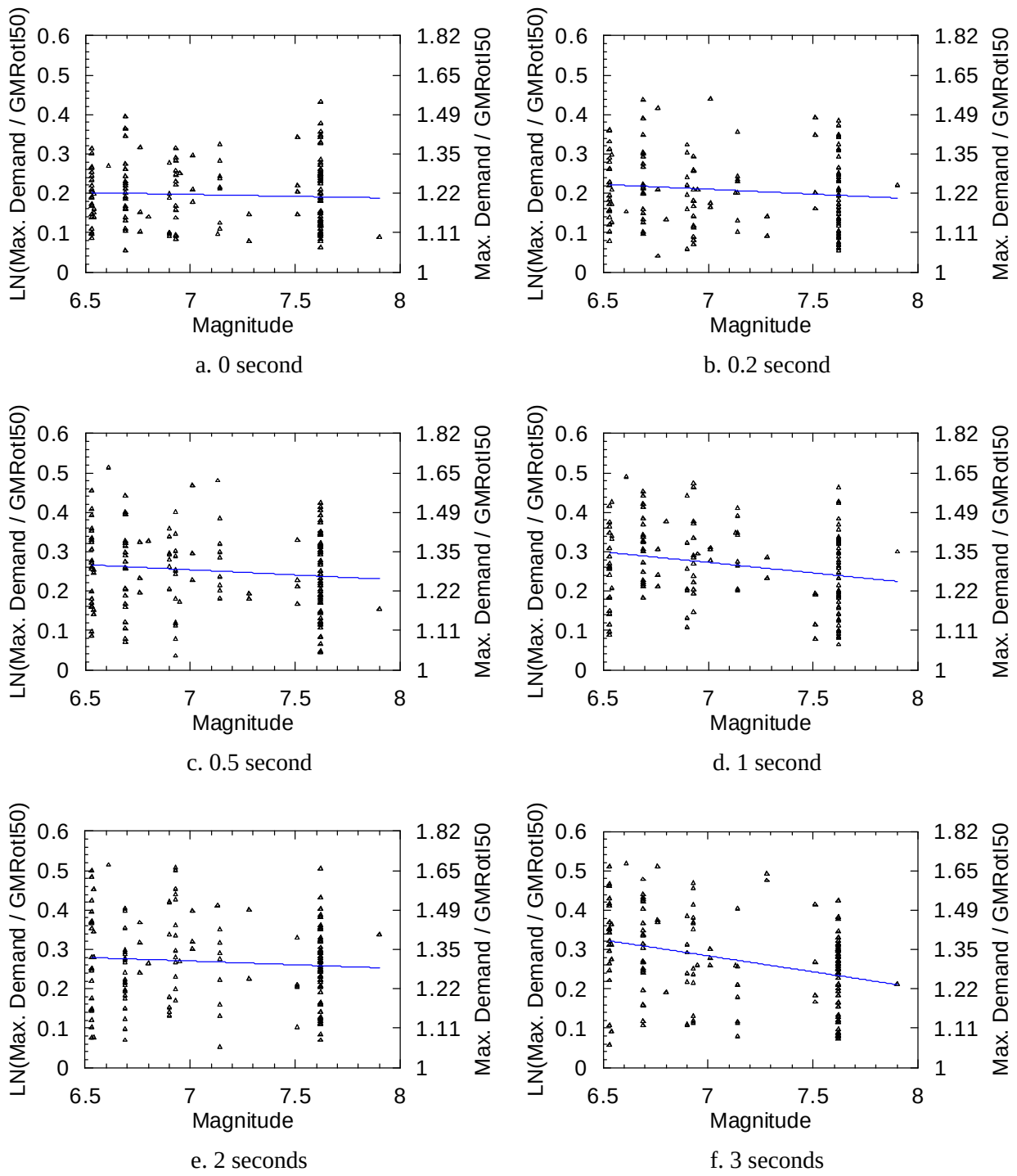

Figure 3-5. Ratios of maximum spectral demand to GMRotI50 at periods of 0, 0.2, 0.5, 1, 2 and 3 seconds as a function of magnitude for the records of Table 3-1

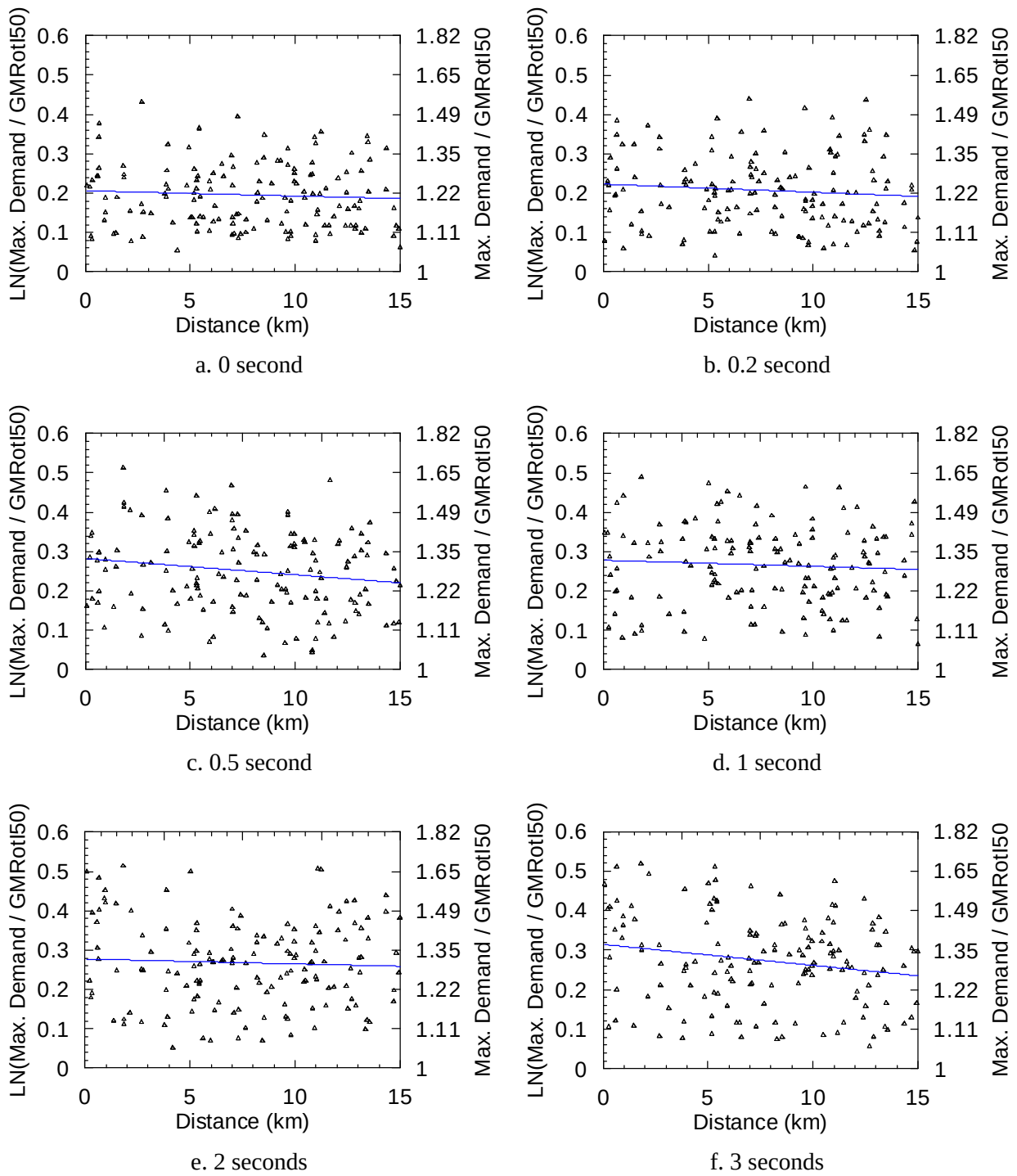

Figure 3-6. Ratios of maximum spectral demand to GMRotI50 at periods of 0, 0.2, 0.5, 1, 2 and 3 seconds as a function of distance for the records of Table 3-1

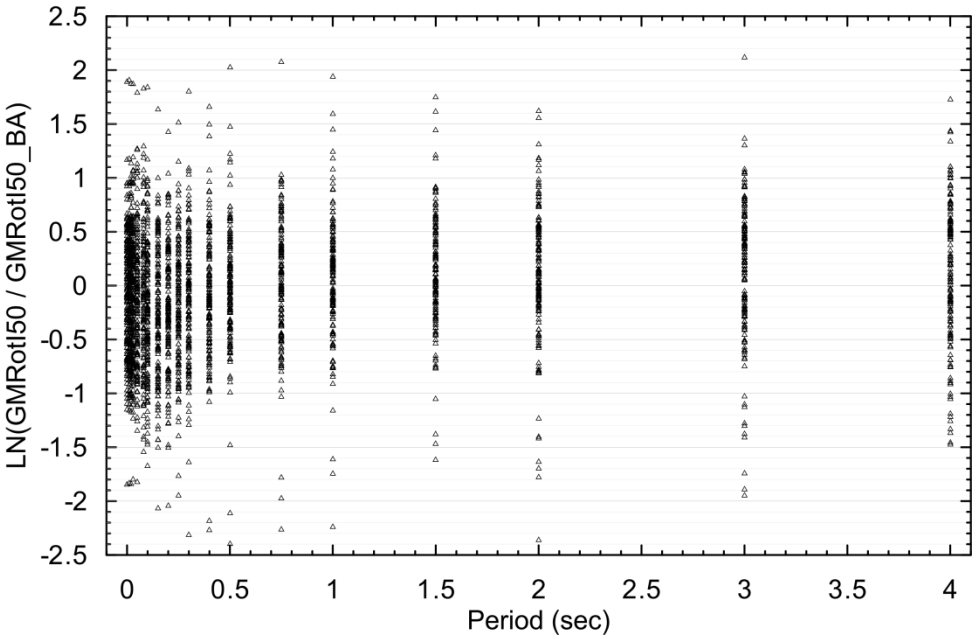

Figure 3-7. Ratios of GMRotI50 to GMRotI50_BA for the records of Table 3-1

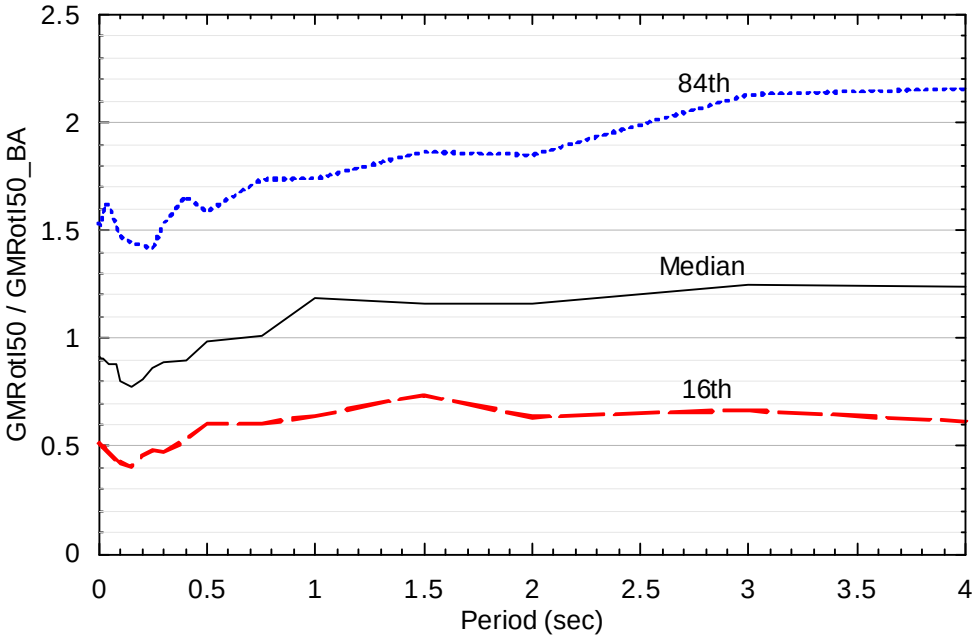

Figure 3-8. Median and 84th and 16th percentiles of the ratios of GMRotI50 to GMRotI50_BA for the records of Table 3-1

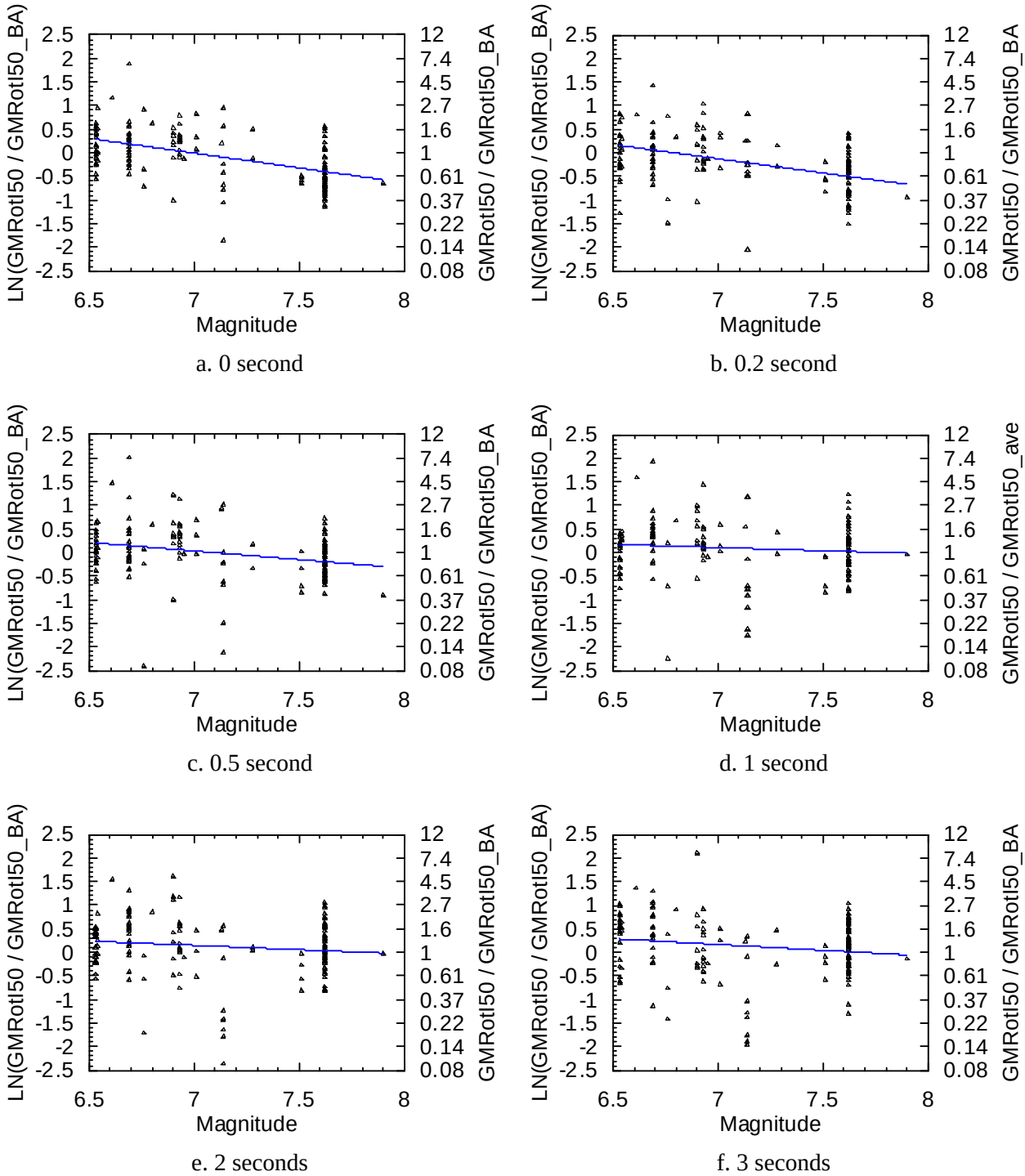

Figure 3-9. Ratios of GMRotI50 to GMRotI50_BA at periods of 0, 0.2, 0.5, 1, 2 and 3 seconds as a function of magnitude for the records of Table 3-1

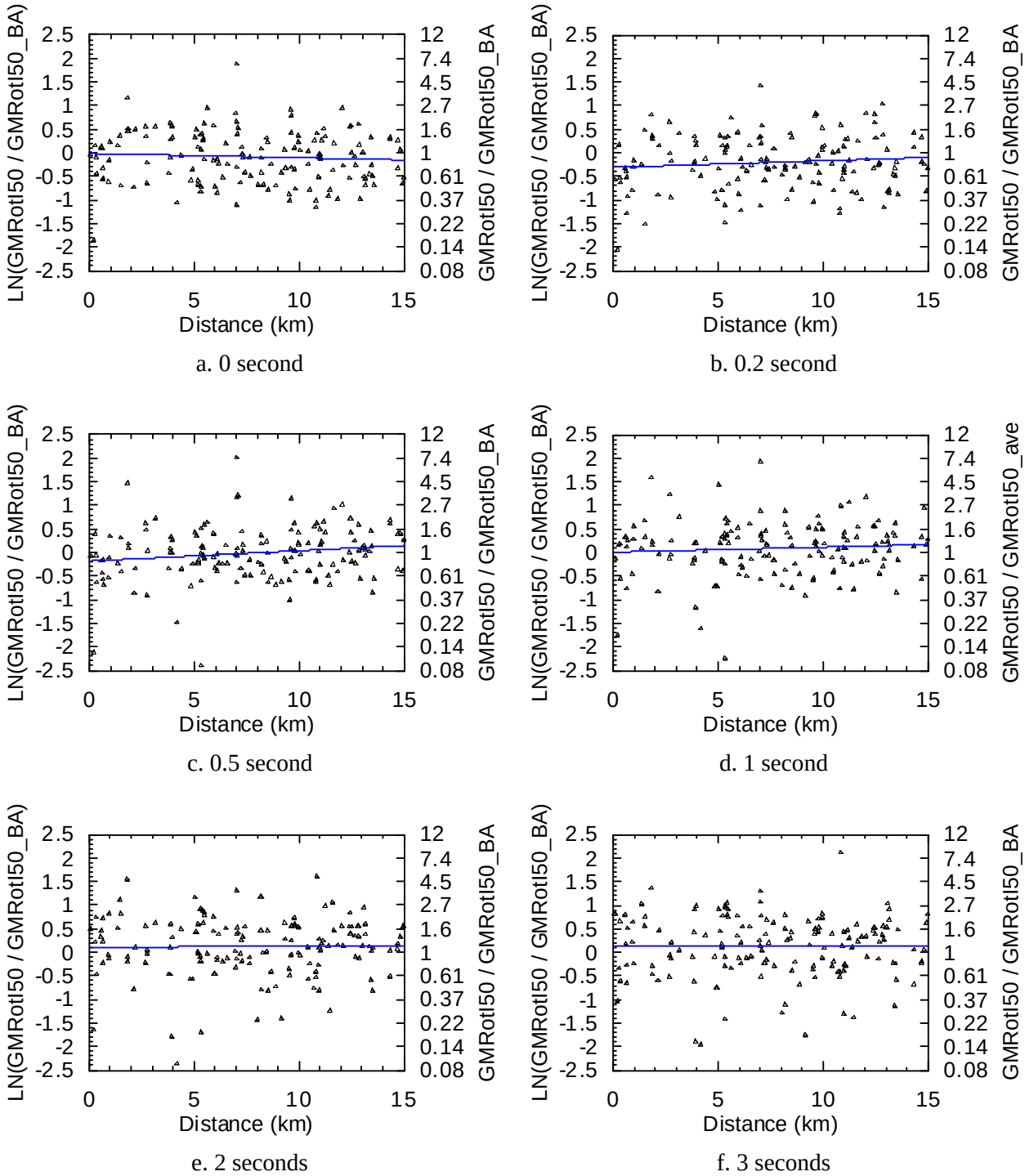

Figure 3-10. Ratios of GMRotI50 to GMRotI50_BA at periods of 0, 0.2, 0.5, 1, 2 and 3 seconds as a function of distance for the records of Table 3-1

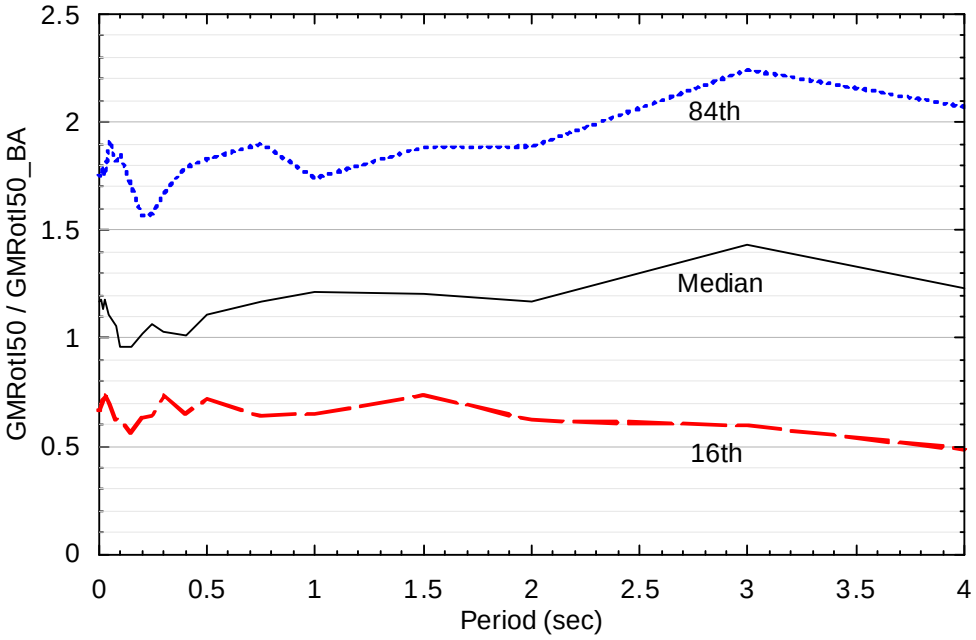

Figure 3-11. Median and 84th and 16th percentiles of the ratios of GMRotI50 to GMRotI50_BA for all of the records of Table 3-1 except those of the 1999 Chi-Chi earthquake

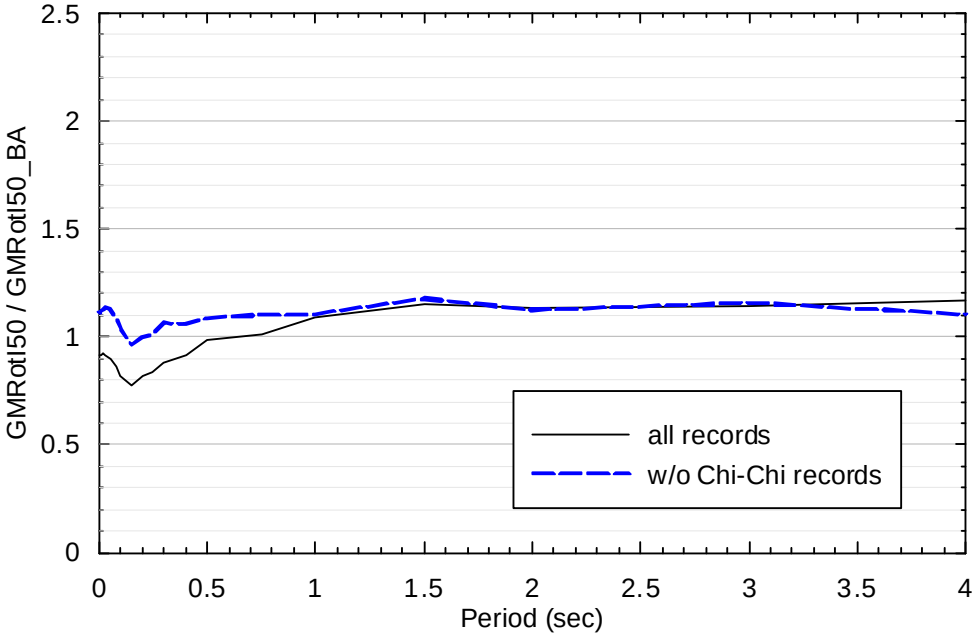

Figure 3-12. Median ratios of GMRotI50 to GMRotI50_BA computed using (3.1) for all of the records of Table 3-1 and for all of the records except those of the 1999 Chi-Chi earthquake

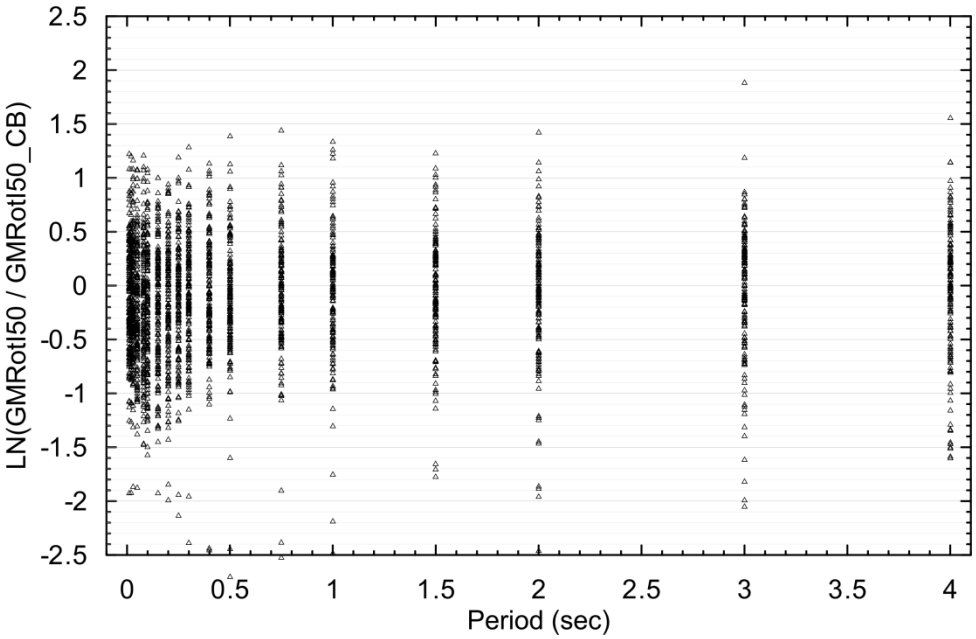

Figure 3-13. Ratios of GMRotI50 to GMRotI50_CB for the records of Table 3-1

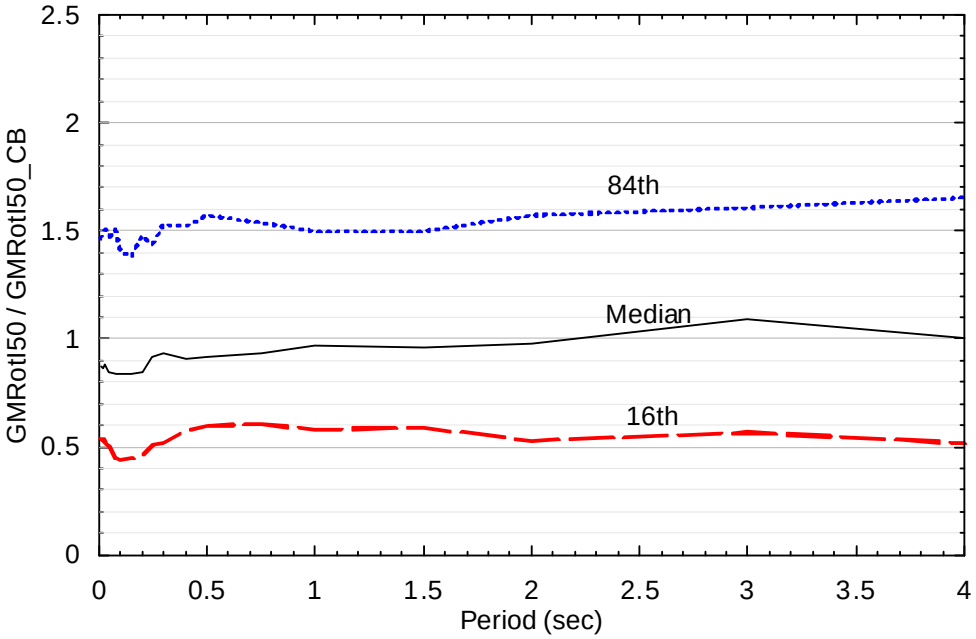

Figure 3-14. Median and 84th and 16th percentiles of the ratios of GMRotI50 to GMRotI50_CB for the records of Table 3-1

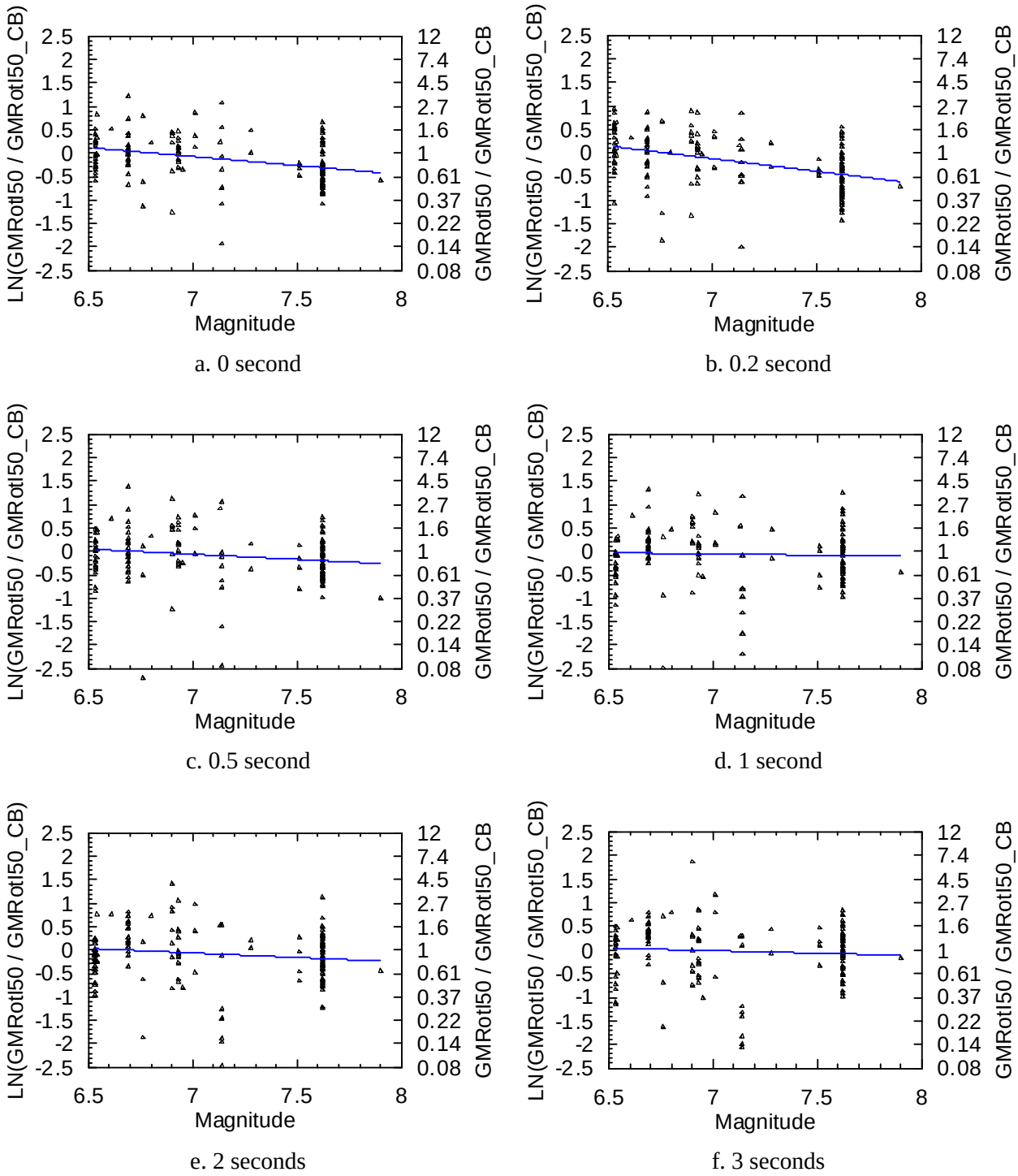

Figure 3-15. Ratios of GMRotI50 to GMRotI50_CB at periods of 0, 0.2, 0.5, 1, 2 and 3 seconds as a function of magnitude for the records of Table 3-1

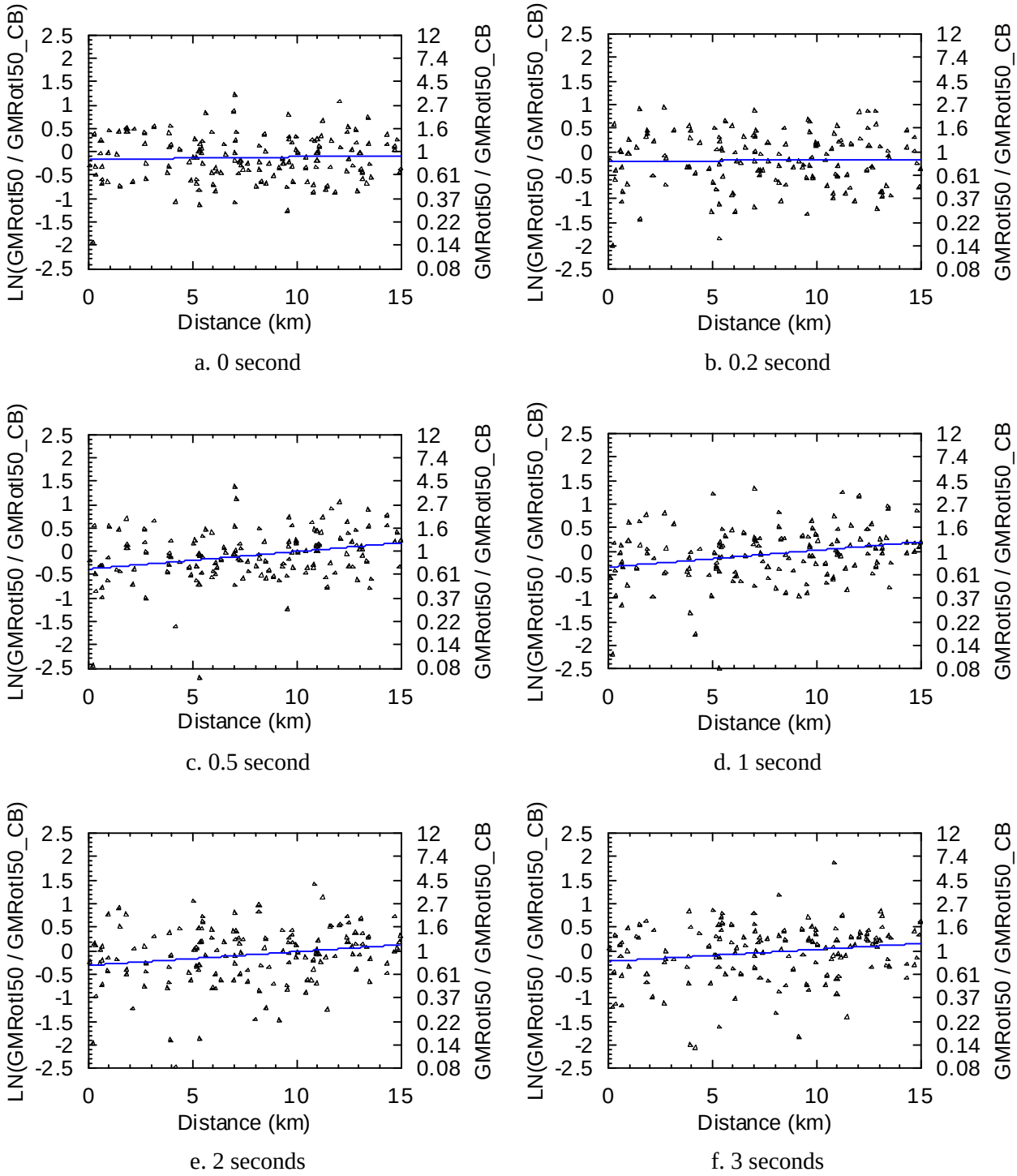

Figure 3-16. Ratios of GMRotI50 to GMRotI50_CB at periods of 0, 0.2, 0.5, 1, 2 and 3 seconds as a function of distance for the records of Table 3-1

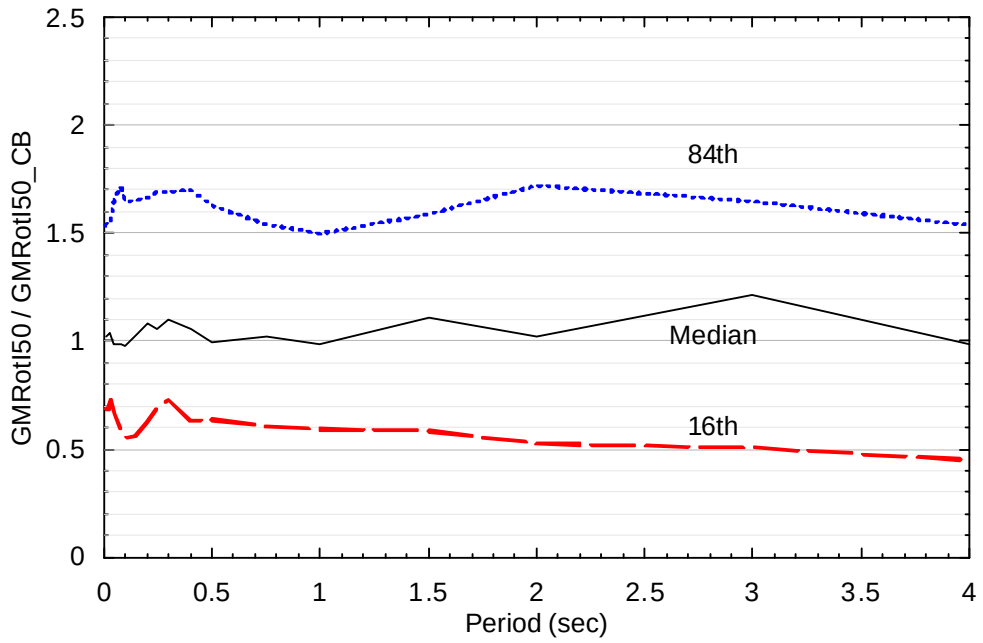

Figure 3-17. Median and 84th and 16th percentiles of the ratios of GMRotI50 to GMRotI50_CB for all the records of Table 3-1 except those of the 1999 Chi-Chi earthquake

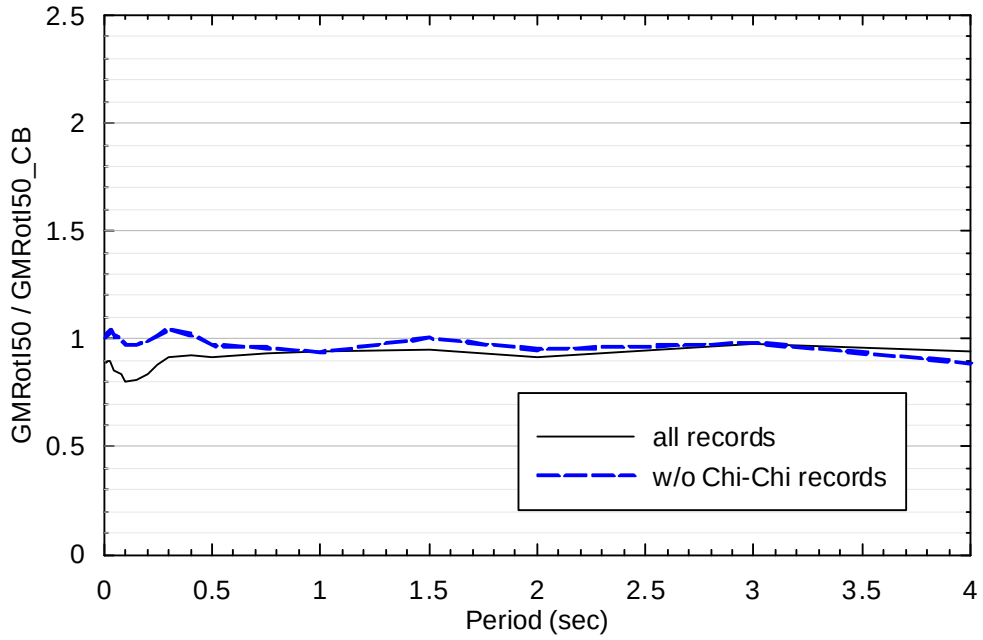

Figure 3-18. Median ratios of GMRotI50 to GMRotI50_CB computed using (3.1) for all of the records of Table 3-1 and for all of the records except those of the 1999 Chi-Chi earthquake

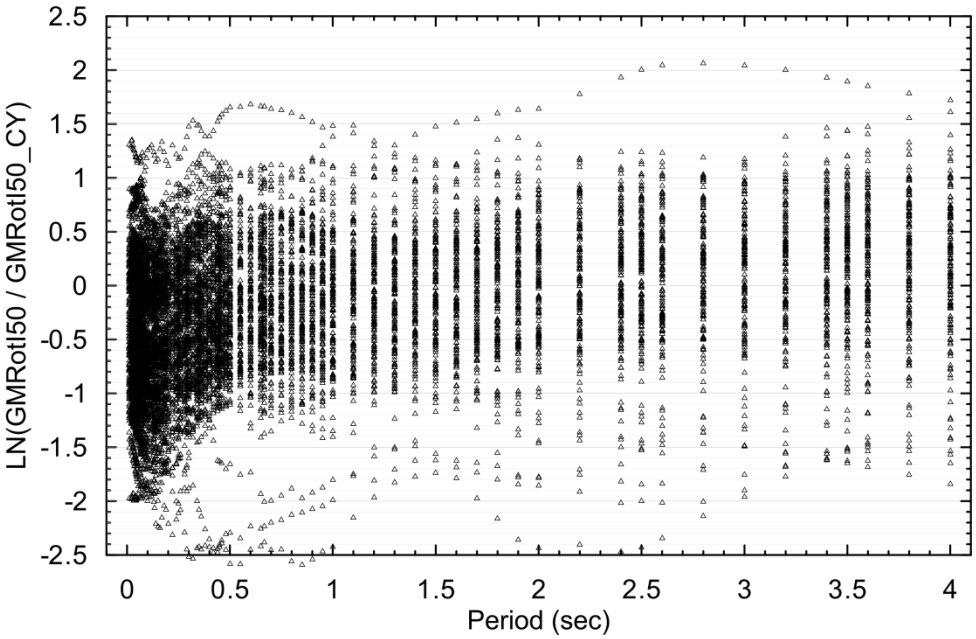

Figure 3-19. Ratios of GMRotI50 to GMRotI50_CY for the records of Table 3-1

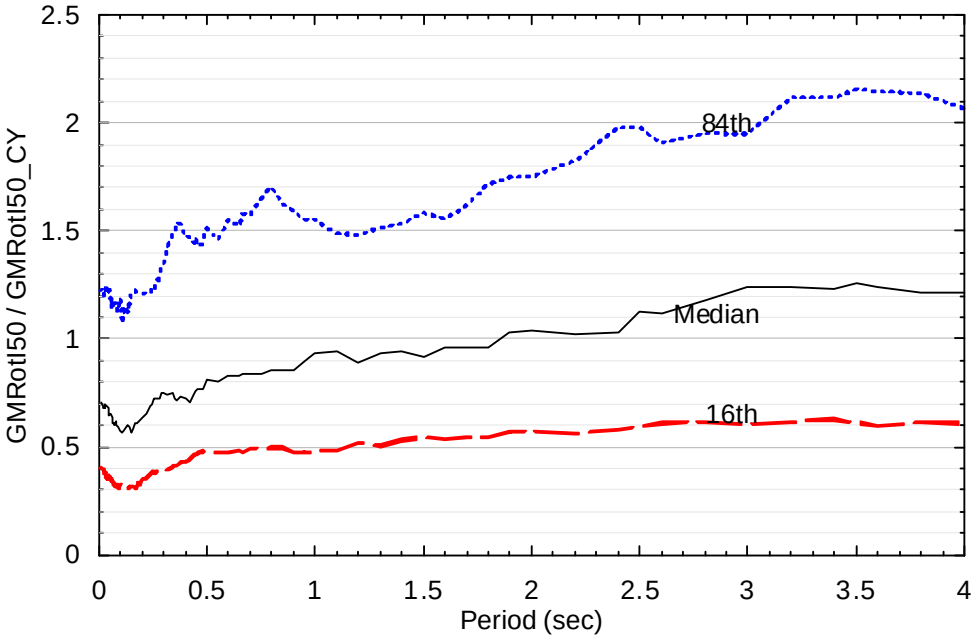

Figure 3-20. Median and 84th and 16th percentiles of the ratios of GMRotI50 to GMRotI50_CY for the records of Table 3-1

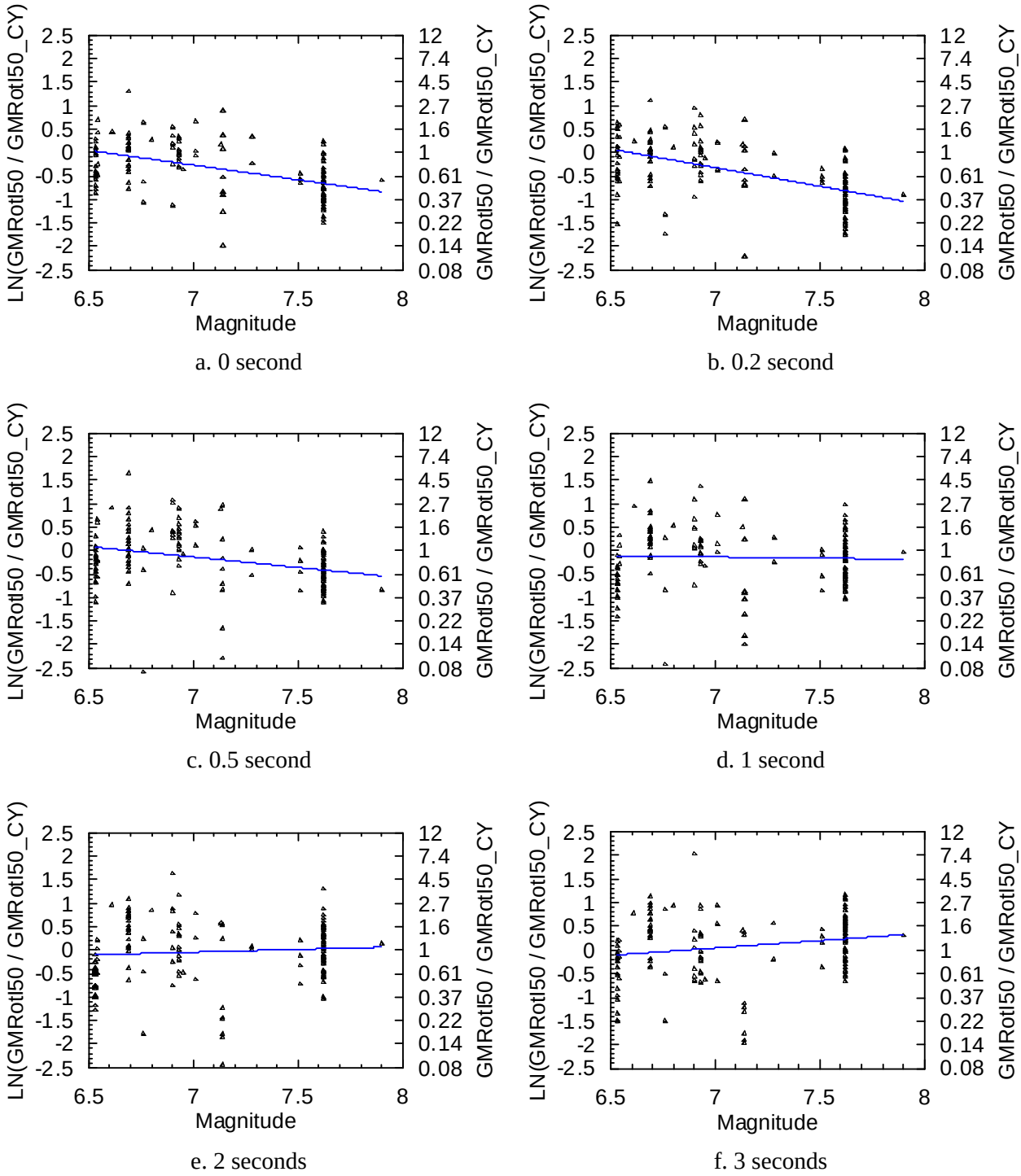

Figure 3-21. Ratios of GMRotI50 to GMRotI50_CY at periods of 0, 0.2, 0.5, 1, 2 and 3 seconds as a function of magnitude for the records of Table 3-1

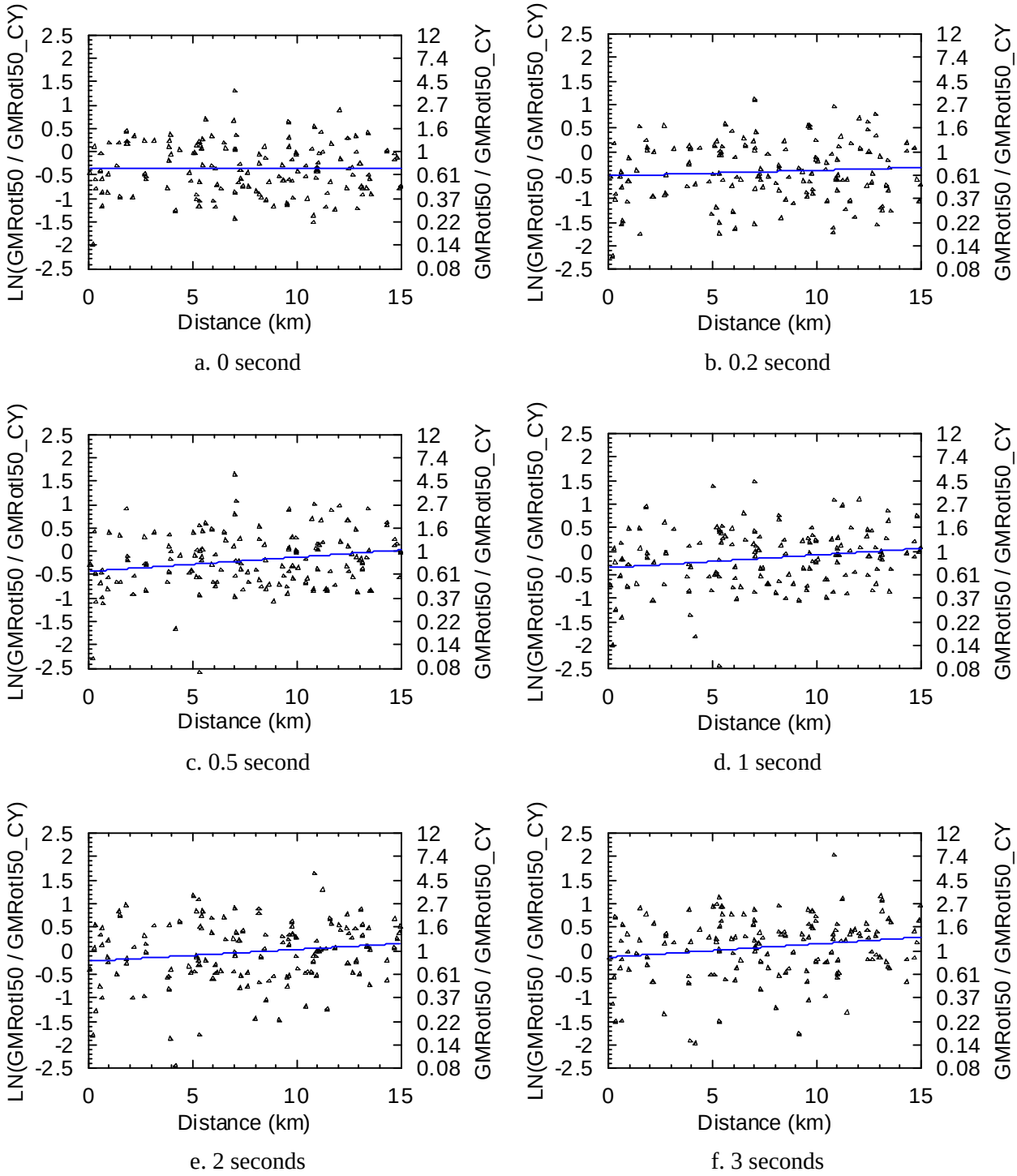

Figure 3-22. Ratios of GMRotI50 to GMRotI50_CY at periods of 0, 0.2, 0.5, 1, 2 and 3 seconds as a function of distance for the records of Table 3-1

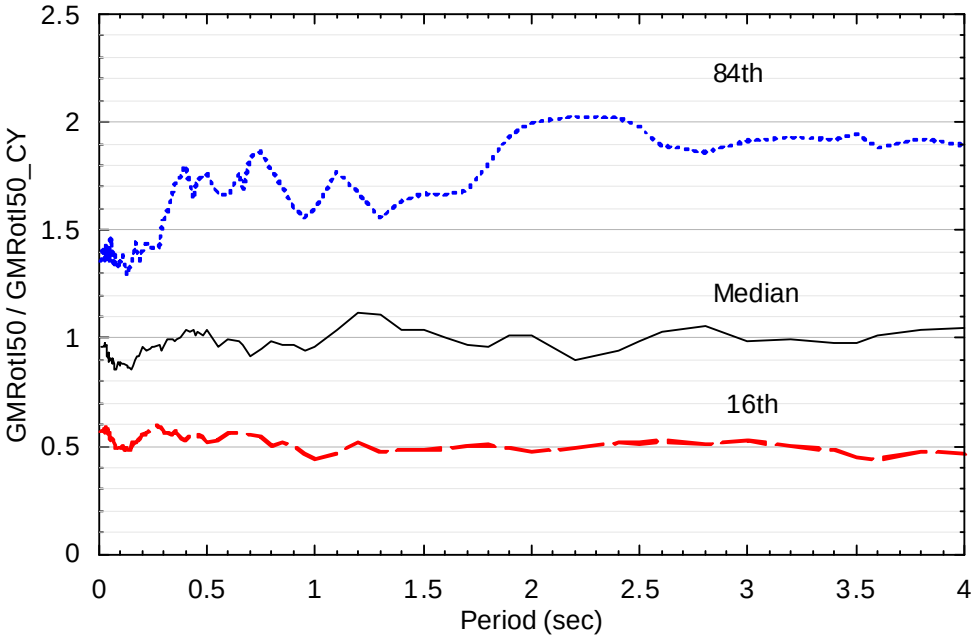

Figure 3-23. Median and 84th and 16th percentiles of the ratios of GMRotI50 to GMRotI50_CY for all of the records of Table 3-1 except those of the 1999 Chi-Chi earthquake

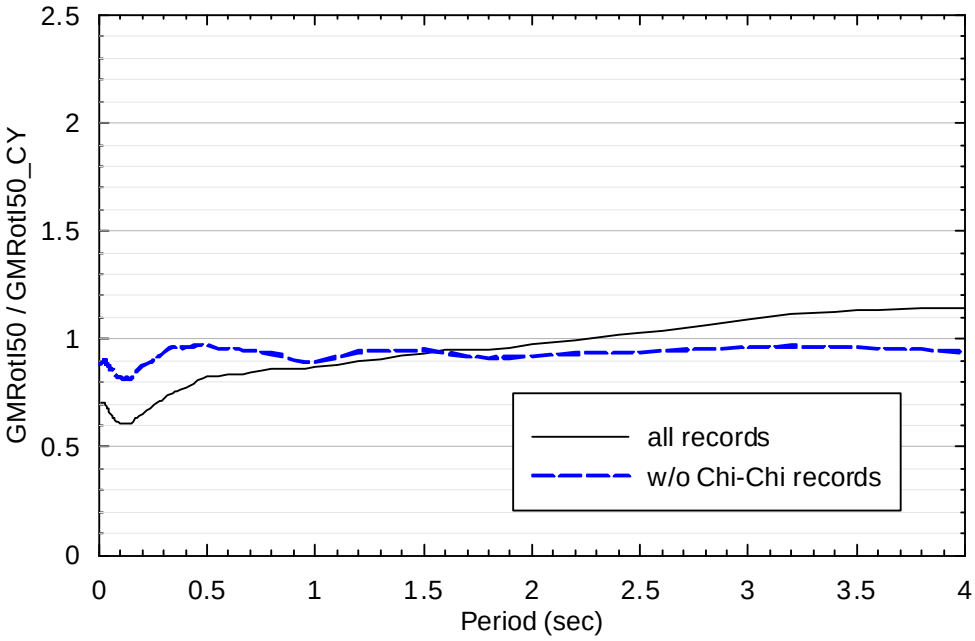

Figure 3-24. Median ratios of GMRotI50 to GMRotI50_CY computed using (3.1) for all of the records of Table 3-1 and for all of the records except those of the 1999 Chi-Chi earthquake

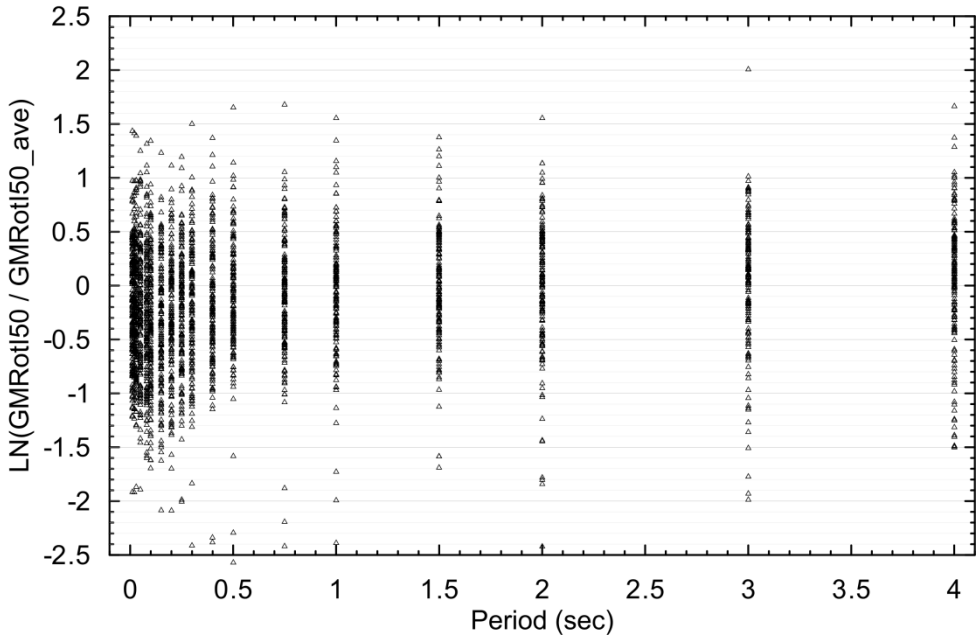

Figure 3-25. Ratios of GMRotI50 to GMRotI50_ave for the records of Table 3-1

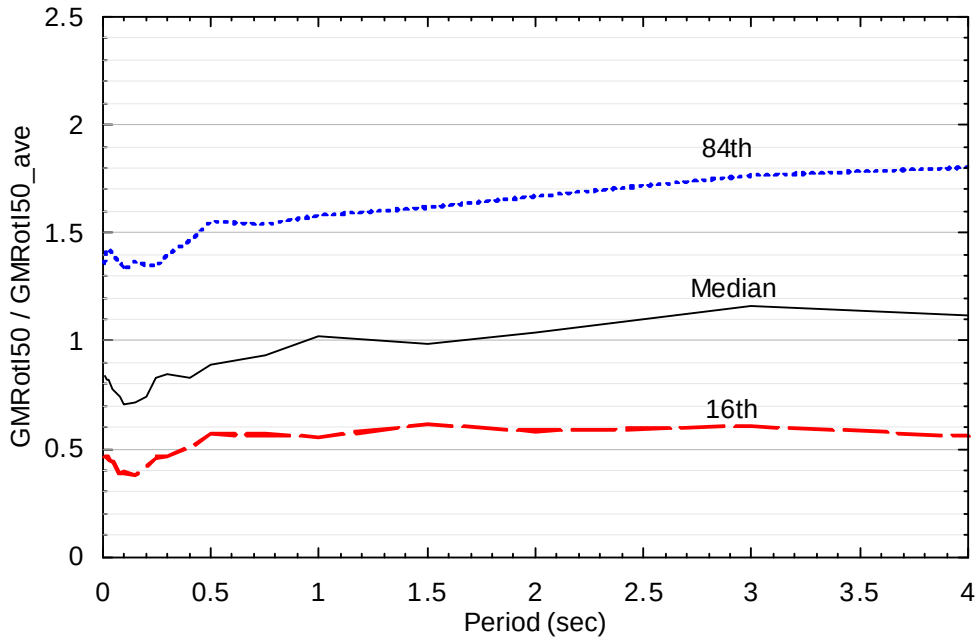

Figure 3-26. Median and 84th and 16th percentiles of the ratios of GMRotI50 to GMRotI50_ave for the records of Table 3-1

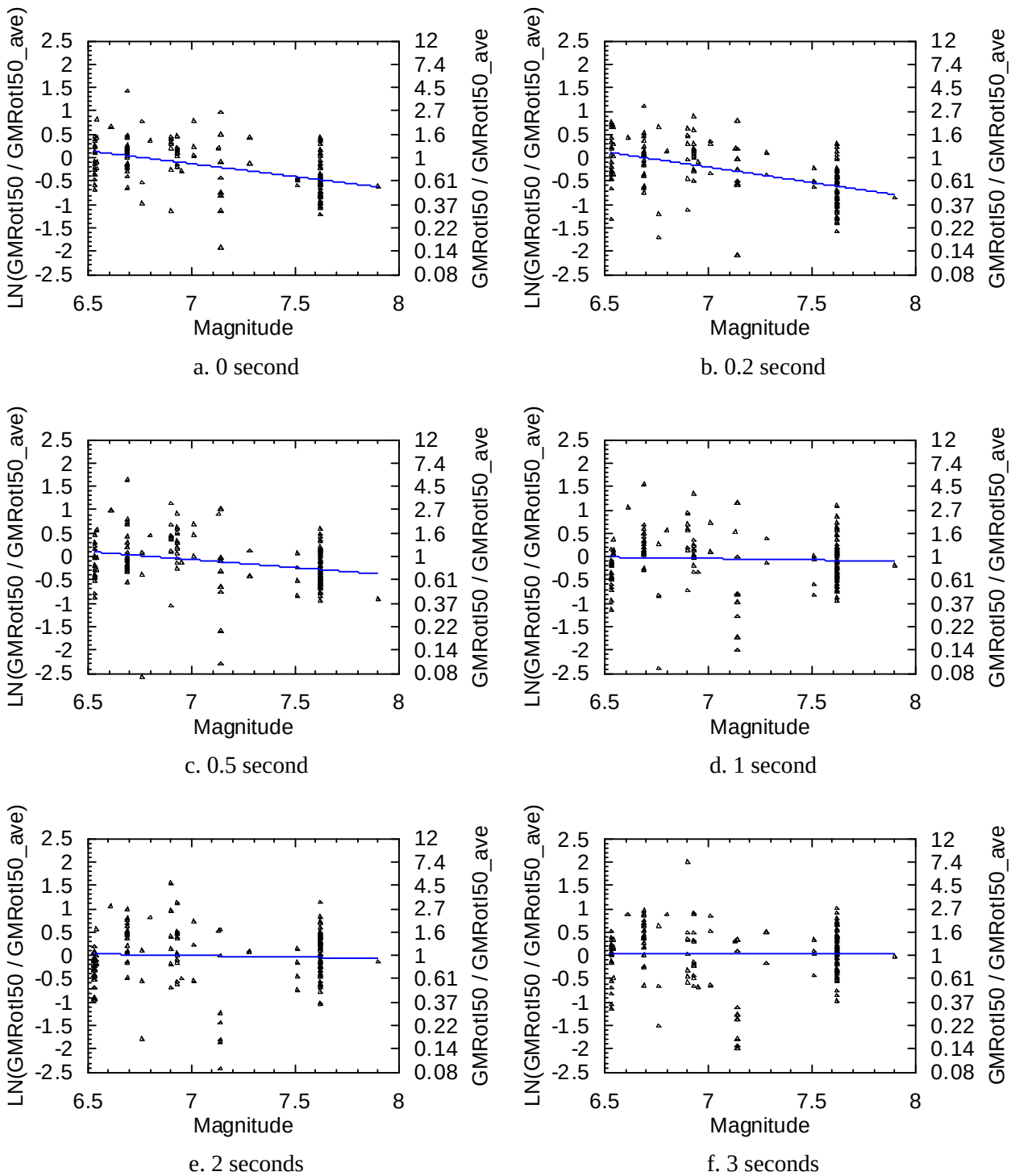

a. 0 second

b. 0.2 second

c. 0.5 second

d. 1 second

e. 2 seconds

f. 3 seconds

Figure 3-27. Ratios of GMRotI50 to GMRotI50_ave at periods of 0, 0.2, 0.5, 1, 2 and 3 seconds as a function of magnitude for the records of Table 3-1

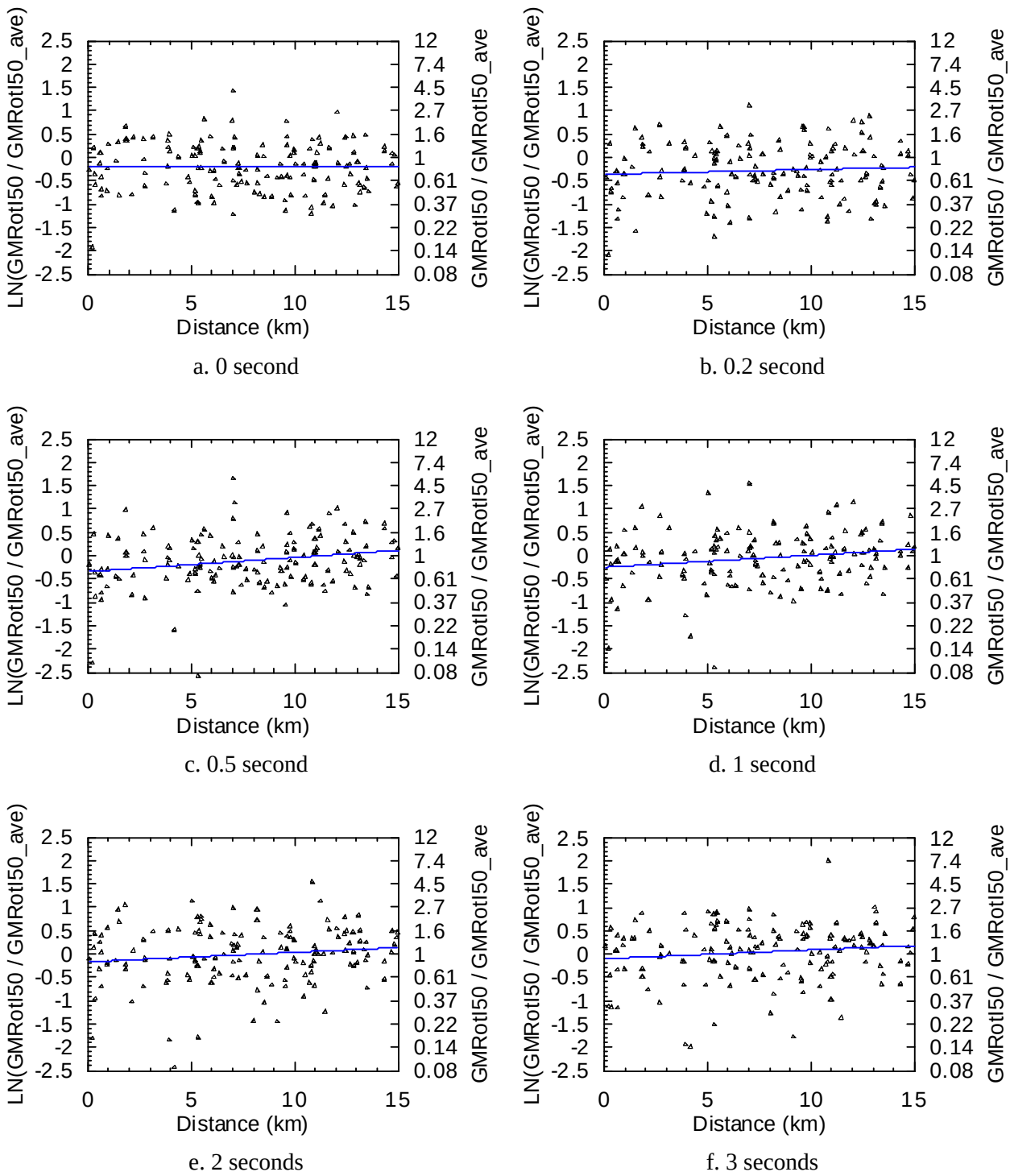

Figure 3-28. Ratios of GMRotI50 to GMRotI50_ave at periods of 0, 0.2, 0.5, 1, 2 and 3 seconds as a function of distance for the records of Table 3-1

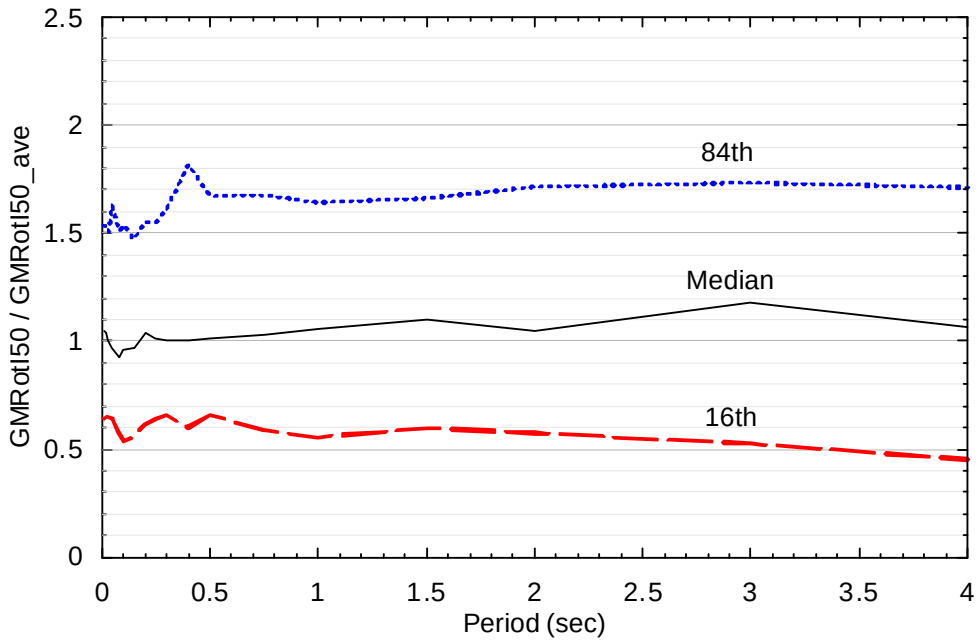

Figure 3-29. Median and 84th and 16th percentiles of the ratios of GMRotI50 to GMRotI50_ave for all of the records of Table 3-1 except those of the 1999 Chi-Chi earthquake

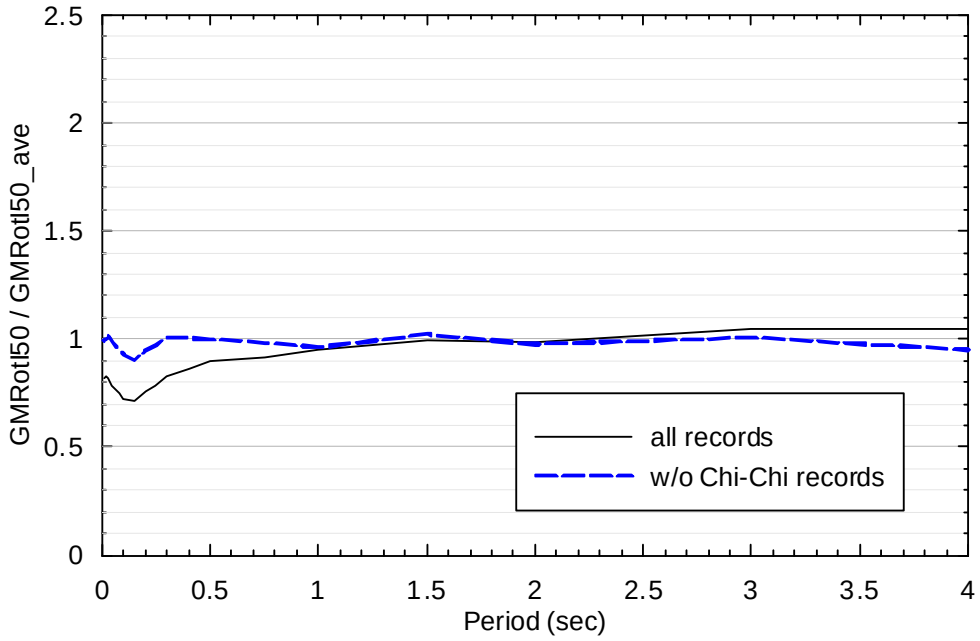

Figure 3-30. Median ratios of GMRotI50 to GMRotI50_ave computed using (3.1) for all of the records of Table 3-1 and for all of the records except those of the 1999 Chi-Chi earthquake

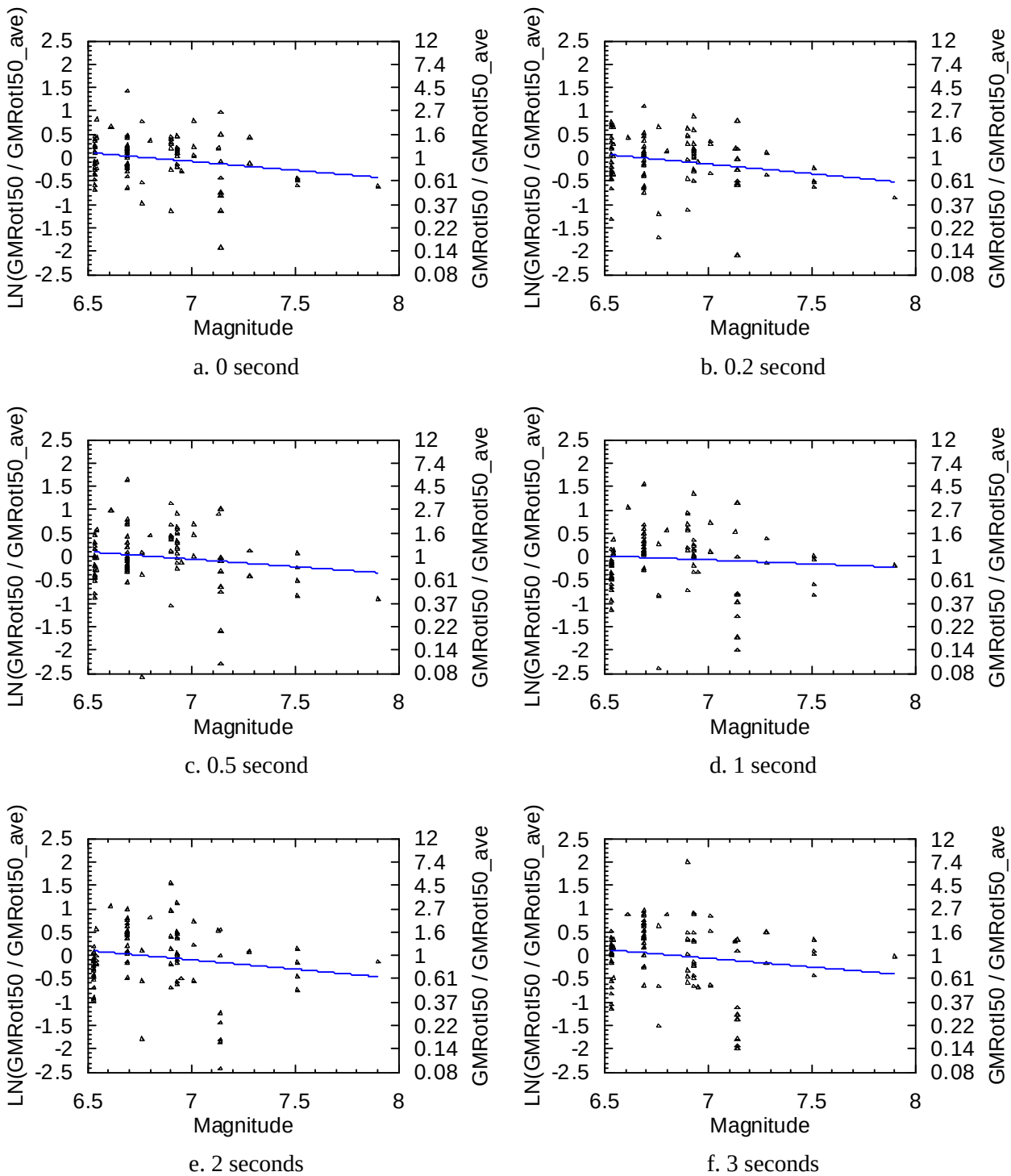

a. 0 second

b. 0.2 second

c. 0.5 second

d. 1 second

e. 2 seconds

f. 3 seconds

Figure 3-31. Ratios of GMRotI50 to GMRotI50_ave at periods of 0, 0.2, 0.5, 1, 2 and 3 seconds as a function of magnitude for all of the records of Table 3-1 except those of the 1999 Chi-Chi earthquake

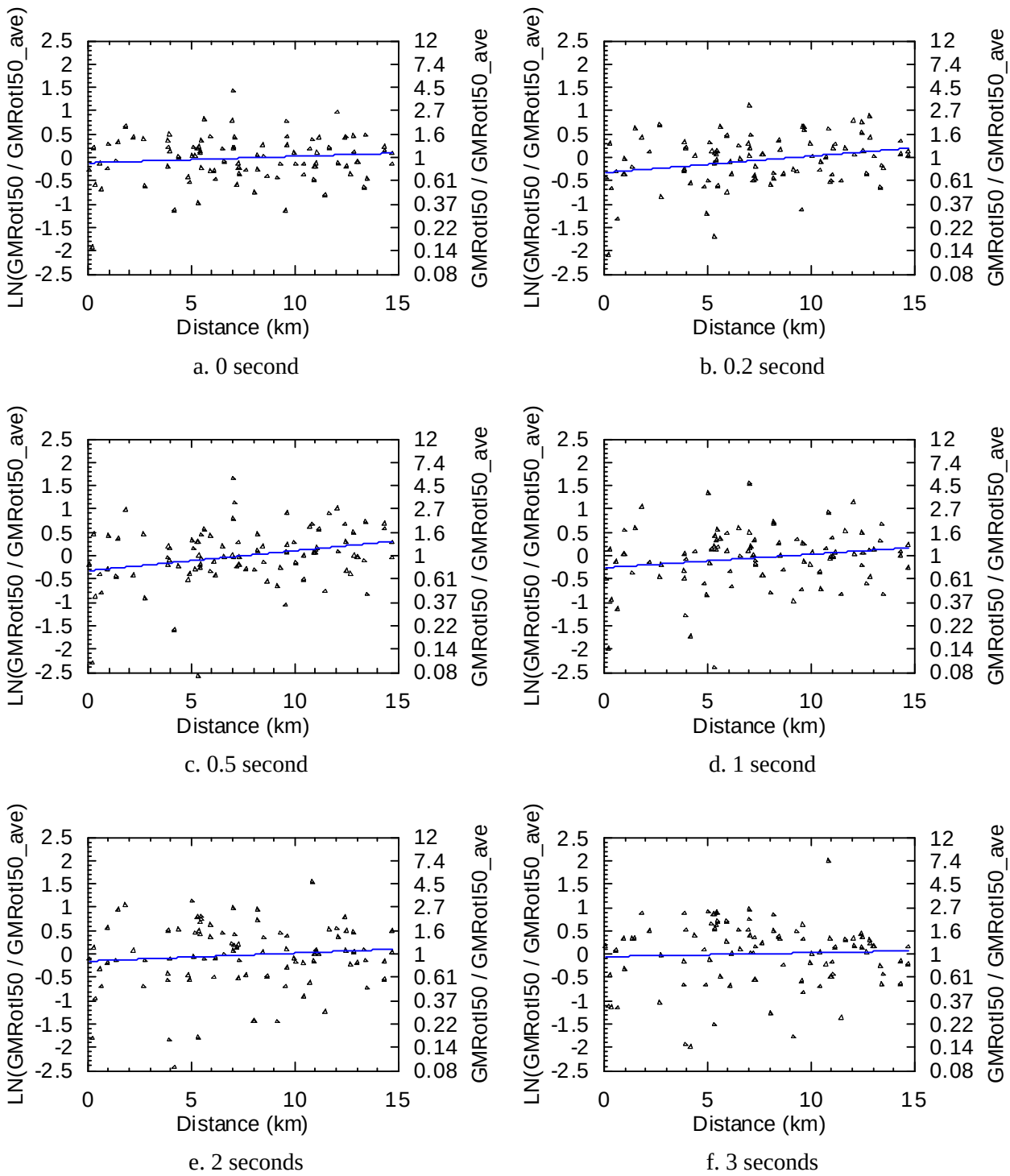

Figure 3-32. Ratios of GMRotI50 to GMRotI50_ave at periods of 0, 0.2, 0.5, 1, 2 and 3 seconds as a function of distance for all of the records of Table 3-1 except those of the 1999 Chi-Chi earthquake

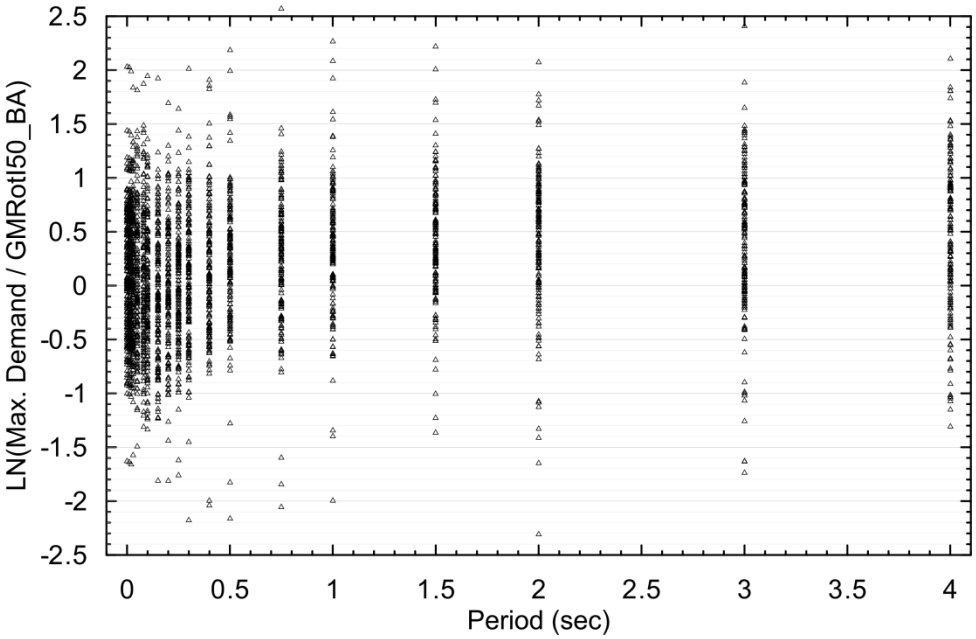

Figure 3-33. Ratios of maximum spectral demand to GMRotI50_BA for the records of Table 3-1

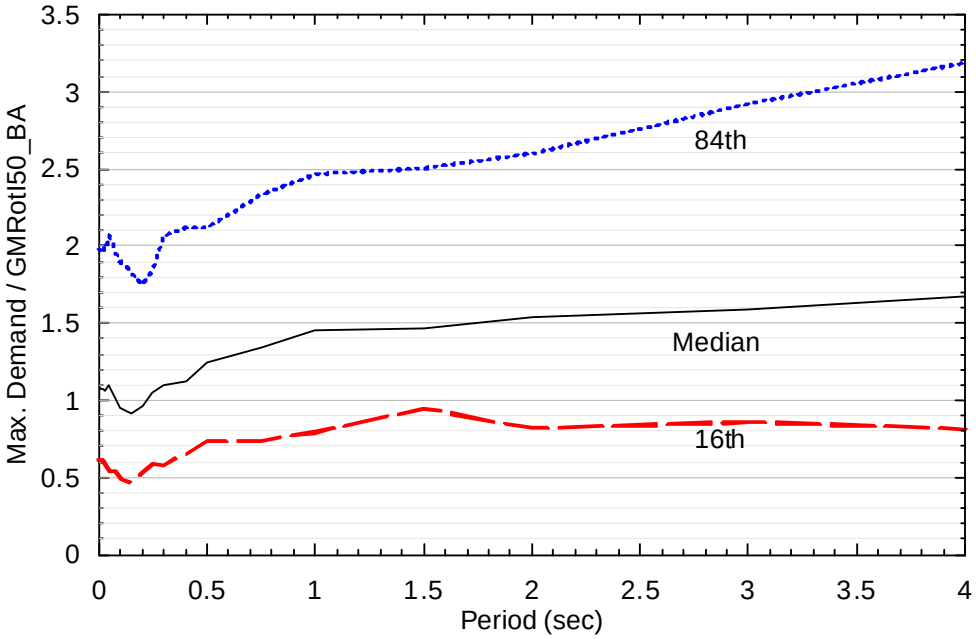

Figure 3-34. Median and 84th and 16th percentiles of the ratios of maximum spectral demand to GMRotI50_BA for the records of Table 3-1

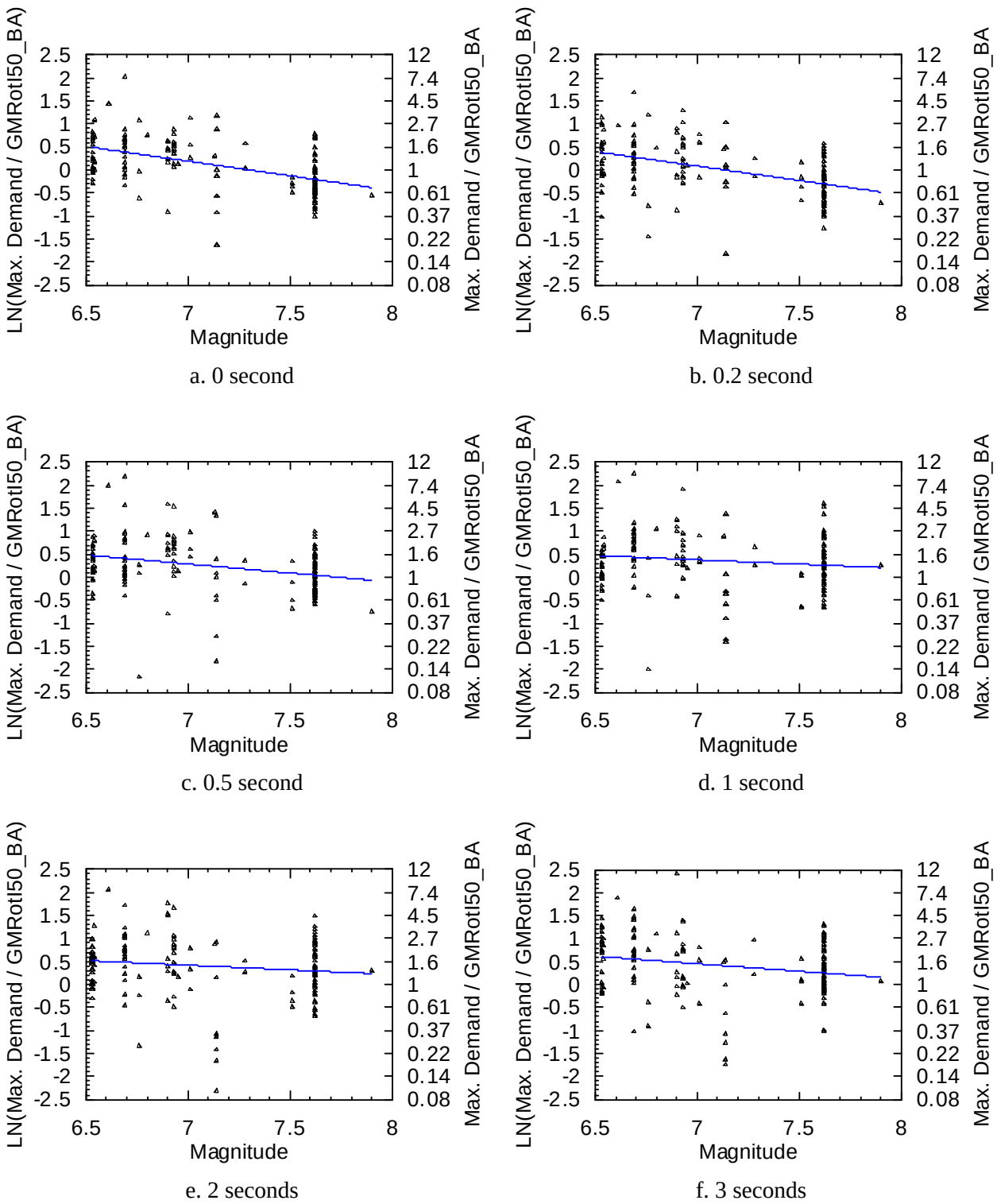

Figure 3-35. Ratios of maximum spectral demand to GMRotI50_BA at periods of 0, 0.2, 0.5, 1, 2 and 3 seconds as a function of magnitude for the records of Table 3-1

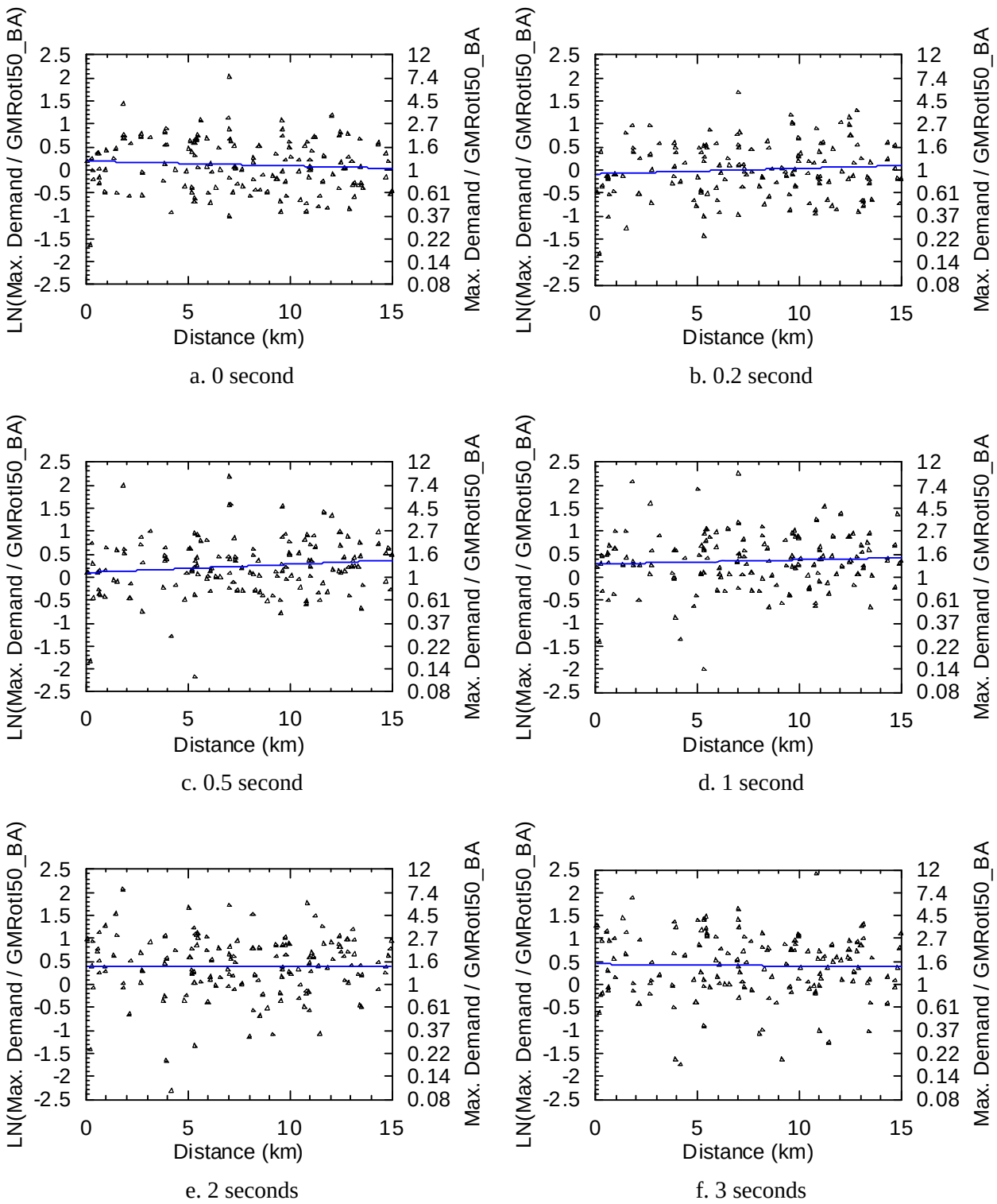

Figure 3-36. Ratios of maximum spectral demand to GMRotI50_BA at periods of 0, 0.2, 0.5, 1, 2 and 3 seconds as a function of distance for the records of Table 3-1

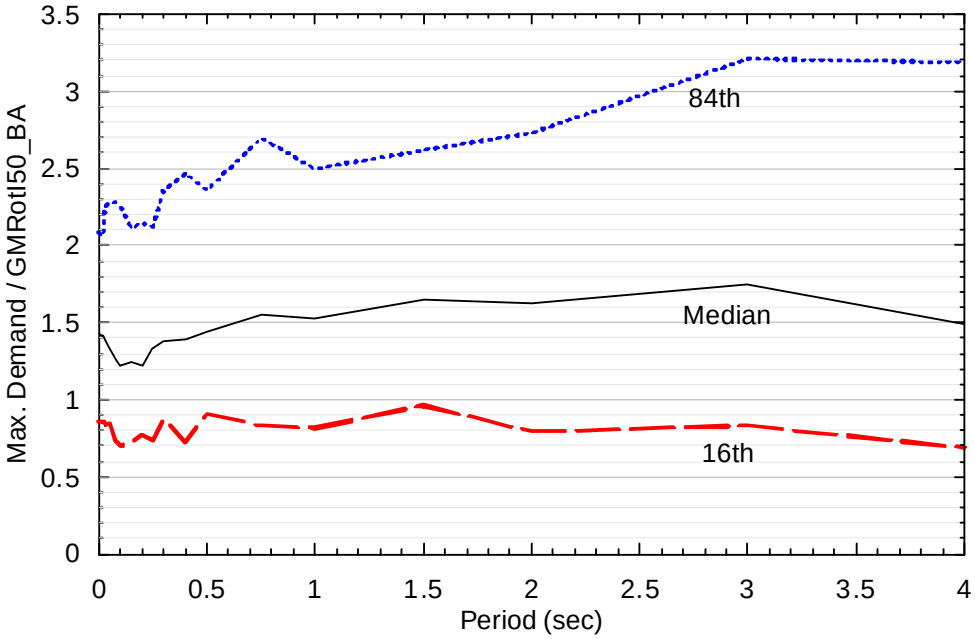

Figure 3-37. Median and 84th and 16th percentiles of the ratios of maximum spectral demand to GMRotI50_BA for all of the records of Table 3-1 except those of the 1999 Chi-Chi earthquake

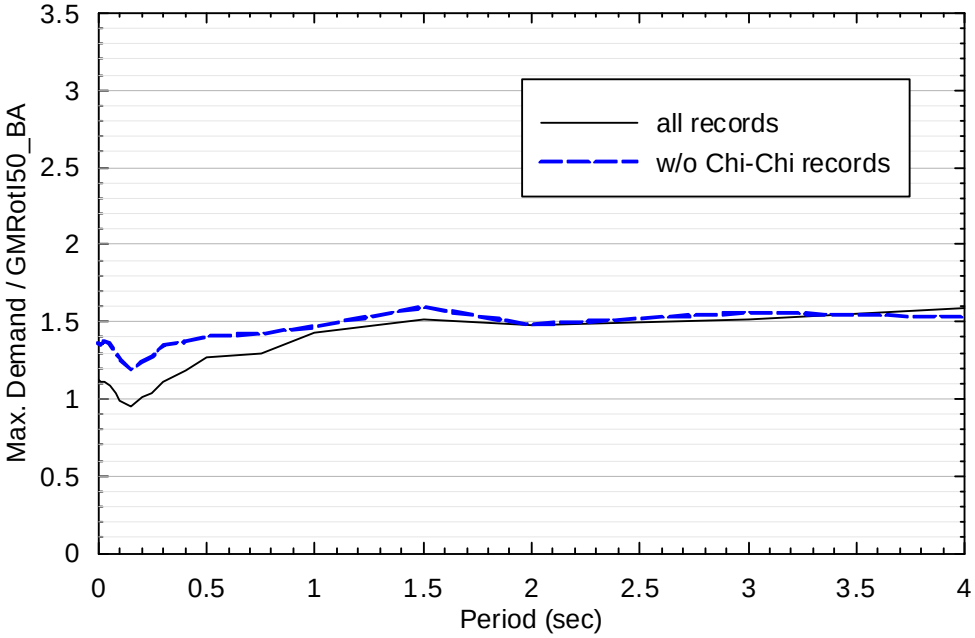

Figure 3-38. Median ratios of maximum spectral demand to GMRotI50_BA computed using (3.1) for all of the records of Table 3-1 and for all of the records except those of the 1999 Chi-Chi earthquake

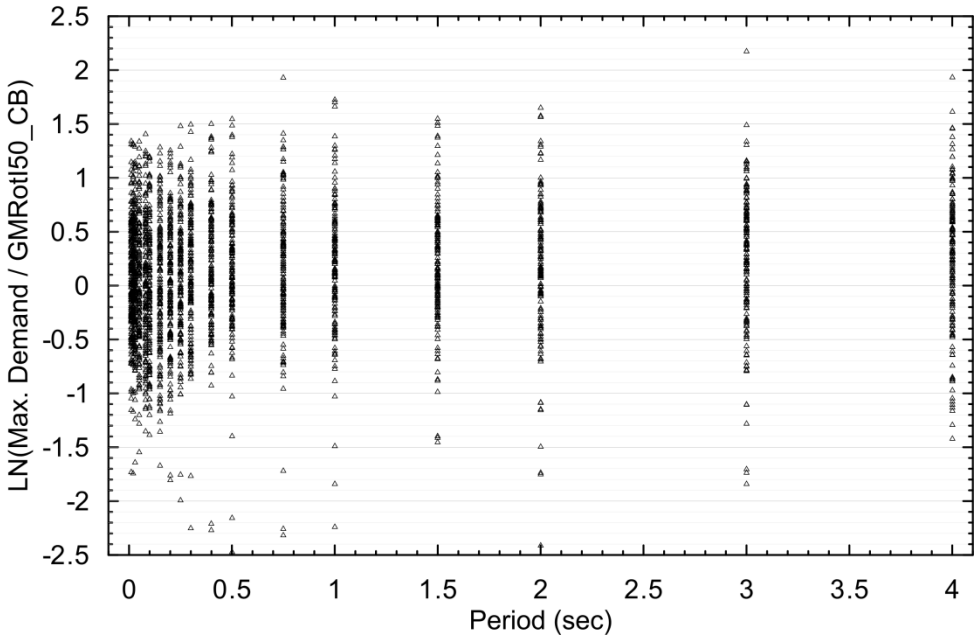

Figure 3-39. Ratios of maximum spectral demand to GMRotI50_CB for the records of Table 3-1

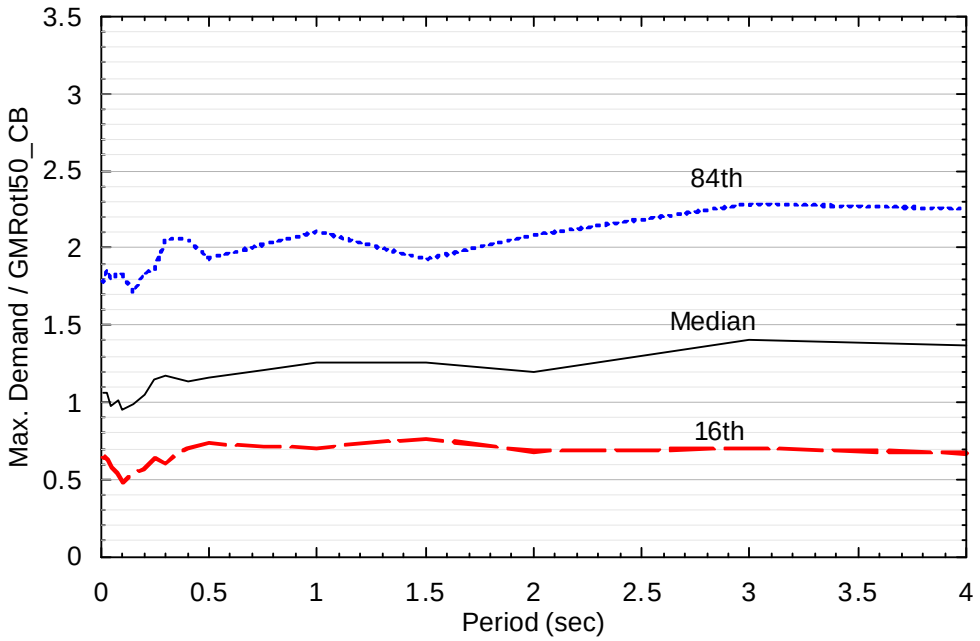

Figure 3-40. Median and 84th and 16th percentiles of the ratios of maximum spectral demand to GMRotI50_CB for the records of Table 3-1

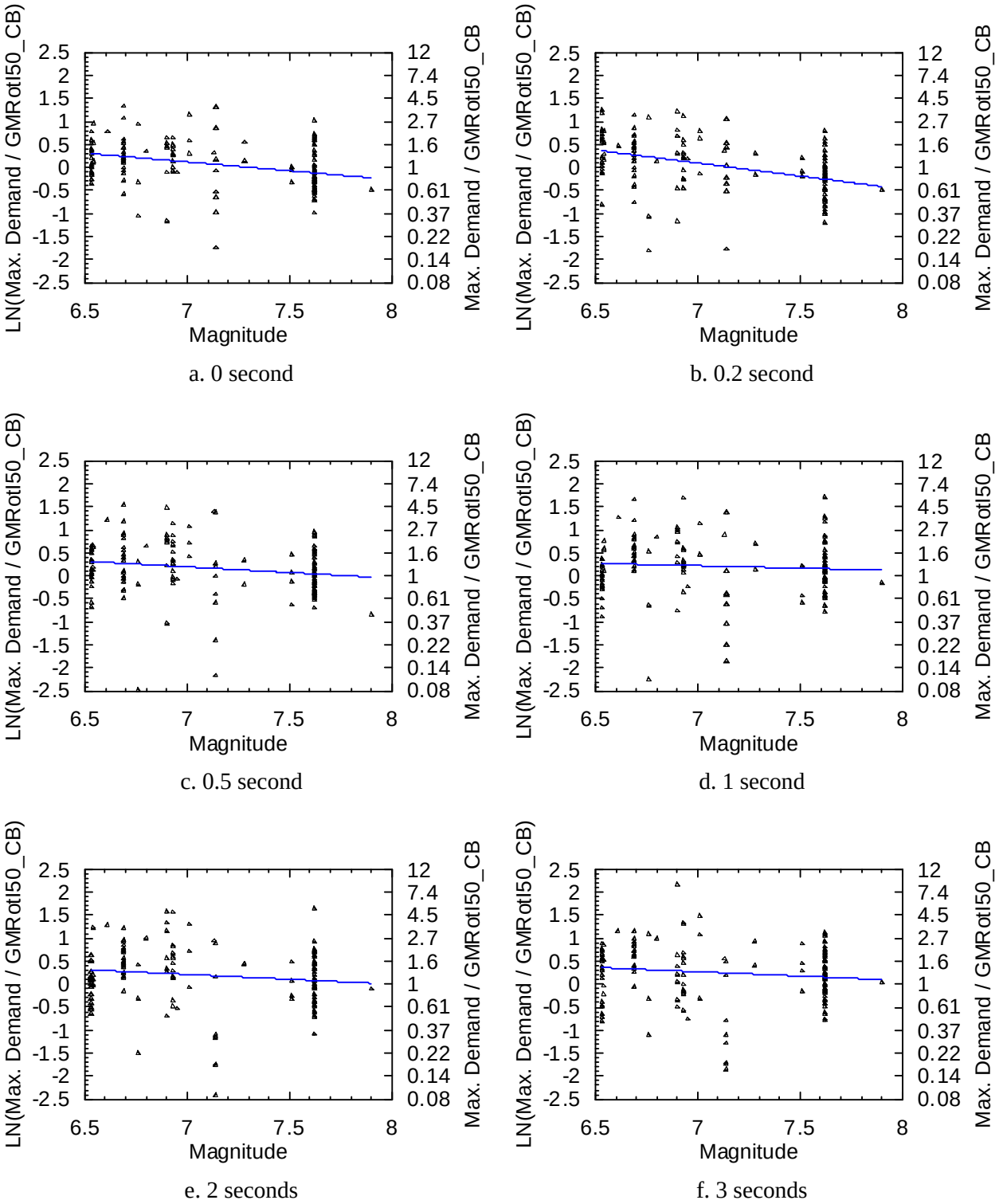

Figure 3-41. Ratios of maximum spectral demand to GMRotI50_CB at periods of 0, 0.2, 0.5, 1, 2 and 3 seconds as a function of magnitude for the records of Table 3-1

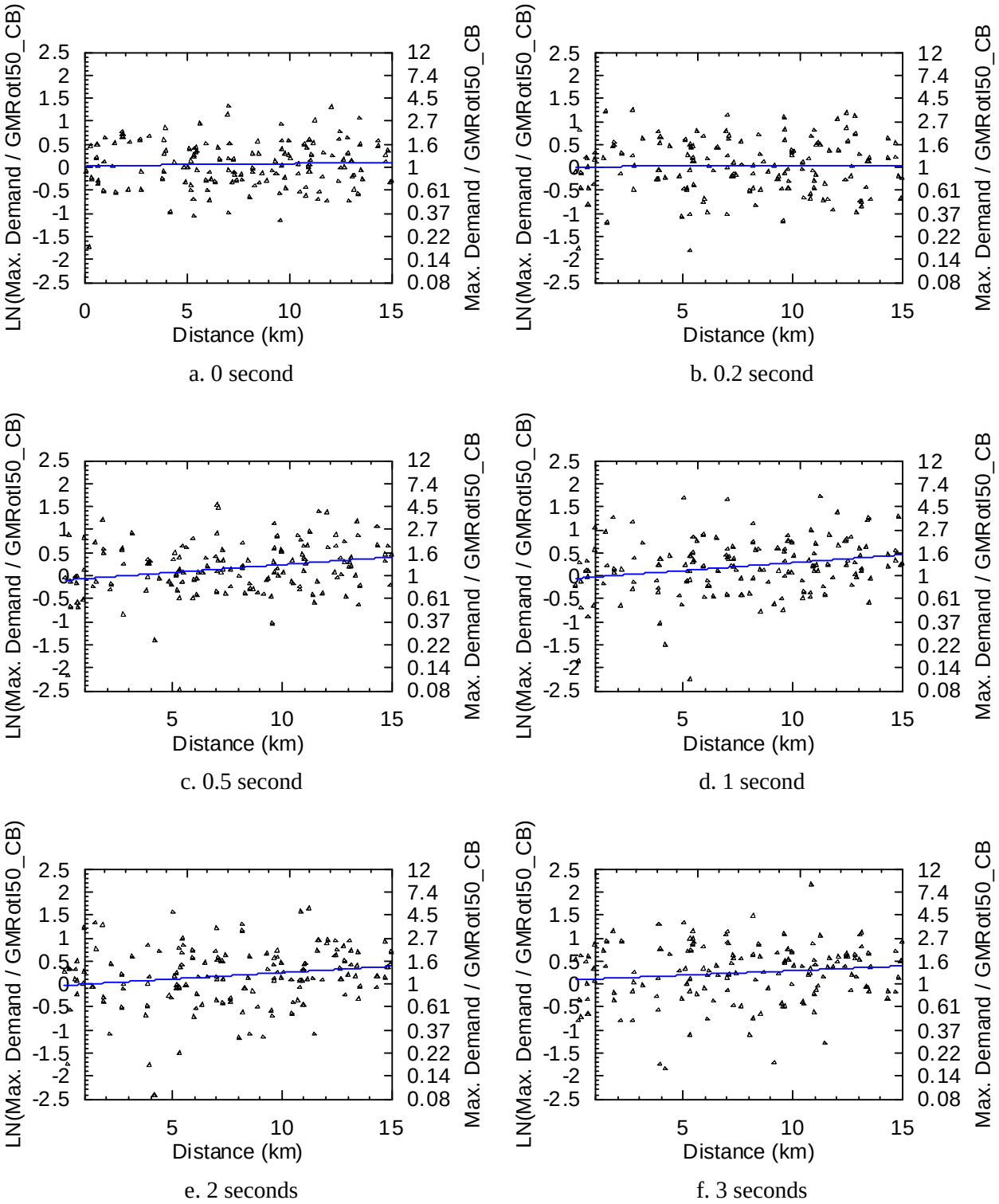

Figure 3-42. Ratios of maximum spectral demand to GMRotI50_CB at periods of 0, 0.2, 0.5, 1, 2 and 3 seconds as a function of distance for the records of Table 3-1

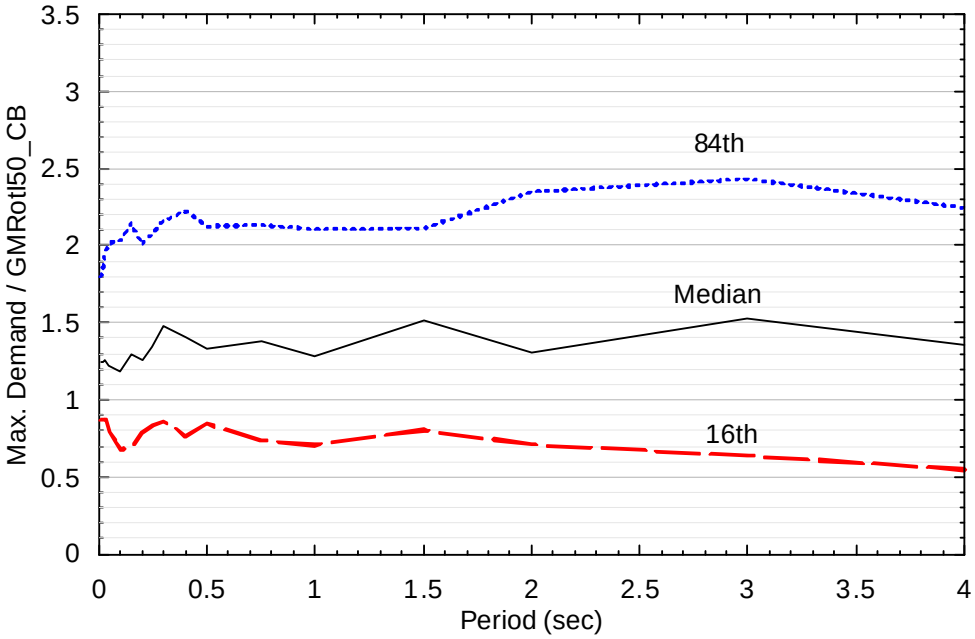

Figure 3-43. Median and 84th and 16th percentiles of the ratios of maximum spectral demand to GMRotI50_CB for all of the records of Table 3-1 except those of the 1999 Chi-Chi earthquake

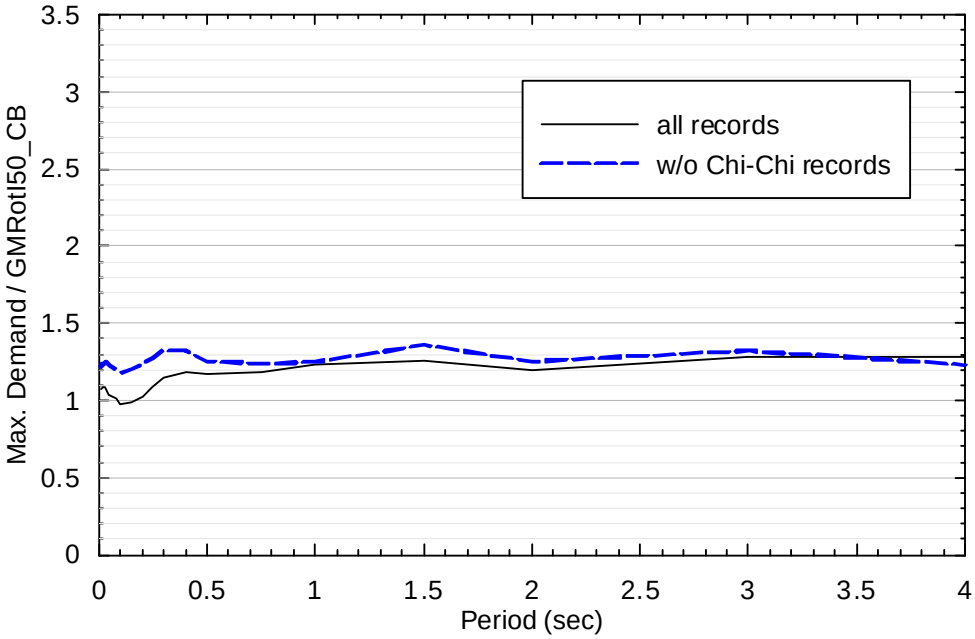

Figure 3-44. Median ratios of maximum spectral demand to GMRotI50_CB computed using (3.1) for all the records of Table 3-1 and for all of the records except those of the 1999 Chi-Chi earthquake

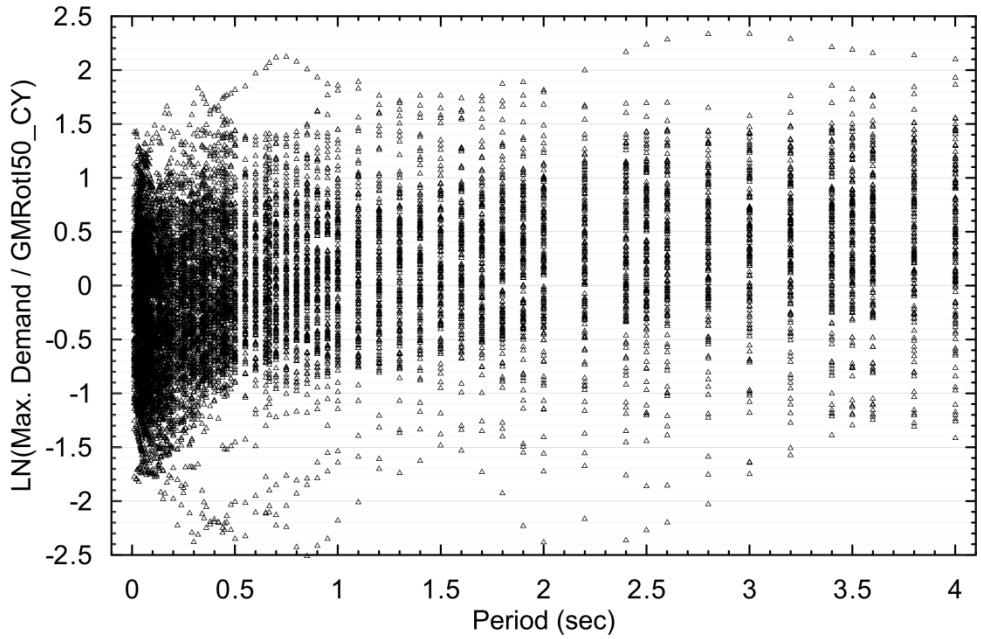

Figure 3-45. Ratios of maximum spectral demand to GMRotI50_CY for the records of Table 3-1

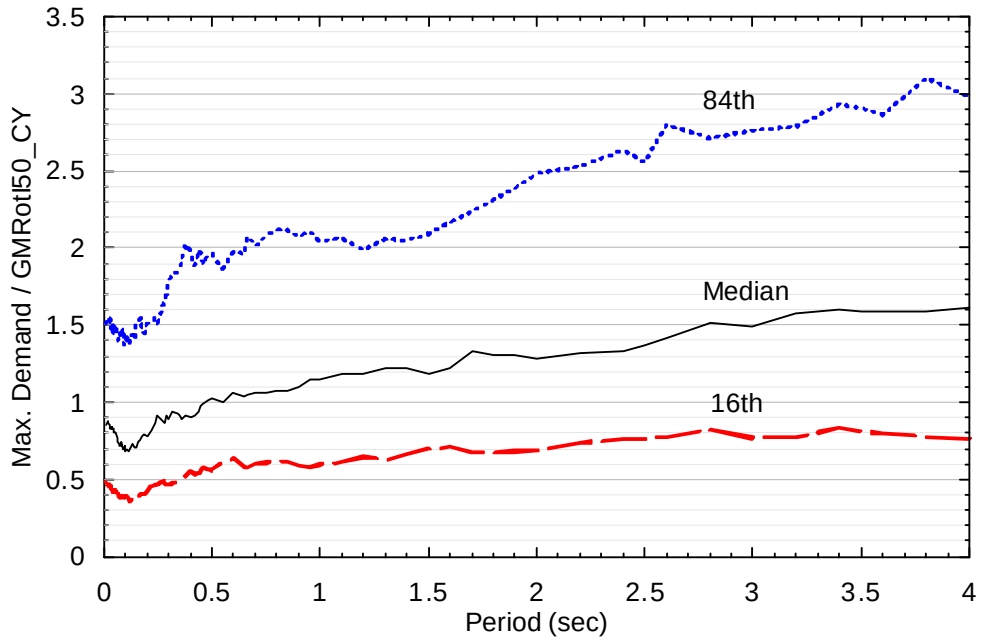

Figure 3-46. Median and 84th and 16th percentiles of the ratios of maximum spectral demand to GMRotI50_CY for the records of Table 3-1

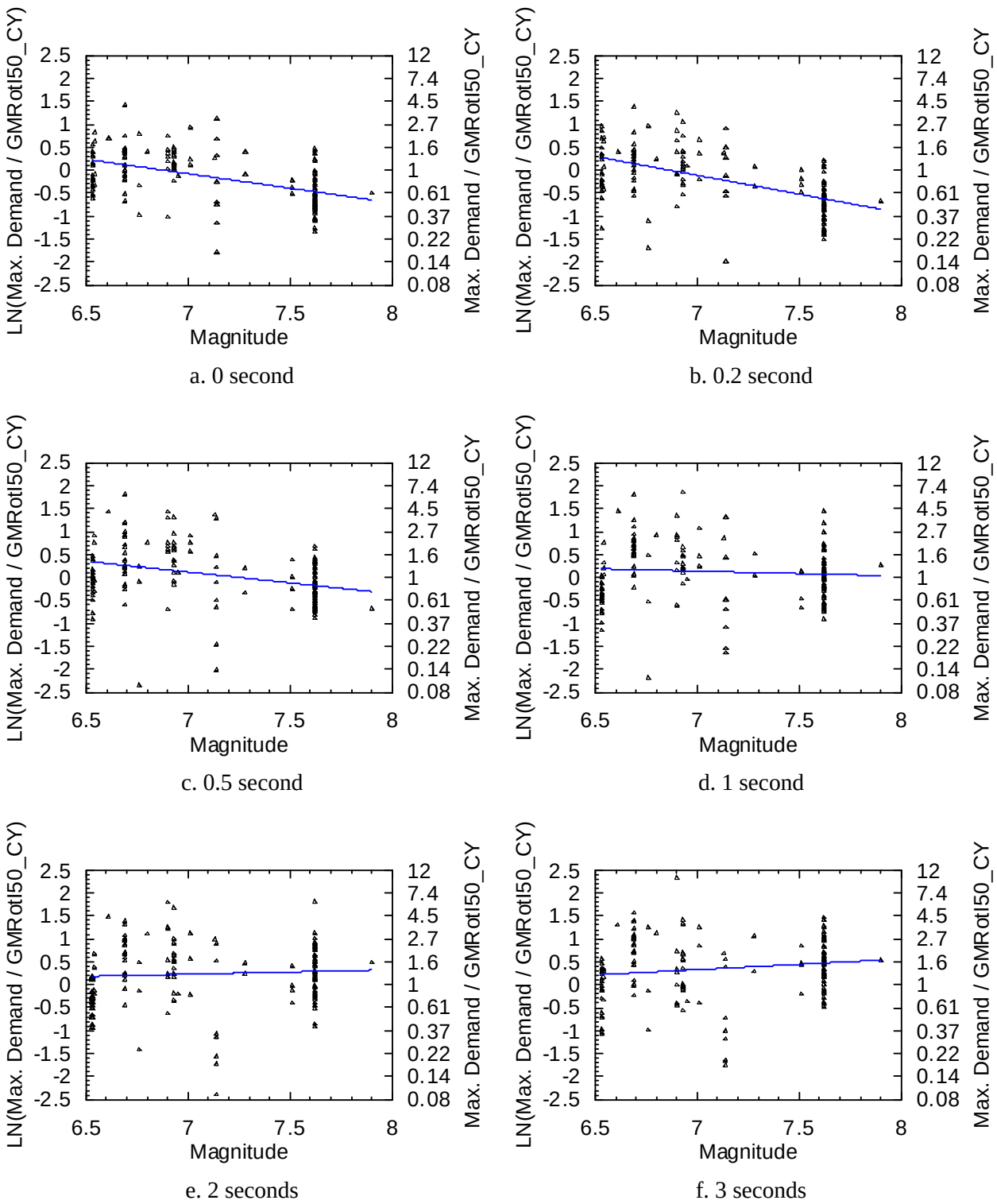

Figure 3-47. Ratios of maximum spectral demand to GMRotI50_CY at periods of 0, 0.2, 0.5, 1, 2 and 3 seconds as a function of magnitude for the records of Table 3-1

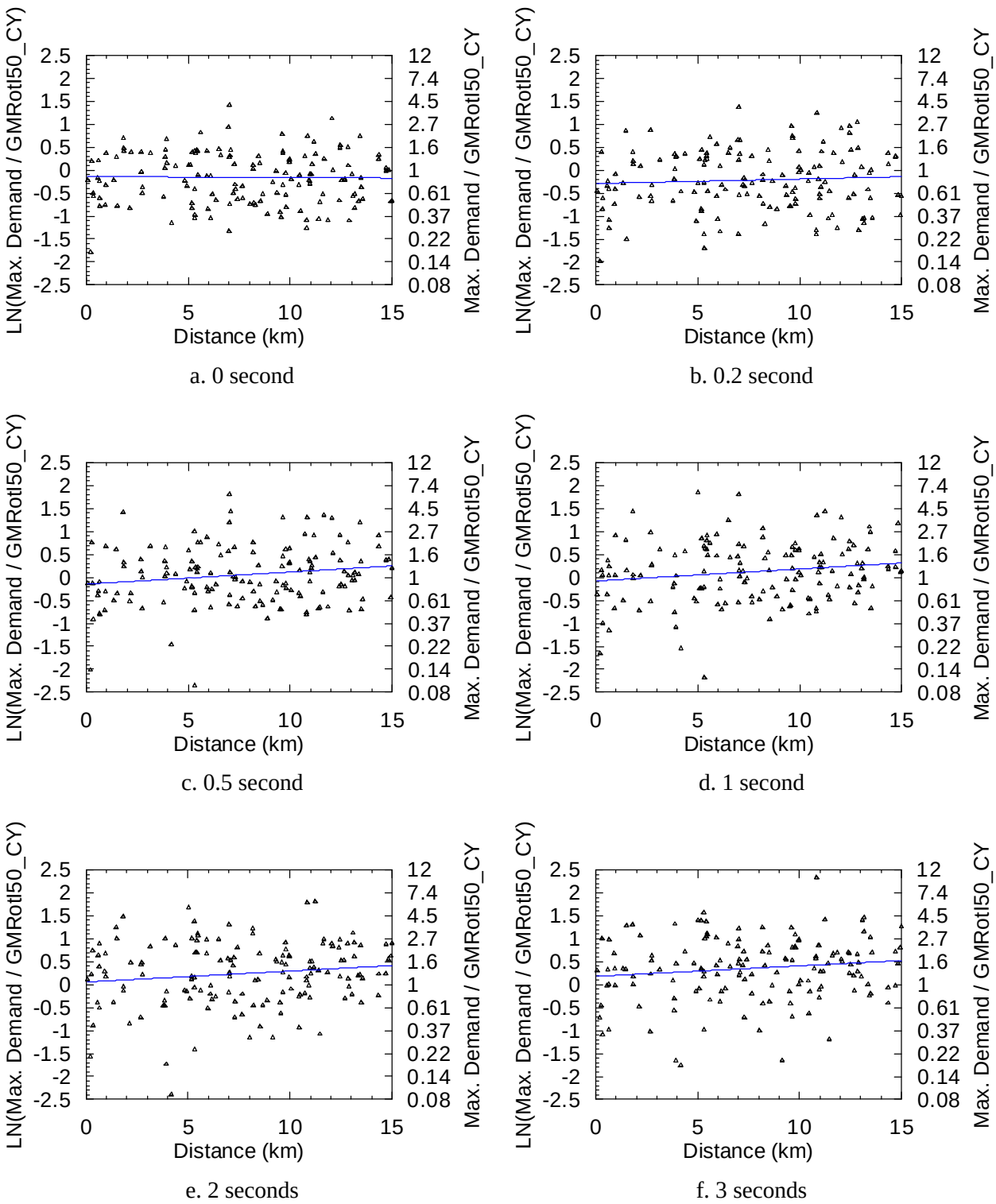

Figure 3-48. Ratios of maximum spectral demand to GMRotI50_CY at periods of 0, 0.2, 0.5, 1, 2 and 3 seconds as a function of distance for the records of Table 3-1

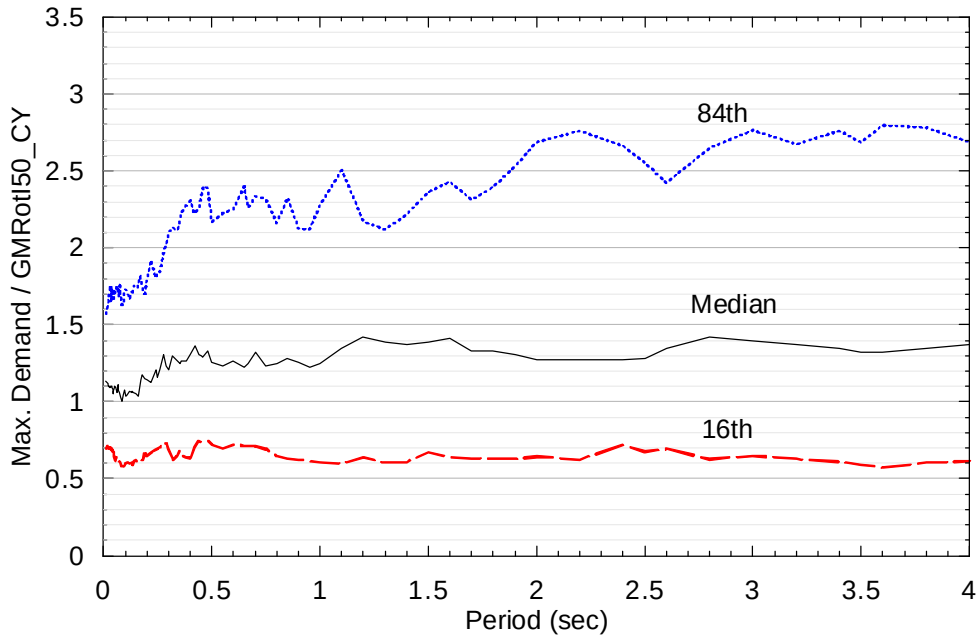

Figure 3-49. Median and 84th and 16th percentiles of the ratios of maximum spectral demand to GMRotI50_CY for all of the records of Table 3-1 except those of the 1999 Chi-Chi earthquake

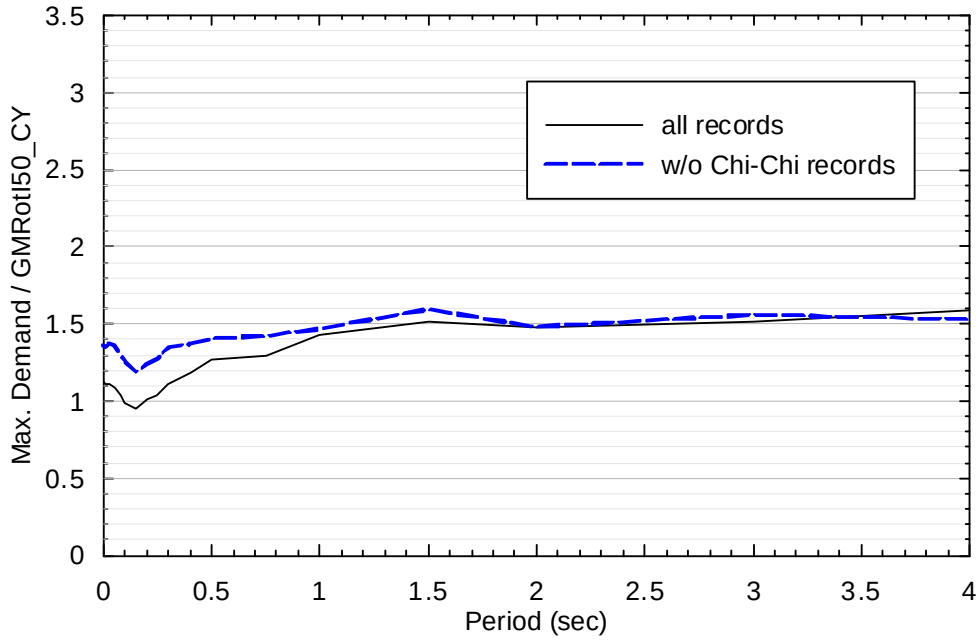

Figure 3-50. Median ratios of maximum spectral demand to GMRotI50_CY computed using (3.1) for all the records of Table 3-1 and for all of the records except those of the 1999 Chi-Chi earthquake

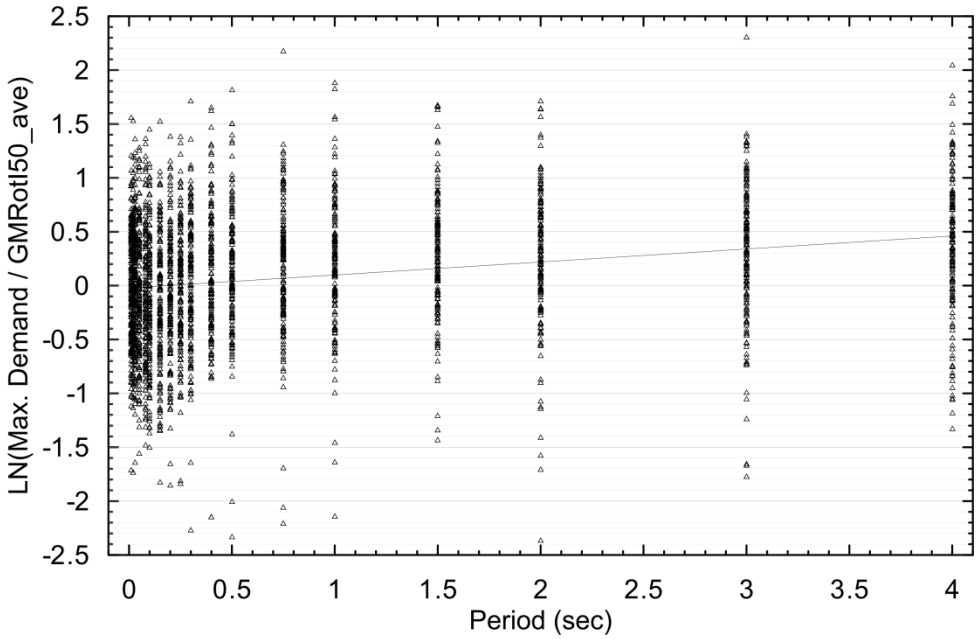

Figure 3-51. Ratios of maximum spectral demand to GMRotI50_ave for the records of Table 3-1

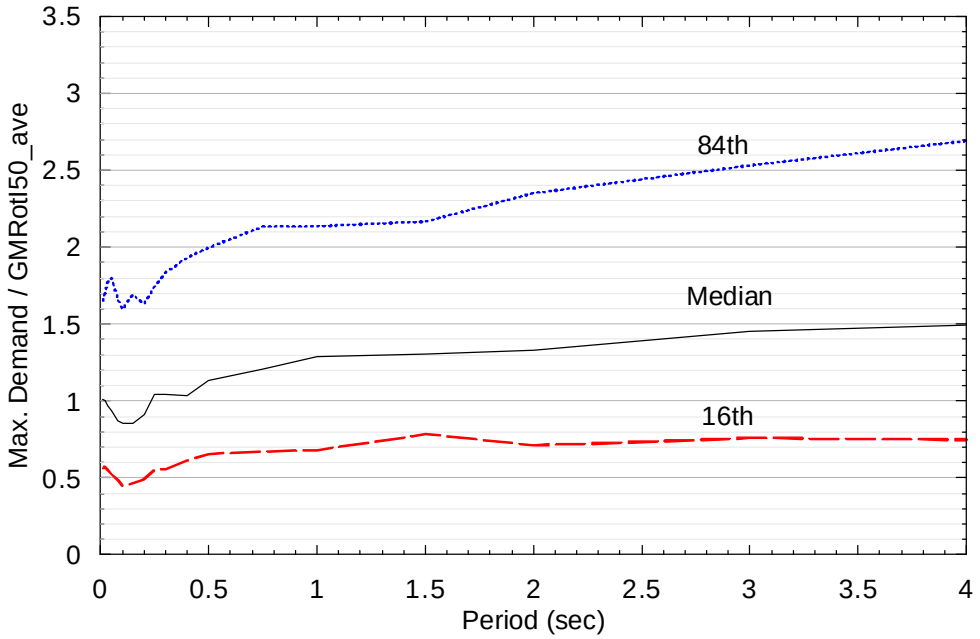

Figure 3-52. Median and 84th and 16th percentiles of the ratios of maximum spectral demand to GMRotI50_ave for the records of Table 3-1

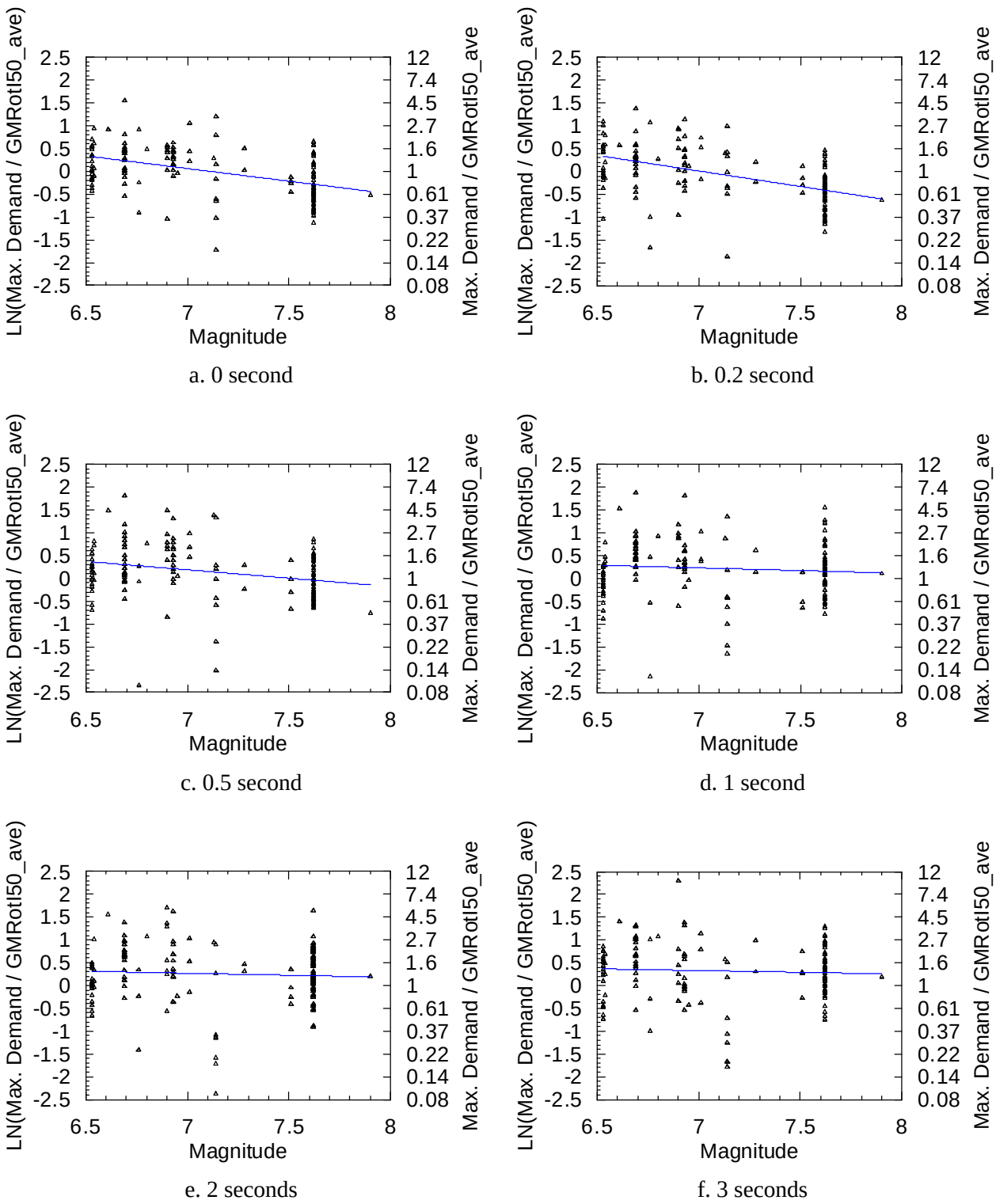

a. 0 second

b. 0.2 second

c. 0.5 second

d. 1 second

e. 2 seconds

f. 3 seconds

Figure 3-53. Ratios of maximum spectral demand to GMRotI50_ave at periods of 0, 0.2, 0.5, 1, 2 and 3 seconds as a function of magnitude for the records of Table 3-1

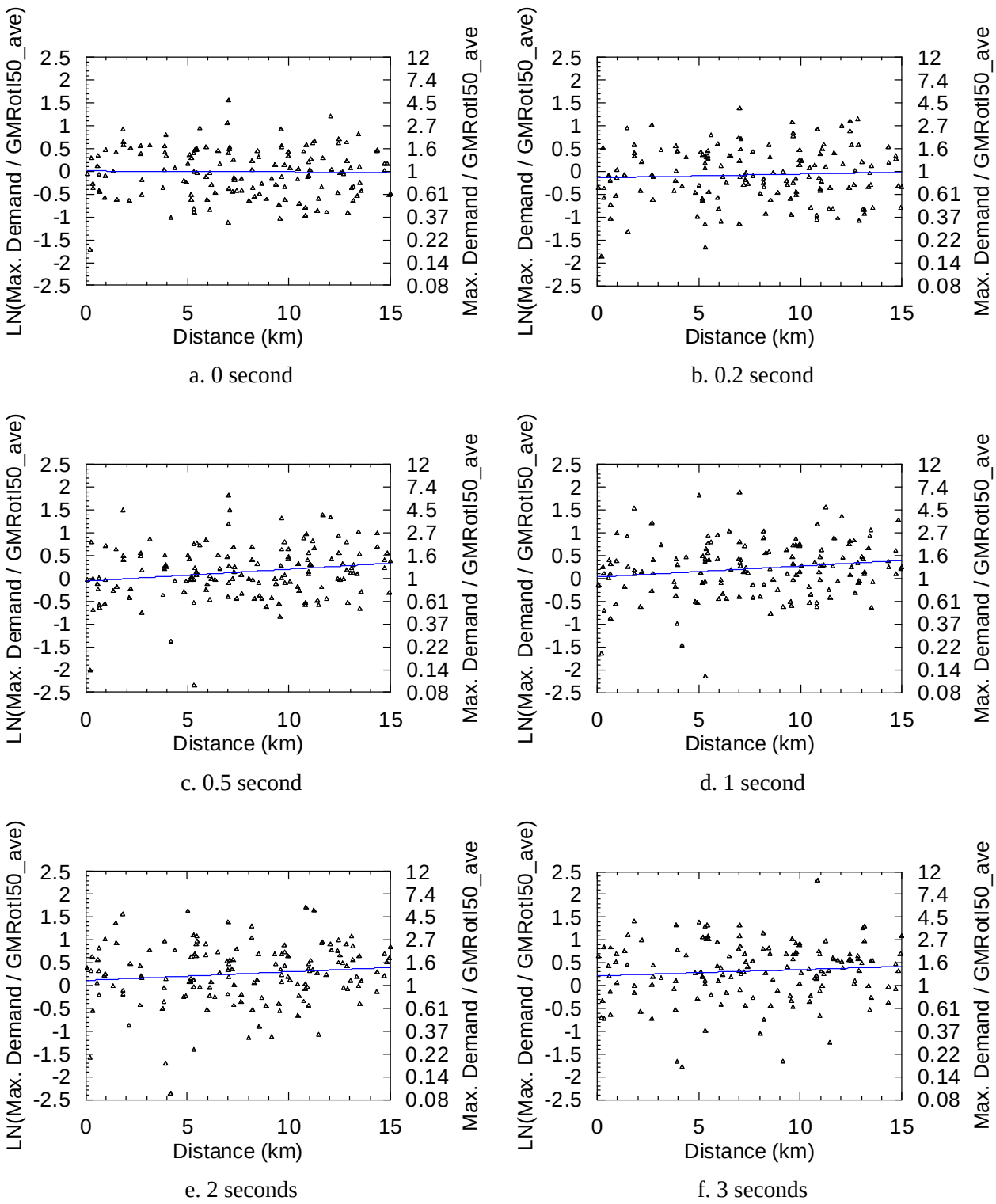

Figure 3-54. Ratios of maximum spectral demand to GMRotI50_ave at periods of 0, 0.2, 0.5, 1, 2 and 3 seconds as a function of distance for the records of Table 3-1

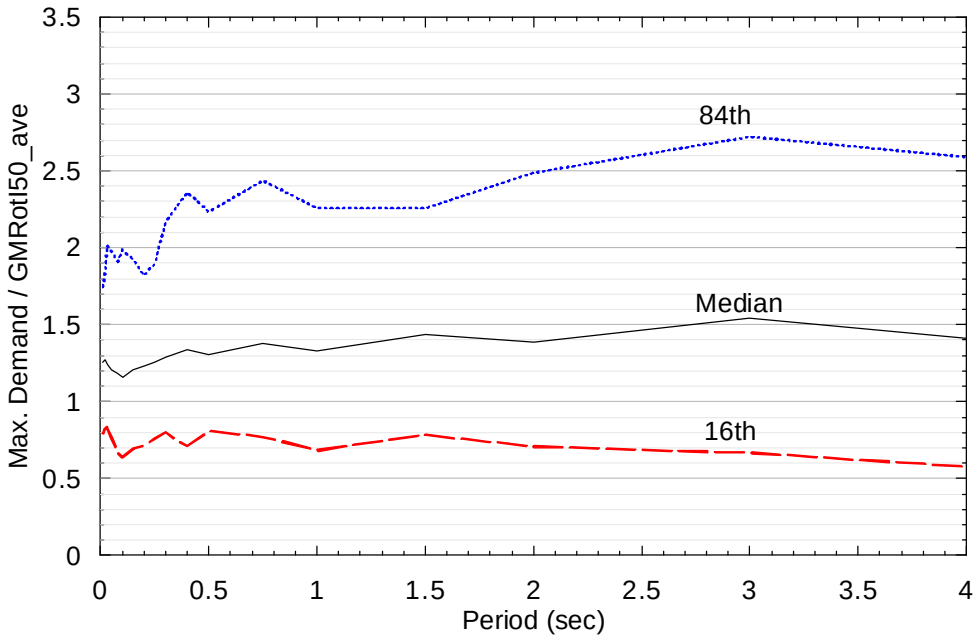

Figure 3-55. Median and 84th and 16th percentiles of the ratios of maximum spectral demand to GMRotI50_ave for all of the records of Table 3-1 except those of the 1999 Chi-Chi earthquake

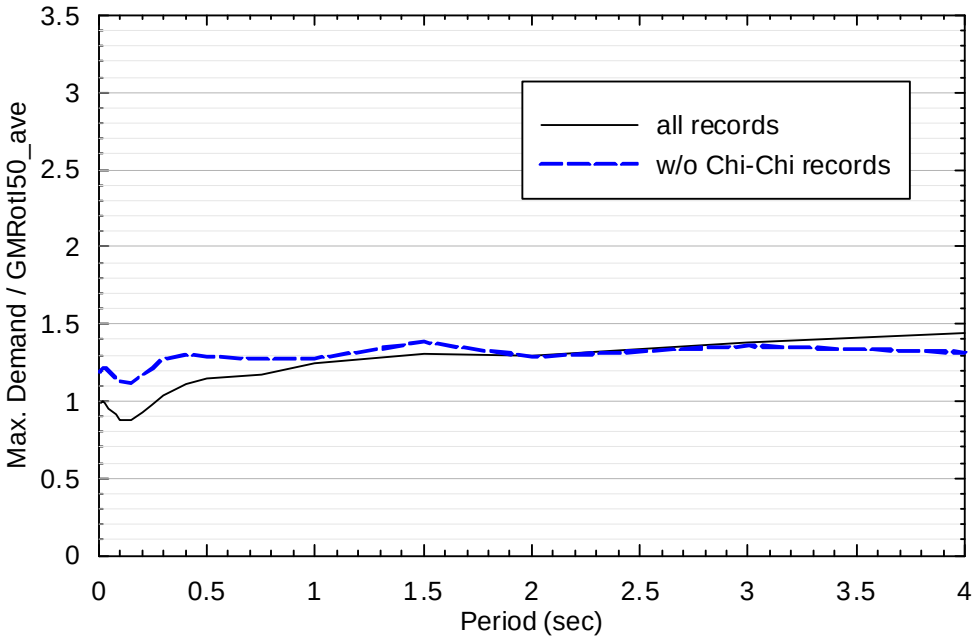

Figure 3-56. Median ratios of maximum spectral demand to GMRotI50_ave computed using (3.1) for all of the records of Table 3-1 and for all of the records except those of the 1999 Chi-Chi earthquake

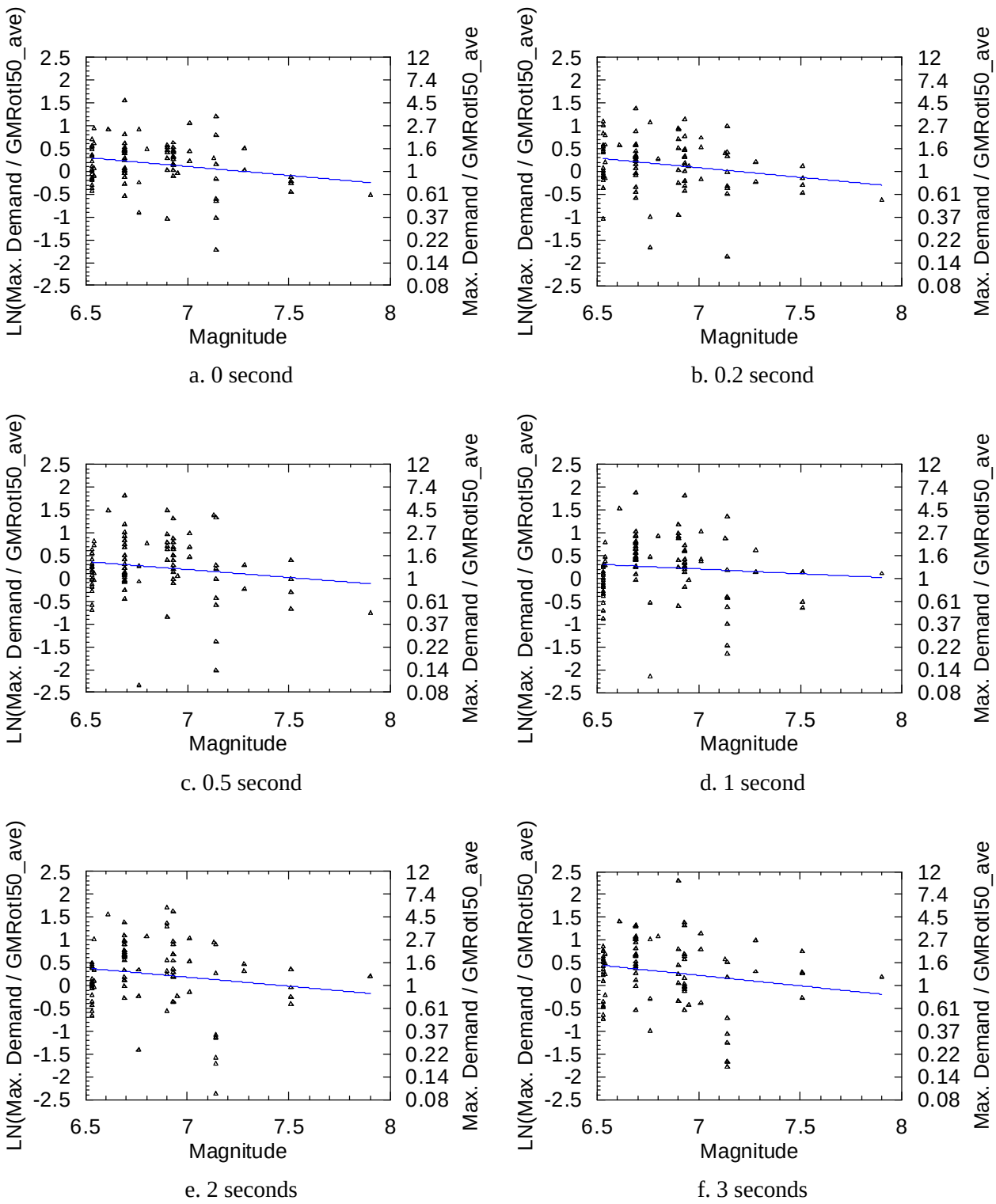

a. 0 second

b. 0.2 second

c. 0.5 second

d. 1 second

e. 2 seconds

f. 3 seconds

Figure 3-57. Ratios of maximum spectral demand to GMRotI50_ave at sample periods as a function of magnitude for all of the records of Table 3-1 except those of the Chi-Chi earthquake

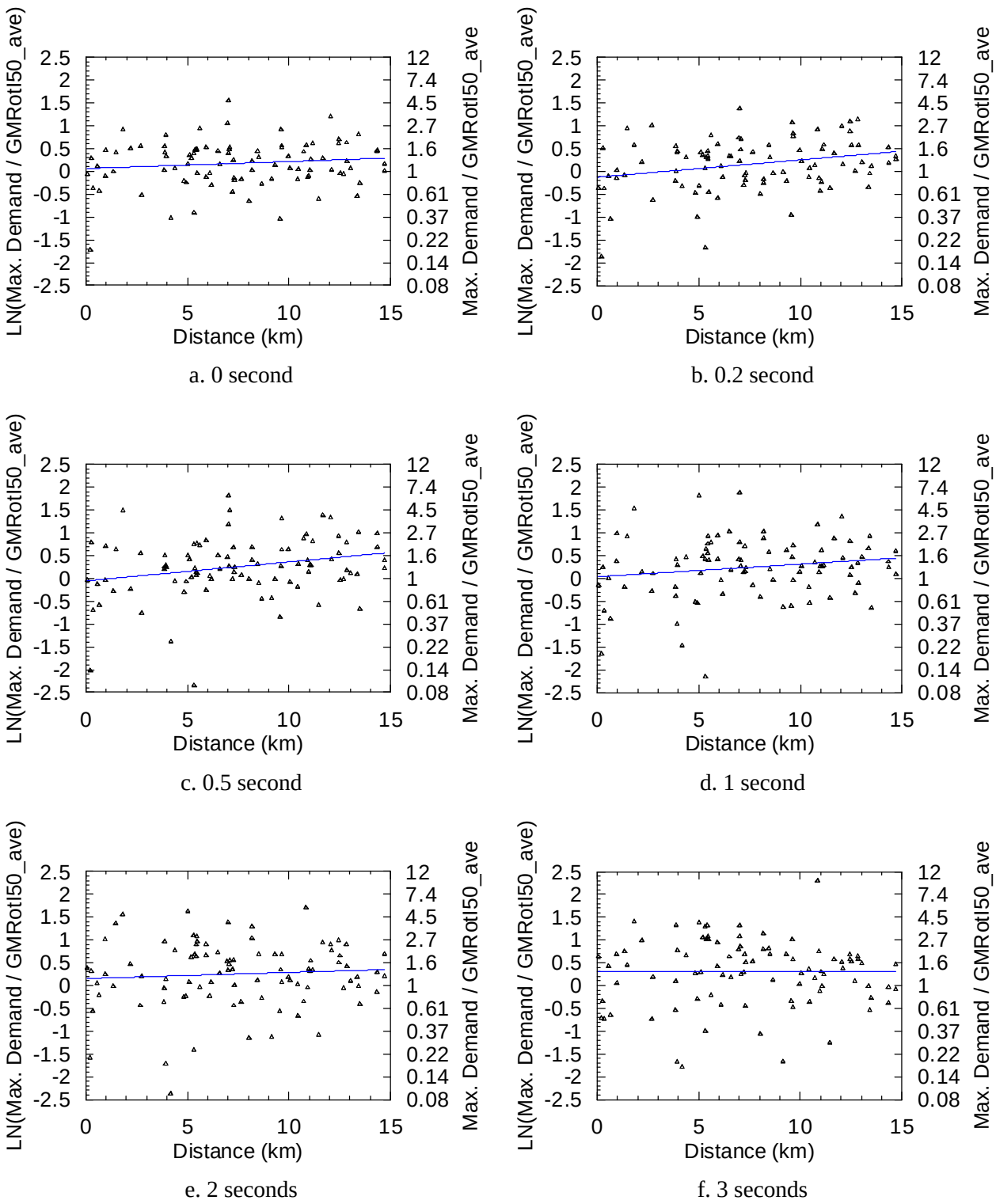

Figure 3-58. Ratios of maximum spectral demand to GMRotI50_ave at sample periods as a function of distance for all of the records of Table 3-1 except those of the Chi-Chi earthquake

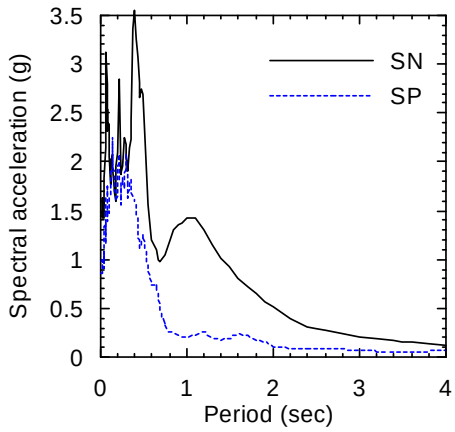

a. SN and SP spectra

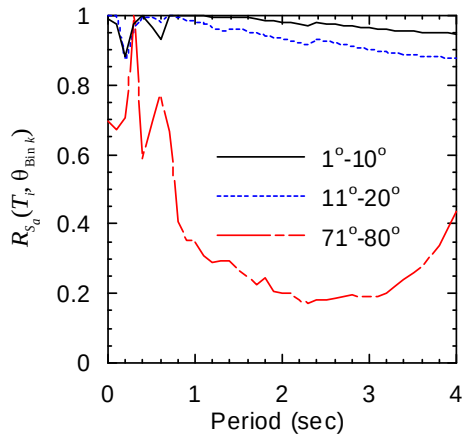

b. R_{S_a} : 1°-10°, 11°-20°, 71°-80°

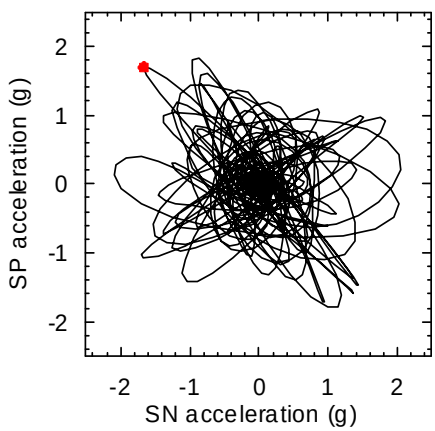

c. acceleration orbit at T_i = 0.2 sec

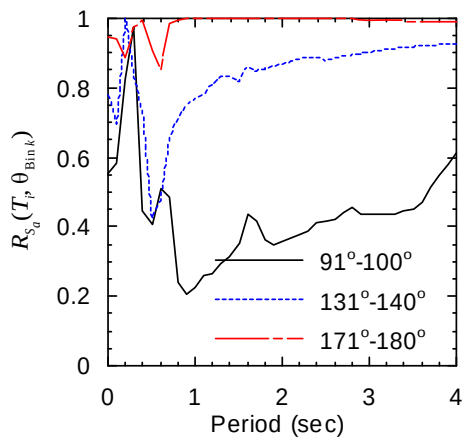

d. R_{S_a} : 91°-100°, 131°-140°, 171°-180°

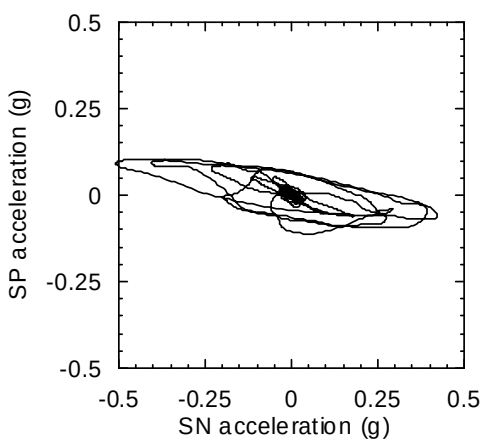

e. acceleration orbit at T_i = 2 secs

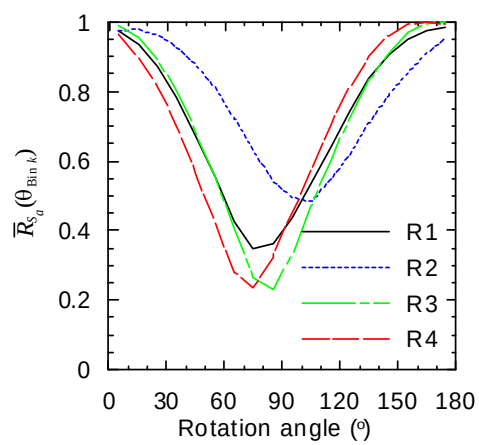

f. $\bar{R}_{S_a}$

Figure 3-59. Sample results for EQ77 of Table 3-1

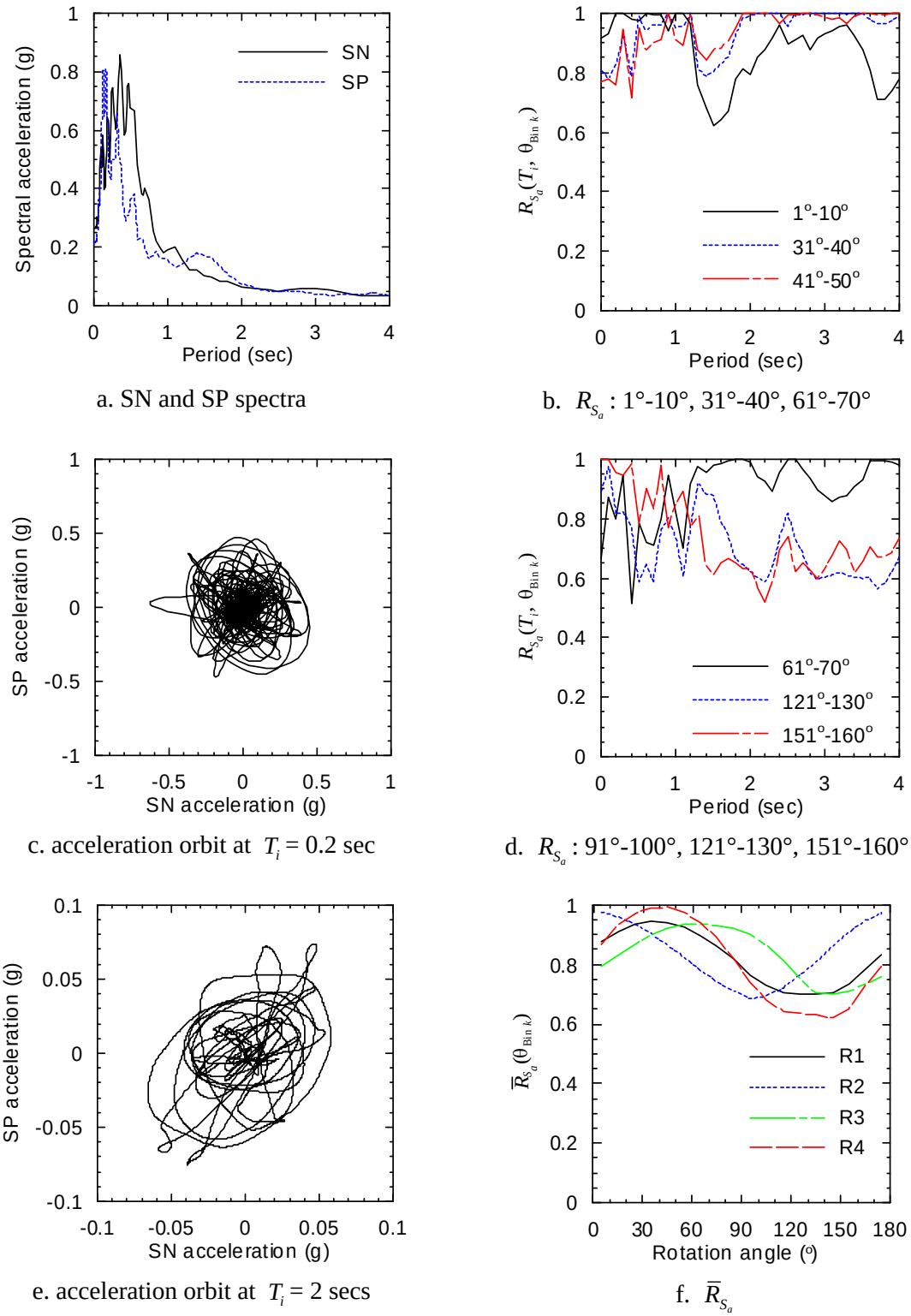

a. SN and SP spectra

b. R_{S_a} : 1°-10°, 31°-40°, 61°-70°

c. acceleration orbit at T_i = 0.2 sec

d. R_{S_a} : 91°-100°, 121°-130°, 151°-160°

e. acceleration orbit at T_i = 2 secs

f. $\bar{R}_{S_a}$

Figure 3-60. Sample results for EQ162 of Table 3-1

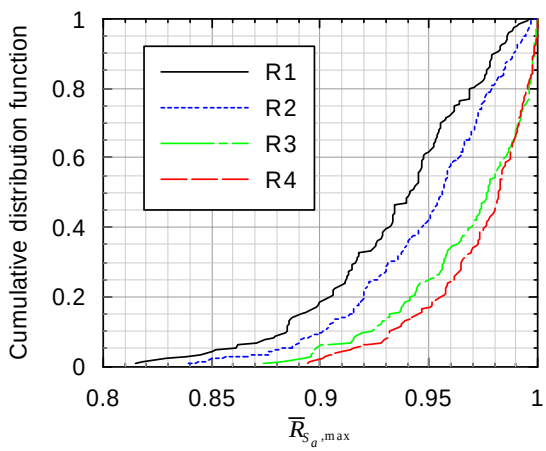

Figure 3-61. Cumulative distribution function for $\overline{R}_{S_a,\max}$ for period ranges R1 through R4 of Table 3-11

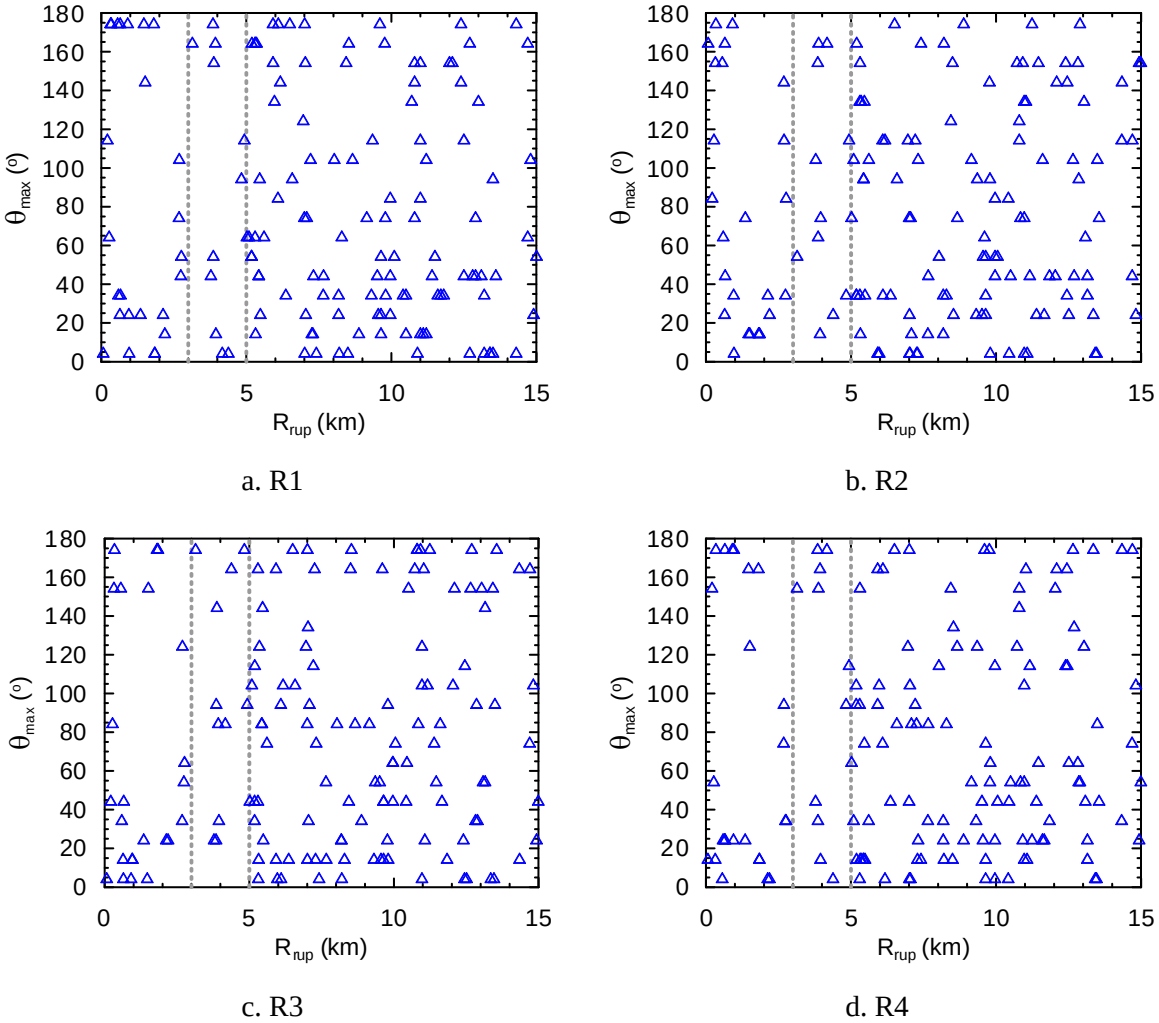

Figure 3-62. Distributions of $\theta_{\max}$ as a function of r for period ranges R1 through R4 of Table 3-11

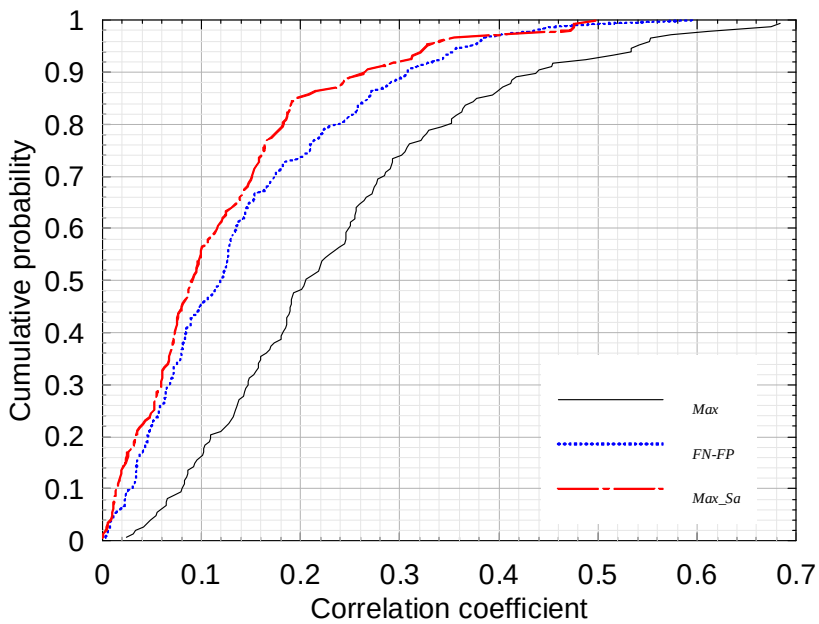

Figure 3-63. Cumulative distribution functions for ρ_{Max}, ρ_{FN_FP} and $\rho_{Max_S_a}$ for the records of Table 3-1

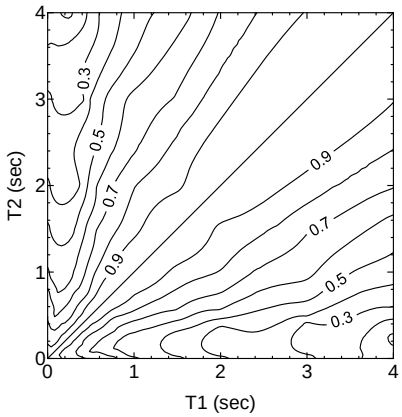

a. B-A model

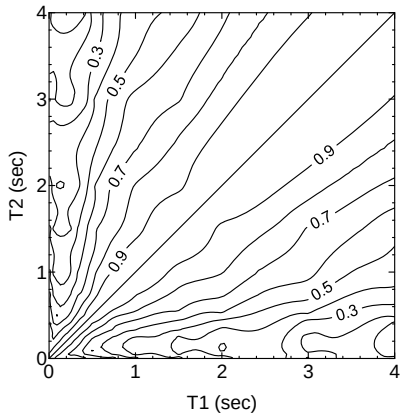

b. C-B model

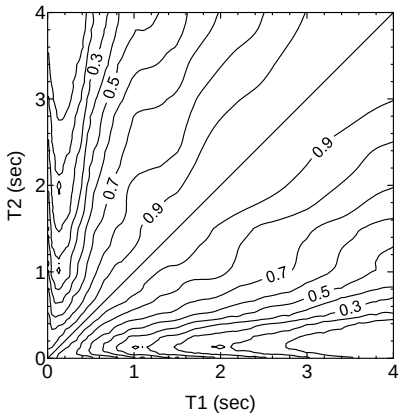

c. C-Y model

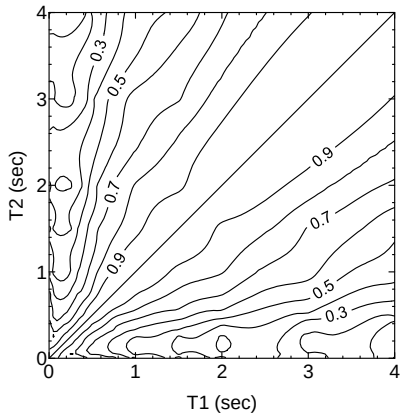

d. averaged NGA results

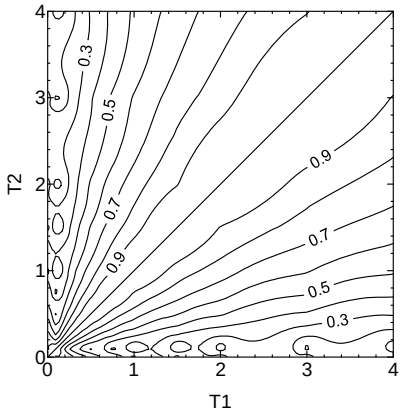

e. Baker and Jayaram (2008)

Figure 3-64. Contours of correlation coefficients between the maximum spectral demands at T_1 and T_2 computed using the B-A, C-B, C-Y and averaged NGA models for the records of Table 3-1 and the model of Baker and Jayaram (2008)

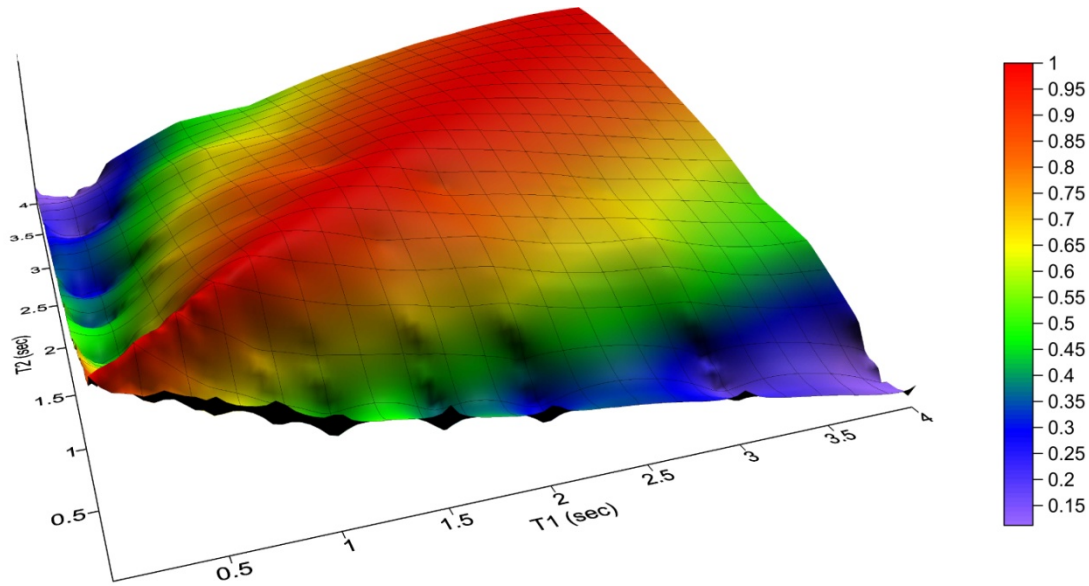

a. averaged NGA results

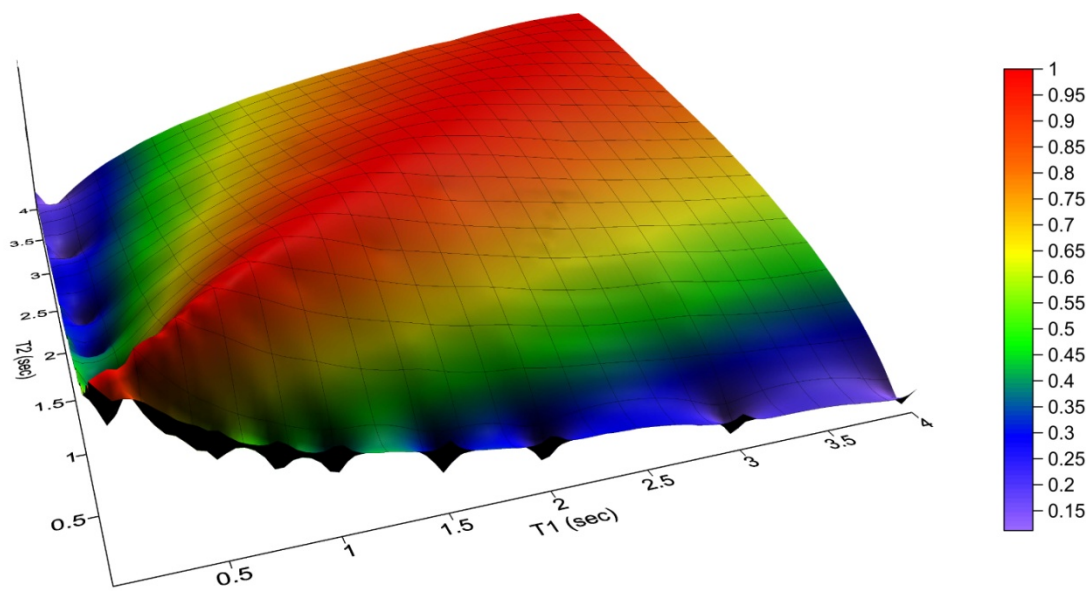

b. Baker and Jayaram (2008)

Figure 3-65. Correlation coefficients between the maximum spectral demands at T_1 and T_2 computed using the averaged NGA results for the records of Table 3-1 and the model of Baker and Jayaram (2008)

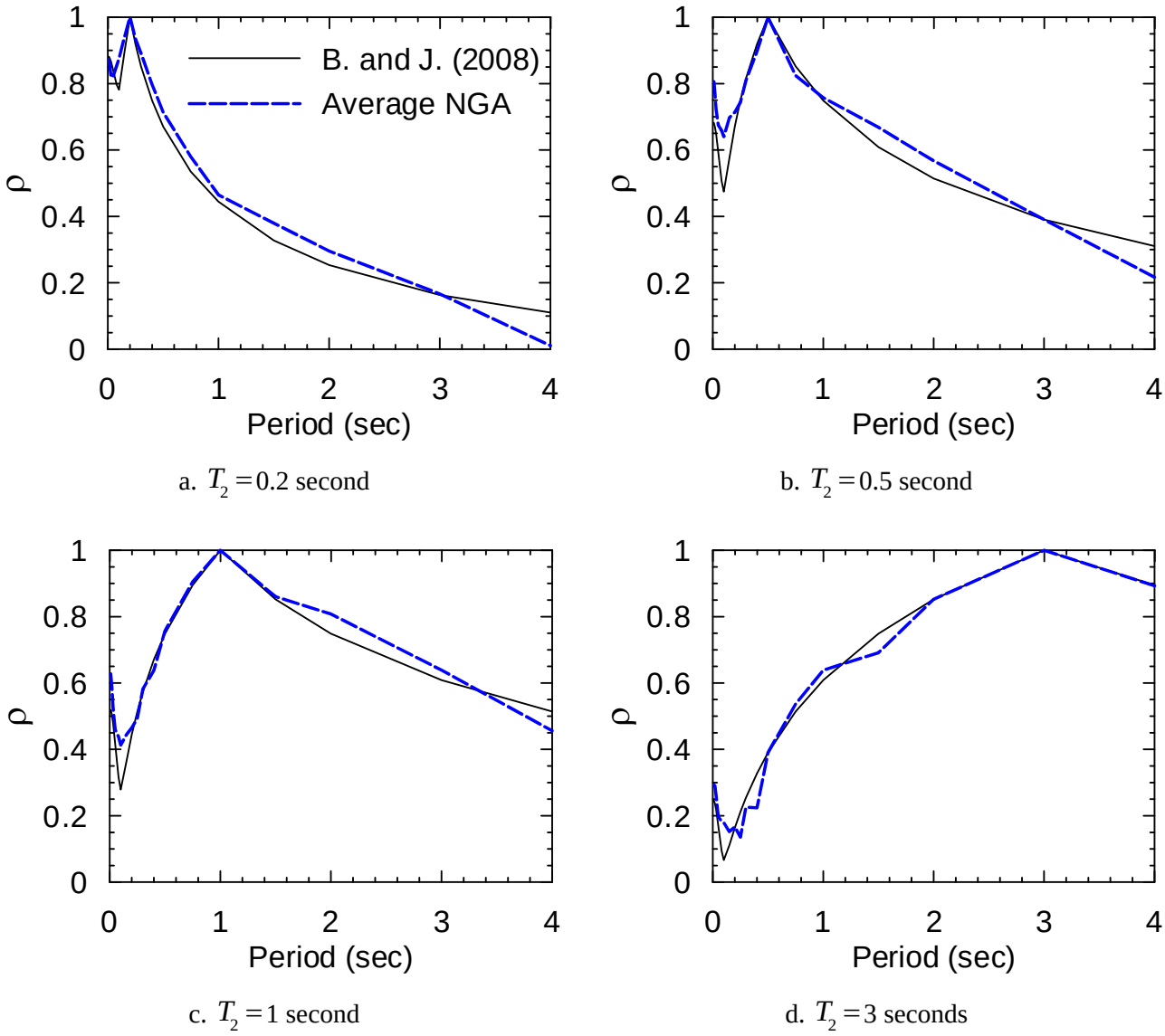

a. $T_2 = 0.2$ second

b. $T_2 = 0.5$ second

c. $T_2 = 1$ second

d. $T_2 = 3$ seconds

Figure 3-66. Correlation coefficients between the maximum spectral demands at T_1 and a given T_2 computed using the averaged NGA results for the records of Table 3-1 and the model of Baker and Jayaram (2008)

SECTION 4
CEUS GROUND MOTIONS

4.1 Datasets

Table 4-1 lists the earthquakes included in the study for the Central and Eastern United States (CEUS). Events 1 through 8 of Table 4-1 are a subset of the datasets used by Atkinson and Boore (1998) and for the EPRI CEUS Ground Motion Project (EPRI 2004). The digital recordings for many events included in those two datasets are not available and those events were not considered here. The records for Events 1 through 8 of Table 4-1 were collected from the PEER NGA ground motion database and COSMOS Virtual Data Center (http://db.cosmos-eq.org).

Atkinson and Boore (1998) justified the inclusion of records from the 1985 Nahanni earthquake, which occurred in northwest Canada, and other earthquakes outside Eastern North America (ENA) in their study of ENA earthquake data. The data for the Nahanni earthquake are used because the study of Wetmiller et al. (1988) concluded that the thrust mechanisms, regional stress regime, shallow focal depth and high-velocity sedimentary rocks for the event make it appropriate engineering design data for critical facilities in ENA. The rock records from the 1976 Gazli, USSR, 1978 Tabas, Iran, and 1991 Georgia, USSR are included since "they are from large intra-plate earthquakes and improve the magnitude-distance distribution of the database significantly at large magnitudes" (Atkinson and Boore 1998).

The records for Events 9 through 11 and 13 through 18 of Table 4-1 were obtained from the website "Engineering Seismology Toolbox" (http://www.seismotoolbox.ca/index.html), where the southeast Canada ground-motion database includes records from stations of the Canadian National Seismograph Network (CNSN) and Portable Observatories for Lithospheric Analysis and Research Investigating Seismicity (POLARIS) since 1992. The numbers in the third columns of Table 4-1 for each of Events 9 through 11 and 13 through 18 indicate the latitude and longitude of the epicenter of the event. The database provides the magnitudes of those events in Nuttli magnitude (M_N), which is based on the maximum amplitude of the Rayleigh's surface waves at a frequency of 1 Hz. The values of M_N for those events (the fifth column of Table 4-1) were converted into moment magnitude (M_W) using the relationships between M_N and M_W presented

in Filiatrault (2002) for intraplate earthquakes. The results are presented in the fourth column of Table 4-1. Only those pairs of ground motions 1) for earthquakes with M_N of 4.0 and greater, and 2) with peak ground acceleration (PGA) greater than 0.01 g in one or both horizontal components are included in this study.

The records for Event 12 of Table 4-1 (the 2002 Au Sable Forks earthquake) were provided by Dr. Christopher Cramer at the University of Memphis, who collected the data from the Incorporated Research Institutions for Seismology (IRIS) data center and the Canadian National Data Centre (CNDC) and then processed the data for the NGA East Project (http://peer.berkeley.edu/ngaeast/). Only those pairs of ground motions with a PGA greater than 0.01 g in one or both horizontal components are included in this study.

A significant number of ground-motion histories were recorded during the Val-des-Bois, Qubec earthquake on June 23rd, 2010, which is Event 19 of Table 4-1. This moment magnitude 5 earthquake generated the strongest shaking experienced in the Canadian province of Ottawa in recent history (Atkinson and Assatourians 2010). Atkinson and Assatourians (2010) collected ground-motion records from 120 stations at epicentral distances between 20 and 1200 km to study the attenuation and source characteristics of this event. We downloaded the 111 pairs of time series used in their study from the website “Engineering Seismology Toolbox”. Only the twelve pairs of motions with a PGA greater than 0.01 g in one or both horizontal components are included in the database we used for the CEUS analysis.

Table 4-2 lists the event, station, M_W, distance between the station and epicenter of the event (r_{epi}) and the PGAs of the two horizontal components of the 63 ground-motion pairs used in this study. Figure 4-1 presents the distribution of the 63 ground-motion pairs as a function of M_W and r_{epi}. Approximately 60 percent of the records are associated with M_W smaller than 6 and r_{epi} smaller than 100 km. Panels a and b of Figure 4-2 present the distributions of PGA as a function of M_W and r_{epi}, respectively. Of the 126 records studied, 76 have a PGA smaller than 0.05 g.

Section 4.2 presents the time difference between the peak accelerations in the two orthogonal horizontal directions for the records of Table 4-2. Section 4.3 presents the relationship between maximum spectral demand and GMRotI50. Section 4.4 presents information on the orientation of

maximum spectral demand. Section 4.5 presents information on the correlation of components of ground motion.

4.2 Geomean spectral demand representation

The analyses of Section 2.3 were repeated using the records of Table 4-2 to study the time difference between the peak spectral acceleration response at a given period in two perpendicular directions for each pair of ground motions of Table 4-2. Each pair of records of Table 4-2 was rotated to be parallel and perpendicular to the orientation of GMRotI50 using the procedures presented in Section 1.2.1. For a given pair of ground motions, the time difference between the two spectral accelerations at a given period was computed and normalized by the period.

Panel a of Figure 4-3 presents the 84th, 50th and 16th percentiles of the normalized time difference for the 63 pairs of records of Table 4-2. The median normalized time differences are a) greater than 1 at periods smaller than 0.6 second and b) smaller than 0.5 at periods greater than 1 second. Panel b of Figure 4-3 presents the cumulative distribution functions of the normalized time difference at periods of 0.2, 0.5, 1 and 2 seconds. The percentages of the records with normalized time difference smaller than 1 at periods of 0.2, 0.5, 1 and 2 seconds are 40%, 44%, 59% and 70%, respectively. The median normalized time difference of Figure 4-3a is much smaller than that of Figures 2-2a and 3-2a for WUS ground motions.

Although the median normalized time difference is smaller in the CEUS than in the WUS, it is greater than 1 at periods smaller than 0.6 second. For most of the records of Table 4-2, the spectral demand at periods greater than 0.5 second is insignificant. Panels a and b of Figure 4-4 presents the 16th, 50th and 84th percentiles of spectral acceleration for the records of Table 4-2 at periods between 0 and 4 seconds and 1 and 4 seconds, respectively. The median spectral acceleration at a period of 0.5 (1) second is smaller than 0.02 (0.005) g.

4.3 Maximum and geomean spectral demands

Figure 4-5 presents the residual between maximum spectral demand and GMRotI50 as a function of period for the records of Table 4-2. Figure 4-6 presents the maximum, minimum, median and 84th and 16th percentiles of the ratios of maximum spectral demand to GMRotI50 for the records

of Table 4-2. The median and 84th percentile of the ratios of Figure 4-6 at periods of 0, 0.2, 0.5, 1, 2, 3 and 4 seconds are presented in Table 4-3. The median ratios range between 1.2 and 1.4 across most of the period range of Figure 4-6 and the 84th percentile ratios range between 1.4 and 1.6 at periods greater than 0.1 second. The median and 84th percentile results increase slightly with period, which is similar to that observed for far-field and near-fault WUS records.

To study the dependence of the residual between maximum spectral demand and GMRotI50 on M_W and r_{epi}, the residuals of Figure 4-5 at periods of 0, 0.2, 0.5, 1, 2 and 3 seconds were re-plotted in the six panels of Figure 4-7 (Figure 4-8), respectively, as a function of M_W (r_{epi}). The blue line in each panel presents a linear regression fit to the data. The residual show clear dependence on both M_W and r_{epi}. The results of Figure 4-7 and Figure 4-8 should be interpreted with care since the most of the records are for M_W less than 6 and r_{epi} less than 100 km. Only 9 pairs of records are associated with r_{epi} greater than 200 km.

4.4 Orientation of maximum spectral demand

4.4.1 Sample computations

The analyses of Section 2.5 were repeated using the records of Table 4-2 to study the orientation of maximum spectral demand for CEUS ground motions.

Sample results are presented using the eighth pair of ground motions of Table 4-2, termed EQ8. The pair was recorded at the Union Village Dam, Vermont during the 1982 Gaza earthquake. The values of M_W and r_{epi} for EQ77 are 4.3 and 60.8 km, respectively. The analysis of Figure 2-55 was repeated using EQ8. Panel a of Figure 4-9 presents the response spectra for the two horizontal components of EQ8. The values of spectral acceleration at periods greater than 0.5 second are much smaller than the short-period demands for both components. Panels c and e present the acceleration orbits of 0.2- and 2-second oscillators, respectively. For T_i = 0.2 second, the maximum acceleration demand occurs at θ_j = 1°. For T_i = 2 second, the response is highly polarized at 45° to the SN direction.

Panel b of Figure 4-9 presents R_{S_a}, which is a function of period and bin of rotation angles θ_j, for Bins 1 (θ_j = 1° through 10°), 4 (31° through 40°) and 7 (61° through 70°) at periods of 0

through 4 seconds. Panel d presents R_{S_a} for Bins 10 (91° through 100°), 13 (121° through 130°) and 16 (151° through 160°). In panel b, the values of R_{S_a} for Bin 1 are greater than 0.95 in the period range between 0 and 0.4 second: an observation supported by the orbit shown in panel c. At a period close to 2 seconds, the values of R_{S_a} between 31° through 70° (Bins 4 through 7) are much higher than those in the perpendicular direction (Bins 13 through 16): an observation supported by the orbit shown in panel e.

Panel f of Figure 4-9 presents values of $\overline{R}_{S_a}(\theta_{\text{Bin } k})$ for four ranges of period at the midpoint rotation angle for each bin. The four ranges of period are 0 to 4 seconds (R1), 0 to 1 second (R2), 1 to 2 seconds (R3) and 2 to 4 seconds (R4). The trend in the curve for the short period range (R2) is different from that at longer periods (R3 and R4). For range R1, the maximum value of $\overline{R}_{S_a}$ over the 18 bins of angles ($\overline{R}_{S_a,\max}$) is 0.95 and the corresponding midpoint rotation angle ($\theta_{\max}$) is 25°. For ranges R3 and R4, the values of $\overline{R}_{S_a,\max}$ are both close to 1 and the values of $\theta_{\max}$ are between 35° and 45°. The difference between the maximum and minimum values of $\overline{R}_{S_a}$ for R2 is much smaller than those for R3 and R4, which implies that the degree of polarization in the oscillator response is higher in the longer period range.

4.4.2 Overall analysis results

Figure 4-10 presents the cumulative distribution functions of $\overline{R}_{S_a,\max}$ for R1, R2, R3 and R4 for all 63 pairs of records of Table 4-2. The medians, (arithmetic) means and standard deviations of the 63 values of $\overline{R}_{S_a,\max}$ for R1 through R4 are presented in Table 4-4. The median values of $\overline{R}_{S_a,\max}$ for all cases are greater than 0.97. Both the median and mean values of Table 4-4 are higher than those for WUS ground motions. The results of Figure 4-10 and Table 4-4 indicate clearly that there is typically an axis of strongest shaking.

4.5 Correlation of ground motions

4.5.1 Time series

The analyses of Sections 2.6.1 and 2.6.2 were repeated using the records of Table 4-2 and presented in Sections 4.5.1 and 4.5.2, respectively. The notation presented in Section 2.6 is used here. Section 4.5.1 presents the correlation between two orthogonal horizontal acceleration *time*

series for each pair of the ground-motion records of Table 4-2. Section 4.5.2 presents the correlation of *spectral demands* (maximum demand at different periods) for each pair of the records of Table 4-2.

For the records of Table 4-2, the distributions of three correlation coefficients of orthogonal horizontal ground-motion time series were investigated, namely, ρ_{Max}, ρ_{C1_C2} and $\rho_{Max_S_a}$, where ρ_{Max} is the maximum correlation coefficient of a pair of ground motions over all rotation angles; ρ_{C1_C2} is the correlation coefficient of the two as-recorded ground-motion components; and $\rho_{Max_S_a}$ is the correlation coefficient in the orientations parallel and perpendicular to the direction associated with $\bar{R}_{S_a,\max}$. The correlation coefficient for a given pair of ground motions was computed using (2.3).

The CDFs of ρ_{Max}, ρ_{C1_C2} and $\rho_{Max_S_a}$ are presented in Figure 4-11. For the three CDFs of Figure 4-11, the values of correlation coefficient at cumulative probabilities of 0.5 and 0.9 and the cumulative probability at a correlation coefficient of 0.3 are presented in Table 4-5 together with the mean and standard deviation of the 63 realizations for each of ρ_{Max}, ρ_{C1_C2} and $\rho_{Max_S_a}$.

In Table 4-5, the mean and standard deviation for ρ_{Max} are 0.27 and 0.19, respectively. The probabilities for ρ_{Max}, ρ_{FN_FP} and $\rho_{Max_S_a}$ less than 0.3 are 66% , 86% and 84%, respectively. The data of Figure 4-11 and Table 4-5 do not support the use of a number smaller than 0.3 as the upper bound on the correlation coefficient of ground-motion time series: the same conclusion as that drawn for far-field and near-fault WUS ground motions.

4.5.2 Spectral demand

4.5.2.1 Attenuation relationship

This subsection presents the correlation of maximum spectral demands at periods of T_1 and T_2, which is represented by the correlation coefficients between $\varepsilon_{\max}(T_1)$ and $\varepsilon_{\max}(T_2)$, termed $\rho_{\varepsilon_{\max}(T_1),\varepsilon_{\max}(T_2)}$. The computation of $\varepsilon_{\max}$ requires the use of attenuation relationships. To establish the relationship between the maximum spectral demand of CEUS ground motions, magnitude and distance, we performed a regression analysis using the records of Table 4-2 and a simple model as presented in (4.1) (Bozorgnia and Campbell 2004):

$$\ln S_{a,\max} = \ln \theta_{CEUS} + \mathrm{E} = a_1 + a_2 M_W + a_3 \ln r_{epi} + a_4 r_{epi} + \mathrm{E} \tag{4.1}$$

where $S_{a,\max}$ is the maximum spectral demand for a given combination of period, M_W and r_{epi}; θ_{CEUS} is the median estimation of $S_{a,\max}$; E is a random error term with a mean of zero and a standard deviation of β_{CEUS}; and a_1, a_2, a_3 and a_4 are coefficients for the median ground motion θ_{CEUS}. The values of a_1, a_2, a_3, a_4 and β_{CEUS} are presented in Table 4-6 as a function of period.

The residual between the maximum spectral demand of the records of Table 4-2 and θ_{CEUS} of (4.1) at periods of 0, 0.2, 0.5, 1, 2 and 3 seconds was plotted in the six panels of Figure 4-12 (Figure 4-13), respectively, as a function of M_W (r_{epi}). The blue line in each panel presents a linear regression fit to the data. The residual is independent of M_W and r_{epi} although the dispersion in the residual is greater at distances less than 100 km. Note that the number of pairs of ground motions with r_{epi} smaller than 100 km (45) is much greater than that with r_{epi} between 100 and 615 km (18). The value of β_{CEUS} in Table 4-6 ranges between 0.78 and 1.18. The values can be reduced using a more robust model than (4.1) to account for site conditions, faulting type, and alternate distance definitions, all of which are beyond the scope of this study.

4.5.2.2 Correlation coefficient of maximum spectral demands at different periods

For the CEUS study, the variable $\varepsilon_{\max}(T_i)$ is defined as:

$$\varepsilon_{\max}(T_i) = \frac{\ln(x_{\max}(T_i)) - \ln \theta_{CEUS}}{\beta_{CEUS}} \tag{4.2}$$

where $x_{\max}(T_i)$ is the maximum spectral demand at the period T_i for a set of ground motions of Table 4-2, and θ_{CEUS} and β_{CEUS} are defined below (4.1) above.

The correlation coefficients $\rho_{\varepsilon_{\max}(T_1),\varepsilon_{\max}(T_2)}$ were computed and the contours of $\rho_{\varepsilon_{\max}(T_1),\varepsilon_{\max}(T_2)}$ are presented in panel a of Figure 4-14. The results are significantly different from the contours of correlation coefficients per the model of Baker and Jayaram (2008), as described in (2.8) through (2.12) (see panel e of Figure 2-59). Panel a of Figure 4-15 presents $\rho_{\varepsilon_{\max}(T_1),\varepsilon_{\max}(T_2)}$ for the CEUS ground motions in a 3-dimensional format. For a given T_2, the decay of $\rho_{\varepsilon_{\max}(T_1),\varepsilon_{\max}(T_2)}$ along T_1 is less significant than that for WUS ground motions (see panel a of Figures 2-60 and 3-65).

The model of Baker and Jayaram (2008) can easily be modified to capture the distribution of Figure 4-15a. The modified model is presented below:

$$
\begin{aligned}
&\text{if } T_{\max} < \mathbf{0.06} \quad \rho_{\varepsilon(T_1),\varepsilon(T_2)} = C_2 \\
&\text{else if } T_{\min} > \mathbf{0.06} \quad \rho_{\varepsilon(T_1),\varepsilon(T_2)} = C_1 \\
&\text{else if } T_{\max} < 0.2 \quad \rho_{\varepsilon(T_1),\varepsilon(T_2)} = \min(C_2,\ C_4) \\
&\text{else} \quad \rho_{\varepsilon(T_1),\varepsilon(T_2)} = C_4
\end{aligned}
\tag{4.3}
$$

where $T_{\min} = \min(T_1, T_2)$, $T_{\max} = \max(T_1, T_2)$ and

$$
C_1 = 1 - \cos\left(\frac{\pi}{2} - \mathbf{0.09}\ln\left(\frac{T_{\max}}{\max(T_{\min}, \mathbf{0.06})}\right)\right) \tag{4.4}
$$

$$
C_2 = \begin{cases} 1 - 0.105\left(1 - \dfrac{1}{1 + e^{100T_{\max} - 5}}\right)\left(\dfrac{T_{\max} - T_{\min}}{T_{\max} - 0.0099}\right) & \text{if } T_{\max} < 0.2 \\ 0 & \text{otherwise} \end{cases} \tag{4.5}
$$

$$
C_3 = \begin{cases} C_2 & \text{if } T_{\max} < \mathbf{0.06} \\ C_1 & \text{otherwise} \end{cases} \tag{4.6}
$$

$$
C_4 = C_1 + 0.5\left(\sqrt{C_3} - C_3\right)\left(1 + \cos\left(\frac{\pi T_{\min}}{\mathbf{0.06}}\right)\right) \tag{4.7}
$$

The differences between the original and modified models of Baker and Jayaram (2008) are presented in (4.3) through (4.7) using the bold numbers. Figure 4-14b and Figure 4-15b present the contours and 3-dimensional distribution, respectively, of correlation coefficients per (4.3) through (4.7).

Panels a through d of Figure 4-16 present the values of $\rho_{\varepsilon_{\max}(T_1),\varepsilon_{\max}(T_2)}$ as a function of T_1 given that T_2 is equal to 0.2, 0.5, 1 and 3 seconds, respectively. The solid and dashed lines in each panel present the data for (4.3) through (4.7) and the records of Table 4-2, respectively. The correlation coefficients per (4.3) through (4.7) are similar to those for the records of Table 4-2, except for 1) T_2 = 0.2 second and 2) T_2 = 0.5 second and T_1 smaller than 0.5 second, where the model of (4.3) through (4.7) overestimates the correlation coefficients for the records of Table 4-2.

The results of Figure 4-14 through Figure 4-16 suggest that the model of (4.3) through (4.7), which is that of Baker and Jayaram (2008) with minor modifications, is an acceptable model to capture the correlation between the maximum spectral demands at different periods for the CEUS ground motions of Table 4-2.

Table 4-1. List of earthquakes for the CEUS study

Event No.	Date	Earthquake	M_W	M_N	Number of records
1	5/17/1976	Gazli (Russia)	6.8	--	1
2	9/16/1978	Tabas (Iran)	7.4	--	2
3	1/19/1982	Gaza (US)	4.3	--	6
4	3/31/1982	New Brunswick (CA)	4	--	3
5	12/23/1985	Nahanni (CA)	6.8	--	3
6	1/31/1986	Painesville (US)	4.8	--	1
7	11/25/1988	Saguenay (CA)	5.8	--	1
8	6/15/1991	Georgia (Russia)	6.2	--	1
9	11/17/1992	(45.77, -74.93)* (CA)	4**	4.3	1
10	9/25/1994	(45.77, -69.96)* (CA)	4.1**	4.4	1
11	10/28/1997	(47.67, -69.91)* (CA)	4.5**	4.7	4
12	4/20/2002	Au Sable Forks (US)	5	--	14
13	6/13/2003	(47.7, -70.09)* (CA)	3.9**	4.1	2
14	3/6/2005	(47.75, -69.73)* (CA)	5.4**	5.4	6
15	10/20/2005	(44.68, -80.48)* (CA)	4**	4.3	1
16	2/25/2006	(45.65, -75.23)* (CA)	4.2**	4.5	1
17	4/7/2006	(47.38, -70.46)* (CA)	3.9**	4.1	1
18	11/15/2008	(47.74, -69.74)* (CA)	3.9**	4.2	2
19	6/23/2010	Val-des-Bois (CA)	5	--	12

* The latitude and longitude of the epicenter of the event.

** The value is converted from M_N .

Table 4-2. Earthquake ground motion records for the CEUS study

Record Sequence Number	Earthquake	Station Name	M_W	r_{epi} (km)	PGA of Comp. 1 (g)	PGA of Comp. 2 (g)
1	Gazli (Russia)	Karakyr	6.8	12.8	0.60	0.71
2	Tabas (Iran)	Dayhook	7.4	20.6	0.33	0.41
3	Tabas (Iran)	Ferdows	7.4	117.7	0.09	0.11
4	Gaza (US)	Ball Mountain Dam	4.3	103.2	0.01	0.01
5	Gaza (US)	Franklin Falls Dam	4.3	10.4	0.13	0.31
6	Gaza (US)	North Hartland Dam	4.3	82.4	0.04	0.04
7	Gaza (US)	North Springfield Dam	4.3	74.6	0.03	0.02
8	Gaza (US)	Union Village Dam	4.3	60.8	0.04	0.02
9	Gaza (US)	White River JCT. VA Hospital	4.3	59.1	0.02	0.03
10	New Brunswick (CA)	Indian Brook II	4	0.8	0.34	0.09
11	New Brunswick (CA)	Hickey Lakes, Loggie Lodge	4	4.1	0.19	0.40
12	New Brunswick (CA)	Mitchell Lake Road	4	3.9	0.15	0.25
13	Nahanni (CA)	6097 Site 1	6.8	6.8	0.98	1.10
14	Nahanni (CA)	6098 Site 2	6.8	6.5	0.49	0.32
15	Nahanni (CA)	6099 Site 3	6.8	22.4	0.15	0.14
16	Painesville (US)	Perry Plant, Bldg Foundation	4.8	16.8	0.18	0.10
17	Saguenay (CA)	Dickey	5.8	194.8	0.06	0.09
18	Georgia (Russia)	Ambralauri	6.2	72.4	0.02	0.02
19	(45.77, -74.93) (CA)	Glen Almond	4	43.2	0.06	0.06
20	(45.77, -69.96) (CA)	La Malbaie	4.1	36.9	0.10	0.22
21	(47.67, -69.91) (CA)	Rivière Ouelle	4.5	23.3	0.02	0.02
22	(47.67, -69.91) (CA)	Saint Andre	4.5	16.9	0.02	0.03
23	(47.67, -69.91) (CA)	Sainte Mathilde	4.5	13.7	0.06	0.06
24	(47.67, -69.91) (CA)	Saint Siméon	4.5	17.5	0.03	0.01
25	Au Sable Forks (US)	Acton	5	516.0	0.01	0.01
26	Au Sable Forks (US)	Bruce Peninsula	5	613.4	0.01	0.01
27	Au Sable Forks (US)	Glen Almond	5	189.3	0.01	0.02
28	Au Sable Forks (US)	Kingston	5	222.2	0.02	0.02

Record Sequence Number	Earthquake	Station Name	M_W	r_{epi} (km)	PGA of Comp. 1 (g)	PGA of Comp. 2 (g)
29	Au Sable Forks (US)	Montreal	5	108.5	0.02	0.02
30	Au Sable Forks (US)	Pickering	5	430.0	0.03	0.04
31	Au Sable Forks (US)	Saint Catharines	5	460.1	0.02	0.02
32	Au Sable Forks (US)	Tyneside	5	517.7	0.02	0.03
33	Au Sable Forks (US)	Wesleyville	5	377.9	0.01	0.02
34	Au Sable Forks (US)	Adirondack Community College	5	127.5	0.11	0.08
35	Au Sable Forks (US)	Cobleskill	5	215.7	0.03	0.04
36	Au Sable Forks (US)	Binghamton	5	316.9	0.01	0.01
37	Au Sable Forks (US)	Lisbon	5	146.9	0.04	0.05
38	Au Sable Forks (US)	Newcomb	5	73.6	0.13	0.11
39	(47.7, -70.09) (CA)	Sainte Mathilde	3.9	0.8	0.03	0.02
40	(47.7, -70.09) (CA)	Saint Siméon	3.9	20.4	0.01	0.01
41	(47.75, -69.73) (CA)	Rivière Ouelle	5.4	37.4	0.02	0.03
42	(47.75, -69.73) (CA)	Saint Andre	5.4	6.0	0.07	0.08
43	(47.75, -69.73) (CA)	Misere	5.4	60.7	0.01	0.02
44	(47.75, -69.73) (CA)	Sainte Mathilde	5.4	27.7	0.05	0.06
45	(47.75, -69.73) (CA)	Saint Siméon	5.4	14.8	0.04	0.04
46	(47.75, -69.73) (CA)	La Malbaie	5.4	50.1	0.02	0.03
47	(44.68, -80.48) (CA)	Collingwood	4	29.4	0.01	0.01
48	(45.65, -75.23) (CA)	Glen Almond	4.2	20.2	0.01	0.01
49	(47.38, -70.46) (CA)	La Malbaie	3.9	21.3	0.01	0.01
50	(47.74, -69.74) (CA)	Saint Andre	3.9	5.5	0.07	0.05
51	(47.74, -69.74) (CA)	Saint Siméon	3.9	14.9	0.02	0.02
52	Val-des-Bois (CA)	Algonquin Park	5	198.3	0.04	0.04
53	Val-des-Bois (CA)	Ottawa (OTT1)	5	60.1	0.03	0.02
54	Val-des-Bois (CA)	Pembroke	5	138.8	0.01	0.02
55	Val-des-Bois (CA)	Ottawa (OTT2)	5	58.7	0.04	0.03
56	Val-des-Bois (CA)	Ottawa (OTGH)	5	57.5	0.05	0.03
57	Val-des-Bois (CA)	Ottawa (OTNM)	5	56.2	0.05	0.08
58	Val-des-Bois (CA)	Ottawa (OTRS)	5	48.9	0.08	0.09
59	Val-des-Bois (CA)	Ottawa (OT002)	5	47.3	0.06	0.05
60	Val-des-Bois (CA)	Ottawa (OT004)	5	63.3	0.06	0.05

Record Sequence Number	Earthquake	Station Name	M_W	r_{epi} (km)	PGA of Comp. 1 (g)	PGA of Comp. 2 (g)
61	Val-des-Bois (CA)	Ottawa (OT006)	5	53.6	0.07	0.04
62	Val-des-Bois (CA)	Ottawa (OT008)	5	62.2	0.06	0.06
63	Val-des-Bois (CA)	Ottawa (OT012)	5	58.7	0.03	0.03

Table 4-3. Median and 84th percentile of the ratio of maximum spectral demand to GMRotI50 for the ground motions of Table 4-2

Period (sec)	$\frac{\text{Maximum demand}}{\text{GMRotI50}}$	
	Median	84th percentile
0	1.23	1.41
0.2	1.28	1.45
0.5	1.32	1.48
1	1.35	1.54
2	1.39	1.53
3	1.35	1.54
4	1.40	1.60

Table 4-4. Medians, means and standard deviations of $\overline{R}_{S_a,\max}$ and T_L and T_U for R1 through R4 for the ground motions of Table 4-2

Bin	T_L (sec)	T_U (sec)	Median	Mean	Standard deviation
R1	0	4	0.97	0.96	0.03
R2	0	1	0.97	0.96	0.03
R3	1	2	0.99	0.98	0.02
R4	2	4	~1.00	0.99	0.02

Table 4-5. Statistics of the correlation coefficients of Figure 4-11

Type of correlation coefficient	**Mean**	**Standard deviation**	**Median**	**Ninetieth percentile**	**Cumulative probability for $\rho = 0.3$**
ρ_{Max}	0.27	0.19	0.22	0.49	0.66
ρ_{FN_FP}	0.17	0.15	0.12	0.37	0.86
$\rho_{Max_S_a}$	0.15	0.15	0.10	0.35	0.84

Table 4-6. Coefficients for the attenuation relationship of (4.1)

Period (sec)	C_1	C_2	C_3	C_4	β_{CEUS}
0	-4.23	0.63	-0.50	0.000751	0.78
0.05	-3.05	0.56	-0.51	-0.000506	0.84
0.1	-4.70	0.69	-0.23	-0.000919	0.92
0.15	-5.98	0.87	-0.21	-0.000021	0.92
0.2	-6.90	1.04	-0.32	0.002425	0.95
0.3	-8.34	1.22	-0.29	0.002599	1.02
0.35	-8.87	1.27	-0.27	0.002121	1.06
0.4	-9.48	1.33	-0.22	0.001676	1.10
0.45	-9.81	1.38	-0.27	0.001840	1.10
0.5	-10.24	1.45	-0.31	0.002302	1.12
0.6	-10.69	1.49	-0.32	0.002465	1.15
0.7	-11.30	1.55	-0.29	0.002073	1.11
0.8	-11.77	1.59	-0.27	0.001845	1.12
0.9	-11.90	1.58	-0.29	0.001794	1.14
1	-12.17	1.59	-0.27	0.001367	1.18
1.2	-12.37	1.60	-0.31	0.001579	1.11
1.4	-12.61	1.60	-0.32	0.002020	1.12
1.5	-12.70	1.60	-0.32	0.001878	1.14
1.6	-12.78	1.60	-0.33	0.001995	1.16
1.8	-12.89	1.58	-0.32	0.001613	1.18
2	-13.06	1.60	-0.34	0.001642	1.16
2.2	-13.14	1.58	-0.35	0.001347	1.16
2.4	-13.20	1.56	-0.34	0.001211	1.16
2.5	-13.25	1.56	-0.34	0.001377	1.17
2.6	-13.29	1.56	-0.35	0.001438	1.18
2.8	-13.49	1.59	-0.37	0.001515	1.18
3	-13.75	1.63	-0.38	0.001366	1.18
3.5	-14.14	1.67	-0.38	0.001117	1.18
4	-14.43	1.70	-0.39	0.001258	1.18

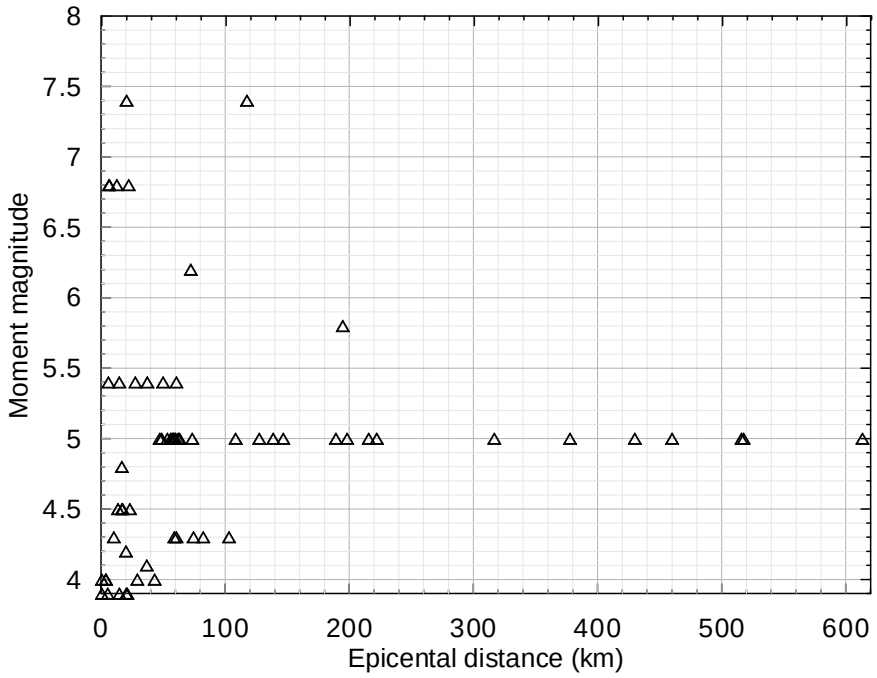

Figure 4-1. Magnitude and distance distribution of the ground motions of Table 4-2

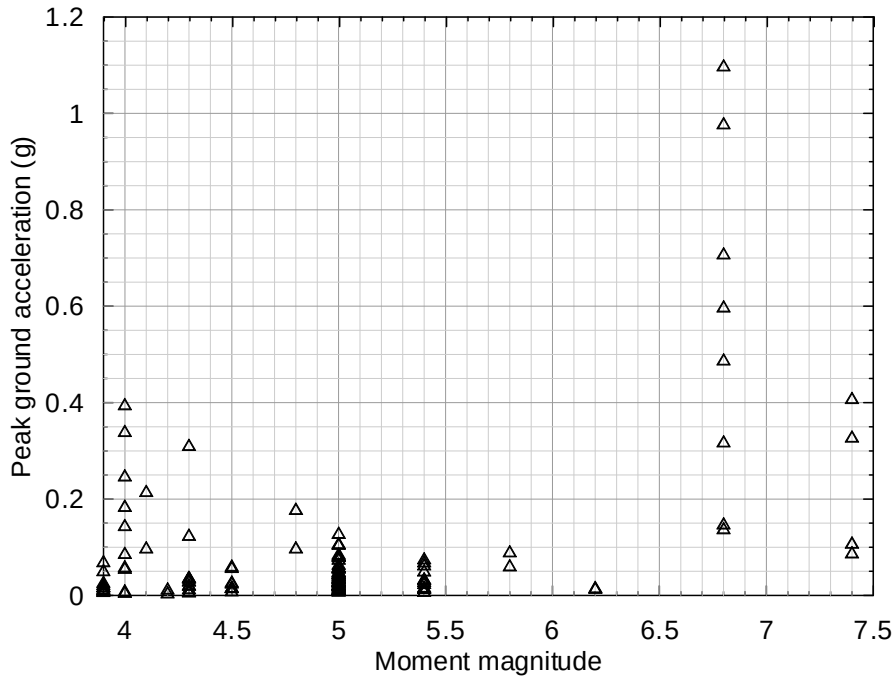

a. PGA as a function of magnitude

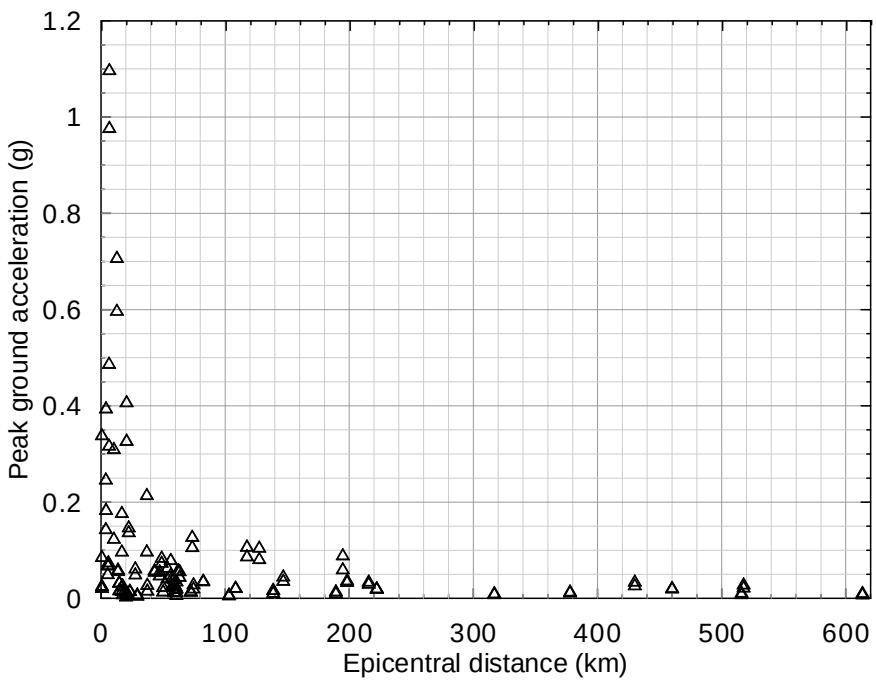

b. PGA as a function of distance

Figure 4-2. Distributions of peak ground acceleration as a function of a) moment magnitude and b) epicentral distance for the ground motions of Table 4-2

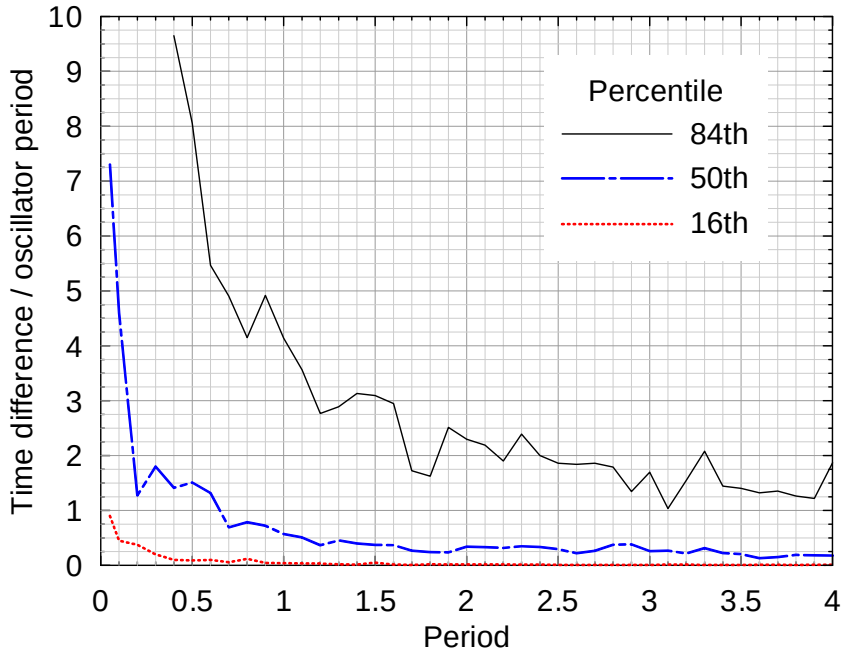

a. 84th, 50th and 16th percentiles

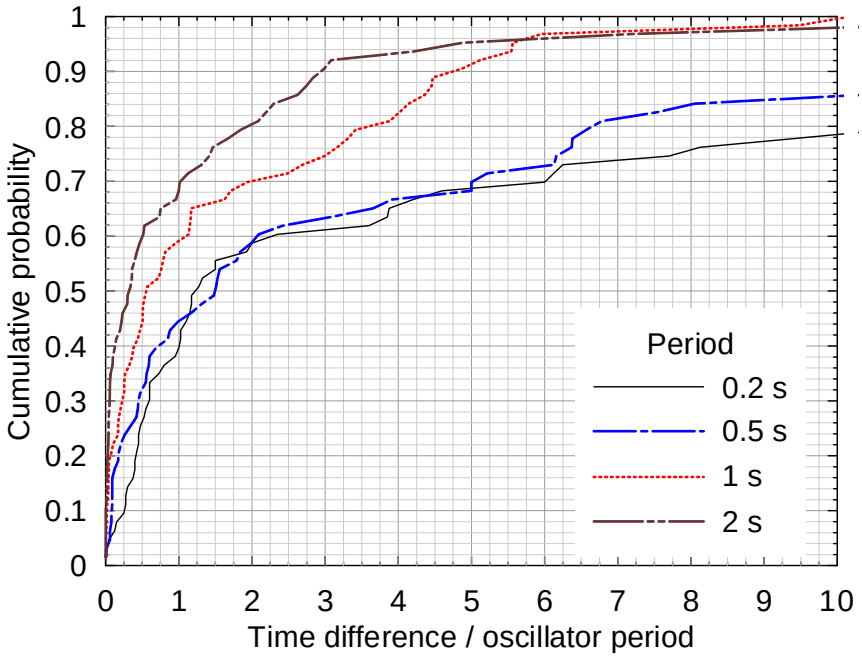

b. CDFs

Figure 4-3. a) Eighty-fourth, 50th and 16th percentiles and b) cumulative distribution functions of normalized time difference between the peak accelerations parallel and perpendicular to the GMRotI50 direction for the records of Table 4-2

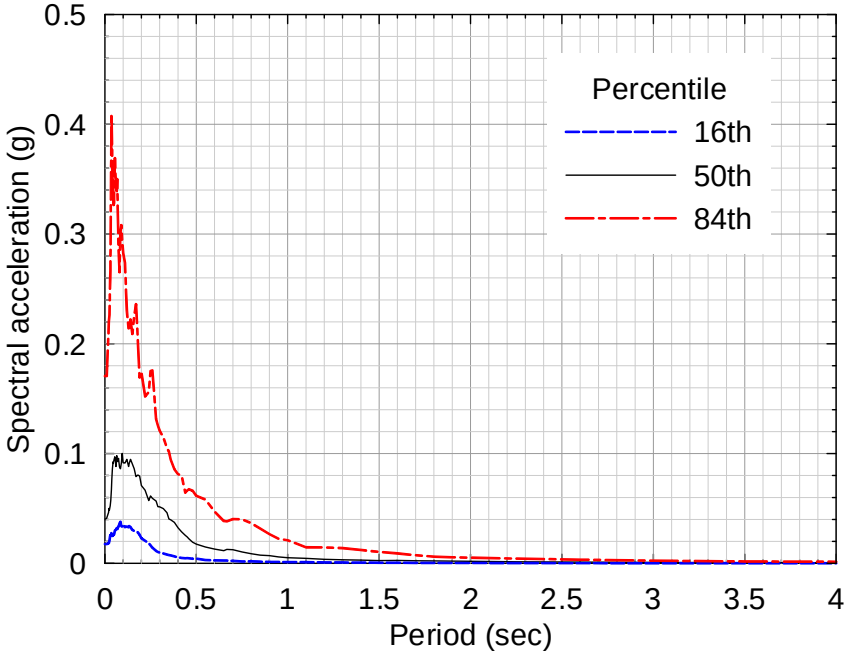

a. 0 through 4 seconds

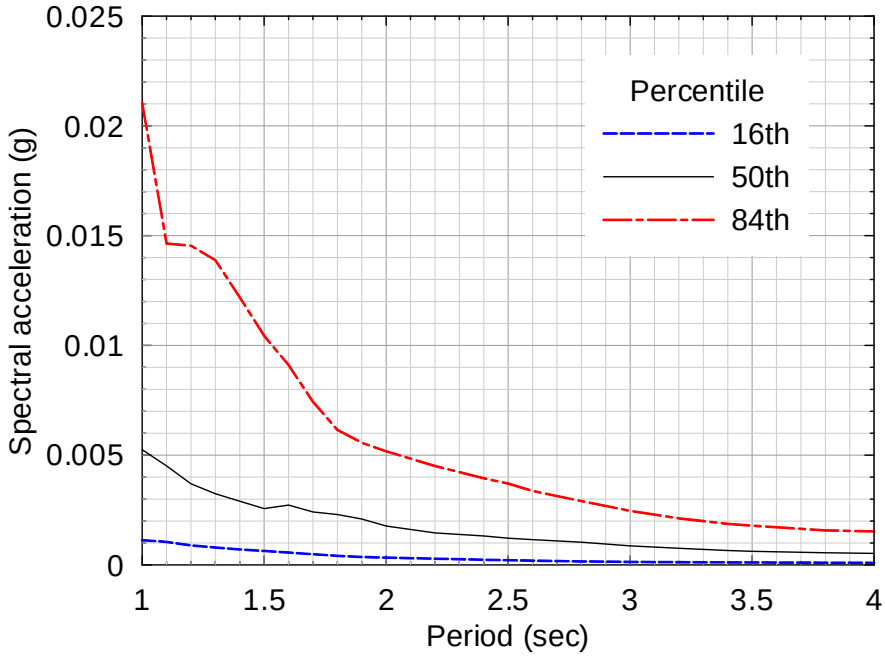

b. 1 through 4 seconds

Figure 4-4. Eighty-fourth, 50th and 16th percentiles of spectral acceleration for the records of Table 4-2

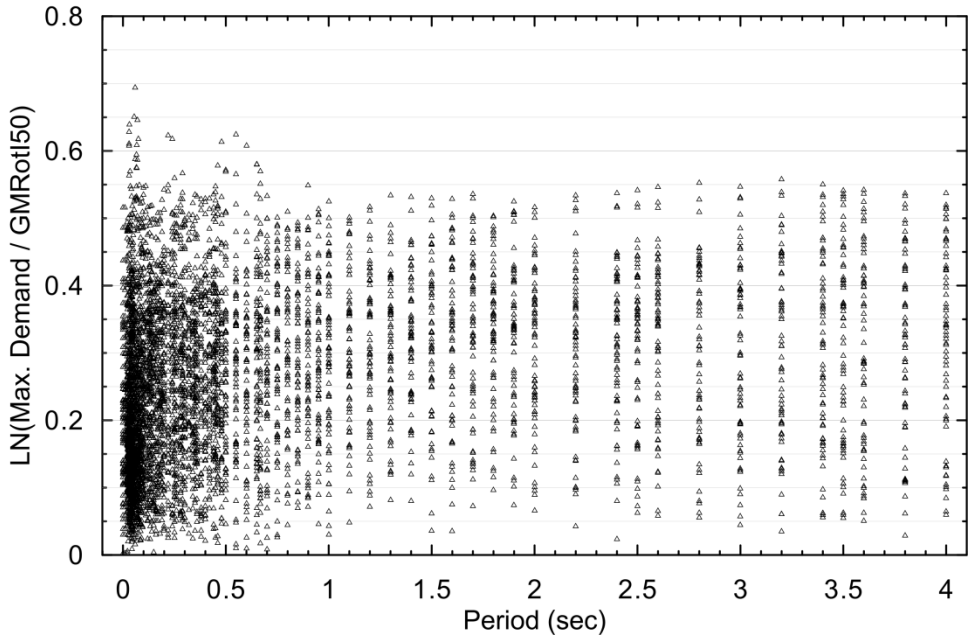

Figure 4-5. Ratios of maximum spectral demand to GMRotI50 for the records of Table 4-2

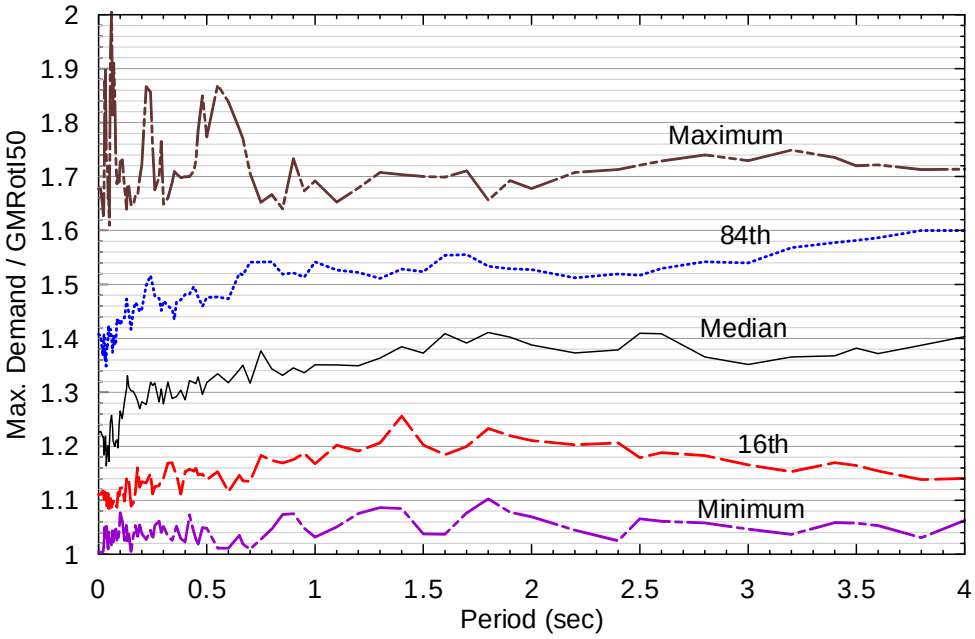

Figure 4-6. Maximum, minimum, median and 84th and 16th percentiles of the ratios of maximum spectral demand to GMRotI50 for the records of Table 4-2

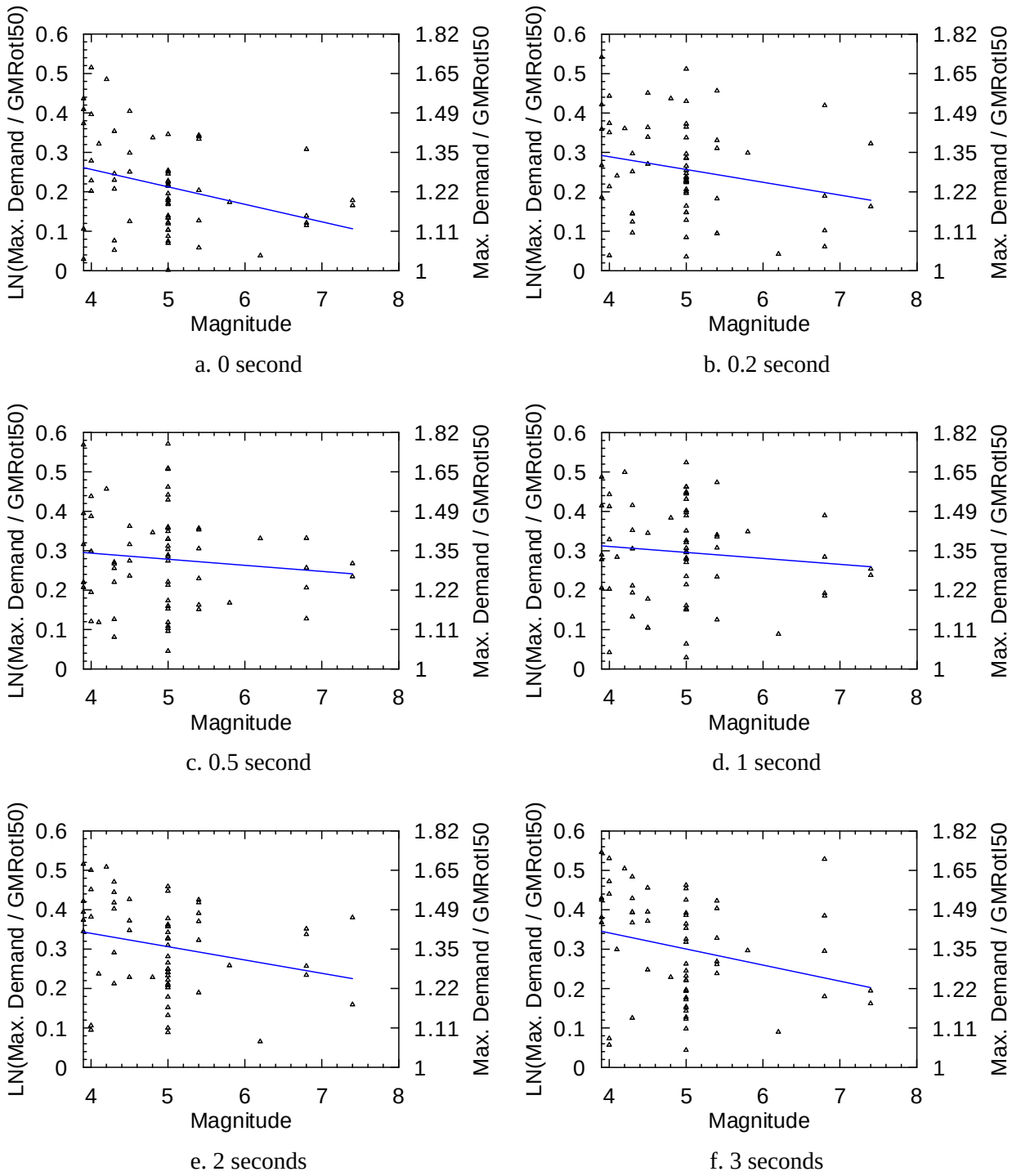

Figure 4-7. Ratios of maximum spectral demand to GMRotI50 at periods of 0, 0.2, 0.5, 1, 2 and 3 seconds as a function of magnitude for the records of Table 4-2

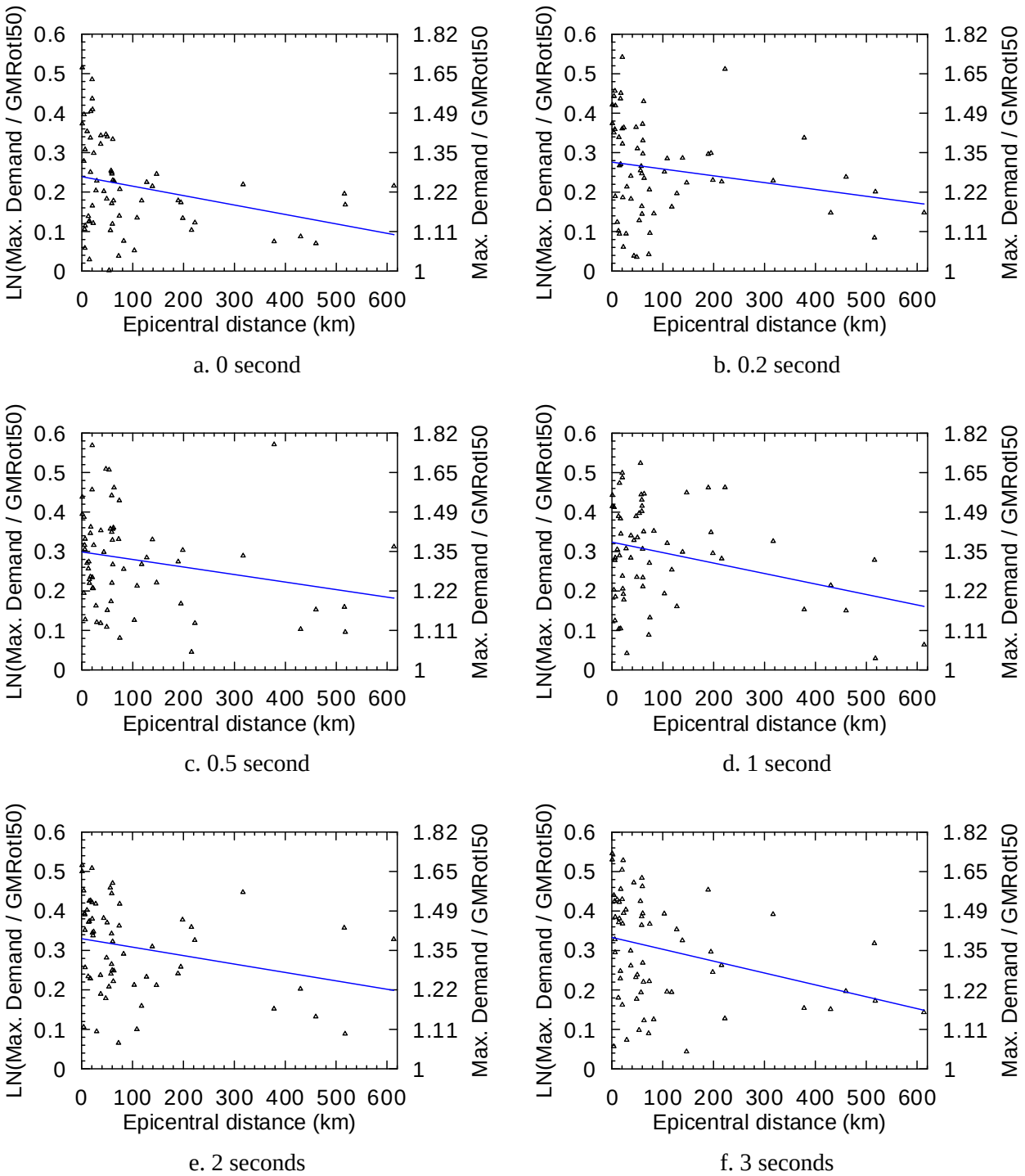

Figure 4-8. Ratios of maximum spectral demand to GMRotI50 at periods of 0, 0.2, 0.5, 1, 2 and 3 seconds as a function of distance for the records of Table 4-2

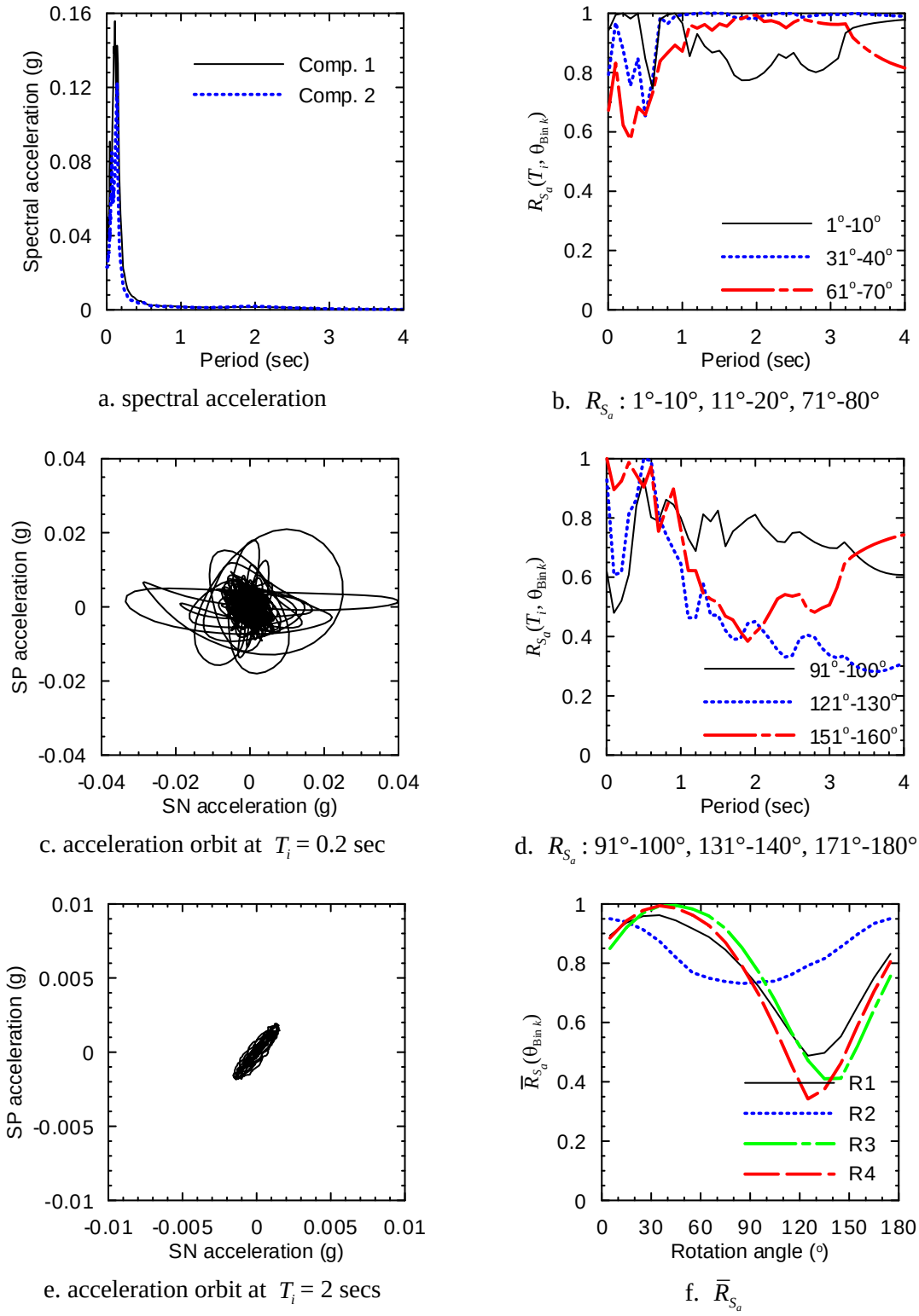

a. spectral acceleration

b. R_{S_a} : 1°-10°, 11°-20°, 71°-80°

c. acceleration orbit at T_i = 0.2 sec

d. R_{S_a} : 91°-100°, 131°-140°, 171°-180°

e. acceleration orbit at T_i = 2 secs

f. $\bar{R}_{S_a}$

Figure 4-9. Sample results for EQ8 of Table 4-2

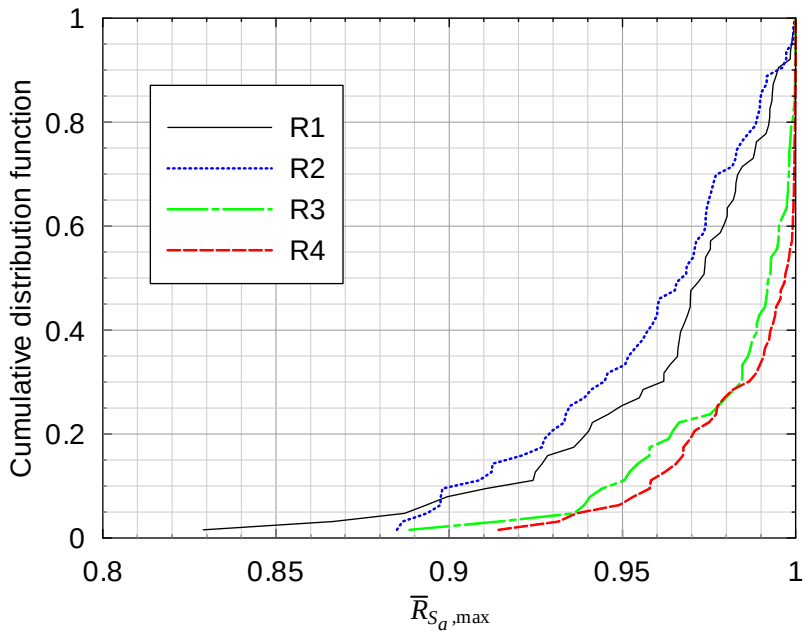

Figure 4-10. Cumulative distribution function for $\overline{R}_{S_a,\max}$ for period ranges R1 through R4 of Table 4-4

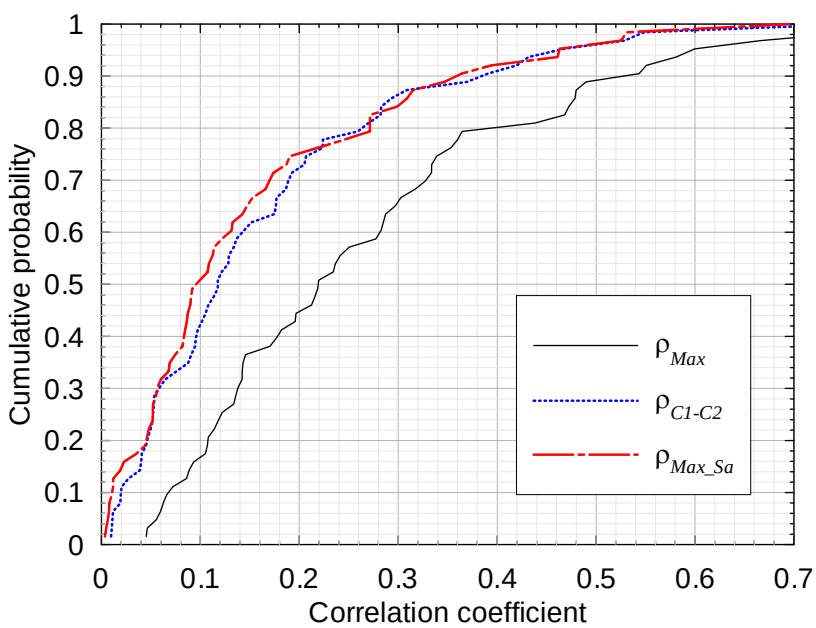

Figure 4-11. Cumulative distribution functions for ρ_{Max}, ρ_{C1_C2} and $\rho_{Max_S_a}$ for the records of Table 4-2

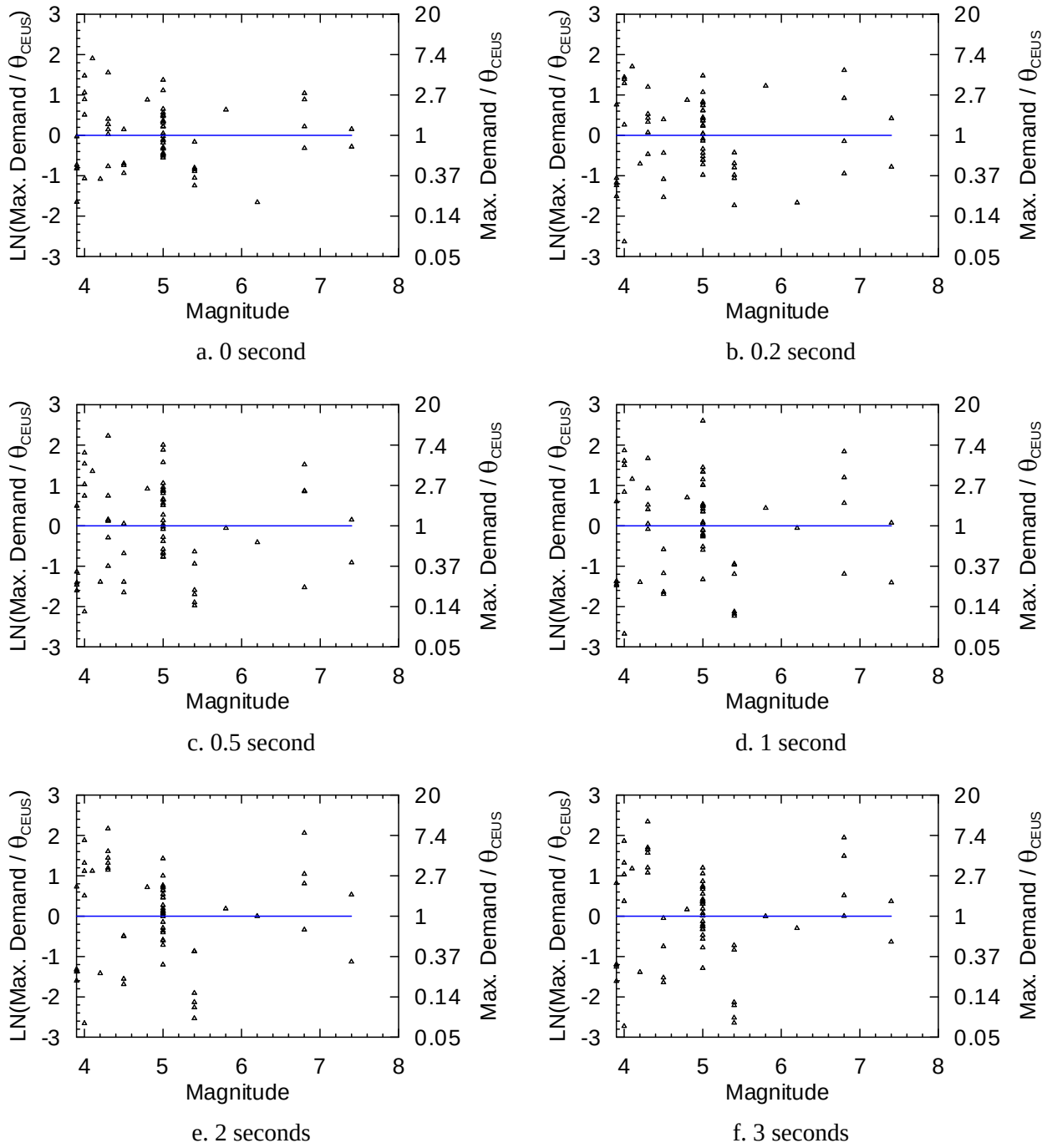

Figure 4-12. Ratios of maximum spectral demand to θ_{CEUS} at sample periods as a function of magnitude for all of the records of Table 4-2

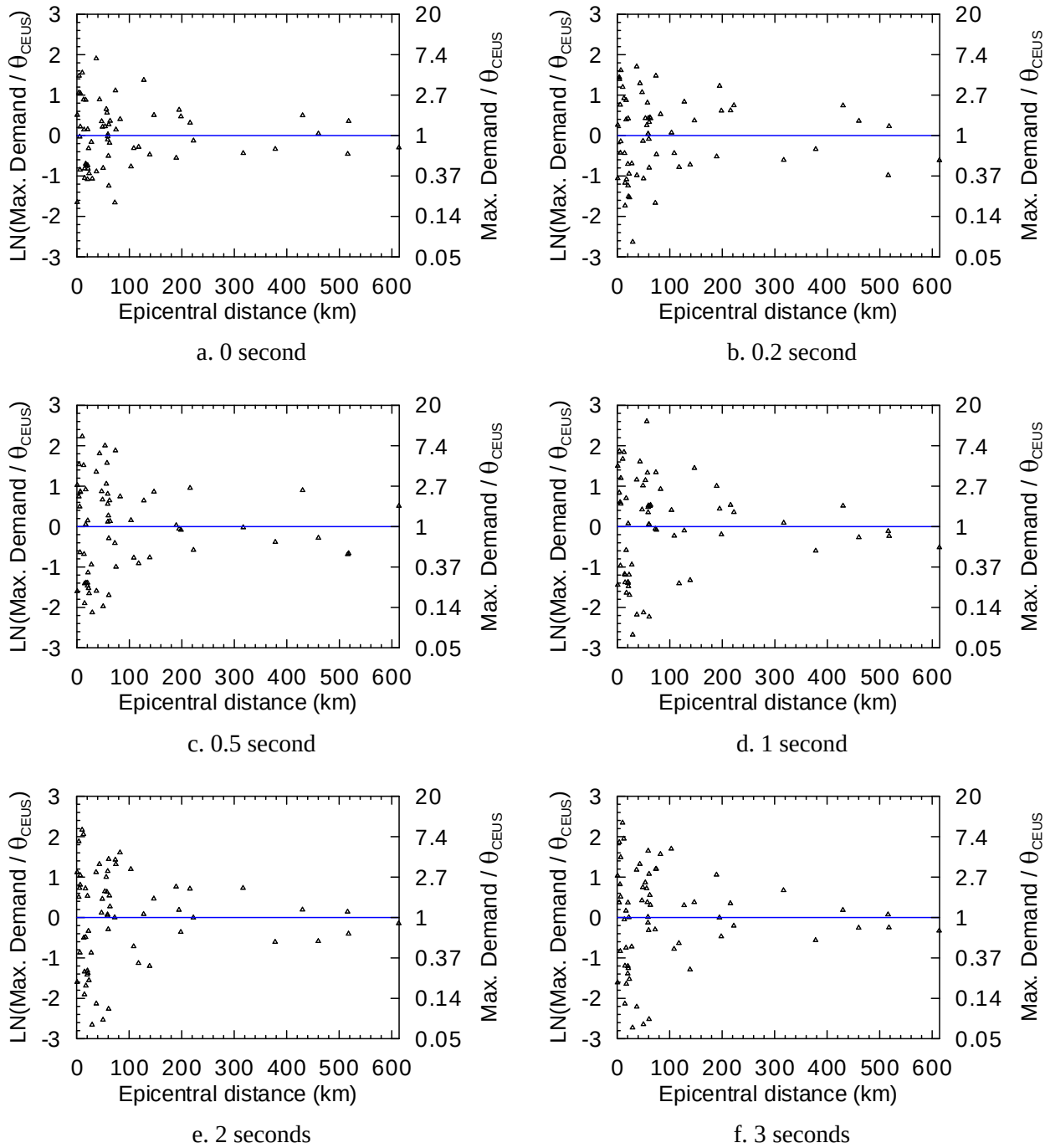

Figure 4-13. Ratios of maximum spectral demand to θ_{CEUS} at sample periods as a function of distance for all of the records of Table 4-2

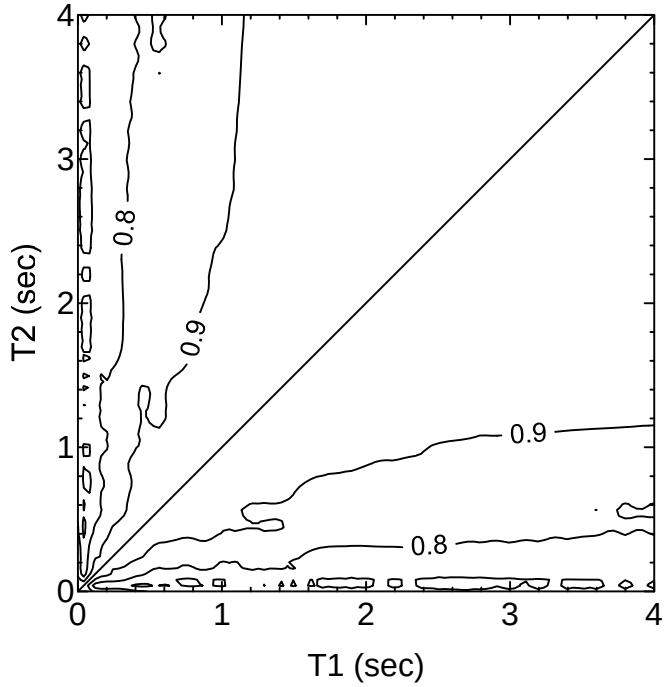

a. recorded

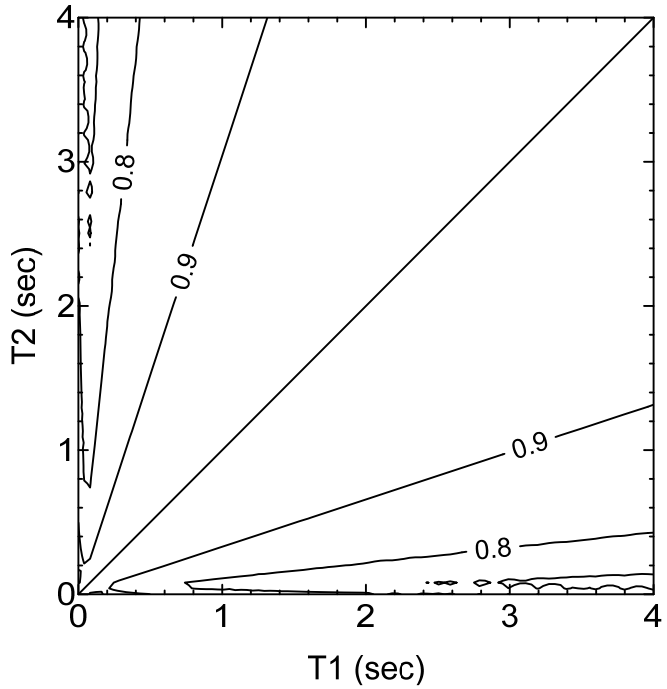

b. the model of (4.3) through (4.7)

Figure 4-14. Contours of correlation coefficients between the maximum spectral demands at T_1 and T_2 for the records of Table 4-2 and the model of (4.3) through (4.7)

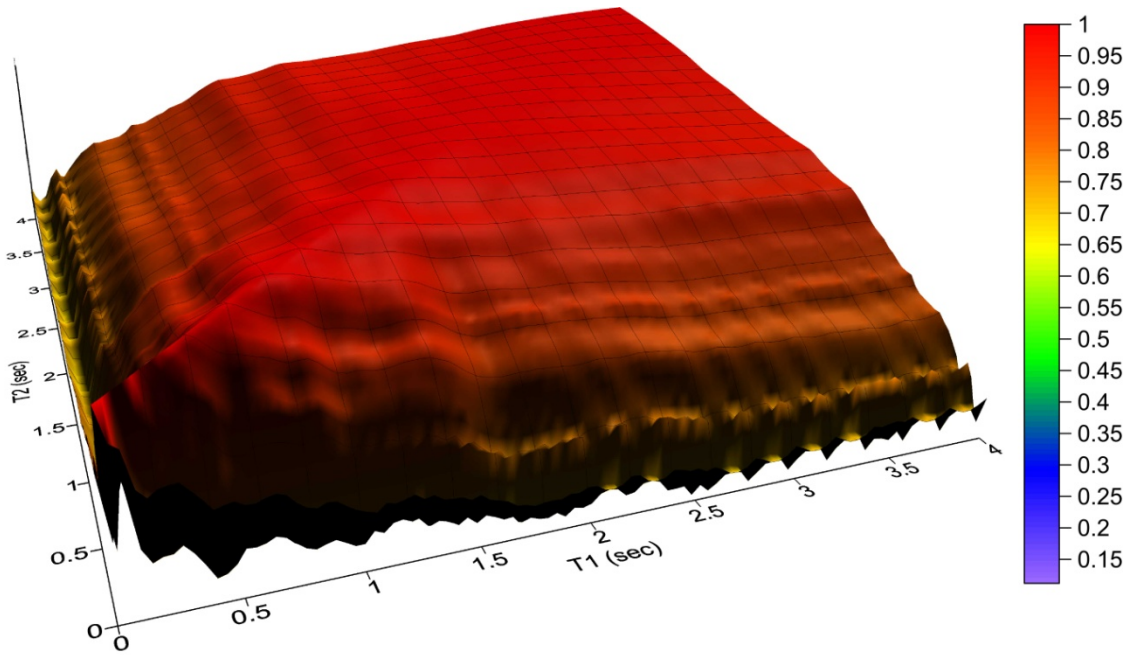

a. recorded

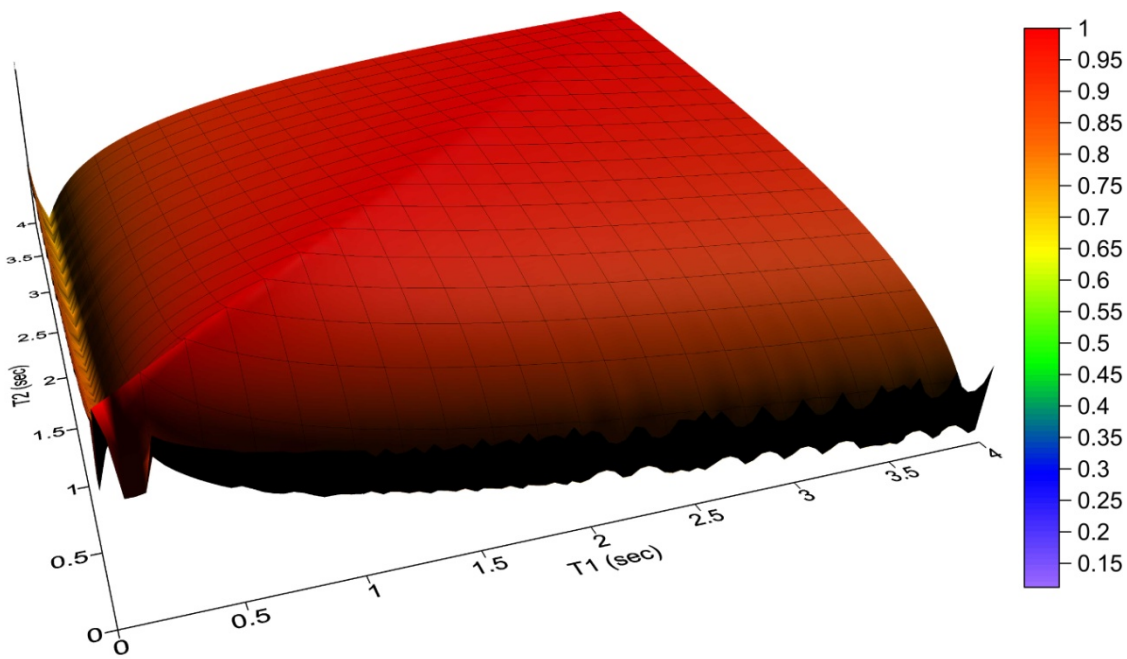

b. the model of (4.3) through (4.7)

Figure 4-15. Correlation coefficients between the maximum spectral demands at T_1 and T_2 for the records of Table 4-2 and the model of (4.3) through (4.7)

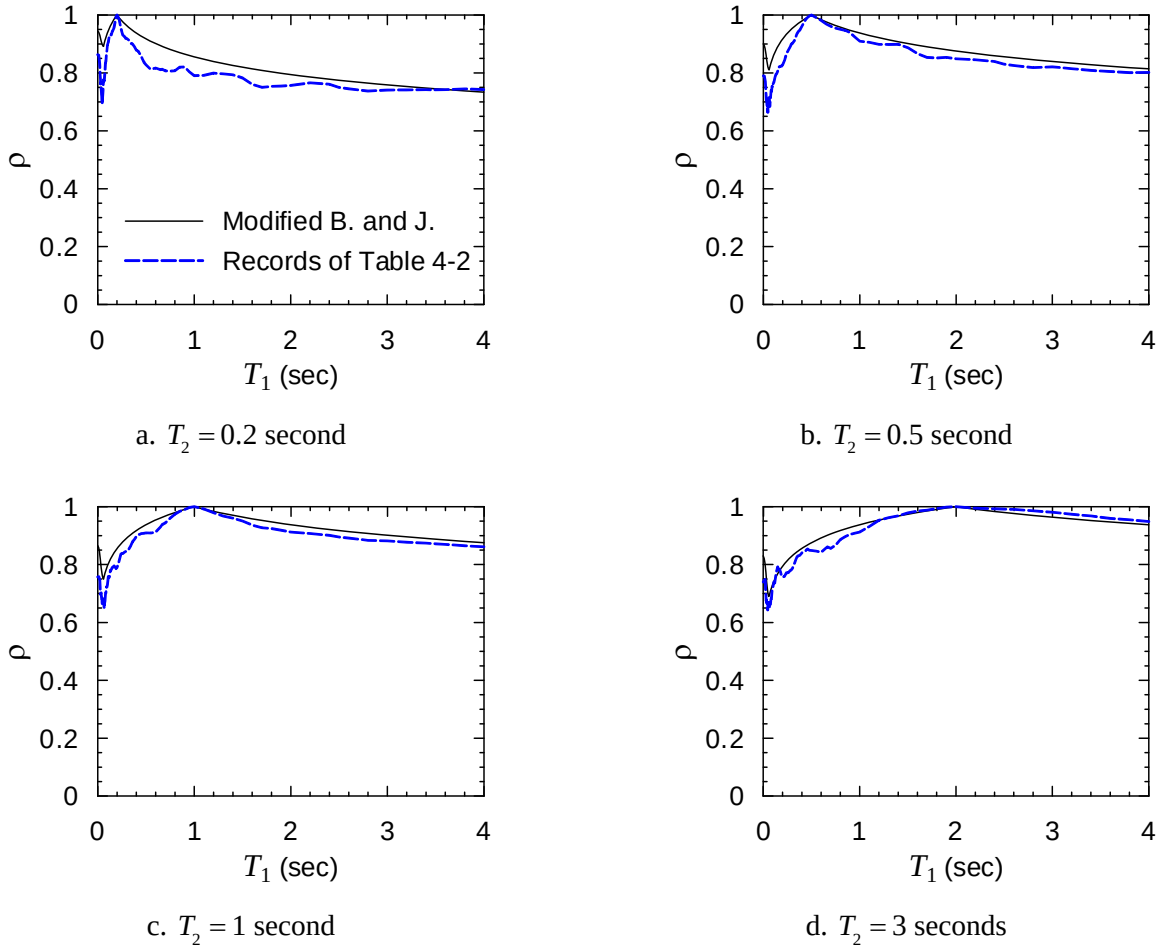

a. $T_2 = 0.2$ second

b. $T_2 = 0.5$ second

c. $T_2 = 1$ second

d. $T_2 = 3$ seconds

Figure 4-16. Correlation coefficients between the maximum spectral demands at T_1 and a given T_2 for the records of Table 4-2 and the model of (4.3) through (4.7)

SECTION 5
SUMMARY AND CONCLUSIONS

5.1 Summary

Both the probabilistic and deterministic values of the ground-motion design parameters reported in ASCE/SEI 7-10 and FEMA P-750 are defined in terms of maximum spectral demand. The major goal of this study is to enable calculation of maximum spectral demand for all regions of seismic hazard in the United States. Other goals of the study include developing an understanding of the orientation of maximum spectral demand across different ranges of period and the correlation of the demand at different periods.

Three earthquake ground-motion databases are compiled for far-field Western United States (WUS), near-fault WUS and the Central and Eastern United States (CEUS). For each pair of ground motions therein these databases, the following parameters are computed and discussed:

1. The normalized time difference between the peak spectral acceleration response at a given period in two orthogonal horizontal directions;
2. The distribution of the ratio of maximum spectral demand to GMRotI50;
3. The orientation of maximum spectral demand;
4. The correlation between two orthogonal horizontal acceleration time series;
5. The correlation of maximum spectral demands at different periods.

The relationships 1) between measured and NGA-predicted GMRotI50, and 2) between maximum spectral demand and NGA-predicted GMRotI50 are reported for the far-field and near-fault WUS ground motions.

5.2 Conclusions

5.2.1 WUS far-field ground motions

The database for the far-field WUS ground motions includes 165 pairs of ground motions with moment magnitude of 6.5 and greater and closest site-to-fault distance between 30 and 50 km. The ground-motion pairs were selected from the PEER NGA ground motion database. The key conclusions of the study for the far-field WUS ground motions are:

1. The peak structural responses of a building in two perpendicular horizontal directions seldom occur at the same time. At periods of 0.2 and 0.5 second (1 and 2 seconds), over 80% (70%) of the 165 pairs of records have a normalized time difference between the peak spectral acceleration response in the two perpendicular directions of greater than 1, where the time difference is normalized by the period of the oscillator.

2. The median ratios of maximum spectral demand to GMRotI50 range between 1.1 and 1.3 and the 84th percentile ratios range between 1.3 and 1.5. Both the median and 84th percentile results tend to increase slightly with period.

3. The median ratios of GMRotI50 to GMRotI50_ave range between 0.8 and 0.9 and the 84th percentile ratios range between 1.3 and 1.8. The bias in the median ratio of measured to NGA-predicted GMRotI50 in the short period range is due mainly to the inter-event residual for the Chi-Chi earthquake. At a period of 0.2 second, the median ratios of GMRotI50 to each of GMRotI50_BA, GMRotI50_CB, GMRotI50_CY and GMRotI50_ave are 0.73, 0.86, 0.83 and 0.81, respectively. When analysis is performed without the records of the Chi-Chi earthquake, the four median ratios are 0.96, 0.99, 1.04 and 0.97, respectively.

4. The median ratios of maximum spectral demand to GMRotI50_ave range between 0.9 and 1.2 and the 84th percentile ratios range between 1.6 and 2.5 for analysis performed using all 165 pairs of ground motions. The ratios at periods equal to or less than 0.2 second are smaller than those at longer periods. For the analysis performed without the records of the Chi-Chi earthquake, the median ratios of maximum spectral demand to

GMRotI50_ave range between 1.1 and 1.3, and the 84th percentile ratios range between 1.7 and 2.8.

5. An orientation-dependent parameter, $\bar{R}_{S_a}(\theta)$, is used to investigate the orientation of maximum spectral demand. The upper bound on $\bar{R}_{S_a}(\theta)$, equal to 1, occurs when the spectral demands for an orientation θ are equal to the maximum demands at all periods considered. The maximum value of $\bar{R}_{S_a}(\theta)$ is termed $\bar{R}_{S_a,\max}$ and the corresponding orientation is termed $\theta_{\max}$.

   The percentages of the records with $\bar{R}_{S_a,\max}$ greater than 0.95 are 73% in the long period range R4 (2 to 4 seconds) and 42% in the short period range R2 (0 to 1 second). The median and mean of the 165 realizations of $\bar{R}_{S_a,\max}$ for each of R1 (0 to 4 seconds), R2, R3 (1 to 2 seconds) and R4 range between 0.93 and 0.97 and the standard deviation is 0.03 for each case. These results indicate that there is typically an axis of strongest shaking.

6. The distributions of three correlation coefficients of orthogonal horizontal ground-motion time series were investigated, namely, ρ_{Max}, ρ_{FN_FP} and $\rho_{Max_S_a}$. The probabilities for ρ_{Max}, ρ_{FN_FP} and $\rho_{Max_S_a}$ less than 0.3 are 0.79, 0.91 and 0.96, respectively. The results support the upper bound of 0.3 on the correlation coefficient between two orthogonal horizontal ground acceleration time series as specified in ASCE Standard 4-98 and ASCE Standard 43-05.

7. Although originally developed to predict the correlation of GMRotI50 at two different periods, the model of Baker and Jayaram (2008) can also capture the correlation of maximum spectral demands at different periods for the far-field WUS ground motions.

5.2.2 WUS near-fault ground motions

The database for the near-fault WUS ground motions includes 147 pairs of ground motions with moment magnitude of 6.5 and greater and closest site-to-fault distance of 15 km and less. These ground-motion pairs were extracted from the PEER NGA ground motion database. The key conclusions of the study for the WUS near-fault ground motions are:

1. At periods of 0.2, 0.5, 1 and 2 seconds, over 75%, 70%, 55% and 55%, respectively, of the 147 pairs of records have a normalized time difference between the peak spectral acceleration response in two perpendicular directions greater than 1. The percentages are lower than those for the far-field WUS ground motions but are still significant.

2. The median ratios of maximum spectral demand to GMRotI50 range between 1.2 and 1.4 and the 84th percentile ratios range between 1.3 and 1.5. Both the median and 84th percentile results increase slightly with period, similar to the trend for the far-field WUS records.

3. The median ratios of GMRotI50 to GMRotI50_ave range between 0.7 and 1.2 and the 84th percentile ratios range between 1.3 and 1.8. Similar to the observation for the far-field WUS records, the bias in the median ratio of measured to NGA-predicted GMRotI50 in the short period range is due mainly to the inter-event residual for the Chi-Chi earthquake. At a period of 0.2 second, the median ratios of GMRotI50 to each of GMRotI50_BA, GMRotI50_CB, GMRotI50_CY and GMRotI50_ave are 0.81, 0.84, 0.64 and 0.74, respectively. When analysis is performed without the records of the Chi-Chi earthquake, the four median ratios are 1.02, 1.08, 0.96 and 1.04, respectively, greatly reducing the bias.

4. The median ratios of maximum spectral demand to GMRotI50_ave range between 0.9 and 1.5 and the 84th percentile ratios range between 1.6 and 2.7 for the analysis performed using all 147 pairs of ground motions. The ratios in the short period range are smaller than those at longer periods. For the analysis performed without the records of the Chi-Chi earthquake, the median ratios of maximum spectral demand to GMRotI50_ave range between 1.2 and 1.6 and the 84th percentile ratio ranges between 1.7 and 2.8.

5. The percentages of the records with $\bar{R}_{S_a,\max}$ greater than 0.95 are 82% in the long period range (R4) and 55% in the short period range (R2). The median and mean of the 147 realizations of $\bar{R}_{S_a,\max}$ for each of R1 through R4 range between 0.94 and 0.98 and the standard deviation is small: either 0.03 or 0.04 for each case. The results indicate clearly

that there is typically an axis where the spectral demands are close or equal to the maximum demands.

6. For distance smaller than 5 km, the percentages of records with $\theta_{\max}$ between ±30° of the SN direction are 64%, 53%, 61% and 72% for R1 through R4, respectively. For distance greater than 5 km, the corresponding percentages are 44%, 39%, 48% and 46%. The SN direction cannot be assumed as the direction of maximum shaking for a) distance greater than 5 km, and b) distance less than 5 km and periods smaller than 1 second; the orientation of maximum direction shaking for these cases should be assumed to be random.

7. The probabilities for ρ_{Max}, ρ_{FN_FP} and $\rho_{Max_S_a}$ less than 0.3 are 0.74, 0.89 and 0.92, respectively. The results support the upper bound of 0.3 on the correlation coefficient between two orthogonal horizontal ground acceleration time series as specified in ASCE Standard 4-98 and ASCE Standard 43-05.

8. The correlation of maximum spectral demands at two different periods for the near-fault WUS ground motions can be captured reasonably well using the model of Baker and and Jayaram (2008).

5.2.3 CEUS ground motions

The database for the CEUS ground motions includes 63 pairs of ground motions recorded from 19 earthquakes that occurred mostly in Eastern North America between 1976 and 2010. Only those pairs of ground motions for earthquakes with moment magnitude of 4.0 and greater and with peak ground acceleration (PGA) greater than 0.01 g in one or both horizontal components are included in this study. The key conclusions of the study for the CEUS ground motions are:

1. The percentages of the records with normalized time difference greater than 1 at periods of 0.2, 0.5, 1 and 2 seconds are 60%, 56%, 41% and 30%, respectively. Although the percentages are much smaller than those for the WUS ground motions, we note that the spectral demand at periods greater than 0.5 second is insignificant for the records included in the CEUS study.

2. The median ratios of maximum spectral demand to GMRotI50 range between 1.2 and 1.4 and the 84th percentile ratios range between 1.4 and 1.6. Both the median and 84th percentile results tend to increase slightly with period.

3. The percentages of the records with $\bar{R}_{S_a,\max}$ greater than 0.95 are 93% in the long period range (R4) and 75% in the short period range (R2). The median values of $\bar{R}_{S_a,\max}$ for R1 through R4 are greater than 0.97: a value higher than those for the WUS ground motions. The results indicate clearly that there is typically an axis of strongest shaking.

4. The probabilities for ρ_{Max}, ρ_{FN_FP} and $\rho_{Max_S_a}$ less than 0.3 are 0.66, 0.86 and 0.84, respectively. The results do not support the use of an upper bound on the correlation coefficient between two orthogonal horizontal ground acceleration time series smaller than 0.3.

5. The correlation coefficients of maximum spectral demands at different periods for the CEUS ground motions are significantly different from the coefficients per the model of Baker and Jayaram (2008). However, with some minor modification, the model still can capture reasonably well the correlation of maximum spectral demands for the CEUS ground motions.

SECTION 6

ACKNOWLEDGEMENT

The authors gratefully acknowledge the National Earthquake Hazards Reduction Program, External Research Grant No. 08HQGR0017. The opinions expressed in this document are solely those of the authors and do not represent the view of the sponsor.

REFERENCES

Abrahamson, N. A. (2000). Effects of rupture directivity on probabilistic seismic hazard analysis, *Proceedings*, 6th International Conference on Seismic Zonation, Palm Springs, CA.

Abrahamson, N., and Silva, W. J. (2008). "Summary of the Abrahamson & Silva NGA ground-motion relations." *Earthquake Spectra*, 24(1), 67-97.

American Society of Civil Engineers (ASCE). (2000). "Seismic analysis of safety-related nuclear structures and commentary." *ASCE 4-98*, ASCE, Reston, VA.

American Society of Civil Engineers (ASCE). (2005). "Seismic design criteria for structures, systems, and components in nuclear facilities." *ASCE/SEI 43-05*, ASCE, Reston, VA.

American Society of Civil Engineers (ASCE). (2010). "Minimum design loads for buildings and other structures." *ASCE/SEI 7-10*, American Society of Civil Engineers, Reston, Virginia.

Atkinson, G. M., and Assatourians, K. (2010). Attenuation and source characteristics of the June 23, 2010 M5.0 Val-des-Bois, Quebec earthquake, *Seismological Research Letters*, in press.

Baker, J. W., and Cornell, C. A. (2005). "A vector-valued ground motion intensity measure consisting of spectral acceleration and epsilon." *Earthquake Engineering and Structural Dynamics*, 34(10), 1193-1217.

Baker, J. W., and Cornell, C. A. (2006a). "Correlation of response spectral values for multicomponent ground motions." *Bulletin of the Seismological Society of America*, 96(1), 215-227.

Baker, J. W., and Cornell, C. A. (2006b). "Spectral shape, epsilon and record selection." *Earthquake Engineering and Structural Dynamics*, 35(9), 1077-1095.

Baker, J. W., and Jayaram, N. (2008). "Correlation of spectral acceleration values from NGA ground motions models." *Earthquake Spectra*, 24(1), 299-317.

Baker, J. W., Bozorgnia, Y., Goulet, C. A., Haselton, C. B., Kalkan, E., Luco, N., Shantz, T., Shome, N., Stewart, J. P., Tothong, P., Watson-Lamprey, J., and Zareian, F. (2009). "Evaluation of ground motion selection and modification methods: Predicting median interstory drift response of buildings." *PEER 2009/01*, C. B. Haselton, ed., Pacific Earthquake Engineering Research Center, University of California, Berkeley.

Beyer K., and Bommer, J. J. (2006). "Relationships between median values and between aleatory variabilities for different definitions of the horizontal component of motion." *Bulletin of the Seismological Society of America*, 96(4A), 1512-1521.

Boore, D. M., and Atkinson, G. M. (2008). "Ground-motion prediction equations for the average horizontal component of PGA, PGV, and 5%-Damped PSA at spectral periods between 0.01 s and 10.0 s." *Earthquake Spectra*, 24(1), 99-138.

Boore, D. M., Watson-Lamprey, J., and Abrahamson, N. A. (2006). "Orientation-independent measures of ground motion." *Bulletin of the Seismological Society of America*, 96(4A), 1502-1511.

Bozorgnia, Y., and Campbell, K. W. (2004). "Engineering characterization of ground motion." *Earthquake engineering : from engineering seismology to performance-based engineering*, Y. Bozorgnia, and V. V. Bertero, eds., CRC Press, Boca Raton, Florida.

Campbell, K. W., and Bozorgnia, Y. (2007). Campbell-Bozorgnia NGA ground motion relations for the geometric mean horizontal component of peak and spectral ground motion parameters, *PEER 2007/02*, Pacific Earthquake Engineering Research Center, Berkekey, California.

Campbell, K. W., and Bozorgnia, Y. (2008). "NGA ground motion model for the geometric mean horizontal component of PGA, PGV, PGD and 5% damped linear elastic response spectra for periods ranging from 0.01 to 10 s." *Earthquake Spectra*, 24(1), 139-171.

Chiou, B. S.-J., and Youngs, R. R. (2008). "A NGA model for the average horizontal component of peak ground motion and response spectra." *Earthquake Spectra*, 24(1), 173-215.

Federal Emergency Management Agency (FEMA). (2009). "NEHRP recommended seismic provisions for new buildings and other structures." *FEMA P-750*, Federal Emergency Management Agency, Washington, D.C.

Filiatrault, A. (2002). *Elements of earthquake engineering and structural dynamics*, Polytechnic International Press, Montréal, Canada.

Hadjian, A. H. (1978). "On the correlation of the components of strong ground motion." *Proceedings*, Second International Conference on Microzonation, San Francisco, California, 1999-1210.

Hadjian, A. H. (1981). "On the correlation of the components of strong ground motion - Part 2." *Bulletin of the Seismological Society of America*, 71(4), 1323-1331.

Howard, J. K., Tracy, C. A., and Burns, R. G. (2005). "Comparing observed and predicted directivity in near-source ground motion." *Earthquake Spectra*, 21(4), 1063-1092.

Huang, Y.-N., Whittaker, A. S., and Luco, N. (2008). "Maximum spectral demands in the near-fault region." *Earthquake Spectra*, 24(1), 319-341.

Idriss, I. M. (2008). "An NGA empirical model for estimating the horizontal spectral values generated by shallow crustal earthquakes." *Earthquake Spectra*, 24(1), 217-242.

McGuire, R. K. (1995). "Probabilistic seismic hazard analysis and design earthquakes: closing the loop." *Bulletin of the Seismological Society of America*, 85(5), 1275-1284.

Power, M., Chiou, B., Abrahamson, N., Bozorgnia, Y, Shantz, T., and Roblee, C. (2008). "An overview of the NGA project." *Earthquake Spectra*, 24(1), 3-21.

Somerville, P. G., Smith, N. F., and Graves, R. W. (1997). Modification of empirical strong ground motion attenuation relations to include the amplitude and duration effects of rupture directivity, *Seismological Research Letters*, 68(1), 94-127.

Soong, T. T. (2004). *Fundamentals of probability and statistics for engineers*. Wiley, Hoboken, NJ.

Watson-Lamprey, J. A., and Boore, D. M. (2007). "Beyond Sa_{GMRotI}: conversion to Sa_{Arb}, Sa_{SN} and Sa_{MaxRot}." *Bulletin of the Seismological Society of America*, 97(5), 1511-1524.